KONINKLIJK BELGISCH INSTITUUT VOOR NATUURWETENSCHAPPEN
OD NATUUR – BEHEERSEENHEID VAN HET MATEMATISCH MODEL

MOnitoring en MOdellering van het cohesieve sedimenttransport en evaluatie van de effecten op het mariene ecosysteem ten gevolge van bagger- en stortoperatie (MOMO)

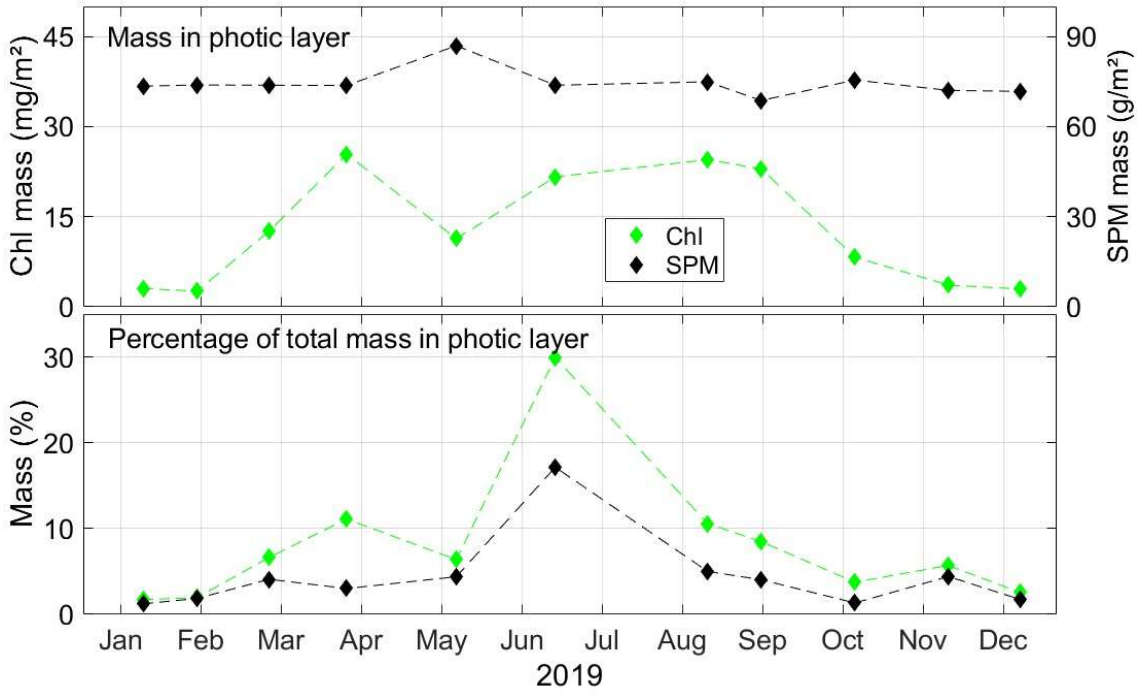

Activiteitsrapport (1 juli - 31 december 2023)

Michael Fettweis, Saumya Silori, Xavier Desmit

MOMO/10/MF/202403/NL/AR/4

KBIN-OD Natuur - BMM
Vautierstraat 29
B–1000 Brussel
België

Inhoudstafel

1. Inleiding

1.1. Voorwerp van deze opdracht

Het MOMO-project (monitoring en modellering van het cohesieve sedimenttransport en de evaluatie van de effecten op het mariene ecosysteem ten gevolge van bagger- en stortoperatie) maakt deel uit van de algemene en permanente verplichtingen van monitoring en evaluatie van de effecten van alle menselijke activiteiten op het mariene ecosysteem waaraan België gebonden is overeenkomstig het verdrag inzake de bescherming van het mariene milieu van de noordoostelijke Atlantische Oceaan (1992, OSPAR-Verdrag). De OSPAR Commissie heeft de objectieven van haar Joint Assessment and Monitoring Programme (JAMP) gedefinieerd tot 2021 met de publicatie van een holistisch "quality status report" van de Noordzee en waarvoor de federale overheid en de gewesten technische en wetenschappelijke bijdragen moeten afleveren ten laste van hun eigen middelen.

De menselijke activiteit die hier in het bijzonder wordt beoogd, is het storten in zee van baggerspecie waarvoor OSPAR een uitzondering heeft gemaakt op de algemene regel "alle stortingen in zee zijn verboden" (zie OSPAR-Verdrag, Bijlage II over de voorkoming en uitschakeling van verontreiniging door storting of verbranding). Het algemene doel van de opdracht is het bestuderen van de cohesieve sedimenten op het Belgisch Continentaal Plat (BCP) en dit met behulp van zowel numerieke modellen als het uitvoeren van metingen. De combinatie van monitoring en modellering zal gegevens kunnen aanleveren over de transportprocessen van deze fijne fractie en is daarom fundamenteel bij het beantwoorden van vragen over de samenstelling, de oorsprong en het verblijf ervan op het BCP, de veranderingen in de karakteristieken van dit sediment ten gevolge van de bagger- en stortoperaties, de effecten van de natuurlijke variabiliteit, de impact op het mariene ecosysteem in het bijzonder door de wijziging van habitats, de schatting van de netto input van gevaarlijke stoffen op het mariene milieu en de mogelijkheden om deze laatste twee te beperken.

Een samenvatting van de resultaten uit de vergunningsperioden 2017-2021 kan gevonden worden in het "Vooruitgangsrapport (juni 2019) over de effecten op het mariene milieu van baggerspeciestortingen" (Lauwaert et al. 2019) en het Syntheserapport over de effecten op het mariene milieu van baggerspeciestortingen" (Lauwaert et al., 2021) die gepubliceerd werden conform art. 10 van het K.B. van 12 maart 2000 ter definiëring van de procedure voor machtiging van het storten in de Noordzee van bepaalde stoffen en materialen.

1.2. Algemene doelstellingen

Het onderzoek uitgevoerd in het MOMO project kadert in de algemene doelstellingen om de baggerwerken op het BCP en in de kusthavens te verminderen, om de effecten van het storten van baggerspecie te kwantificeren en om een gedetailleerd inzicht te verwerven van de fysische processen die plaatsvinden in het mariene kader waarbinnen deze baggerwerken worden uitgevoerd. Dit impliceert enerzijds beleidsondersteunend onderzoek naar de vermindering van de sedimentatie op de baggerplaatsen en het evalueren van alternatieve stortmethoden. Anderzijds is vernieuwend onderzoek noodzakelijk om beter de effecten van het storten van baggerspecie in te schatten. Dit onderzoek is specifiek gericht op het dynamische gedrag van slib in de waterkolom en op de bodem en de interacties tussen fysische en biologische processen en zal uitgevoerd worden met behulp van modellen, in situ metingen en remote sensing data.

De specifieke acties die binnen dit onderzoek uitgevoerd worden om de algemene doelstellingen in te vullen zijn:

1. Streven naar een efficiënter stortbeleid door een optimalisatie van de stortlocaties.

2. Continue monitoring van het fysisch en biogeochemisch milieu waarbinnen de baggerwerken worden uitgevoerd (Taak 1) en aanpassing van de monitoring aan de nog op te stellen targets voor het bereiken van de goede milieutoestand (GES), zoals gedefinieerd zal worden binnen MSFD;

3. Uitbouw en optimalisatie van het numerieke modelinstrumentarium, ter ondersteuning van het onderzoek (Taak 2.1).

1.3. Algemeen Onderzoek 2012-2026

Het onderzoek heeft als doel om de effecten van baggerspeciestortingen op het mariene ecosysteem (fysische en biogeochemische aspecten) te onderzoeken. Hiervoor worden in situ metingen verzameld, gebruik gemaakt van remote sensing data en worden numerieke modellen ingezet. Voor de vergunningsperiode 2022-2026 worden volgende taken voorzien:

1) In situ en remote sensing metingen en data-analyse

De monitoring van effecten van baggerspeciestortingen gebeurd met behulp van een vast meetstation in de nabijheid van MOW1, en met meetcampagnes met de RV Belgica (een 10-tal meetcampagnes voor het verzamelen van traject informatie, profielen en de calibratie van sensoren; en een 10-tal campagnes voor het onderhoud van het meetstation te MOW1). De geplande monitoring is gericht op het begrijpen van processen, zodoende dat de waargenomen variabiliteit en de effecten van baggerspeciestortingen in een correct kader geplaatst kunnen worden. Een belangrijk deel is daarom gericht op zowel het uitvoeren van de in situ metingen, het garanderen van kwalitatief hoogwaardige data en het archiveren, rapporteren en interpreteren ervan. Remote sensing data afkomstig van onder andere satellieten worden gebruikt om een ruimtelijk beeld te bekomen.

2) Uitbouw en optimalisatie van het modelinstrumentarium

Het tijdens de voorbije jaren verbeterde en aangepaste slibtransportmodel zal verder worden ontwikkeld. Dit zal parallel gebeuren met de nieuwe inzichten die voorvloeien uit de metingen en de procesgerichte interpretatie van de metingen.

3) Ondersteunend wetenschappelijke onderzoek

Monitoring gebaseerd op wetenschappelijke kennis is essentieel om de effecten van menselijke activiteiten (hier het storten van baggerspecie) te kunnen inschatten en beheren. Om te kunnen voldoen aan de door OSPAR opgelegde verplichtingen van monitoring en evaluatie van de effecten van menselijke activiteiten is het ontwikkelen van nieuwe monitorings- en modelleractiviteiten nodig. Dit houdt in dat onderzoek dat de actuele stand van de wetenschappelijke kennis weerspiegelt wordt uitgevoerd en dat de hieruit voortvloeiende nieuwe ontwikkelingen geïntegreerd zullen worden in zowel de verbetering van het modelinstrumentarium als voor het beter begrijpen van het kustnabije ecosysteem.

1.4. Onderzoek Januari 2022 – December 2024

Voor de periode 2019-2021 werd rekening gehouden werd met de aanbevelingen voor de minister ter ondersteuning van de ontwikkeling van een versterkt milieubeleid zoals geformuleerd in het “Syntheserapport over de effecten op het mariene milieu van baggerspeciestortingen (2021)” dat uitgevoerd werd conform art. 10 van het K.B. van 12 maart 2000 ter definiëring van de procedure voor machtiging van het storten in de Noordzee van bepaalde stoffen en materialen.

Taak 1: In situ en remote sensing metingen en data-analyse

Taak 1.1 Langdurige metingen te MOW1 en W05

Sinds eind 2009 worden er continue metingen uitgevoerd te MOW1 met behulp van een meetframe (tripode). Met dit frame worden stromingen, slibconcentratie, korrelgrootte-verdeling van het suspensiemateriaal, saliniteit, temperatuur, waterdiepte en zeebodem altimetrie gemeten. Om een continue tijdreeks te hebben, wordt gebruik gemaakt van 2 tripodes. Na ongeveer 1 maand wordt de verankerde tripode voor onderhoud aan wal gebracht en wordt de tweede op de meetlocatie verankerd. Op de meetdata wordt een kwaliteitsanalyse uitgevoerd, zodat de goede data onderscheiden kunnen worden van slechte of niet betrouwbare data.

Veranderingen in kustnabije ecosystemen zijn dikwijls gecorreleerd met veranderingen van de helderheid van het water of de concentratie aan particulair suspensiemateriaal (SPM) en dus ook met het gehalte aan particulair organisch materiaal. De zone waar de invloed van het minerale en kustnabij suspensiemateriaal overgaat in een zone met dominantie van organisch suspensiemateriaal van mariene origine is van bijzonder belang. De monitoring wordt uitgebreid met de verankering van een meetboei in locatie W05 (51°N 24.96', 2°E 48.7'). W05 is één van de drie monitoringspunten waar waterstalen en sensormetingen maandelijks worden uitgevoerd.

Taak 1.2 Calibratie van sensoren tijdens in situ metingen

Tijdens meetcampagnes met de R/V Belgica zullen een voldoende aantal 13-uursmetingen uitgevoerd worden met als hoofddoel het kalibreren van optische of akoestische sensoren en het verzamelen van verticale profielen. De metingen zullen plaatsvinden in het kustgebied van het BCP (MOW1, W05). De optische metingen (Optical Backscatter Sensor) zullen gekalibreerd worden met de opgemeten hoeveelheid materie in suspensie (gravimetrische bepalingen na filtratie) om te komen tot massa concentraties

Taak 1.2 Bio-geo-chemische monitoring van het SPM (BGCMonit)

SPM bestaat uit minerale deeltjes van fysicochemische (b.v. kleimineralen, kwarts, veldspaat) en biogene oorsprong (b.v. calciet, aragoniet, opaal), levend (bacteriën, fyto- en zoöplankton) en niet-levend organisch materiaal (b.v. fecale pellets, detritus, exopolymeren), en partikels van menselijke oorsprong (microplastiek). Het SPM kan door hydrofobe organische polluenten of metalen gecontamineerd zijn. De samenstelling en concentratie van het SPM inclusief de hydrofobe polluenten verandert in functie van de tijd en de locatie. Deze variaties worden beïnvloed door de interacties tussen de fysische processen (getij, meteo, klimaat), biologische cycli (algenbloei), chemische processen (koolstofcyclus) en menselijke activiteiten (aanvoer van nutriënten, bagger- en stortactiviteiten, offshore constructies). De samenstelling van het particulair en opgelost suspensiemateriaal zal bepaald worden tijdens meetcampagnes met de RV Belgica tijdens een 10-tal campagnes per jaar. Naast de totale hoeveelheid aan SPM worden ook de concentraties aan verschillende organische bestanddelen (POC, PON, TEP, chlorofyl en phaeofytine) bepaald. De opgeloste stoffen zijn inorganische nutriënten, DOC, DIC en alkaliniteit. Stalen van suspensiemateriaal zullen genomen worden met de centrifuge om de samenstelling ervan te bepalen.

Taak 1.4: Archivering en verwerking van de data

De meetdata worden gearchiveerd en er wordt een kwaliteitsanalyse uitgevoerd, zodat de goede data onderscheiden kunnen worden van slechte of niet betrouwbare data. Slechte data kunnen bv optreden doordat het instrument slecht heeft gewerkt en verkeerd werd ingesteld. Niet betrouwbare data zijn typisch geassocieerd met bv biofouling. De data en metadata worden gearchiveerd. De metingen worden verwerkt en geïnterpreteerd. En

zullen dienen als basis voor het verder gebruik bij wetenschappelijke vraagstellingen.

Taak 2: Uitbouw en optimalisatie van het modelinstrumentarium

Taak 2.1: Opstellen van een slibtransportmodel voor het BCP met Coherens V2

Een slibtransportmodel zal worden geïmplementeerd met de software Coherens V2. De software laat toe om rekening te houden met gemengde sedimenten en dus met de interactie tussen zand en slib en laat morfologische berekeningen toe door een verbeterde implementatie van het schema voor het massabehoud en gebruik van lagen met gemengde sedimenten. Verdere aanpassingen en verbeteringen aan het model zullen worden uitgevoerd, meer bepaald:

- Kritische bodemschuifspanning voor erosie van gemengde sedimenten,
- Formulering voor de bodemschuifspanning,
- Koppeling van het model met het TILES voxel model voor een betere voorstelling van de bodemkarakteristieken.

Taak 2.2: Validatie van het slibtransportmodel voor het jaar 2013 (stortproef)

Een eerste toepassing van het model kan het jaar 2013 zijn, waarin de terreinproef voor alternatieve stortplaats alsook een intensieve monitoring plaatsvond. Deze laatste zal gebruikt worden voor de validatie van het model. Verder zal het model vergeleken worden met andere modellen van het BCP.

Taak 2.3: Optimalisatie baggerwerken

Een operationeel stortmodel zal worden opgezet in overleg met aMT. Dit model zal geïntegreerd worden in de binnen BMM-OD Natuur beschikbare operationele modellen. Het model zal gebruikt worden om in functie van de voorspelde fysische (wind, stroming, golven, sedimenttransport, recirculatie), economische (afstand, grootte baggerschip) en ecologische aspecten op korte termijn een keuze te kunnen maken tussen de beschikbare stortlocaties. Een eerste test hiervoor werd uitgevoerd in Van den Eynde en Fettweis (2011) waarin werd aangetoond dat door een optimale positie te kiezen voor het storten van baggerspecie in functie van de meteorologische omstandigheden, een vermindering van de aanslibbing van de vaargeulen en haven van Zeebrugge kan worden verwacht.

Het model zal worden gebruikt voor de optimalisatie van de baggerwerken. Verschillende simulaties kunnen worden uitgeoefend waarbij de invloed van de verschillende mogelijke stortplaatsen kunnen worden geëvalueerd.

Taak 2.4: Flocculatiemodel

De inzichten die voortvloeien uit de in situ data (Taken 1.4, 3.1 en 3.2) zullen worden geïntegreerd in een numeriek model dat het verband tussen SPM, TEP en flocculatie langsheen temporele (getij, seizoenen) en geografische (waterkolom, onshore-offshore) schalen combineert. Het model zal worden opgezet als 1D verticaal en zal gekoppeld worden met het 2 klassen populatie model van Lee et al. (2011). Hierdoor zal de verticale verdeling van de minerale en de organische fractie van het SPM en hun interactie kunnen worden voorspeld.

Taak 3: Ondersteunend wetenschappelijk onderzoek

Monitoring gebaseerd op wetenschappelijke kennis is essentieel om de effecten van menselijke activiteiten (hier het storten van baggerspecie) te kunnen inschatten en beheren. Om te kunnen voldoen aan de door OSPAR opgelegde verplichtingen van monitoring en evaluatie van de effecten van menselijke activiteiten is een verdere implementatie van huidige en het ontwikkelen van nieuwe monitoringsactiviteiten nodig. Meer specifiek gericht op de activiteit ‘storten van baggerspecie’ worden hier – wat het fysische milieu betreft - turbiditeit, samenstelling van de zeebodem, bathymetrie en

hydrografische condities beoogt. Deze taak speelt hierop in door de ontwikkeling en de implementatie van nieuwe tools die de actuele stand van de wetenschappelijke kennis weerspiegelen teneinde de mathematische modellen te optimaliseren en verfijnen.

Taak 3.1: SPM samenstelling - minerale fractie

Door de aanwezigheid van gemengde sedimenten in de zeebodem (zand en slib) zal tijdens sterke stroming en of hoge golven ook een gemengde minerale fractie in suspensie komen. Dit heeft twee consequenties voor monitoring. Ten eerste reageren akoestische en optische sensoren verschillend op zand en slib, zodat de verzamelde tijdreeksen een grotere onnauwkeurigheid hebben tijdens zo'n momenten (Fugate & Friedrichs, 2002; Baschek et al., 2017; Schwarz et al, 2017; Fettweis et al., 2019). Ten tweede bevatten zandkorrels geen mineraal-gebonden organisch materiaal en stalen genomen tijdens dit soort momenten kunnen dus de onzekerheid van het SPM-POM model vergroten. Indien er geen rekening gehouden wordt hiermee zal de SPM concentratie onder- of overschat worden alsook de afgeleid organische fracties. Doel is om de zand en slibfractie te identificeren door gebruik te maken van innovatieve meettechnieken (Pearsons et al., 2021) die optische en akoestische sensoren combineren. Het ultieme doel is om te komen tot tijdreeksen van zand- en slibconcentratie te MOW1.

Uit visuele inspecties van de bodemsamenstelling te MOW1 tijdens de laatste jaren blijkt dat het sediment zandiger is geworden. De hypothese is, dat dit verband houdt met erosie van de vooroever na de strandopspuitingen die de voorbije jaren werden uitgevoerd. Aan de hand van de boven aangehaalde methode zal nagegaan worden of er een trend naar zandaanrijking kan vastgesteld worden in de omgeving van MOW1.

Taak 3.2: SPM samenstelling - organische fractie

Het semi-empirisch POM-SPM model (Fettweis et al., 2022) zal verfijnd worden met de nieuwe data verzameld in taak 1.3. Hierdoor zal de inschatting van de minerale en de vers en mineraal-gebonden organische fractie nauwkeuriger kunnen worden gedaan.

Op basis van dit POM-SPM model kan de samenstelling van het suspensiemateriaal (minerale fractie, vers en mineraal gebonden POC, PON en TEP) worden berekend voor de tijdreeksen te MOW (vanaf 2005) en voor de satellietdata (vanaf 1997). Dit zal toelaten om de geografische en temporele variabiliteit van de transitiezone tussen het kustgebonden turbiditeitsmaximum en de offshore wateren te kwantificeren. De dynamica van het suspensiemateriaal in beide gebieden is verschillend, wat consequenties heeft naar de modellering ervan. Verder kan uit de lange tijdsreeksen gekeken worden of het gebruik van de stortplaatsen, meer bepaald S1, geleid heeft tot een zeewaartse uitbreiding van het turbiditeitsmaximum.

Taak 3.3: Trends in SPM concentratie

Om significante statistische trends te kunnen documenteren in SPM concentratie over de laatste decades, zijn metingen nodig die een lange tijdspanne omvatten en een groot gebied omvatten. Deze data zijn helaas niet beschikbaar. Wat er wel beschikbaar is zijn de tripode metingen te MOW1 (vanaf 2005) en op andere locaties, de puntmetingen verzameld met onderzoeksschepen in het Belgisch Deel van de Noordzee sinds ongeveer 1970 (cf. Belspo 4DEMON project) en satellietbeelden (vanaf 1997). De tripode data geven de temporele variabiliteit weer, maar zijn heel beperkt wat ruimtelijke spreiding betreft. De 4DEMON en satellietbeelden zijn beschikbaar over een lange periode en over een groot gebied, maar kunnen de temporele schaal niet oplossen. Om deze heterogene datasets samen te kunnen gebruiken, zal gekeken worden naar de statistische verschillen tussen de datasets en naar een manier om deze te combineren. Doel is om mogelijke trends in de SPM concentratie te identificeren en deze te linken aan natuurlijke veranderingen of aan menselijke activiteiten.

De trendanalyse van de historische data zal de basis vormen om de verandering van de SPM concentratie in de nabijheid van de nieuwe stortplaats ZBW te kwantificeren.

Taak 4: Rapportage en outreach

Om de zes maanden zal er een activiteitenrapport worden opgesteld dat de onderzoeksresultaten beschrijft. Jaarlijks wordt er een 'factual data' rapport opgesteld van de verzamelde meetgegevens. De resultaten uit het onderzoek zullen tevens worden voorgesteld op workshops, conferenties en in de wetenschappelijke literatuur.

1.5. Gerapporteerde en uitgevoerde taken

Periode Januari 2022 - Juni 2022

Taak 1.1: De meetreeks te MOW1 werd verdergezet.

Taak 1.2: Calibratie van OBS sensoren werd uitgevoerd tijdens RV Begica campagnes 2022/01, 2022/03, 2022/06, 2022/09 en 2022/14.

Taak 3.1: De akoestische en optische sensoren werden gebruikt om veranderingen in sedimentsamenstelling te zien te MOW1. Eerste resultaten worden getoond in hoofdstuk 2.

Taak 3.2: Intensieve bio-geochemische monitoring werd uitgevoerd te MOW1, W05 en W08 tijdens RV Belgica campagnes 2022/01, 2022/03, 2022/07, 2022/11, 2022/14). Eerste resultaten worden besproken in hoofdstuk 3.

Periode Juli 2022 - December 2022

Taak 1.1: De meetreeks te MOW1 werd verdergezet.

Taak 1.2: Calibratie van OBS sensoren werd uitgevoerd tijdens RV Begica campagnes 2022/17, 2022/19, 2022/21, 2022/24, 2022/28 en 2022/32.

Taak 2.4: De interactie van phytoplankton en SPM resulteert in de vorming van grotere vlokken met hogerer valsnelheden. In een labo experiment werd de flocculatie bestudeerd tussen klei en phytoplankton deeltjes. Een twee-klassen flocculatiemodel werd opgesteld om de experimentele data kwantitatief te analyseren, zie paper in appendix 1.

Taak 3.2: Intensieve bio-geochemische monitoring werd uitgevoerd te MOW1, W05 en W08 tijdens RV Belgica campagnes 2022/17, 2022/19, 2022/21, 2022/24, 2022/28 en 2022/32). Eerste resultaten worden besproken in hoofdstuk 3.

Taak 3.3: Het informatieverlies van niet continue tijdreeksen werd bepaald. Dit zal de basis vormen voor de trendanalyse in SPM concentratie over een langere periode, zie hoofdstuk 2.

Periode Januari 2023 - Juni 2023

Taak 1.1: De meetreeks te MOW1 werd verdergezet.

Taak 1.2: Calibratie van OBS sensoren werd uitgevoerd tijdens RV Begica campagnes 2023/01, 2023/04, 2023/06, 2023/08 en 2023/10.

Taak 2.4: Een 2D horizontaal flocculatiemodel werd gevalideerd voor het BCP (zie appendix 3). De resultaten tonen het nut van een flocculatiemodel voor grootschalig SPM transport modellering. Tegelijkertijd onderstrepen ze tekortkomingen die het gevolg zijn van de transitie tussen kust en offshore en die zich uiten in verschillende SPM dynamica (zie ook hoofdstuk 2). Dit dient opgenomen te worden in toekomstige modelleringen.

Taak 3: De resultaten beschreven in hoofdstuk 2 hebben mogelijks consequenties voor het storten van baggerspecie. Zij tonen immers aan dat er een duidelijk verschil tussen een kustnabije zone die gedomineerd wordt door minerale deeltjes en een offshore zone die vooral uit organische deeltjes bestaat. Er is geen (of weinig) uitwisseling tussen deze twee zones, zie hoofdstuk 3.

Taak 3.1: Analysen werden uitgevoerd gebaseerd op akoestische en optische sensoren van de tripode te MOW1 om de slib en zand fractie van het SPM te bepalen.

Taak 3.2: De bio-geochemische monitoring werd verdergezet te MOW1, W05 en W08 tijdens RV Belgica campagnes 2023/01, 2023/04, 2023/06, 2023/08 en 2023/10.

Periode Juli 2023 – December 2023

Taak 1.1: De meetreeks te MOW1 werd verdergezet.

Taak 1.2: Calibratie van OBS sensoren werd uitgevoerd tijdens RV Belgica campagnes 2023/17 en 2023/25.

Taak 2.4: De interactie tussen phytoplankton en minerale partikels werd verdergezet, resultaten werden voorgesteld op de INTERCOH conferentie (zie Appendix 1).

Taak 3.1: De analysen gebaseerd op akoestische en optische sensoren van de tripode te MOW1 om de slib en zand fractie van het SPM te bepalen, werden verdergezet. Eerste resultaten werden op de INTERCOH conferentie voorgesteld (zie Appendix 1)

Taak 3.2: De bio-geochemische monitoring werd verdergezet te MOW1, W05 en W08 tijdens RV Belgica campagnes 2023/17 en 2023/25. De verandering in samenstelling van het SPM werd bestudeerd over de waterkolom, conclusies met betrekking tot de gehele waterkolom in turbide gebieden worden besproken in hoofdstuk 2 (en Appendices 2-12) en werden voorgesteld op de INTERCOH conferentie (zie Appendix 1).

1.6. Publicaties

Hieronder wordt een overzicht gegeven van publicaties met directe betrokkenheid van het KBIN waar resultaten en data uit het MOMO project in worden gebruikt.

Activiteits-, Meet- en Syntheserapporten

Fettweis M, Silori S, Desmit X. 2024. MOMO activiteitsrapport (1 juli - 31 december 2023). BMM-rapport MOMO/10/MF/202309/NL/AR/4, 29pp + app.

Fettweis M, Desmit X. 2023 MOMO activiteitsrapport (1 januari - 30 juni 2023). BMM-rapport MOMO/10/MF/202310/NL/AR/3, 28pp + app.

Fettweis M, Desmit X. 2023 MOMO activiteitsrapport (1 juli – 31 december 2022). BMM-rapport MOMO/10/MF/202303/NL/AR/2, 27pp + app.

Fettweis M, Baeye M, Desmit X. 2022 MOMO activiteitsrapport (1 januari – 30 juni 2022). BMM-rapport MOMO/10/MF/202210/NL/AR/1, 21pp + app.

Conferenties/Workshops

Fettweis M, Delhaye L, Lee BJ, Riethmüller R, Schartau M, Silori S, Desmit X. 2023. Vertical variations of suspended particle composition reflect particle dynamics. INTERCOH, 18-22 September, Inha University, Incheon (Korea).

Ho QN, Fettweis M, Hur J, Lee SD, Lee BJ. 2023. The role of microalgae in cohesive sediment flocculation: Insights from stochastic modeling and laboratory experiments. INTERCOH, 18-22 September, Inha University, Incheon (Korea).

Huynh TT, Fettweis M, Lee BJ. 2023. Application of an 1-DV TCPBE model with Bayesian calibration to diagnose the flocculation potential in the laboratory experiments and field measurement. INTERCOH, 18-22 September, Inha University, Incheon (Korea).

Pham TTTP, Ho QN, Lee SD, Fettweis M, Lee BJ. 2023. Isolation and characterization of the molecular composition of algal dissolved organic matter. INTERCOH, 18-22 September, Inha University, Incheon (Korea).

Tran D, Desmit X, Verney R, Fettweis M. 2023. Application of sediment composition index to predict suspended particulate matter concentration in the North Sea. INTERCOH, 18-22 September, Inha University, Incheon (Korea).

Kallend A, Dujardin J, De Rijcke M, Fettweis M, Sabbe K, Vyverman W, Desmit X. 2023. Interactions between phytoplankton, marine gels and suspended particulate matter in a dynamic, shallow coastal system before and during the phytoplankton spring bloom. ASLO Aquatic Sciences Meeting, 4–9 June, Palma de Mallorca (Spain).

Schartau M, Fettweis M, Desmit X, Terseleer N, Riethmüller R. 2023. From brown to blue water: Unraveling spatio-temporal variations in organic matter composition of suspended particulate matter. ASLO Aquatic Sciences Meeting, 4–9 June, Palma de Mallorca (Spain).

Baeye M, Delhaye L, Fettweis M. 2022. Acoustic and optical turbidity response to altering particle size distribution during extreme events. EuroSea/OceanPredict workshop, 29

June – 1 July, Exeter (UK).

Fettweis M, Desmit X, Terseleer N, Parmentier K, Van der Zande D, Schartau M, Lee BJ, Riethmüller R. 2022. The characteristics of the organic matter in biomineral flocs. Ocean Science Meeting, 24 February – 4 March, Honolulu (USA).

Peer reviewed artikels

Desmit X, Schartau M, Terseleer N, Van der Zande D, Riethmüller R, Fettweis M. 2024. The transition between coastal and offshore areas in the North Sea unraveled by the suspended particle composition. Science of the Total Environment 915, 169966. doi:10.1016/j.scitotenv.2024.169966

Escobar S, Bi Q, Fettweis M, Monbaliu J, Wongsoredjo S, Toorman E. 2023. A 2DH flocculation model for coastal domains. Ocean Dynamics 73, 333-358. doi:10.1007/s10236-023-01554-y

Fettweis M, Riethmüller R, Van der Zande D, Desmit X. Water quality monitoring in coastal seas: How significant is the information loss of patchy time series? Science of the Total Environment 873, 162273. doi:10.1016/j.scitotenv.2023.162273.

Fettweis M, Schartau M, Desmit X, Lee BJ, Terseleer N, Van der Zande D, Parmentier K, Riethmüller R. 2022. Organic matter composition of biomineral flocs and its influence on suspended particulate matter dynamics along a nearshore to offshore transect. Journal of Geophysical Research Biogeosciences, 126, e2021JG006332. doi:10.1029/2021JG006332

Ho NQ, Fettweis M, Hur J, Desmit X, Kim JI, Jung DW, Lee SD, Lee S, Choi YY, Lee BJ. 2022. Flocculation kinetics and mechanisms of microalgae- and clay-containing suspension in different microalgae growth phases. Water Research 226, 119300. doi:10.1016/j.watres.2022.119300

Ho QN, Fettweis M, Spencer KL, Lee BJ. 2022. Flocculation with heterogeneous composition in water environments: A review. Water Research. 118147. doi:10.1016/j.watres.2022.118147

2. Interaction of phytoplankton and mineral particles at MOW1

The complex hydrodynamics in coastal waters result from a combination of constantly evolving physical forces (tidal currents, waves, density driven currents etc.), which lead to a significant variability in the distribution and composition of suspended particulate matter (SPM) (Jones et al., 1998). SPM composition, more specifically its particulate organic matter (POM) fraction, changes in a characteristic way with SPM concentration. An observed trend shows a progressive increase in POM fraction with decreasing SPM concentrations from nearshore to offshore waters (Schartau et a., 2019; Fettweis et al., 2022). This shift in the SPM composition across the cross-shore gradient, coupled with the influence of the physical forcing, is recognised to significantly impact the behaviour of SPM. In the offshore, the combination of lower turbulence levels and a higher POM fraction, acting as a binding agent for mineral particles, creates favourable conditions for the formation of low-density organic aggregates (Fettweis et al., 2006, Lee et al., 2019). Conversely, in nearshore shallow waters, lower organic fraction and greater turbulence governed by meteorological and tidal forcing can disrupt the formation of large low density organic aggregates (Fugate and Friedrichs, 2003).

In addition to its spatial variation, SPM composition also undergoes a seasonal variation while its organic fraction changes during and after phytoplankton blooms. In certain regions, the distinctive seasonality observed in SPM concentrations is an outcome of the seasonal shifts in SPM composition (Jago et al., 2007, Van Beusekom et al., 2012). Given the same hydrodynamic forcing, the SPM concentration is lower by about a factor of two in summer than in winter in the coastal turbidity maximum of the Southern Bight of the North Sea (Fettweis et al., 2016). This decrease is attributed to the interaction between mineral and organic particles (Engel et al., 2020; Fettweis et al., 2022). Higher fraction of phytoplankton-derived sticky transparent exopolymer particles (TEP) during biologically productive periods appear to promote formation and subsequent deposition of biomineral aggregates (Fettweis & Baeye, 2015), thereby lowering the SPM concentrations.

Existing studies establish an apparent relationship between the concentrations and composition of SPM, influencing its behavior, fate, and transport on broader spatial and temporal scales. However, the translation of these patterns to relatively smaller scales, particularly within shallow water columns and across tidal cycles, remains unexplored. This finer-scale investigation is particularly crucial in the coastal waters of the North Sea, where spring phytoplankton blooms develop over alternating spring-neap cycles (Blauw et al., 2012). Variations on tidal scales assume significance, with the difference between minimum and maximum SPM concentrations often contributing to a substantial gradient within the water column (Winterwerp, 2001, Sommerfield & Wong, 2011). Drawing directly from the observed cross-shore gradient in the particulate organic matter (POM) fraction of SPM, we expect analogous variations in SPM composition within the water column. Specifically, we anticipate a greater organic fraction near the surface compared to the deeper waters. However, the variation in hydrodynamic forcing across the cross-shore gradient (spanning a few tens of kilometers) is likely to differ markedly from the vertical variations within the shallow water column (extending over a few meters). Simultaneously, phytoplankton production is likely constrained by nutrient availability across the cross-shore, contrasting with the light limitation experienced in the vertical water column. These considerations prompt a closer examination of changes occurring at the surface and bottom of the water column.

A minor yet significant component of SPM is Chlorophyll-a (Chl*a*). In coastal waters, POM

often originates from diverse sources, encompassing a substantial amount of detritus, and becomes independent from both phytoplankton growth and Chla (Boyer et al., 2009; Chen et al., 2021). Therefore, investigating Chl*a* profiles in addition to POM provides insights into phytoplankton dynamics and enhances our understanding of sustaining phytoplankton blooms in turbid waters. Unlike the predominantly mineral composition of SPM, Chl*a* is influenced not only by the physical environment but also by a complex interplay of biological processes. Consequently, its distribution in continuously mixing water columns is likely determined by how biological processes compete with tidal mixing. As a result, its distribution may or may not consistently mirror that of SPM in the water column (Zhao et al., 2019). However, in shallow waters, characterized by intense vertical mixing we expect Chl*a* and SPM to follow the same vertical dynamics, that is, the dynamics of flocculation during the tidal cycle: floc formation and settling during the slack and floc breaking-up and resuspension above a critical current velocity. Therefore, we hypothesize that the Chl*a* content of SPM follows a similar pattern as POM content. Consequently, most vertical profiles are expected to show higher Chl*a* concentrations close to the bottom and lower concentrations close to the surface. In this study, we utilize data collected at a well-mixed shallow turbid station within the Belgian Coastal Zone over several tidal cycles. Our objective is to assess the changes in the POM and Chl*a* content of SPM within the water column. By examining these variations, we aim to explore potential implications for phytoplankton dynamics in turbid waters.

2.1. Methods

2.1.1. Study Area

The sampling station (MOW1) lies within the turbidity maximum in the Belgian Coastal Zone, and the typical SPM values vary between 20 and 100 mg/L at the surface and between 100 and 3000 mg/L near the bed (Fettweis et al., 2014). This shallow region with 10 m water depth at Mean Lower Low Water Spring (MLLWS) experiences a semi-diurnal tidal regime, with mean tidal range of 4.3 m (Spring Tide) and 2.8 m (Neap Tide). The water column remains well-mixed with negligible gradients in temperature and salinity, owing to strong tidal currents and low freshwater discharge (Lacroix et al., 2004). A significant event in phytoplankton bloom dynamics is the Spring bloom, which initiates in March and is particularly notable in April and May coinciding with the highest Chl-a concentrations. (Muylaert et al., 2006). Thereafter, Chl-a concentrations are relatively lower but remain moderate (3-10 µg/L) during the summer and autumn months. The phytoplankton succession observed in the Belgian coastal zone follows a distinct pattern (Rousseau et al., 2002). During winter, the dominant group comprises bentho-pelagic diatoms. As spring progresses, these small colonial diatoms are replaced by large-sized diatoms. Later in the spring bloom, Phaeocystis colonies become dominant. Subsequently, in summer and autumn, large diatoms regain prominence, only to be succeeded by smaller diatoms thereafter

2.1.2. In-situ Sample Collection and Analysis

Water samples were collected at MOW1 over monthly tidal cycles (12.5 hours) during a period spanning from 2019 to 2022. Twenty-nine such tidal cycles were sampled during this period. Every hour, 5 or 10 l Niskin bottles on the Sea-Bird SBE09 CTD carousel were closed at about 2 m above bed and 2 m below the surface and the carousel was taken on board and the bottles emptied. The water samples were filtered on board and analysed in the laboratory to obtain the concentration of SPM, POC, PON, Chla, and Phaeophytin*a* (Pheo*a*). At every sampling occasion, three subsamples for SPM concentration were taken and filtered on board using pre-combusted (405°C, 24 hr), rinsed, dried for 24 hr at 105°C and

pre-weighted 47 mm GF/C filters. After sampling the filters were rinsed with ultrapure water (resistivity 18.2 MΩcm normalized at 25°C) and immediately stored at -20°C, before being dried during 24 hr at 50°C and weighted to obtain the concentration. The samples for POC and PON were filtered on board using 25 mm GF/C filters (pretreated as above for SPM), stored immediately at -20°C, before being analysed using a Thermo Finnigan Flash EA1112 elemental analyser (for details see Ehrhardt & Koeve, 1999). The analytical uncertainty for POC and PON are 12% and 18%. The sample for pigment concentration was filtered on 47 mm GF/C filters, stored in liquid nitrogen, and determined in the lab using ultra high-performance liquid chromatography with fluorometric detection.

2.1.3. Sensor Measurements

Profiles of sensor measurements (OBS, LISST 100) have been collected during monthly (except in July) tidal cycles (12.5 hours) at MOW1 in 2019. In total 143 profiles with sample data and sensor data during 11 tidal cycles were collected. An Optical Backscatter Sensor (OBS3+) was connected to the SBE09 CTD and a LISST 100X was attached to the carousel. The LISST 100X was used to measure the volume concentrations of the SPM in 32 logarithmically spaced size groups over the range of 2.5–500 µm (Agrawal & Pottsmith, 2000). The OBS output was calibrated in the laboratory against a laboratory standard (AMCO clear) to convert the sensor output (in Volt) to a backscatter turbidity unit, then the sample SPM concentration was used to convert the turbidity into mass concentration. The linear regression between turbidity and sample SPM concentration had always a R^2>0.9. The sensor measurements provided data over the whole up- and downcast.

2.1.4. Statistical Analysis

We conducted a Shapiro-Wilk normality test to assess the normality of the differences between surface and bottom samples. The results indicated that, for most parameters, the differences deviated significantly from a normal distribution ($p < 2.2\times10^{-16}$). Consequently, to test for significant differences between the surface and bottom samples, we employed the non-parametric Wilcoxon signed-rank test for paired samples.

2.1.5. Vertical profiles of SPM, Chla and POC concentration

The OBS data cover the water column from about 2-3 m above the bed towards about 1-2 m below the surface, while the sample data are limited to the near bed and near-surface. The missing values near the bed, near the surface and in between have been calculated based on a power function (Zheng et al., 2013). The profile was calculated by a linear regression between the water depth and the logarithm of the SPM, POC, Phaeophytine a and Chl*a* concentration respectively. Both sample and OBS derived SPM concentration data have been used for constructing the SPM concentration profiles. The Chl*a* and Phaeo*a* concentration profiles have been built only with the sample data. The POC profiles have been calculated based on the relationship between the POM (=POC) content and the SPM concentration (see Fettweis et al., 2022):

$$POM_{fres} = f_1 \times \frac{K_{POM}}{\frac{K_{POM}}{SPM}+1} \times \frac{1}{m_{POM}+1} \quad (2.1)$$

$$POM_{mineral} = f_2 \times \frac{m_{POM}}{m_{POM}+1} \times SPM \quad (2.2)$$

2.1.6. Mass of SPM, Chla and POC in the euphotic layer

The fitted profiles have been used to calculate the amount of SPM, POC and Chl*a* mass in the euphotic layer. The euphotic depth, D_{euph}, is mainly controlled by the relationship between the SPM concentration and its relationship with the vertical light attenuation coefficient, K_d, as (Cloern, 1987):

$$D_{euph} = \frac{4.6}{K_d} \quad (2.3)$$

The vertical attenuation coefficient, k_d, was derived from the relationship proposed by Devlin et al. (2008) for combined coastal, offshore, and transitional UK waters:

$$K_{PAR} = 0.086 + 0.067 \times SPM_{surf} \quad (2.3)$$

where SPM_{surf} is the SPM concentration at the surface. The mass of SPM, POC and Chl*a* in the euphotic layer was then calculated for every profile. The fraction of SPM, POC and Chl*a* in the euphotic layer was estimated for every tidal cycle separately by relating the mass in the euphotic layer in each profile to the total available mass for resuspension during the tidal cycle. The latter was set equal to the maximum mass of SPM, POC and Chl*a* available in a profile during the cycle. The total mass in the euphotic layer during a tidal cycle was then scaled by the total mass available for resuspension.

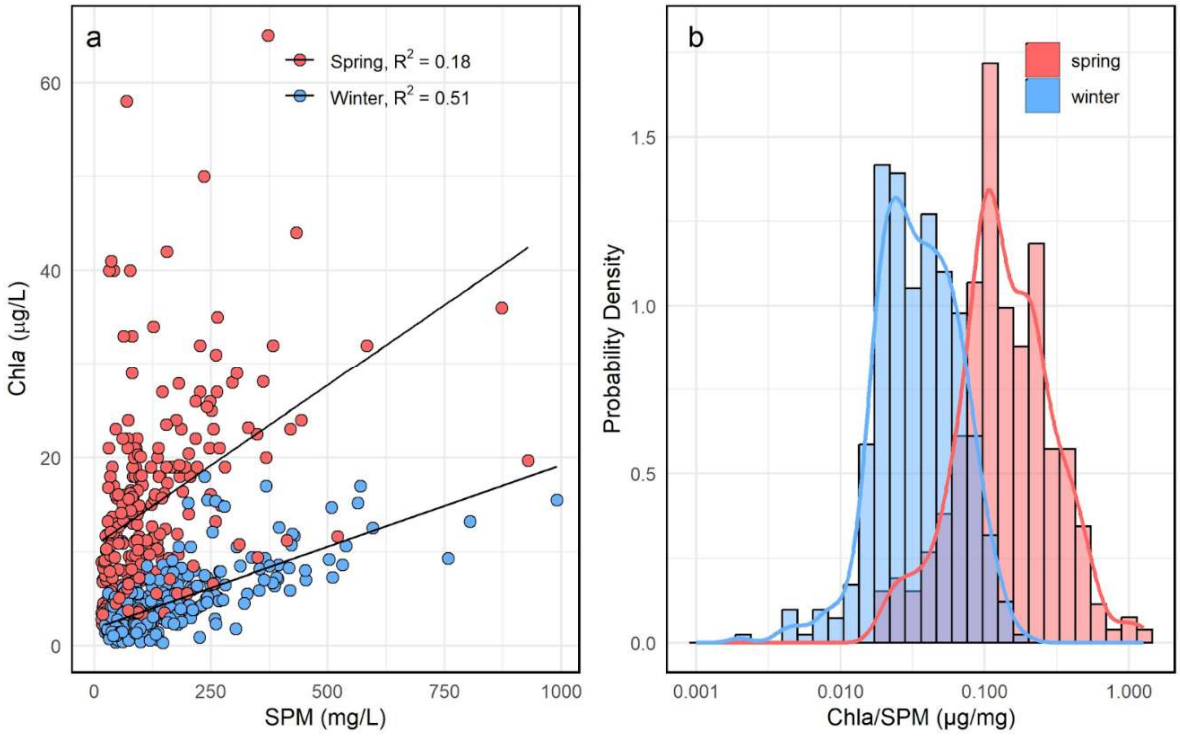

Figure 2.1: Correlation between SPM (mg/L) and Chla (µg/L) (a) and Probability Density of Chla/SPM ratio (b) during spring (Mar-May) and winter (Dec-Feb). Data was collected between 2012–2022 at MOW1.

2.2. Results

2.2.1. Probability density distribution of sample SPM, POC and Chla

The sample data from the tidal cycles has been divided into the following seasonal categories: December, January, and February representing winter; March, April, and May denoting spring; June, July, and August indicating summer; and September, October, and November representing autumn. SPM, POC and Chl*a* concentrations exhibited large variations at tidal and seasonal scales. During spring, SPM ranged from 14 to 988 mg/L, in summer from 8 to 487 mg/L, in autumn from 11 to 573 mg/L, and in winter from 20 to 990 mg/L. Variations in POC concentrations were similar to the SPM concentrations and the two parameters exhibited a significant positive correlation at seasonal and tidal scales. During spring, POC ranged from 0.73 to 34 mg/L, in summer from 0.52 to 16 mg/L, in autumn from 0.38 to 16 mg/L, and in winter from 0.39 to 34 mg/L. Elevated POC fractions (POC/SPM) were observed during spring (1-13%) and summer (1–19%), compared to the tidal cycles in

autumn (2–10%) and winter (1-8%). Like the POC fraction, the highest Chla concentrations were recorded during the productive months of spring (2–65 µg/L) and summer (3–40 µg/L), while lower Chla concentrations were seen in autumn (1–24 µg/L) and winter (0.3–18 µg/L). On an average higher POC and Chla contents were measured in the surface than bottom waters (Table 2.1).

To establish a robust correlation between SPM and Chl*a*, we expanded our dataset from MOW1. In addition to the data gathered during tidal cycles between 2019-2022, we incorporated information from earlier periods spanning 2012-2018. Notably, the data collected during these earlier cycles was exclusively obtained near the bed, omitting measurements from the surface. A significant positive correlation between SPM and Chl*a* was identified during winter (Figure 2.1a). However, greater phytoplankton production in spring, evidenced by significantly higher Chla/SPM ratios may have contributed to the lack of correlation between SPM and Chl*a* during these months (Figure 2.1b).

Table 2.1. Geometric means (/ standard deviation) of parameters measured at the surface (surf) and bottom (bot) depths at MOW1. Data was collected across four seasons (spring, summer, autumn, and winter) spanning from 2018 to 2022. Number of observations = n*

	Spring	n	Summer	n	Autumn	n	Winter	n
SPM_{surf} (mg/l)	71.3*/2.1	109	29.6*/1.8	98	60.0*/2.1	99	82.3*/2.1	124
SPM_{bot} (mg/l)	114.6*/2.3	129	51.1*/2.3	98	85.3*/2.2	96	110.2*/2.3	162
POC_{surf} (mg/l)	2.4*/1.9	109	1.3*/1.4	92	1.9*/1.9	99	2.4*/2.0	109
POC_{bot} (mg/l)	3.5*/2.1	116	2.0*/1.9	88	2.7*/2.0	96	3.2*/2.2	125
Chla_{surf} (µg/l)	10.8*/1.9	95	8.2*/1.6	97	5.4*/2.0	99	3.8*/1.9	124
Chla_{bot} (µg/l)	11.8*/2.0	103	10.3*/1.7	96	6.5*/1.9	95	4.2*/1.9	135
Pheoa_{surf} (µg/l)	0.5*/1.9	95	0.2*/1.7	98	0.3*/2.0	99	0.3*/2.6	122
Pheoa_{bot} (µg/l)	0.6*/2.1	103	0.3*/1.9	97	0.4*/2.1	95	0.4*/2.8	137
POC:SPM_{surf} (%)	3.4*/1.3	109	4.6*/1.4	91	3.2*/1.3	99	3.0*/1.3	109
POC:SPM_{bot} (%)	3.3*/1.3	116	4.1*/1.5	88	3.2*/1.3	96	2.9*/1.3	125
Chl*a*:SPM_{surf} (%)	0.014*/2.0	95	0.028*/1.8	96	0.009*/2.2	99	0.004*/1.8	124
Chl*a*:SPM_{bot} (%)	0.011*/2.0	103	0.020*/2.2	96	0.008*/2.1	95	0.004*/1.7	134
$POC:PON_{surf}$	8.1*/1.2	105	7.7*/1.1	90	8.3*/1.2	88	8.6*/1.2	102
$POC:PON_{bot}$	8.6*/1.2	112	7.9*/1.1	87	8.7*/1.2	87	9.1*/1.2	112
Chl*a*:$Pheo_{surf}$	20.3*/1.6	95	35.3*/1.6	97	18.8*/1.9	99	11.3*/1.7	122
Chl*a*:Pheoa_{bot}	18.2*/1.5	103	30.3*/1.6	96	16.6*/1.8	95	10.5*/1.7	135

2.2.2. Vertical variations in SPM composition

The collected samples, obtained a few meters from the surface and bed during multiple tidal cycles during 2019-2022, allowed investigating the vertical variations in SPM composition. At MOW1, the SPM, POC, and Chl*a* concentrations are significantly influenced by tidal mixing, as particles are subject to settling and resuspension processes. This influence is evident in the observed concentration patterns where, for most instances, the highest concentrations, as indicated by the Wilcoxon signed-rank tests, are found near the bottom compared to the surface values (Fig. 2.2a-c). The observed vertical gradient in Chl*a* concentrations contrasts with previous findings in the Belgian coastal zone, where surface waters (3 m from the surface) and bottom waters (1 m from the bed) exhibited similar Chl*a* concentrations (Franco et al. 2007). Relevant to the topic, their sampling did not consider the tidal phase. Investigating the SPM composition in the vertical water column, we

observed that POC contents between bottom and surface waters were significantly different (Figure 2.3a), the difference in the POC content between surface and the bottom seems to increase in spring and reaches a maximum in summer (Figure 2.3b). The depth-based variation in POC content is likely driven by the gradient in SPM concentrations along the vertical water column, indicating an increase in the POC content of SPM as the SPM concentration decreases towards the surface. Such a relationship between the POC content and the SPM concentration is a well-documented feature (e.g., Manheim et al., 1972; Fettweis et al., 2006; Schartau et al., 2019).

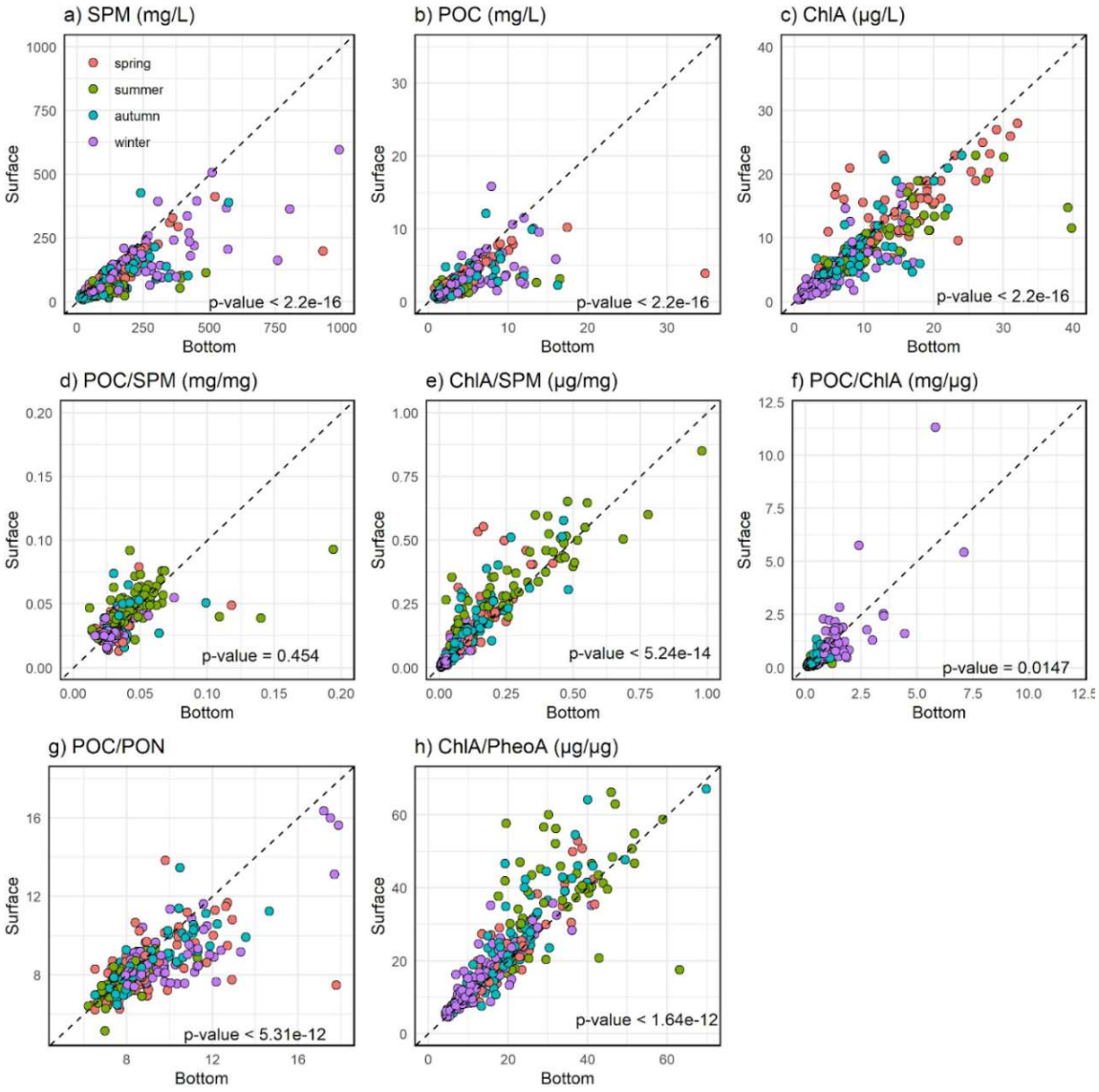

Figure 2.2: Scatter plots (1:1 line shown) comparing SPM (mg/L) concentrations (a), POC (mg/L) concentrations (b), Chla (µg/L) concentrations (c), POC:SPM (mg/mg) ratios (d), Chla:SPM (µg/mg) ratios (e), POC:Chla (mg/µg) ratios (f), POC:PON (molar ratio) (g), and Chla:Pheoa (µg/µg) ratios (h) between surface (2 m below surface) and bottom (2-3 m above bed) depths .p-values for t-paired tests.

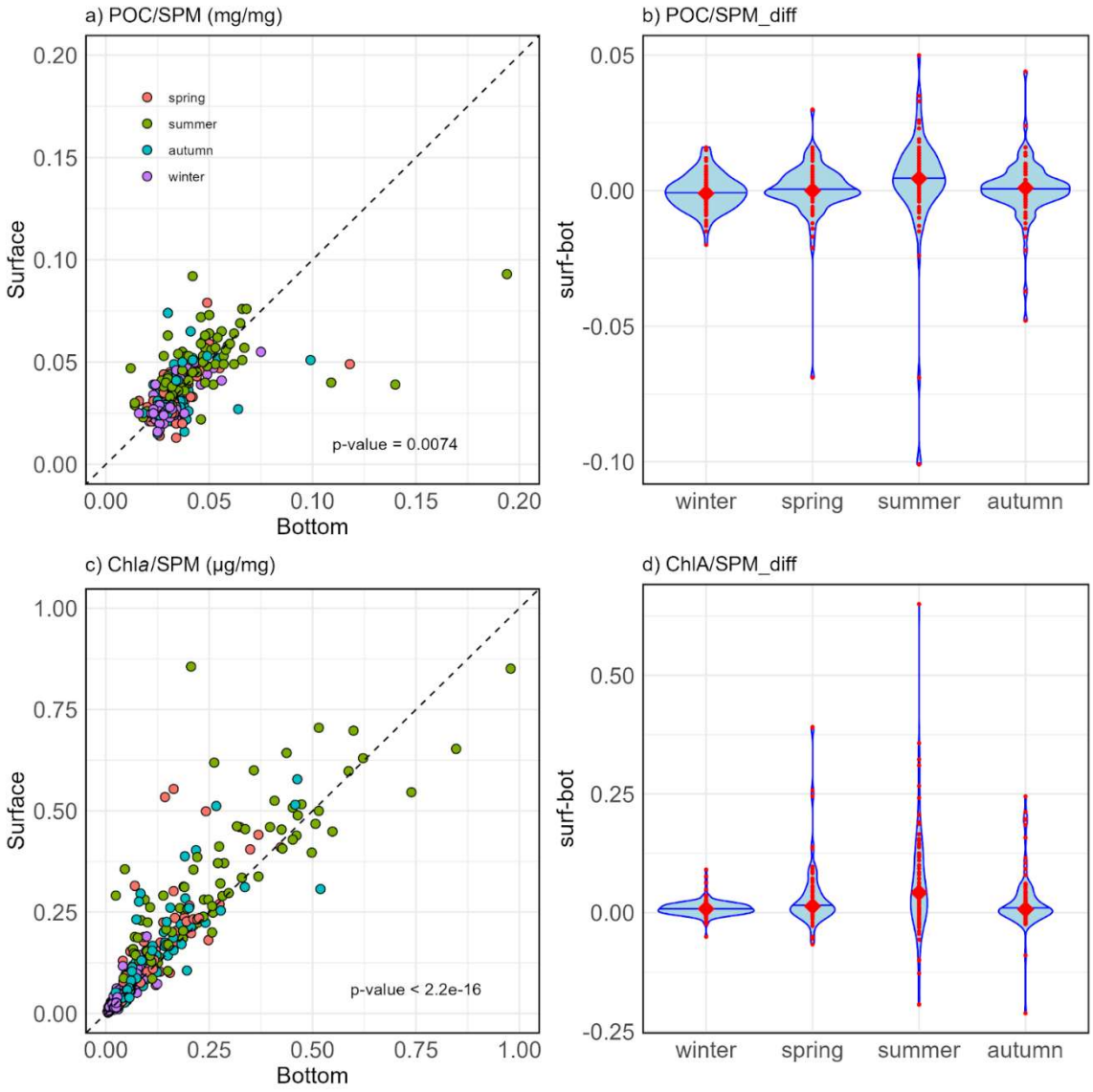

Figure 2.3: (a) Scatter plot comparing surface and bottom POC:SPM (mg/mg) ratios. (b) Violin plot showing the difference (surf-bot) between surface and bottom POC:SPM (mg/mg) ratios during different seasons. (c) Scatter plot comparing surface and bottom Chla:SPM (µg/mg) ratios. (d) Violin plot showing the difference (surf-bot) between surface and bottom Chla:SPM (µg/mg) ratios during different seasons. The black dashed line in the scatter plots represents the 1:1 line. In the violin plots the blue horizontal line, bigger red point, and smaller red points indicate median, mean, and the data points, respectively.

The vertical variation in the Chla content (Chla/SPM; Figure 2.3c) is notably more pronounced than the variation in the POC content. We observed significantly higher Chla contents in the upper water column during spring and summer, and occasionally in autumn (Figure 2.3d). Additionally, this evidence for vertical differences in the organic content of the SPM in the water column is supported by significantly lower POC/Chla and POC/PON ratios in surface waters, with concomitant higher Chla/Pheoa ratios (Figure 2.2d, e, f). These ratios may serve as potential proxies indicating the quality of organic matter (Savoye et al., 2003; Bouillon et al., 2011), and our results suggest that the surface waters are generally enriched in organic matter of higher trophic quality.

Analysis of hourly profiles of SPM and Chl*a* concentrations during tidal cycles in spring (April 2019) and winter (November 2019) revealed notable disparities between the two seasons. Throughout both tidal cycles, SPM concentrations exhibited a tendency to increase

towards the bed during periods of maximum current velocities, whereas they remained relatively constant on the vertical exhibiting lower values on average during the slack periods (blue lines in Figure 2.4a, b). Concurrently, Chl*a* profiles in November closely mirrored the corresponding SPM patterns (Figure 2.3b). However, in Apr il, distinct differences emerged between Chl*a* and SPM vertical profiles. Most notably, about half of the Chla profiles in April exhibited inversions, where concentrations decreased towards the bed (Figure 2.4a, Profiles 1-4, 7-8). Similar patterns as in November have been found during the months May-August and October-November and as in April during the months March and September.

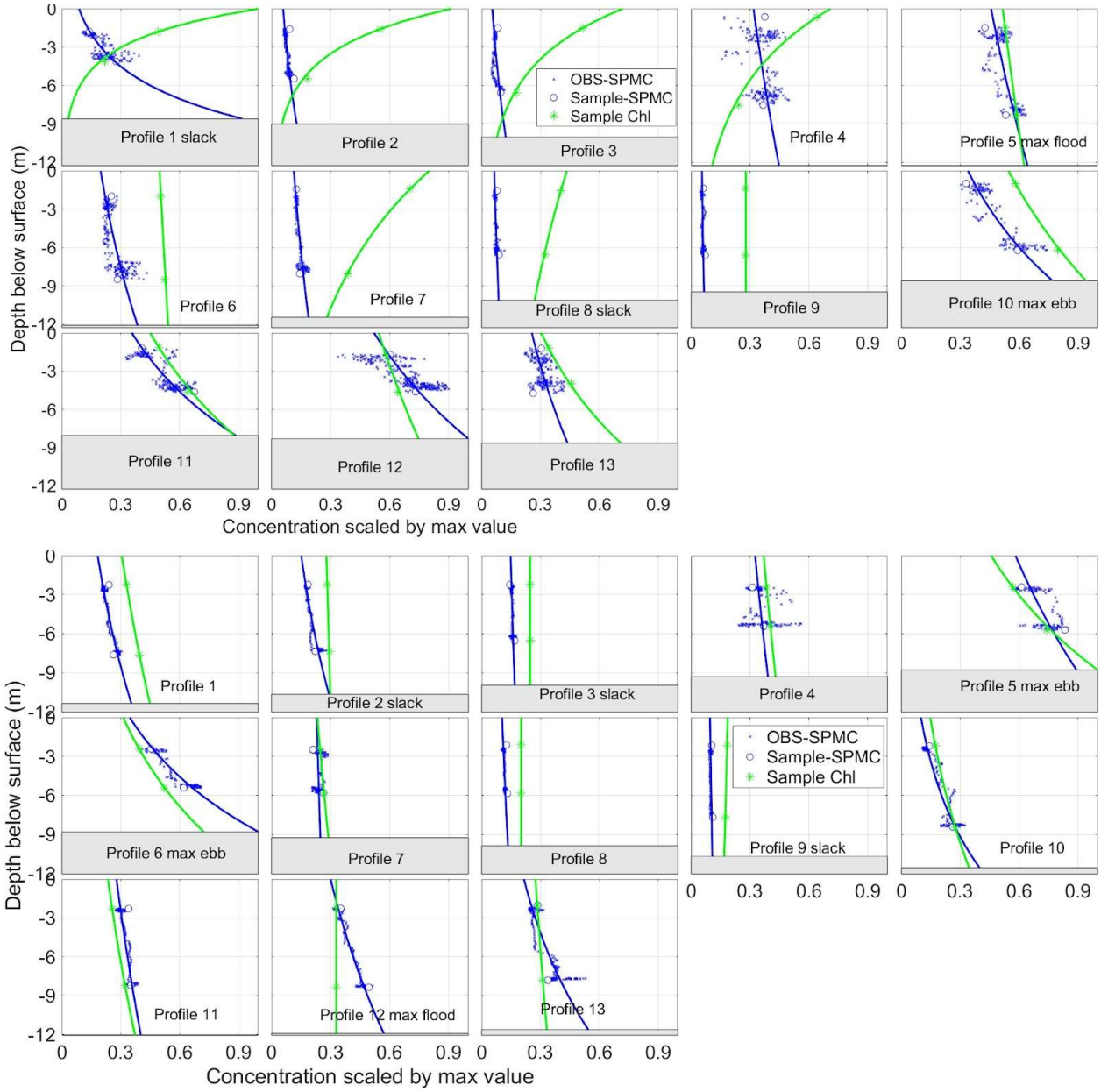

Figure 2.4: Hourly vertical profiles of SPM (blue line) and Chla (green line) concentrations scaled by the maximum value during the tidal cycle in April 2019 (SPM: 366 mg/l, Chla: 33 µg/l) (a) and November 2019 (SPM: 272 mg/l, Chla: 11 µg/l) (b). Sample and OBS-derived data were used to construct SPM concentration profiles, whereas Chla concentration profiles were derived using surface and bottom sample data only.

2.3. Discussion

This study seeks to investigate if significant changes occur in the composition of SPM on smaller spatial (within a few meters of a shallow water column) and temporal (tidal cycle) scales. In contrast to many older studies that are based solely on surface samples, we use field vertical profile observations (hourly water samples at surface and bottom and continuous sensors during a tidal cycle). The objective is to discern the implications of these changes for phytoplankton, as evidenced by shifts in Chl*a* distribution. Our initial hypothesis, suggesting that Chl*a* closely tracks the distribution of SPM in a shallow, well-mixed water column (characterized by uniform temperature and salinity), appears to be supported only during the winter months, when tidal mixing is most likely to be the dominating force influencing the two variables. This is substantiated by a significant positive correlation observed between SPM and Chl*a* in winter. However, during the growing season (spring), the correlation between the two variables becomes less robust. Furthermore, a significant increase in the Chl*a* content of SPM during this period suggests a pronounced influence of primary production/biological processes?? on Chl*a* in addition to tidal mixing. Based on these observations, we propose the existence of two distinct phytoplankton types: a) Floc-associated phytoplankton: This type, physically linked to SPM, is expected to result in synchronized variations in Chl*a* concentrations alongside changes in SPM concentrations. This association is dominant during the winter months. b) Free phytoplankton: This type, lacking a direct association with mineral SPM, exhibits differences in physical properties such as density and settling velocities. Consequently, it is likely to experience variations in settling and resuspension cycles, resulting in a weaker correlation with SPM. This type appears to prevail during the growing season and is likely to accumulate closer to the surface during maximum currents when the flocs break up owing to lower settling velocities than the mineral particles. If correct, this hypothesis contributes to explaining why phytoplankton can sustain a net production in turbid, vertically mixed waters.

2.3.1. Vertical variation in SPM composition

We first examined the sampled data of SPM, Chl*a*, POC, and Pheo*a* collected at two distinct depths at MOW1. The rationale lies in our expectation of observing differences in the composition of SPM, that arise from the anticipated differences in the distribution of both SPM and phytoplankton (Chl*a*). Our results reveal a compositional gradient of SPM within the vertical water column similar to the cross-shore gradient (Figure 2.2, 2.3). Notably, the Chl*a* and POC content of SPM begins to diverge between surface and bottom depths in spring, with the disparity reaching its peak during summer (Figure 2.3b, d). In addition to significantly higher Chl*a* and POC content at the surface, the observations also indicate the disparity in the quality of the organic material between surface and deeper depths. POC/PON, POC/Chl*a*, and Chl*a*/Pheo*a* ratios often used as proxy's indicative of biochemical composition of bulk POM suggests prevalence of degraded POM deeper in the water column (Figure 2.2d, e, f). Most of our observed POC/PON ratios align with the commonly assigned range for marine POM (6-12; Martiny et al., 2013) although there is a seasonal variation (Table 2.1). Previous estimates of $\delta^{13}C_{POC}$ (-24 to -18 ‰) from the bottom waters in the Belgian coastal zone also indicate significant autochthonous production (Franco et al., 2008). But the elevated POC/PON ratios in deeper waters indicate preferential remineralization of nitrogen (Schneider et al., 2003). Lower values closer to the surface suggest greater contribution of non-degraded phytoplanktonic POM. Moreover, higher POC/Chl*a* ratios further support the dominance of degraded material at deeper depth (Savoye et al., 2003). Notably lower Chl*a*/Pheo*a* ratios in deeper waters similarly indicate the accumulation of chlorophyll degradation products through processes such as predation

and degradation of phytoplankton cells (Lorenzen, 1967). Variations in the composition of organic matter based on depth have also been documented within the Delaware Estuary, with the prominence of phytoplankton-derived organic matter in surface waters and more degraded terrestrial organic matter closer to the bed (Hermes & Sikes, 2016). Deng et al., (2022) also reported elevated Chl*a*/SPM ratios closer to the surface than the deeper waters (≈10 m) in the Changjiang Estuary. The depth-based segregation of POM by quality is a further indication that resuspension and settling do not merely result in dilution of the particles that would result in a constant composition independent of concentration. Instead, our data shows that particles do not behave homogeneously and that differential settling occurs. This finding calls for a reconsideration of monitoring strategies to include samples from surface and bottom depths during a tidal cycle.

2.3.2. Free and floc-attached phytoplankton

At the tidal scale, the hourly profiles of SPM and Chl*a* during most of the year consistently exhibit similar distribution. In contrast, during the bloom periods (spring and late summer), the observations of higher Chl*a* concentrations near the surface in the vertical profiles suggest instances during the tidal cycle where Chl*a* distribution deviates from its association with SPM. During most of the year, resuspension results in an increase in SPM and Chl*a* concentrations at the surface but the higher concentrations are still found at the bottom. While the specific interactions between phytoplankton and SPM remain unclear, high SPM concentrations at MOW1, coupled with tidal turbulence, create favorable conditions for collisions and attachments between phytoplankton and mineral particles forming biomineral flocs (Wheatland et al., 2020). We reason that the inverse Chl*a* profiles, which is a simultaneous increase at the surface and decrease at the bottom in Chl*a* concentrations observed during the growing season result from the vertical transport towards the surface at maximum currents velocities. The inverse Chl*a* profiles partly result from the difference in buoyancy between released phytoplankton cells and mineral microflocs after the flocs break up during maximum current velocity. Although the phytoplankton cells are subject to an upward flux and settling akin to the mineral particles, they are likely to have lower settling velocities due to lower densities compared to mineral-enriched flocs. Additionally, phytoplankton employ strategies to decrease their buoyancy. Smaller phytoplankton cells, such as cyanobacteria, are buoyant and accumulate near the surface waters (Huisman et al., 2004), while in certain cases improved nutrient levels increase the buoyancy of the cells, resulting in reduced sinking velocities (Steele & Yentsch 1960). Notably, *Phaeocystis* colonies with cells embedded in a mucilaginous matrix dominate the late phase of spring bloom in the Belgian coastal waters (Rousseau et al., 1994). Evidence from the German Bight indicates that *Phaeocystis* colonies exhibit a lower aggregation potential, often observed either freely floating or loosely attached to the flocs. In contrast, the diatom cells were found to be firmly embedded within the flocs (Riebesell, 1993). Furthermore *Phaeocystis*-rich flocs may have lower sinking velocities prolonging their residence closer to the surface (Riebesell, 1992). The inverse Chl*a* profiles, supports our assumption of a substantial abundance of free-floating phytoplankton in the growing season. Profiles with higher Chl*a* concentrations in the upper water column are also observed in shallow waters (10-15 m) during summer in the German Bight (Zhao et al., 2019). Although floc breaking during the maximum current occurs throughout the year, the increase in Chl*a* at the surface seems to be less pronounced during winters and late-autumn due to high SPM and low phytoplankton abundance (low Chl*a*) with dominance of small colonial bentho-pelagic diatoms (Rousseau et al., 2002; Muylaert et al., 2006). Whereas, during summer, the accumulation of fresh TEP not only increases the abundance of the aggregates but strengthens the flocs, thus reducing the probability of floc breakup (Fettweis et al., 2014).

The vertical profile data in summer do not show inverse profiles of Chl*a* with respect to SPM and support that free phytoplankton is less probable.

2.3.3. Photo-acclimation

While our hypothesis with free and floc-associated phytoplankton explains the observations at MOW1, it is imperative to consider alternative perspectives. Physiological adaptations of coastal phytoplankton enable photosynthetic production even when the mixing depth is remarkably deeper, reaching up to 20 times the photic depth (Van Spaendonk et al., 1993). Additionally, phytoplankton may alleviate the light limitation to an extent through photo-acclimation mechanisms, such as enhanced Chl*a* production per cell. This implies that Chl*a* alone may not be a reliable proxy for phytoplankton abundance in turbid systems (Jakobsen & Markager, 2016; Striebel et al., 2023). However, such mechanisms may not always be effective, particularly under sustained intense mixing, when the physiological adjustment lag rapidly changing environmental conditions (Falkowski, 1980; McLaughlin et al., 2020). Photoacclimation would typically lead to higher Chl*a* concentrations in phytoplankton cells at deeper depths due to increased light limitation, while Chl*a* concentrations at the surface would decrease due to photoprotective strategies. Furthermore, the observation of inverse profiles even during night sampling (April 2019) eliminates photoacclimation as a factor influencing these profiles. Similarly, the expectation of higher Chl*a* concentrations at the surface and lower concentrations at the bottom, typically attributed to higher primary production and phytoplankton mortality, respectively, may not be justified. Variability in the Chl*a* profile over short time scales such as hourly measurements over a tidal cycle are likely governed by physical processes, such as resuspension, settling or buoyancy rather than biological processes (Blauw et al., 2012). While tidal advection plays a crucial role in horizontally transporting phytoplankton, its impact on shaping the observed Chl*a* profile appears less significant. It is less likely for adjacent shallow and well-mixed areas to display different vertical Chl*a* distributions. Additionally, the consistent observation of inverse profiles during both ebb and flood periods reduces the likelihood of gradients explaining these patterns. Although we cannot completely rule out the possibility of phytoplankton patchiness contributing to the observed high Chl*a* concentrations near the surface, the occurrences of the inverse profiles during high current velocities suggests a more systematic pattern. This contrasts with a more stochastic pattern that we expect from patchiness and points to a lower significance of this phenomenon.

2.3.4. Probability of phytoplankton to be in the photic zone

To better quantify the accumulation of Chl*a* in the surface waters, we attempted to determine the average mass of SPM and Chl*a* within the estimated photic layer during a tidal cycle (11 tidal cycles from the year 2019) from the fitted vertical profiles. The depth-integrated concentration of SPM ([g m^{-2}]) within the photic layer during a tidal cycle remains conservative across seasons (Figure 2.5a). This lack of variability aligns with expectations, considering that the vertical light attenuation coefficient, and hence the photic layer, is mainly controlled by SPM concentrations. However, the mass of Chl*a* within the photic layer during a tidal cycle exhibits seasonal variation, being higher during spring and summer compared to winter and autumn, yet it remains constant within each of these seasons (Figure 2.5a). Further we calculate the percentage of SPM and Chl*a* within the photic layer by assuming the highest concentration in the fitted vertical profile as the maximum SPM and Chl*a* available for resuspension during a tidal cycle (Figure 2.5b). The analysis reveals that the percentages of Chl*a* and SPM within the photic layer are identical during a tidal cycle in winter. However, during spring, the Chl*a* percentage in the photic layer averages around 10%, while the SPM percentage is notably lower at 3%. Similarly, in summer, the

Chl*a* percentage increases up to 30%, whereas the SPM percentage rises to 18% within the photic layer. This observation substantiates the enrichment of Chl*a* in the photic layer and aligns with the established POC/SPM relationship, indicating an inverse correlation between SPM concentration and the POC:SPM ratio (Schartau et al., 2019; Fettweis et al., 2022).

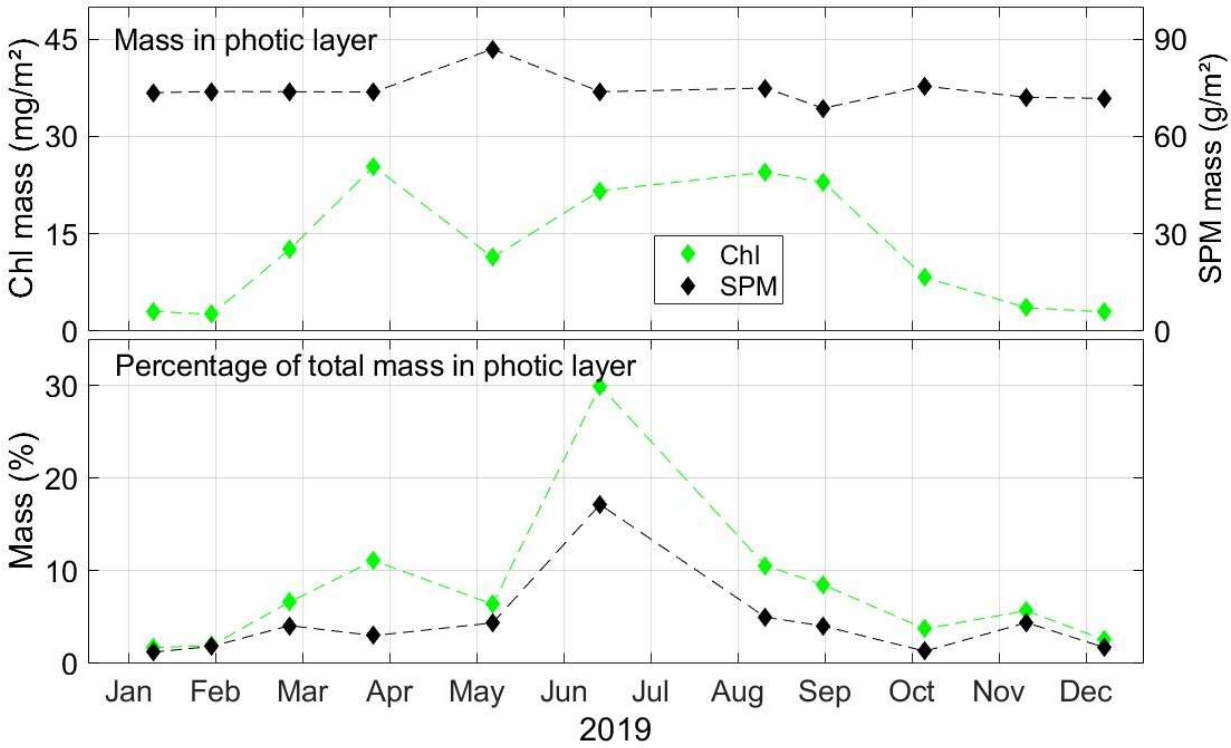

Figure 2.5: (a) Mass of Chla and SPM integrated over the photic layer per tide and unit area. (b) Percentage of Chla and SPM in the photic layer with respect to their total mass available for resuspension during a tide.

2.3.5. How important is water clarity in turbid areas for primary production?

A typical occurrence in Belgian nearshore waters is an elevated surface Chl*a* concentration (10-25 µg/l) co-occurring with SPM varying between 20 and 100 mg/l (Fettweis et al., 2014). High Chl*a* concentrations in such turbid waters suggest prominence of mechanisms that aid in increasing the probability of the phytoplankton cells to be retained in the photic zone. The insignificant differences in the SPM concentrations between winter and early spring (March) in the Belgian Coastal Waters suggests that the photic depth, a measure of water clarity, may not be different during these months, though there will be potential variations due to spring-neap tides. The observed increase in Chl*a* concentrations during early spring hence indicates a relaxation of winter light limitation and not necessarily an increase in the photic depth. This indicates that once the minimum irradiance threshold for photosynthesis is met, phytoplankton cells can initiate production despite high SPM concentrations. In turbid waters during early spring, free phytoplankton types have a distinct advantage. Due to differential settling, they are likely to spend more time within the shallow photic zone compared to floc-attached phytoplankton cells. The differential settling, as evidenced by the inverted Chla profiles, appears to be an important mechanism for further enhancing and sustaining the phytoplankton bloom until late April, when SPM concentrations begin to decrease. Thereafter, as photic depths increase, the advantage of free phytoplankton types diminishes, given the higher likelihood of cells to be within the photic zone (Figure 2.5b).

This line of reasoning also calls in to examine the hypothesis that the phytoplankton in turbid waters have an evolutionary benefit to produce TEP to clear the water column to thus have more light.

2.3.6. Effects of dumping of dredged material

The findings of our study ask for an evaluation of the effect of dumping of dredged material as these activities may modify the physicochemical, biochemical, and biological properties of the ecosystem. The effects on the water column mainly involve an increase in SPM concentration, a change in organic matter composition and concentration, a change in the sediment structure and a release of pollutants, such as microplastics (Simmoni et al., 2005; Cesar et al., 2014; Laskar & Kumar, 2019; Fettweis et al., 2022).

Turbidity increase reduces the light available for photosynthesis and as such may affect phytoplankton growth and primary production. Our results show that with decreasing SPM concentration, the probability of a particle to be in the photic layer increases (Figure 2.5). Vice versa, high SPM concentrations, such as occurring in winter, decreases this probability. This suggests that water clarity is a limiting factor especially in winter when solar radiation is low. Phytoplankton starts to grow at the end of February, even under light limited conditions. Phytoplankton starts in April, when Phaeocystis cells grow exponentially. These cells are accumulating at the surface to avoid light limitation. After the bloom, the SPM concentration decreases, and the probability of being in the surface layer increases. The limiting factor for primary production is now nutrient rather than light availability. Further, differential settling of organic and mineral particles, results in a lower effect of water clarity on primary production than it would be if the composition of the SPM would not change as a function of concentration, see Figure 2.5 where Chla has always a similar or higher probability than SPM.

If the increase in turbidity and thus the decrease in probability of a particle to be in the photic zone due to dumping of dredged material is limited in space and time, it may have a small impact on turbid pelagic ecosystems. Further work needs to be done to understand this process better and the effect of increased turbidity on more offshore ecosystems where turbidity is lower, such as the dumping site B&W S1.

2.4. Conclusion

Our results show that the vertical enrichment of POM at the surface follows the same processes as along the horizontal nearshore-offshore gradient, i.e. differential settling of mineral vs organic rich particles, which is a fundamental property of SPM in turbid areas. Additionally, the seasonal variation in the composition of SPM between surface and bottom waters, peaking in summer, corresponds to notable differences in the quality of POM at these depths. This highlights the importance of sampling at surface and bottom, particularly for particulate parameters exhibiting vertical gradients, even in well-mixed waters like those observed in MOW1. While tidal currents primarily control the vertical gradients in SPM and Chl*a* concentrations, our observations reveal instances with higher Chl*a* concentrations near the surface compared to the bottom during the phytoplankton growing period, without a decrease in SPM concentrations. This suggests that Chl*a* concentrations can escape the influence of tidal currents during this period, possibly due to changes in phytoplankton dominance from floc-attached to free forms. Free phytoplankton cells during the growing period appear to spend more time in the photic zone due to differential settling, likely an adaptation to low irradiance conditions. In contrast, floc attachment is not as limiting in summer, where the probability of residing in the photic layer is high due to lower SPM concentrations. Our analysis of the mass of SPM within the photic layer, which remains conservative across months, suggests that the seasonally varying composition of

SPM (Chl*a*/SPM) plays a more significant role. This calls for looking in more detail at the strategies deployed by different types of phytoplankton to increase their buoyancy or associate with mineral particles.

3. Referenties

Agrawal YC, Pottsmith HC, 2000. Instruments for particle size and settling velocity observations in sediment transport. Marine Geology 168, 89-114.

Blauw AN, Benincà E, Laane RWPM, Greenwood N, Huisman J. 2012. Dancing with the tides: Fluctuations of coastal phytoplankton orchestrated by different oscillatory modes of the tidal cycle. PLoS ONE 7(11): e49319.

Bolam SG, Rees HL, Somerfield P, Smith R, Clarke KR, Warwick RM, Atkins M, Garnacho E.2006. Ecological consequences of dredged material disposal in the marine environment: a holistic assessment of activities around the England and Wales coastline. Marine Pollution Bulletin 52, 415-26.

Bouillon S, Connolly RM, Gillikin D.P. 2011. Use of stable isotopes to understand food webs and ecosystem functioning in estuaries. Treatise on estuarine and coastal science, 7.

Boyer JN, Kelble CR, Ortner PB., Rudnick DT. 2009. Phytoplankton bloom status: Chlorophyll a biomass as an indicator of water quality condition in the southern estuaries of Florida, USA. Ecological indicators, 9(6), S56-S67.

Cesar A, Lia LR, Pereira CD, Santos AR, Cortez FS, Choueri RB, De Orte MR, Rachid BR. 2014.Environmental assessment of dredged sediment in the major Latin American seaport (Santos, São Paulo—Brazil): An integrated approach. Science of the Total Environment 497, 679-87.

Cloern JE. 1987. Turbidity as a control on phytoplankton biomass and productivity in estuaries. Continental shelf research, 7, 1367-1381.

Deng Z, He Q, Chassagne C. Wang ZB. 2021. Seasonal variation of floc population influenced by the presence of algae in the Changjiang (Yangtze River) Estuary. Marine Geology 440, 106600.

Devlin MJ, Barry J, Mills DK, Gowen RJ, Foden J, Sivyer D, Tett P. 2008. Relationships between suspended particulate material, light attenuation and Secchi depth in UK marine waters. Estuarine, Coastal and Shelf Science, 79(3), 429-439.

Ehrhardt M, Koeve W. 1999. Determination of particulate organic carbon and nitrogen. In Grasshoff K, Kremling K, Ehrhardt M (Eds.), Methods of seawater analysis (3rd ed., pp. 437–444). Wiley.

Engel A, Endres S, Galgani L, Schartau M. 2020. Marvelous marine microgels: on the distribution and impact of gel-like particles in the oceanic water-column. Front. Mar. Sci. 7. doi:10.3389/FMARS.2020.00405/FULL

Falkowski PG, Greene RM, Geider RJ. 1992. Physiological limitations on phytoplankton productivity in the ocean. Oceanography 5(2), 84-91.

Fettweis M, Francken F, Pison V, Van den Eynde D. 2006. Suspended particulate matter dynamics and aggregate sizes in a high turbidity area. Marine Geology 235, 63-74. doi:10.1016/j.margeo.2006.10.005

Fettweis M, Baeye, M, Cardoso C, Dujardin A, Lauwaerts B, Van den Eynde D, Van Hoestenberghe T, Vanlede J, Van Poucke L, Velez C, Martens C. 2016. The impact of disposal of fine grained sediments from maintenance dredging works on SPM concentration and fluid mud in and outside the harbor of Zeebrugge. Ocean Dynamics 66, 1497–1516.

Fettweis M, Baeye M. 2015. Seasonal variation in concentration, size, and settling velocity of muddy marine flocs in the benthic boundary layer. Journal of Geophysical Research: Oceans 120, 5648-5667.

Fettweis M, Schartau M, Desmit X, Lee BJ, Terseleer N, Van der Zande D, Parmentier K, Riethmüller R. 2022. Organic matter composition of biomineral flocs and its influence on suspended particulate matter dynamics along a nearshore to offshore transect. Journal of Geophysical Research Biogeosciences, 126, e2021JG006332. doi:10.1029/2021JG006332

Franco MA, De Mesel I, Diallo MD, Van Der Gucht K, Van Gansbeke D, Van Rijswijk P, Costa MJ, Vincx M, Vanaverbeke J. 2007. Effect of phytoplankton bloom deposition on benthic bacterial communities in two contrasting sediments in the southern North Sea. Aquatic Microbial Ecology 48, 241-254..

Franco MA, Soetaert K, Van Oevelen D, Van Gansbeke D, Costa MJ, Vincx M, Vanaverbeke J. 2008. Density, vertical distribution and trophic responses of metazoan meiobenthos to phytoplankton deposition in contrasting sediment types. Marine Ecology Progress Series. 358: 51-62.

Fugate DC, Friedrichs CT. 2002. Determining concentration and fall velocity of estuarine particle populations using ADV, OBS and LISST. Continental Shelf Research, 22, 1867–1886

Hartmann NB, Hüffer T, Thompson RC, Hassellöv M, Verschoor A, Daugaard AE, Rist S, Karlsson T, Brennholt N, Cole M, Herrling MP, Hess MC, Ivleva NP, Lusher AL, Wagner M. 2019. Are we speaking the same language? Recommendations for a definition and categorization framework for plastic debris. Environmental Science and Technology 53, 1039-1047,

Hermes AL, Sikes EL. 2016. Particulate organic matter higher concentrations, terrestrial sources and losses in bottom waters of the turbidity maximum, Delaware Estuary, USA. Estuarine, Coastal and Shelf Science 180, 179-189.

Huisman J, Sharples J, Stroom JM, Visser PM, Kardinaal WEA, Verspagen JM, Sommeijer B. 2004. Changes in turbulent mixing shift competition for light between phytoplankton species. Ecology 85 2960-2970.

Jago CF, Kennaway GM, Novarino G, Jones SE. 2007. Size and settling velocity of suspended flocs during a Phaeocystis bloom in the tidally stirred Irish Sea, NW European shelf. Marine Ecology Progress Series, 345, 51-62.

Jakobsen HH, Markager S. 2016. Carbon-to-chlorophyll ratio for phytoplankton in temperate coastal waters: Seasonal patterns and relationship to nutrients. Limnology and Oceanography 61, 1853–1868

Jones SE, Jago CF, Bale AJ, Chapman D, Howland RJM, Jackson J. 1998. Aggregation and resuspension of suspended particulate matter at a seasonally stratified site in the southern North Sea: physical and biological controls. Continental Shelf Research 18, 1283-1309.

Lacroix G, Ruddick K, Ozer J, Lancelot C. 2004. Modelling the impact of the Scheldt and Rhine/Meuse plumes on the salinity distribution in Belgian waters (southern North Sea). Journal of Sea Research, 52, 149–163.

Laskar N, Kumar U. 2019. Plastics and microplastics: A threat to environment. Environ. Tech. Innov. 14, 100352.

Lauwaert B, Fettweis M, De Witte B, Van Hoei G, Timmermans S, Hermans L. 2019. Vooruitgangsrapport (juni 2019) over de effecten op het mariene milieu van baggerspeciestortingen (Vergunningsperiode 01/01/2017 – 31/12/2021). RBINS-ILVO-AMT-CD rapport. BL/2019/01, 28pp.

Lauwaert B, De Witte B, Festjens F, Fettweis M, Hermans L, Lesuisse A, Le H-M, Seghers S, Timmermans S, Vanavermaete D, Van Hoey G. 2021. Synthesis report on the effects of dredged material dumping on the marine environment (licensing period 2017-2021). RBINS-ILVO-AMT-AMCS-FHR report BL/2021/10, 67pp.

Lee BJ, Kim J, Hur J, Choi I-H, Toorman E, Fettweis M, Choi J.W. 2019. Seasonal dynamics of organic matter composition and its effects on suspended sediment flocculation in river water. Water Resources Research, 55, 6968-6985. doi:10.1029/2018WR024486

Liénart C, Savoye N, Bozec Y, Breton E, Conan P, David V, Feunteun E, Grangeré K, Kerhervé P, Lebreton B, Lefebvre S. 2017. Dynamics of particulate organic matter composition in coastal systems: A spatio-temporal study at multi-systems scale. Progress in Oceanography 156, 221-239.

Lorenzen CJ. 1967, December. Vertical distribution of chlorophyll and phaeo-pigments: Baja California. In Deep Sea Research and Oceanographic Abstracts, 14(6) 735-745).

Manheim, F.T., Hathaway, J.C. and Uchupi, E., 1972. Suspended matter in surface waters of the Northern Gulf of Mexico 1. *Limnology and Oceanography*, *17*(1), pp.17-27.

Martiny AC, Vrugt JA, Primeau FW, Lomas MW. 2013. Regional variation in the particulate organic carbon to nitrogen ratio in the surface ocean. Global Biogeochemical Cycles, 27, 723-731

McLaughlin MJ, Greenwood J, Branson P, Lourey MJ, Hanson CE. 2020. Evidence of phytoplankton light acclimation to periodic turbulent mixing along a tidally dominated tropical coastline. Journal of Geophysical Research Oceans, 125(11).

Muylaert K, Gonzales R, Franck M, Lionard M, Van der Zee C, Cattrijsse A, Sabbe K, Chou L, Vyverman W. 2006. Spatial variation in phytoplankton dynamics in the Belgian coastal zone of the North Sea studied by microscopy, HPLC-CHEMTAX and underway fluorescence recordings. Journal of Sea Research *55*(4): 253-265.

Petersen F, Hubbart JA. 2021. The occurrence and transport of microplastics: The state of the science. Science of the Total Environments 758, 143936.

Riebesell U. 1993. Aggregation of Phaeocystis during phytoplankton spring blooms in the southern North Sea. Marine Ecology Progress Series 96, 281-289.

Riebesell U. 1992. The formation of large marine snow and its sustained residence in surface waters. Limnology and Oceanography 37, 63-76.

Rousseau V, Leynaert A, Daoud N, Lancelot C. 2002. Diatom succession, silicification and silicic acid availability in Belgian coastal waters (Southern North Sea). Marine Ecology Progress Series 236, 61-73.

Rousseau V, Vaulot D, Casotti R, Cariou V, Lenz J, Gunkel J, Baumann M. 1994. The life cycle of Phaeocystis (Prymnesiophycaea): evidence and hypotheses. Journal of Marine Systems 5, 23-39.

Savoye N, Aminot A, Tréguer P, Fontugne M, Naulet N, Kérouel R. 2003. Dynamics of particulate organic matter $\delta^{15}N$ and $\delta^{13}C$ during spring phytoplankton blooms in a macrotidal ecosystem (Bay of Seine, France). Marine Ecology Progress Series 255, 27-41.

Schartau M, Riethmüller R, Flöser G, van Beusekom JEE, Krasemann H, Hofmeister R, Wirtz K. 2019. On the separation between inorganic and organic fractions of suspended matter in a marine coastal environment. Progress in Oceanography 171, 231–250.

Schneider B, Schlitzer R, Fischer G, Nöthig EM. 2003. Depth-dependent elemental compositions of particulate organic matter (POM) in the ocean. Global Biogeochemical Cycles, 17(2).

Shen X, Huo H, Zhang Y, Zhu Y, Fettweis M, Bi Q, Lee BJ, Maa JP-Y, Chen Q. 2023. Effects of organic matter on the aggregation of anthropogenic microplastic particles in turbulent environments. Water Research 232, 119706.

Simonini R, Ansaloni I, Cavallini F, Graziosi F, Iotti M, N'siala GM, Mauri M, Montanari G, Preti M, Prevedelli D. 2005. Effects of long-term dumping of harbor-dredged material on macrozoobenthos at four disposal sites along the Emilia-Romagna coast (Northern Adriatic Sea, Italy). Marine Pollution Bulletin 50, 1595-1605.

Sommerfield CK, Wong KC. 2011. Mechanisms of sediment flux and turbidity maintenance in the Delaware Estuary. Journal of Geophysical Research Oceans *116*(C1).

Steele JH, Yentsch CS. 1960. The vertical distribution of chlorophyll. Journal of the Marine Biological Association of the United Kingdom 39(2): 217-226.

Striebel M, Kallajoki L, Kunze C, Wollschläger J, Deininger A, Hillebrand H. 2023. Marine primary producers in a darker future: a meta-analysis of light effects on pelagic and benthic autotrophs. Oikos, 2023(4):09501.

Van Beusekom JE, Buschbaum C, Reise K. 2012. Wadden Sea tidal basins and the mediating role of the North Sea in ecological processes: scaling up of management?. *Ocean & coastal management*, *68*, 69-78.

Van Spaendonk JCM, Kromkamp JC, De Visscher PRM. 1993. Primary production of phytoplankton in a turbid coastal plain estuary, the Westerschelde (The Netherlands). Netherlands Journal of Sea Research 31(3):267-279.

Waldschläger K, Brückner MZ, Almroth BC, Hackney CR, Adyel TM, Alimi OS, Belontz SL, Cowger W, Doyle D, Grey A, Kane I, Kooi M, Kramer M, Lechthaler S, Michie L, Nordam T, Pohl F, Russell C, Thit A, Umar W, Valero D, Varrani A, Warrier AK, Woodall LC, Wu N. 2022. Learning from natural sediments to tackle microplastics challenges: a multidisciplinary perspective. Earth-Science Review 228, 104021.

Wheatland JA, Spencer KL, Droppo IG, Carr SJ, Bushby AJ. 2020. Development of novel 2D and 3D correlative microscopy to characterize the composition and multiscale structure of suspended sediment aggregates. Continental Shelf Research 200:104112.

Winterwerp JC. 2001. Stratification effects by cohesive and non-cohesive sediments. Journal of Geophysical Research Oceans 106, 22559-22574

Zhao C, Maerz J, Hofmeister R, Röttgers R, Wirtz K, Riethmüller R, Schrum C. 2019. Characterizing the vertical distribution of chlorophyll a in the German Bight. Continental Shelf Research 175: 127-146.

Zheng J, Li RJ, Qing FENG, Lu SS. 2013. Vertical profiles of fluid velocity and suspended sediment concentration in nearshore. International Journal of Sediment Research, 28, 406-412

COLOPHON

Dit rapport werd voorbereid door de BMM in maart 2024
Zijn referentiecode is MOMO/10/MF/202403/NL/AR/3

De scheepstijd met de RV Belgica werd voorzien door BELSPO en KBIN-OD Natuur

Indien u vragen hebt of bijkomende copies van dit document wenst te verkrijgen, gelieve een e-mail te zenden naar mfettweis@naturalsciences.be, met vermelding van de referentie, of te schrijven naar:

Koninklijk Belgisch Instituut voor Natuurwetenschappen
OD Natuur – BMM
t.a.v. Michael Fettweis
Vautierstraat 29
B–1000 Brussel
België
Tel: +32 2 627 41 83

BEHEERSEENHEID VAN HET
MATHEMATISCH MODEL VAN DE NOORDZEE

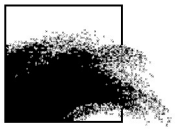

APPENDIX 1

Abstracts

INTERCOH, 18-22 September, Inha University, Incheon (South Korea)

17th International Conference on
Cohesive Sediment Transport Processes
September 18-22, 2023
Inha University, Incheon, Republic of Korea

Changes in suspended particle composition in the water column affect floc dynamics

M. Fettweis[1], L. Delhaye[1], B.J. Lee[2], R. Riethmüller[3], M. Schartau[4], S. Silori[1] and X. Desmit[1]

[1] Royal Belgian Institute of Natural Sciences, Rue Vautier 29, Brussels, Belgium, mfettweis@naturalsciences.be
[2] Department of Environmental and Safety Engineering, Kyungpook National University, Sangju, Korea
[3] Institute of Carbon Cycles, Helmholtz Centre hereon, Geesthacht, Germany
[4] GEOMAR Helmholtz Centre for Ocean Research, Kiel, Germany

1. Introduction

Suspended particulate matter (SPM) consist of solid particles (from clay to sand size), loose particles (biomineral flocs) and particulate organic matter (POM). The structure, composition and size of biomineral flocs variates along time scales from seconds to seasons, and along the cross-shore. Physical processes dominate particle dynamics at short time scales, while biological processes dominate at the seasonal scale. With distance from the coast the portion of terrestrial waters diminishes and the water depth generally increases. These changes generate and form coastal ocean specific hydrodynamic processes that influence the availability of mineral and organic matter of terrestrial origin and primary production and thus the size, composition and texture of biomineral flocs.

Mass concentration of flocs in suspension depends strongly on their density and size, controlled by the rate of inelastic collisions, which in turn depends on the turbulence, the SPM concentration and the particle stickiness (Winterwerp & van Kesteren, 2004). Flocs in the turbid nearshore are smaller, denser and consist mainly of settleable biomineral aggregates, while in the offshore flocs are larger, biomass-enriched and have lower densities (Fettweis et al., 2022). The increase of the POM content with decreasing SPM concentration is a characteristic feature and well described along the nearshore to offshore transect (Riebesell, 1991; Lai et al., 2018; Schartau et al., 2019).

2. Scope of the study

In this study we show that in the high turbid nearshore similar gradients also occur in the vertical, i.e. an organic enrichment of the SPM towards the surface layer, which is most prominent during slack waters. This means that size, composition and density of suspended particles vary with water depth. Although studies (e.g., Ho et al, 2022; Zhu et al., 2022) have revealed that minerals and microorganisms together can change the size and settling velocities of biomineral flocs through the occurrence of Transparent Exopolymer Particles (TEP), our data indicate that during slack water, when the flocs are largest and the settling highest, the organic enriched particles have a lower probability to settle than the biomineral flocs. In addition, also fine mineral particles (~2µm) during slack water escape the incorporation into flocs (see also Alber, 2000).

Our hypotheses are: 1) Two types of phytoplankton coexist: a floc-associated and a free one. The occurrence of free-phytoplankton is controlled by the primary production and thus the age

of a phytoplankton cell. A young phytoplankton cell would thus have a lower probability to be incorporated into a floc than an older one. 2) The fine mineral particles are non-cohesive and occur as wash load.

3. Results

We have used in situ data of SPM, Chlorophyll (Chl) and POM concentration together with particle size data measured by a LISST from 2012 till 2021 in a turbid station in the southern North Sea. The Chl data have been used as proxy measure for the occurrence of phytoplankton, while particulate organic carbon and nitrogen were used as indicator of POM. The data from the turbid nearshore reveal that:

1) In winter SPM and Chl concentration are well correlated (see Figure). We postulate that the phytoplankton is floc-incorporated and behaves similar as biomineral flocs, i.e. tide controlled resuspension and deposition. It occurs in a dormant stage, free phytoplankton is absent.

2) During the biological active period the correlation between SPM and Chl is less good and the probability density distribution of the Chl:SPM ratio is larger than in winter (see Figure). We postulate that only part of the phytoplankton is floc-associated, while the other part is free phytoplankton. The free phytoplankton has a higher probability to be in the euphotic layer than the floc-associated. The TEP produced during photosynthesis will increase the floc sizes. As larger flocs sink faster, they are removed from the water column on the long run. This results in a decrease of the mean SPM concentration to a minimum in summer. In the meantime, the probability of all phytoplankton to be in the photic layer will increase.

3) During slack water, when turbulence is small and the larger flocs have settled, the remaining SPM consist of very large (>250µm) and very small (<20µm) particles. Both do not or only very slowly settle and are interpreted as the free phytoplankton and fine-grained minerals (quartz, amorphous silica, carbonates) that have not collided with flocs or that have a low adhesiveness. These findings have also been found in low turbid offshore locations.

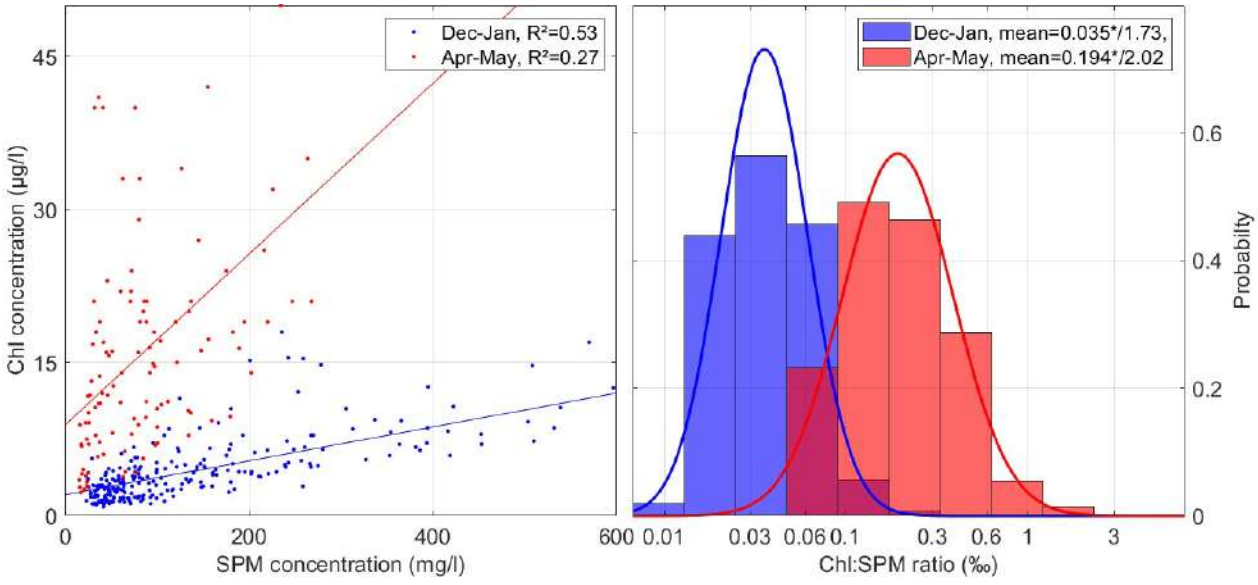

Correlation between winter and spring SPM and Chl concentration (left) and the probability density of the Chl:SPM ratio (right). Data are from 2012-2021.

4. Conclusions

The results underline that the composition of the SPM controls, together with concentration and turbulence, the flocculation of particles. The composition of the SPM changes with concentration, it is getting more organic when the concentration decreases, this occurs along a nearshore to offshore gradient but also along the vertical in the water column. Changes in composition are more pronounced in spring and summer than in winter. The results indicate the presence of mineral and organic particles that are incorporated in flocs and others that are not (free-phytoplankton and wash load). Flocculation models should take into account these heterogenous characteristics, by including non-settleable minerals and phytoplankton cells and by incorporating changes in composition of the SPM. The latter can be estimated with an empirical model that relates the POM content to the SPM concentration as proposed by Schartau et al. (2019) and Fettweis et al. (2022).

Acknowledgments
This research was supported by the Belgian Science Policy (BELSPO) within the BRAIN-be program (BG-PART and PiNS projects), the Maritime Access Division of the Flemish Ministry of Mobility and Public Works (MOMO project), and the RBINS BGCMonit program.

References

Alber, M. 2000. Settleable and Non-Settleable Suspended Sediments in the Ogeechee River Estuary, Georgia, U.S.A. Estuarine, Coastal and Shelf Science (2000) 50, 805–816

Fettweis, M., Schartau, M., Desmit, X., Lee, B.J., Terseleer, N., Van der Zande, D., Parmentier, K., Riethmüller, R. 2022. Organic matter composition of biomineral flocs and its influence on suspended particulate matter dynamics along a nearshore to offshore transect. Journal of Geophysical Research Biogeosciences, 126, e2021JG006332.

Ho, N.Q., Fettweis, M., Hur, J., Desmit, X., Kim, J.I., Jung, D.W., Lee, S.D., Lee, S., Choi, Y.Y., Lee, B.J. 2022. Flocculation kinetics and mechanisms of microalgae- and clay-containing suspension in different microalgae growth phases. Water Research 226, 119300.

Lai, H., Fang, H., Huang, L., He, G., Reible, D. 2018. A review on sediment bioflocculation: Dynamics, influencing factors and modeling. The Science of the Total Environment, 642, 1184–1200.

Riebesell, U., 1991. Particle aggregation during a diatom bloom. II. Biological aspects. Marine Ecolology Progres Series 69, 281–291.

Schartau, M., Riethmuller, R., Flöser, G., van Beusekom, J.E E., Krasemann, H., Hofmeister, R., Wirtz, K. 2019. On the separation between inorganic and organic fractions of suspended matter in a marine coastal environment. Progress in Oceanography, 171, 231–250.

Winterwerp, J.C., van Kesteren, W.G.M. 2004. Introduction to the Physics of Cohesive Sediment in the Marine Environment. Elsevier.

Zhu, Y., Lin, M., Shen, X., Fettweis, M., Zhang, Y., Zhang, J., Bi, Q., Lee, B.J., Maa, J.P.-Y., Chen, Q. 2022. Biomineral flocculation of kaolinite and microalgae: Laboratory experiments and stochastic modeling. Journal of Geophysical Research: Oceans, 127, e2022JC018591.

17th International Conference on
Cohesive Sediment Transport Processes
September 18-22, 2023
Inha University, Incheon, Republic of Korea

The potential of cohesive sediment and diverse microalgae to flocculate in demanding growth conditions.

Que Nguyen Ho[1,2], Michael Fettweis[3], Jin Hur[4], Sang Deuk Lee[5], and Byung Joon Lee[1,6*]

[1] Energy Environment Institute, Kyungpook National University, 2559 Gyeongsang-daero, Sangju, Gyeongbuk 37224, Korea
[2] Faculty of Environment and Labour Safety, Ton Duc Thang University, Ho Chi Minh City, Vietnam
[3] Operational Directorate Natural Environment, Royal Belgian Institute of Natural Sciences, Rue Vautier 29, B-1000 Bruxelles, Belgium
[4] Department of Environment & Energy, Sejong University, Seoul 05006, South Korea.
[5] Nakdonggang National Institute of Biological Resources (NNIBR), Sangju, Gyeongsangbuk-do 37242, South Korea
[6] Department of Advanced Science and Technology Convergence, Kyungpook National University, 2559 Gyeongsang-daero, Sangju, Gyeongbuk 37224, Korea, bjlee@knu.ac.kr

This study investigates the flocculation potential of *Microcystic* and *Chlorella vulgaris* microalgae in low nutrient concentrations, using a standard jar test experiment. Biopolymer and humic substance (HS) concentrations were found to control flocculation potential, with different kinetic patterns observed for each microalgae in the presence of clay suspension particles. The findings suggest that appropriate concentrations of biopolymers can enhance floc-to-floc collision and attachment, but excessive amounts can lead to stabilization due to steric effects. Overall, this study offers insights into the fate of suspended particulate matter in aquatic environments. The flocculation kinetics of *Microcystic* and *Chlorella vulgaris* microalgae with clay suspension can be explained in Figure 1. The flocculation potential of both *Microcystic* and *Chlorella vulgaris* microalgae was observed to begin during the exponential phase due to an increase in cell numbers and secretion of biopolymers, such as extracellular polymeric substances/transparent exopolymer particles (Naveed S et al., 2019) . The production of biopolymers by microalgae was found to increase with time as nitrogen content became depleted (Babiak W et al., 2021). This led to an increase in the flocculation potential of *Chlorella vulgaris* with incubation time, whereas for *Microcystic*, an adequate concentration of biopolymers during the exponential, stationary, and early death phases was necessary for the development of large flocs (Avnimelech Y et al., 1982; Ho QN et al., 2022). However, excessive amounts of biopolymers and humic substances in the final death phase did not significantly change the volumetric faction of flocculi and flocs, as it may simultaneously encourage flocculation and stability. The accumulation of biopolymer and humic substances may enhance stabilization due to steric effects, which can decrease attachment between flocs. At the equilibrium stage, an excess of organic matter concentration may enhance flocculation up to a particular size, after which the build-up of biopolymers and humic substances may cover flocs, leading to enhanced steric stability and decreased attachment between flocs (Ho QN et al., 2022).

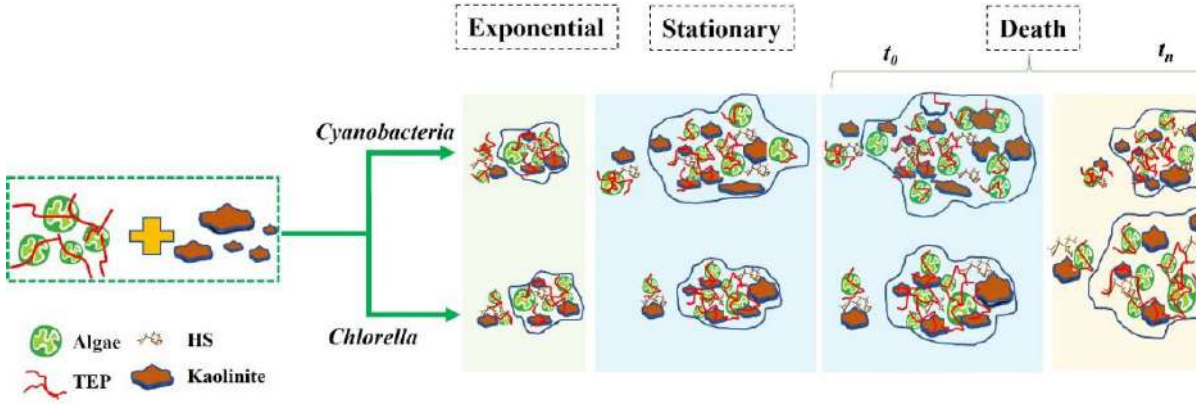

Figure 1. The general model conception of the varying flocculation kinetics of *Microcystic* and *Chlorella vulgaris* with clay-suspended particles is presented in a schematic diagram.

Acknowledgment
This work was supported by the National Research Foundation of Korea (Grant No. NRF-2020R1I1A3A04036895) and the Nakdonggang National Institute of Biological Resources (Grant No. NNIBR-202302104).

References
Naveed S, Li C, Lu X, Chen S, Yin B, Zhang C, Ge Y: Microalgal extracellular polymeric substances and their interactions with metal (loid) s: A review. Critical Reviews in Environmental Science and Technology 2019, 49(19):1769-1802.
Babiak W, Krzemińska I: Extracellular polymeric substances (EPS) as microalgal bioproducts: A review of factors affecting EPS synthesis and application in flocculation processes. Energies 2021, 14(13):4007.
Avnimelech Y, Troeger BW, Reed LW: Mutual flocculation of algae and clay: evidence and implications. Science 1982, 216(4541):63-65.
Ho QN, Fettweis M, Hur J, Desmit X, Kim JI, Jung DW, Lee SD, Lee S, Choi YY, Lee BJ: Flocculation kinetics and mechanisms of microalgae-and clay-containing suspensions in different microalgal growth phases. Water Research 2022:119300.

17th International Conference on
Cohesive Sediment Transport Processes
September 18-22, 2023
Inha University, Incheon, Republic of Korea

Application of an 1-DV TCPBE model with Bayesian calibration to diagnose the flocculation potential in the laboratory experiments and field measurement

T. T. Huynh[1], Michael Fettweis[2], Byung Joon Lee[1]

[1] Department of Advanced Sciences and Technology Convergence, KNU, Sangju 37224, Korea
[2] Royal Belgian Institute of Natural Sciences, Rue Vautier 29, 1000 Brussels, Belgium

Abstract
In the aquatic environment, flocculation plays an important role in determining the size, sellting velocity and deposition rate of the cohesive sediment. The aggregation and breakage of the particles under turbulent flow field regulates the deposition process. This paper describes a Two-Class Population Balance Equation (TCPBE) in couple with the Reynold-averaged Navier Stokes based 1-Dimention Verticlal (1-DV) model to diagnose the flocculation potential in both laboratory experiments and in-situ measurement. The Bayesian analysis is utilized as the calibration tool which examines the unknown posterior parameters, model uncertanties compared with the experimental and field observation data. Results show that, the 1-DV TCPBE with the effect of k-ε turbulent closure and mass balance equation is capable to simulate the bimodal flocculation of the marine and estuarine sediment. In addition, the simplified model also showed its capability on the implementing of the large-scale multimodal flocculation in the flow field of estuary and marine area.

Keywords: *Cohesive sediment, Flocculation, Population Balance Equation, Reynolds-averaged Navier-Stokes.*

The govern equations

The Reynold-averaged Navier Stokes based 1-Dimention Verticlal (1-DV) and Two-Class Population Balance (TCPBE) equation.

$$\frac{\partial N_i}{\partial t} = \frac{\partial}{\partial z}\left(C'_\mu \frac{k^2}{\varepsilon}\frac{\partial N_i}{\partial z}\right) - w_{s,i}\frac{\partial N_i}{\partial z} + (A_i + B_i) \tag{1}$$

$$(A_P + B_P) = \frac{dN_P}{dt} = -\frac{1}{2}\alpha\beta_{PP}N_P N_P\left(\frac{N_C}{N_C - 1}\right) - \alpha\beta_{PF}N_P N_F + fN_C a_F N_F$$

$$(A_F + B_F) = \frac{dN_F}{dt} = +\frac{1}{2}\alpha\beta_{PP}N_P N_P\left(\frac{1}{N_C - 1}\right) - \frac{1}{2}\alpha\beta_{FF}N_F N_F + a_F N_F \tag{2}$$

$$(A_T + B_T) = \frac{dN_T}{dt} = +\frac{1}{2}\alpha\beta_{PP}N_P N_P\left(\frac{N_C}{N_C - 1}\right) + \alpha\beta_{PF}N_P N_F - fN_C a_F N_F$$

Preliminary results

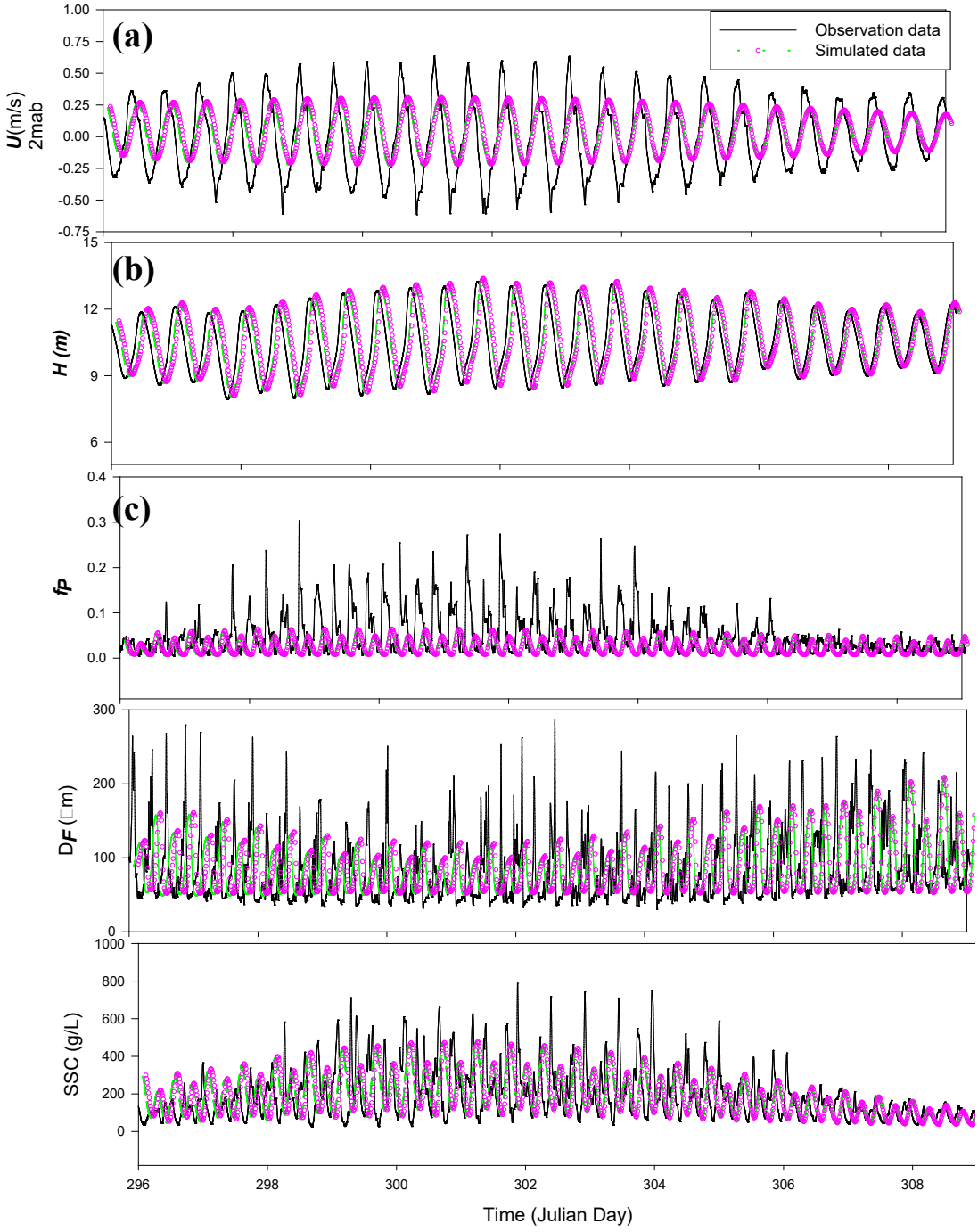

Figure 1. Time series of the measured and simulated results (a) bottom shear velocity U_{2mab}; (b) water depth H; (c) flocculi mass fraction f_P; (d) volume mean floc diameter D_F; (e) Suspended solid concentration SSC.

Acknowledgement

This work was supported by the National Research Foundation of Korea (Grant No. NRF-2020R1I1A3A04036895).

17th International Conference on
Cohesive Sediment Transport Processes
September 18-22, 2023
Inha University, Incheon, Republic of Korea

ISOLATION AND CHARACTERIZATION OF THE MOLECULAR COMPOSITION OF ALGAL DISSOLVED ORGANIC MATTER

Thi Thuy Trang Pham [1], Que Nguyen Ho[1], Sang Deuk Lee[2], Michael Fettweis[3], and B.J. Lee[1]

[1]Department of Advanced Sciences and Technology Convergence, KNU, Sangju 37224, Korea
[2] Nakdonggang National Institute of Biological Resources (NNIBR), Sangju 37242, Korea
[3] Royal Belgian Institute of Natural Sciences, Rue Vautier 29, 1000 Brussels, Belgium

Abstract

In the aquatic environment, dissolved organic matter (OM) can increase either flocculation or stabilization of suspended particulate matter (SPM) (Lee BJ, 2019; Lee Byung Joon, 2017). Colloidal stabilization and flocculation of SPM in a water environment depend on the chemical/molecular composition of DOM. Cell exudates of microalgae are one of the primary sources of DOM. Extracellularly released DOM from microalgae consists of various chemical/molecular components (Findlay Stuart, 2003; Huangfu Xiaoliu, 2013; Qualls, 2013). DOM has been known as critical in controlling the global carbon cycle and the fate and transport of chemical pollutants (Huangfu Xiaoliu, 2013; Wilkinson Kevin J, 1997; Xu Huacheng, 2016). Despite its importance, the chemical/molecular composition of DOM and its roles in SPM flocculation and stabilization are still largely unknown. This study focuses on identification and characterization of the key DOM components, including polysaccharides and Humic substances, which mainly affect the flocculation and stabilization of SPM. The chemical/molecular composition of algal DOM was isolated and quantified by using Nuclear Magnetic Resonate (NMR), Fluorescence Excitation Emission Matrices (FE-EM), and Liquid Chromatography – Organic Carbon Detection (LC-OCD) techniques. In association with laboratory and field studies on SPM behaviours (i.e., flocculation and stabilization), these analytical techniques on the DOM composition will help us to understand the fundamental mechanisms of the biological and physicochemical processes in the aquatic environment containing various DOM and SPM.

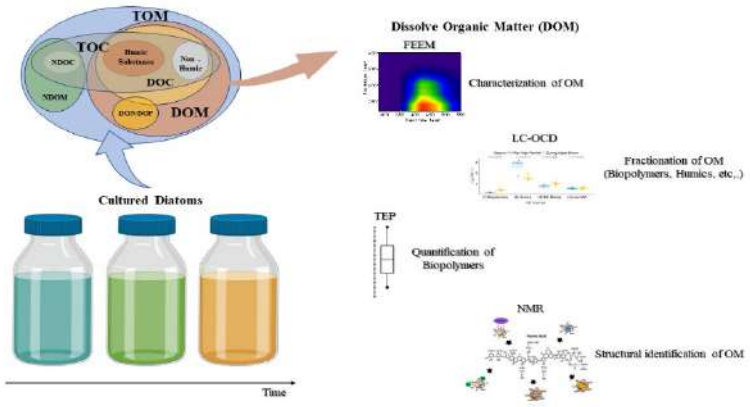

Figure 1. Schematic diagram of the analytical techniques for measuring the chemical/molecular composition of algal dissolved organic matter: Nuclear Magnetic Resonate (NMR),

Fluorescence Excitation Emission Matrices (FE-EM), and Liquid Chromatography – Organic Carbon Detection (LC-OCD) techniques.

Acknowledgement
This work was supported by the National Research Foundation of Korea (Grant No. NRF-2020R1I1A3A04036895) and Nakdonggang National Institute of Biological Resources (Grant No. NNIBR-202302104).

References
Findlay Stuart, Sinsabaugh Robert L. (2003). Aquatic ecosystems: interactivity of dissolved organic matter: Academic press.
Huangfu Xiaoliu, Jiang Jin, Ma Jun, Liu Yongze, Yang Jing. (2013). Aggregation kinetics of manganese dioxide colloids in aqueous solution: influence of humic substances and biomacromolecules. Environmental science & technology, 47(18), 10285-10292.
Lee BJ, Kim J, Hur J, Choi IH, Toorman EA, Fettweis M, Choi JW. (2019). Seasonal dynamics of organic matter composition and its effects on suspended sediment flocculation in river water. Water Resources Research, 55(8), 6968-6985.
Lee Byung Joon, Hur Jin, Toorman Erik A. (2017). Seasonal variation in flocculation potential of river water: Roles of the organic matter pool. Water, 9(5), 335.
Qualls, Robert G. (2013). Dissolved organic matter. Methods in biogeochemistry of wetlands, 10, 317-329.
Wilkinson Kevin J, Negre J-C, Buffle Jacques. (1997). Coagulation of colloidal material in surface waters: the role of natural organic matter. Journal of Contaminant Hydrology, 26(1-4), 229-243.
Xu Huacheng, Yang Changming, Jiang Helong. (2016). Aggregation kinetics of inorganic colloids in eutrophic shallow lakes: influence of cyanobacterial extracellular polymeric substances and electrolyte cations. Water Research, 106, 344-351.

17th International Conference on
Cohesive Sediment Transport Processes
September 18-22, 2023
Inha University, Incheon, Republic of Korea

Application of sediment composition index to predict suspended particulate matter concentration in the North Sea

D. Tran[1], X. Desmit[1], R. Verney[2] and M. Fettweis[1]

[1] Royal Belgian Institute of Natural Sciences, OD Nature, Brussels, Belgium,
dtran@naturalsciences.be
[2] IFREMER, Laboratoire DHYSED, Plouzané, France

1. Introduction

A proper understanding of sediment transport is extremely important in many areas of engineering and socio-economic development. On the time scale of months to years, the knowledge of where sediment accumulates could save billions of dollars on annual port dredging and beach nourishment. On length scales of deltas, estuaries and coastal zones, such knowledge plays a crucial role for decision makers to govern the development of a country or region. Nevertheless, in sand-mud environments, quantifying the variability of suspended particulate matter concentration (SPMC) and their constituents is essential but highly challenging. To better quantify the ratio of sand/mud in suspension, we previously defined a sediment composition index, such as

$$SCI = 10log_{10}(OBS) - SNR \quad (1)$$

Where OBS is the signal measured by an optical backscatter sensor (in NTU) and SNR is the signal measured by an acoustic sensor (in dB) (Pearson et al 2021, Tran et al 2021). In this study, we propose a novel method of applying SCI to predict long-term, high-frequency SPMCs of the North Sea without the need of conducting sensor calibrations.

2. Approach

This study used data collected at station MOW1, situated about 3 km offshore of Zeebrugge, Belgium. Overall, data at MOW1 consists of hourly water samples, particle size distributions, turbidity, hydrodynamic conditions and chlorophyll concentration for the year 2013 during 125 tidal cycles, providing one of the most comprehensive field data sets in the North Sea. Figure 1 shows three steps in applying the SCI method to obtain SPMC from raw signals of OBS (Optical Backscatter Sensor) and ADV (Acoustic Doppler Velocimetry). First, the data was divided into 20 bins, i.e., 0-100, corresponding to the ratio of sand/mud in suspension and OBS and ADV signals (Fig.1 left). Second, the relationship between SCI and bins was plotted (Fig.1 right and Eq.1) to obtain mathematical functions for each mooring during 2013. More specifically, this step provides the relationships between 1) OBS and ADV and the ratio of sand/mud (Fig.1 left), 2) SPMC and raw ADV signal (not shown), and 3) SPMC and raw OBS signal (not shown). The function obtained from Mooring 59 (Jan 24th – Mar 7th, 2013) was chosen to apply for the entire year because it covered almost all ratios of sand/mud that occurred during the year. Last, raw data of OBS and ADV from different moorings were

applied to the functions derived in the previous step to compute the SPMC of the year 2013 and potentially of any other years at the same station.

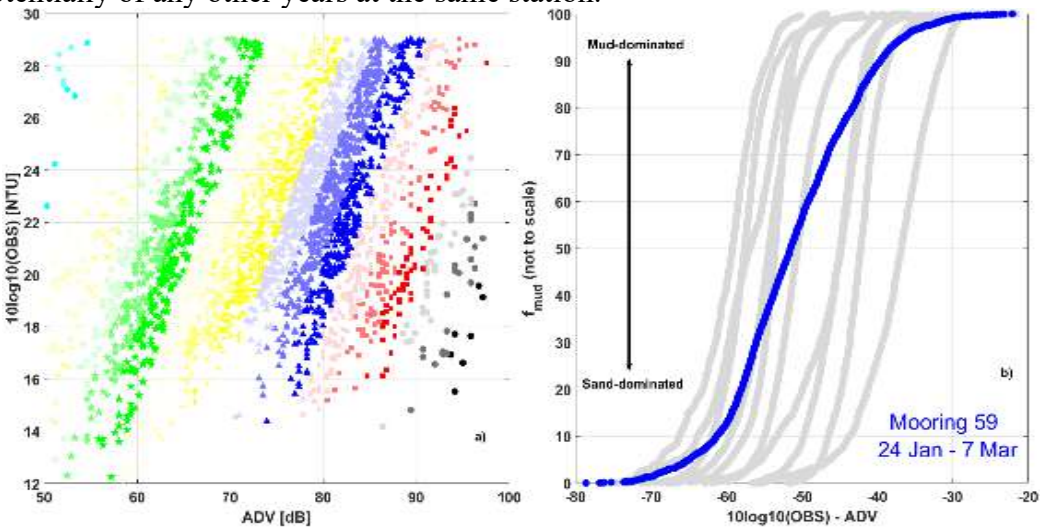

Figure 1. Left: field data illustrates a log-linear relationship between raw OBS and ADV signals of different bins. Right: data from each mooring was divided into 20 bins to derive a mathematical function, describing ratio of sand/mud in suspension as a function of raw OBS and ADV signals.

3. Results and conclusions

Overall, the application of the SCI method provided good predictions of SPMC from raw signals of OBS and ADV (Fig.2). It is worth mentioning that the range of concentration is from 0 – 3 g/L and there is no prior knowledge of particle size distributions and ratios of sand/mud of the suspension. There are two moorings at which the errors were greater than 100 mg/L, i.e., mooring 60 and 73. We noticed a relatively strong correlation between the activities of plankton, represented by the time series of Chlorophyll concentrations (Fig.2 right axis), and the performance of the SCI functions. For example, the Chlorophyll concentrations boosted up during mooring 60 to mooring 62 which might result in a significant error during mooring 60. Similarly, the rapid reduction in Chl concentration from mid-September might also cause the overestimation of concentration for mooring 73. Whereas, other moorings with or without plankton activities do not essentially influence the prediction of SCI functions as long as the Chl concentration is stable. One possible explanation is that under the blooming condition the relationship between OBS and ADV might not be log-linear anymore, or at least at a very different scale in comparison to no blooming. It is noted that in Figure 2, the time in Chl concentrations “timeseries”, i.e., orange stars markers, was relatively scaled to match with the time of each mooring.

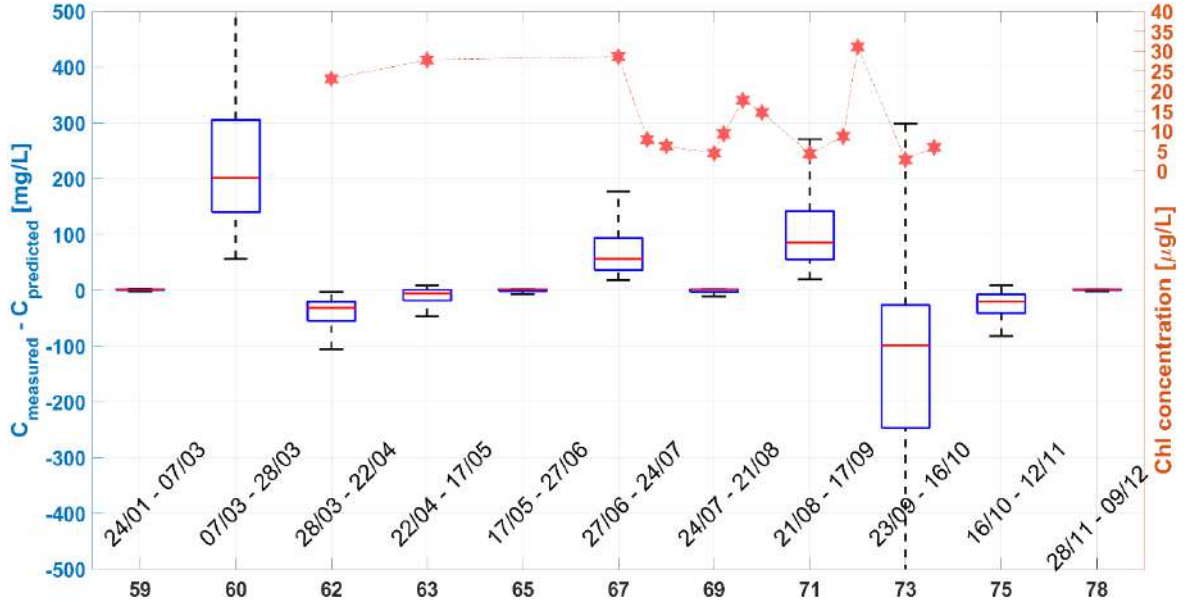

Figure 2. Concentration differences when applying SCI function from Mooring 59 for all the other moorings in the same year. Functions derived from other moorings can also be applied with similar procedure. However, functions obtained from mooring 59 provided the most accurate estimation.

In conclusion, results show that it is possible to develop SCI functions for, at least, a year from a small subset of field data. Such SCI functions then can be applied for the rest of the year in order to predict SPMC without any further requirements of particle size distribution and/or water sample calibrations. Nonetheless, during blooming period a correction coefficient is needed to account for the impact of plankton activities on the behaviours of the OBS and ADV sensors. In the future, we will apply this method for longer historical data and also conduct further investigation on the impact of plankton on the performance of optical and acoustic sensors.

Acknowledgments

This work is part of the research program "PiNS: Particle in the North Sea" funded by Belgian Science Policy and "EU_Sed" funded by Marie Sklodowska-Curie Postdoctoral Fellowship (No 101067047).

References

Pearson, S., Verney, R., Prooijen, B., Tran, D., Hendriks, E., Jacquet, M., and Wang, Z., (2021). Characterizing the composition of sand and mud suspensions in coastal and estuarine environments using combined optical and acoustic measurements. JGR: Ocean. 126(7), e2021JC017354.

Tran, D., Pearson, S.G., Jacquet, M., Verney, R. (2021) Investigating suspended particulate matters from multi-wavelength optical and multi-frequency acoustic measurements. *vEGU 2021.*

APPENDIX 1

Desmit X, Schartau M, Terseleer N, Van der Zande D, Riethmüller R, Fettweis M. 2024. The transition between coastal and offshore areas in the North Sea unraveled by the suspended particle composition. Science of the Total Environment 915, 169966

Science of the Total Environment 915 (2024) 169966

Contents lists available at ScienceDirect

Science of the Total Environment

journal homepage: www.elsevier.com/locate/scitotenv

Research Paper

The transition between coastal and offshore areas in the North Sea unraveled by suspended particle composition

Xavier Desmit [a,*], Markus Schartau [b], Rolf Riethmüller [c], Nathan Terseleer [a], Dimitry Van der Zande [a], Michael Fettweis [a]

[a] OD Natural Environment, Royal Belgian Institute of Natural Sciences, Vautier Street 29, 1000 Brussels, Belgium
[b] GEOMAR Helmholtz Centre for Ocean Research Kiel, Wischhofstr. 1-3 D-24148 Kiel, Germany
[c] Institute of Coastal Ocean Dynamics, Helmholtz-Zentrum Hereon, Max-Planck-Str. 1, 21502 Geesthacht, Germany

HIGHLIGHTS

- SPM concentration and organic fractions are analyzed in coastal-offshore gradients
- Diagnostic model of SPM allows separating fresh, labile from less reactive PON
- Analysis of PON fractions reveals a characteristic area, the transition zone
- There, particle settling is enhanced, fostering their transport back to the coast, which controls the fate of organic matter
- The transition zone is generally confined to water depths below 20 m

GRAPHICAL ABSTRACT

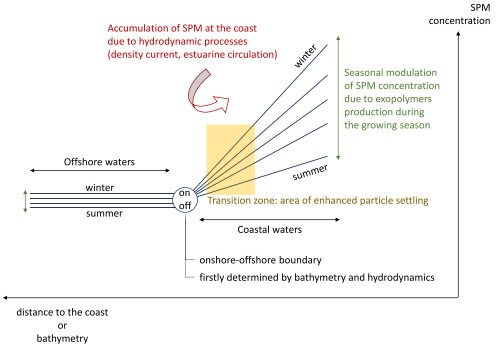

ARTICLE INFO

Editor: Daniel Alessi

Keywords:
Suspended particulate matter (SPM)
Particulate organic nitrogen (PON)
Particle dynamics
Particle composition
Coastal-offshore gradient
North Sea

ABSTRACT

Identifying the mechanisms that contribute to the variability of suspended particulate matter concentrations in coastal areas is important but difficult, especially due to the complexity of physical and biogeochemical interactions involved. Our study addresses this complexity and investigates changes in the horizontal spread and composition of particles, focusing on cross-coastal gradients in the southern North Sea and the English Channel. A semi-empirical model is applied on in situ data of SPM and its organic fraction to resolve the relationship between organic and inorganic suspended particles. The derived equations are applied onto remote sensing products of SPM concentration, which provide monthly synoptic maps of particulate organic matter concentrations (here, particulate organic nitrogen) at the surface together with their labile and less reactive fractions. Comparing these fractions of particulate organic matter reveals their characteristic features along the coastal-offshore gradient, with an area of increased settling rate for particles generally observed between 5 and 30 km from the coast. We identify this area as the transition zone between coastal and offshore waters with respect to particle dynamics. Presumably, in that area, the turbulence range and particle composition favor particle settling, while hydrodynamic processes tend to transport particles of the seabed back towards the coast. Bathymetry plays an important role in controlling the range of turbulent dissipation energy values in the water column, and we observe that the transition zone in the southern North Sea is generally confined to water depths

* Corresponding author.
E-mail address: xdesmit@naturalsciences.be (X. Desmit).

https://doi.org/10.1016/j.scitotenv.2024.169966
Received 11 November 2023; Received in revised form 15 December 2023; Accepted 4 January 2024
Available online 10 January 2024
0048-9697/© 2024 The Authors. Published by Elsevier B.V. This is an open access article under the CC BY-NC-ND license (http://creativecommons.org/licenses/by-nc-nd/4.0/).

below 20 m. Seasonal variations in suspended particle dynamics are linked to biological processes enhancing particle flocculation, which do not affect the location of the transition zone. We identify the criteria that allow a transition zone and discuss the cases where it is not observed in the domain. The impact of these particle dynamics on coastal carbon storage and export is discussed.

1. Introduction

The dynamic nature of shelf regions is responsible for strongly fluctuating concentration patterns of suspended particulate matter (SPM). This variability is particularly pronounced within nearshore areas where fine-grained sediments are abundant. The SPM dynamics are controlled by a combination of physical and biological processes and particle characteristics (Eisma, 1986; Moulton et al., 2023). Also, SPM in a turbulent flow field is further subject to flocculation, which by changing size and excess density of the particles affect the settling velocity (e.g. Eisma, 1986). These dynamics not only depend on the concentration but also on the composition of the SPM, considering the mineral and particulate organic matter (POM) constituents (Dyer, 1989; Maggi and Tang, 2015; Maerz et al., 2016; Blattmann et al., 2019).

Despite the extensive variations in SPM concentration (SPMC), a typical feature is the persistence of a horizontal cross-shore gradient, with higher SPMCs in the shallow coastal waters and lower concentrations offshore. This cross-shore gradient in SPMC is associated with a higher POM content of SPM offshore, in contrast to a lower content found inshore (e.g. Eisma and Kalf, 1987; Jago et al., 1994). For the southern North Sea, with its tidal flats in the Wadden Sea, Postma (1984) stressed the importance of tidal asymmetries and particle trapping by density circulation and proposed the concept of a 'line of no return' located at some distance from the coast. This line would represent a boundary away from the coast beyond which any cross-transport of SPM towards the coast becomes improbable. As a consequence, POM produced nearshore tends to be processed within the coastal area and POM produced beyond the line tends to remain offshore. A nearshore utilisation and recycling of organic compounds is known to be significant when quantifying the fate of nutrient inputs from land (e.g. Asmala et al., 2017). In this perspective, only dissolved compounds (nutrients and dissolved organic matter) are exchanged across the line, which in turn may promote POM production further offshore.

From another perspective, the line of no return can be interpreted as the outer limit of a transition zone between coastal and offshore areas, which depends on the width of a surf zone of a specific depth range. Within a transition zone the aggregated particles or flocs may also exhibit maxima in sinking velocity (Maerz et al., 2016). Likewise, such a transition zone can be associated with comparable concentrations of fresh and mineral-associated POM (Schartau et al., 2019; Fettweis et al., 2022), and it may also reveal significant changes in phytoplankton order richness (Jung et al., 2017). One might thus assume that the cross-shore distribution of SPM relies, at least partially, on different hydrodynamic conditions. Moulton et al. (2023) propose that the inner shelf be the area where turbulent surface and bottom boundary layers overlap. From that perspective, the end of such overlapping could mark the transition between coastal and offshore waters, and we may expect that it affects SPM dynamics. The definition of Moulton et al. (2023), however, does not seem sufficient for some parts of the southern North Sea. For instance, the Belgian waters exhibit a cross-shore gradient in SPMC, salinity and bathymetry, while the water column remains entirely mixed in the vertical throughout the year (van Leeuwen et al., 2015). Besides, the nearshore area of the German Bight and the Seine Bay exhibit stratification due to freshwater input mainly, that weakens towards the offshore as the river plume is getting diluted by sea water (Becker et al., 1992; Brenon and Le Hir, 1999). The occurrence of salinity gradients in the nearshore results in tidal straining, which leads to a near-bottom residual current towards the coast (e.g. Simpson et al., 1990; Becherer et al., 2016; Du et al., 2022). This partially explains the persistent cross-shore gradients in SPMC found in many nearshore areas (Maerz et al., 2016). The above examples suggest that the cross-shore gradient in SPMC may occur independently of the existence of a separation between surface and bottom turbulent layers. It therefore stands to reason that there are specific sedimentological and biogeochemical processes that lead to a particular distribution in the concentration and composition of SPM, in turn influencing the transport of particles. These processes and fluxes may remain hidden or overlooked in a pure analysis of the physical conditions.

In this paper, we aim at inferring information about the transition from nearshore to offshore waters by analyzing spatio-temporal variations in the concentration and composition of SPM. We hypothesize that by disaggregating changes in the amount and composition of SPM over time and space, we can better distinguish between nearshore waters, where particles are controlled primarily by turbulence, resuspension, flocculation and deposition, and offshore regions, where variations in SPMC and composition are significantly controlled by the production and decay of plankton and detritus in the water column. Our approach applies a semi-empirical model onto field data of SPM and POM concentration from the Belgian shelf to extract POM properties (such as fresh and mineral-associated POM) along their cross-shore gradient. The model equations are then applied to remote sensing derived SPMC at the surface of the southern North Sea and the English Channel to derive the POM properties in a larger domain.

2. Methods

2.1. In situ and remote sensing data

2.1.1. In situ data

The in situ data of SPM and Particulate Organic Nitrogen (PON) concentrations have been collected between October 2004 and August 2022 on the Belgian shelf. The data set consists of hourly, 1.5 hourly or 2 hourly water samples collected during 243 tidal cycles or half tidal cycles in 12 stations, 3 of them being more sampled: one located in the nearshore coastal turbidity maximum area (MOW1, water depth about 10 m), one along the outer margin of the coastal turbidity maximum (W05; transition zone; water depth about 20 m), and the third one in the offshore area under complete Channel water influence (W08, water depth about 25 m). The amount of SPM-PON data pairs is equal to 2539. These pairs are well distributed over each month, with slightly less data in summer and autumn than winter and spring.

At every sampling occasion, three subsamples for SPMC were taken and filtered on board using pre-combusted (405 °C, 24 h), rinsed, dried for 24 h at 105 °C and pre-weighted 47 mm GF/C filters. After sampling the filters were rinsed with ultrapure water (resistivity 18.2 MΩ/cm normalized at 25 °C) and immediately stored at −20 °C, before being dried during 24 h at 50 °C and weighted to obtain the concentration. The uncertainty (expressed as the RMSE of the triplicates divided by the mean value) decreases with increasing concentration from 8.5 % (SPMC <5 mg l^{-1}) to 6.7 % (<10 mg l^{-1}), 3.5 % (10–50 mg l^{-1}) and 2.1 % (>100 mg l^{-1}) and represent the random error related to the lack of precision during filtrations. Especially in clearer water, systematic errors due to the offset by salt or other errors become much larger than the random errors (Neukermans et al., 2012). These are not included, and have been estimated based on Stavn et al. (2009) and Röttgers et al. (2014) as 1 mg l^{-1}. The samples for PON were filtered on board using 25 mm GF/C filters (pretreated as above for SPM), stored immediately at −20 °C, before being analyzed using a Thermo Finnigan Flash EA1112

elemental analyzer (for details see Ehrhardt and Koeve, 1999). The analytical uncertainty for PON is 18 % augmented with the uncertainty of the SPMC due to filtration.

2.1.2. Satellite data of SPMC

The satellite-based SPMC was generated using the Nechad et al. (2009, 2010) algorithm applied to the standard Sentinel-3/OLCI remote sensing reflectance product (RRS) provided by the EUMETSAT water processor (PB 2.00, https://earth.esa.int/eogateway/documents/20142/1564943/Sentinel-3-OLCI-Marine-User-Handbook.pdf) after applying recommended quality flags (LAND, CLOUD, CLOUD_AMBIGUOUS, CLOUD_MARGIN, AC_FAIL). While a single band can be used for SPMC estimation the optimal band depends on SPMC. If RRS is too low (e.g. for longer wavelengths in low SPMC waters) then SPMC estimation will be significantly affected by noise or errors in RRS, if it is too high (e.g. for shorter wavelengths in high SPMC waters) then the saturation phenomenon means that RRS becomes insensitive to changes in SPMC. This has led to the development of "switching single band algorithms" (Novoa et al., 2017) using the basic single band formulation of (Nechad et al., 2010) but with different wavelengths used at different SPMC and typically a smooth weighting between two adjacent spectral bands to avoid image artifacts. The Novoa et al. (2017) approach is applied to the SPMC products providing a multi-band SPMC product using two bands (red: 665 nm and near-infrared: 865 nm). Daily images of surface SPMC in the period 2017–2021 were extracted in the North Sea (lon [−4 10], lat [48 59]) with a spatial resolution of 1 km × 1 km. Daily images were then averaged to get monthly images over the same period, and data were extracted along the different transects of the study (Fig. 1).

2.2. Regional domain

The studied domain is the southern North Sea and the English Channel, with a focus on the German Bight, the Thames and East Anglia plume, the Southern Bight and the Seine Bay. The bathymetry in the domain and along four specific transects ('GE', 'UKNL', 'UKBE', 'FR') is shown in Fig. 1. The bathymetry data are gridded on a 15 arc-second geographic latitude and longitude grid, that is, any grid cell size is ~450 m on the latitude axis and ~280 m on the longitude axis (source: GEBCO 2022 Grid; see Acknowledgments). Bathymetry along the transects was smoothed with a LOESS function (span = 0.2) in MATLAB R2019a© to facilitate further interpretation.

The tides in the study area are principally semidiurnal and progress cyclonically around the North Sea, with the largest amplitudes along the coasts of the English Channel, Eastern England, the Southern Bight and the German Bight (e.g., Otto et al., 1990; Huthnance, 1991). In the central Southern Bight, the west of Denmark and the west of South Norway amphidromic points occur. The winds are variable and dominated by eastward moving depressions. The residual circulation along the North Sea coasts is cyclonic, along the English coast a southerly direction dominates up to the East Anglia coast where it turns offshore towards the northeast. Atlantic water enters the North Sea from the North and through the English Channel and the Dover Strait (Prandle et al., 1996). The freshwater inflow from the Seine, Scheldt, Rhine, Weser, Elbe and minor rivers results in coastal water masses with salinities lower than 33 and in density currents up to typically 20–40 km offshore along the southern North Sea (Prandle et al., 1997; Rijnsburger et al., 2016; Kopte et al., 2022). The SPM transport patterns in the North Sea follow the general residual current patterns and are restricted to a narrow band along the coast, except along the East Anglian coast, where

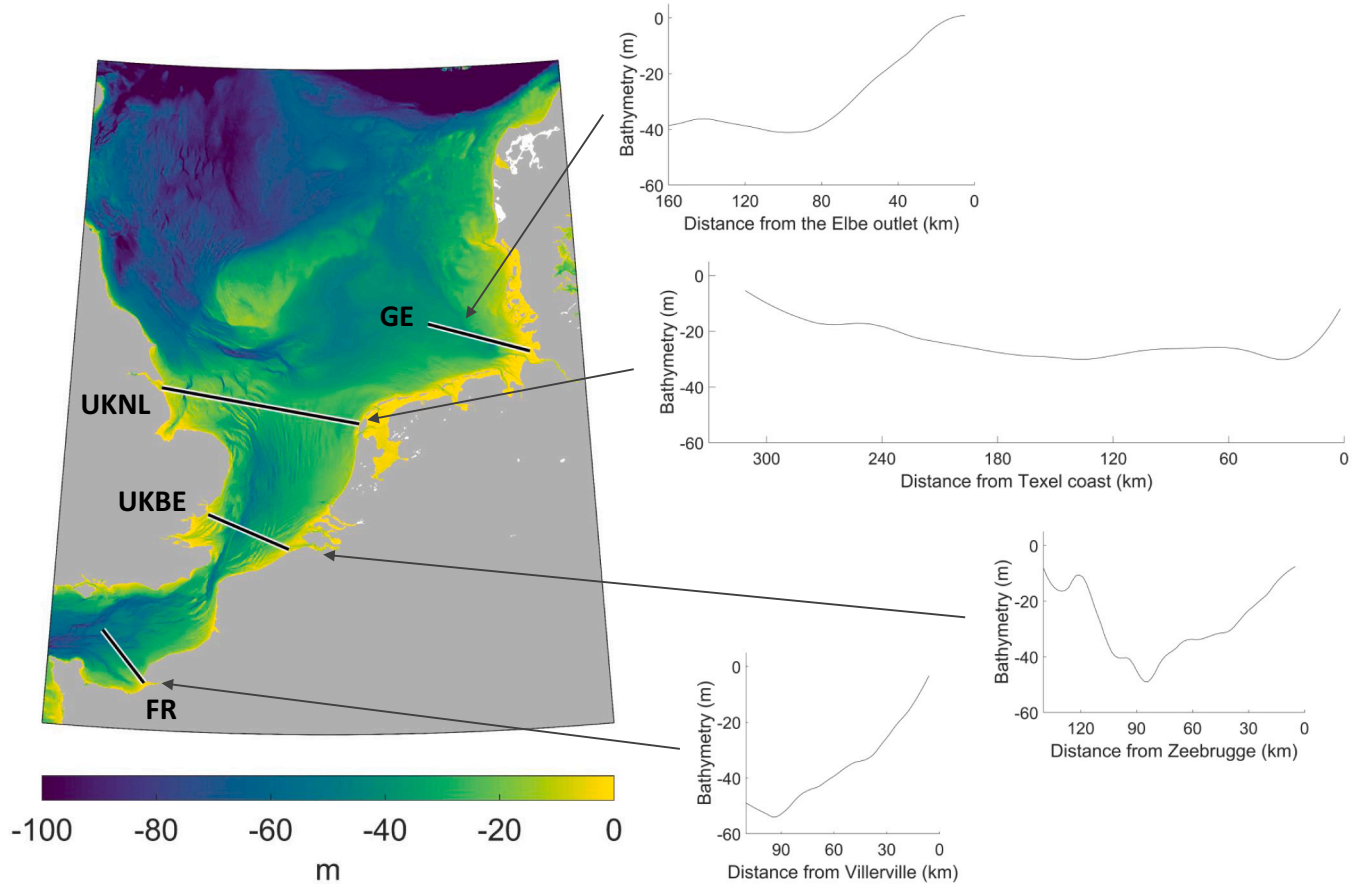

Fig. 1. Bathymetry of the southern North Sea. The black lines are showing the four transects used in this study. Side graphs on the right show the smoothed (LOESS) bathymetry along the transects.

the SPM is transported offshore towards the German Bight and the Norwegian trench (Fig. 2). The origin of the fine-grained sediments is from rivers, erosion of recent and geological layers (e.g. mud banks along the Belgian coast), coastal erosion (English Channel, east of English coast) and human impacts (see, e.g., Eisma, 1981; Dyer and Moffat, 1998; Gerritsen et al., 2001; Fettweis et al., 2009; Adriaens et al., 2018).

Satellite images show a clear difference between winter and summer SPMC, featuring a systematic decrease in summer across the continental shelf (Fig. 2). This decrease is mainly caused by the interaction between mineral and sticky exopolymeric substances that comprise organic microgels such as transparent exopolymer particles (TEP; e.g., Engel et al., 2020). During the growing season, phytoplankton excretes polysaccharides, of which a large fraction can coagulate and form TEP. This sticky TEP promotes the formation of larger flocs, enhancing the settling of the SPM (Fettweis et al., 2022). The seasonal variations in floc size and settling velocity, with higher settling rates in summer than winter, correspond well with the seasonal biological activity, whereas resuspension caused by waves, wind climate, or storms have a weaker correlation with this observed seasonality (Fettweis and Baeye, 2015).

2.3. Model of the PON content versus SPM concentration

It has been shown that the variation of the organic matter content of SPM is nonlinear and depends on the SPMC and the season (Manheim et al., 1972; Eisma and Kalf, 1987; Ittekkot and Laane, 1991). For our study we adopted the diagnostic modeling approach proposed by Schartau et al. (2019). In Fettweis et al. (2022), the usefulness of an extended model version has been documented for describing variations in particulate organic carbon and nitrogen (POC and PON), as well as for resolving changes in concentrations of transparent exopolymer particles (TEP). When calibrated with observational data, the diagnostic model can be well applied to approximate compositional changes of the SPM as a function of SPMC. In general, the POM content of SPM (POM-to-SPM ratio) changes from low to high values when SPMC decreases from highly turbid (brown) waters towards much clearer waters, respectively.

This relationship is not only observed along the inshore-offshore transect in both the German Bight and on the Belgian shelf, but also vertically between the surface and the bottom of the water column during the tidal cycle (Fettweis et al., 2022). The semi-empirical model of Schartau et al. (2019) is based on the discrimination between mineral-associated POM (POM_m), considered less reactive (Keil et al., 1994), and fresh POM (POM_f) considered more labile. The boundary condition of the model is that, when the SPMC approaches zero, the POM content of SPM converges to one, and POM is assumed to be mainly POM_f. At high SPMC, the POM content converges towards an invariant POM fraction of the SPM that is assumed to be mainly mineral-associated POM (POM_m). The remaining POM is described as a time varying fraction of the SPM, which can be attributed to the build up (primary production) and decay (remineralisation) of POM_f. Regarding the transition from highly turbid inshore towards clearer offshore waters, the relative proportion of the POM_f fraction versus the POM_m fraction increases. Accordingly, at low SPMC the POM_f fraction is high, whereas at high SPMC the POM_m fraction dominates. The same relationship can be attributed to any component of POM (e.g., POC, PON, TEP).

For our analysis we focus on the PON component of POM. The fresh fraction of the PON (PON_f) is a proxy for biomass, mainly plankton and detritus. The use of POC data would instead introduce additional uncertainties due to polysaccharide exudation and gel formation as well as physiological variations of the phytoplankton, i.e. the carbon-to-nitrogen ratio. By fitting the model to the PON data (see below), we

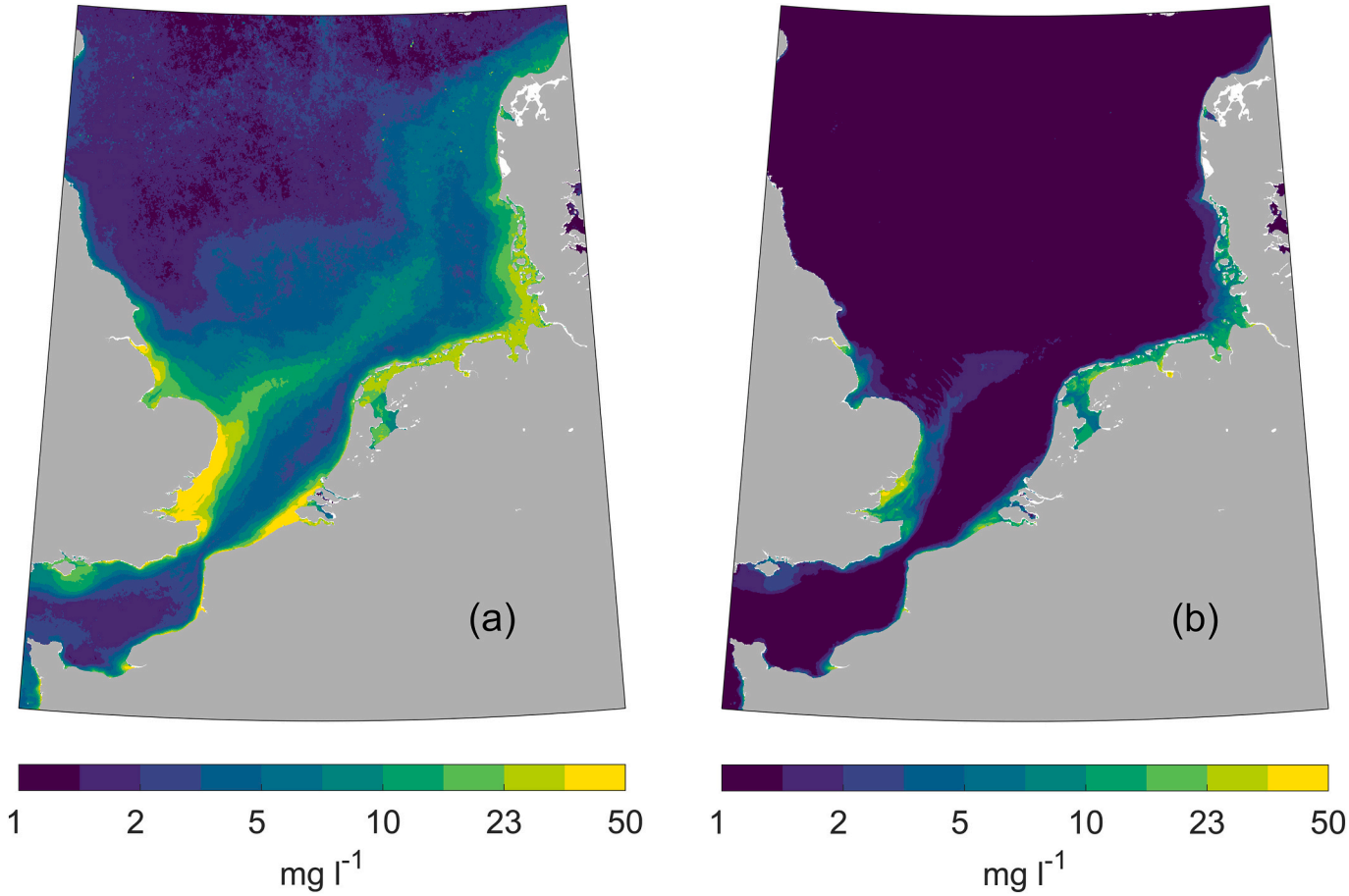

Fig. 2. Multiyear mean (2017–2021) of (a) winter (Jan, Feb, Dec) and (b) summer (Jun, Jul, Aug) surface SPMC [mg l^{-1}] in the southern North Sea.

can apply the optimized parameter values in the model (K_{POM}, $f_{1,PON}$ and $f_{2,PON}$) to recalculate the PON concentration from SPMC, while separating between the components PON_f and PON_m (Eqs. (1)–(3)):

$$PON_{modelled} = SPMC_{observed} * \frac{K_{POM} * \left(f_{2,PON} * m_{POM} + f_{1,PON}\right) + f_{2,PON} * m_{POM} * SPMC_{observed}}{\left(K_{POM} + SPMC_{observed}\right) * \left(m_{POM} + 1\right)} \quad (1)$$

$$PON_f = f_{1,PON} * \frac{K_{POM}}{\frac{K_{POM}}{SPMC_{observed}} + 1} * \frac{1}{m_{POM} + 1} \quad (2)$$

$$PON_m = f_{2,PON} * SPMC_{observed} * \frac{m_{POM}}{m_{POM} + 1}, \quad (3)$$

where m_{POM} is a factor specifying the amount of suspended POM_m along with mineral particles. Variations of m_{POM} are assumed to depend on the sediment composition (Flemming and Delafontaine, 2000), and in this study we assume m_{POM} constant (0.13) across the studied area. K_{POM} is a saturation parameter controlling the net accumulation of POM_f in the water column. Its monthly variation, thus, reflects the seasonal variation of POM_f and is assumed to be a function of available nutrients (see Schartau et al., 2019). The parameter $f_{1,PON}$ expresses the ratio of fresh PON to fresh POM (PON_f/POM_f), and $f_{2,PON}$ is the ratio of mineral-associated PON to mineral-associated POM (PON_m/POM_m), therefore, $f_{1,PON}$ and $f_{2,PON}$ are varying seasonally.

In this study, we apply the semi-empirical diagnostic model presented above to the detailed PON and SPM dataset of the Belgian shelf (Section 2.1.1) in order to derive its parameters on a monthly basis. Best model representations of the PON:SPM data were obtained by identifying model parameter values that minimize a cost function that includes the sum of squared data-model residuals divided by the respective observational errors (variances). When considering these weighted least squared misfits only, a collinearity exists between estimates of the parameters $f_{1,PON}$ and K_{POM}, in particular when individual subsamples yield estimates of K_{POM} below 0.5 mg l^{-1}. To overcome this difficulty, a Gaussian-based prior is added to the weighted least square misfit, imposing a K_{POM} value of 2 mg l^{-1} with a 100 % uncertainty. Such extension of the cost function ensures that the optimization problem is well-defined, leading to robust parameter estimates. To identify the optimal combinations of the three model parameters, we systematically explored the three-dimensional manifold of the cost function. Rather than applying an optimization algorithm, this is simply achieved by evaluating cost function values for a three-dimensional array of parameter combinations. The element of this array with the lowest cost function value represents the best combination of parameter values. The array's individual dimensions cover the variational range for $f_{1,PON}$, $f_{2,PON}$, and K_{POM}, respectively. For $f_{1,PON}$ the interval between $[10^{-3}, 1]$ is covered with a resolution of $\Delta = 10^{-3}$, and for $f_{2,PON}$ the interval covers $[5 \times 10^{-4}, 1]$ with $\Delta = 10^{-4}$. To account for the wide range of possible values for K_{POM}, spanning two orders of magnitude, we implemented a constant resolution on a logarithmic scale within the interval $\log_{10}(K_{POM}) \in [\log_{10}(0.1), \log_{10}(10)]$. This logarithmic scale approximation aims to achieve a precision of approximately 1 %.

The model is, then, applied pixel wise to the satellite SPMC images (Section 2.1.2) in the southern North Sea, assuming the same model parameters for all areas (see Eqs. (1) to (3)). This provides qualitative information on SPM composition, in addition to the original SPMC levels, in order to investigate the coastal-to-offshore patterns of SPM dynamics.

3. Results

3.1. Model-based estimates of PON_f and PON_m

The SPM composition, more specifically its PON fraction, changes in a characteristic way with SPMC. A progressive increase of the PON fraction occurs with decreasing SPMC from nearshore to offshore waters (Fig. 3).

The PON content increases in the spring and summer (Fig. 3 c-g) while phytoplankton blooms and detritic particles accumulate in the bulk, until the fall and winter when heterotrophic processes dominate. Also, the general decrease in SPMC during summer (May–August) compared to the winter period is observable in these graphs (distribution around lower values on the horizontal axis). The model was fitted against the data, reproducing the cross-shore gradient and the seasonal trend, and providing monthly model estimates for its parameters (Table 1). Statistics shown in Table 1 indicate the goodness of fit. The Root Mean Square Error (RMSE) is expressed in the units of PON:SPM and should be small. The normalized cost function would be equal to 1 if the data-model misfit was perfect. While the RMSE does not account for uncertainties in observations, the cost function (weighted least squares) does and thus provides more meaningful assessment of the model fit. The range of uncertainty of the fit increases towards low SPMC due to the lack of data constraints (e.g., February in Fig. 3b). This does not necessarily prevent good model representations of the available observations, as shown by corresponding statistics. Overall, only for June, July and October the model estimates reveal a less good fit to observations. The model parameters allow calculating a modelled PON concentration from the SPMC, and also the fractions PON_f and PON_m (Eqs. (2) and (3)). The values of Table 1, generated by fitting the model on the available Belgian data, are applied to all transects in this study, assuming they are representative of North Sea particle dynamics.

3.2. Multiyear mean winter and summer PON concentration in the North Sea

Using the model's best parameter estimates, we derived PON, PON_m and PON_f concentrations from SPMC and applied it pixel wise to the satellite images in the southern North Sea and the English Channel. The uncertainties in the model parameters enhance the errors of the pixel wise values for POM_f and POM_m in comparison with the satellite SPMC they are derived from. However, for geographical entities, which extend over tens of kilometers and comprise a larger number (10 to 100) of pixels, they still reveal robust patterns. We use ΔPON, the difference between PON_m and PON_f concentrations (PON_m - PON_f), to highlight the spatio-temporal variations of the PON dynamics and composition. It is shown for the months of January 2020 at Fig. 4a and April 2020 at Fig. 4b.

ΔPON varies in time and space as both fractions PON_m and PON_f undergo biogeochemical transformations. In winter, ΔPON shows the highest values at the coast due to the dominance of PON_m and rapidly decreases towards the offshore, where values are typically closer to zero as both PON_m and PON_f are low and closer in concentration (Fig. 4a). A notable exception offshore is the turbid Thames River plume carrying SPM from East Anglia across the sea to the German Bight and the coast of Denmark, and where PON_m dominates. In the spring (Fig. 4b), ΔPON shows its minimum values in a narrow area close to the coast. In that area, the freshly produced fraction of PON in spring is found in higher

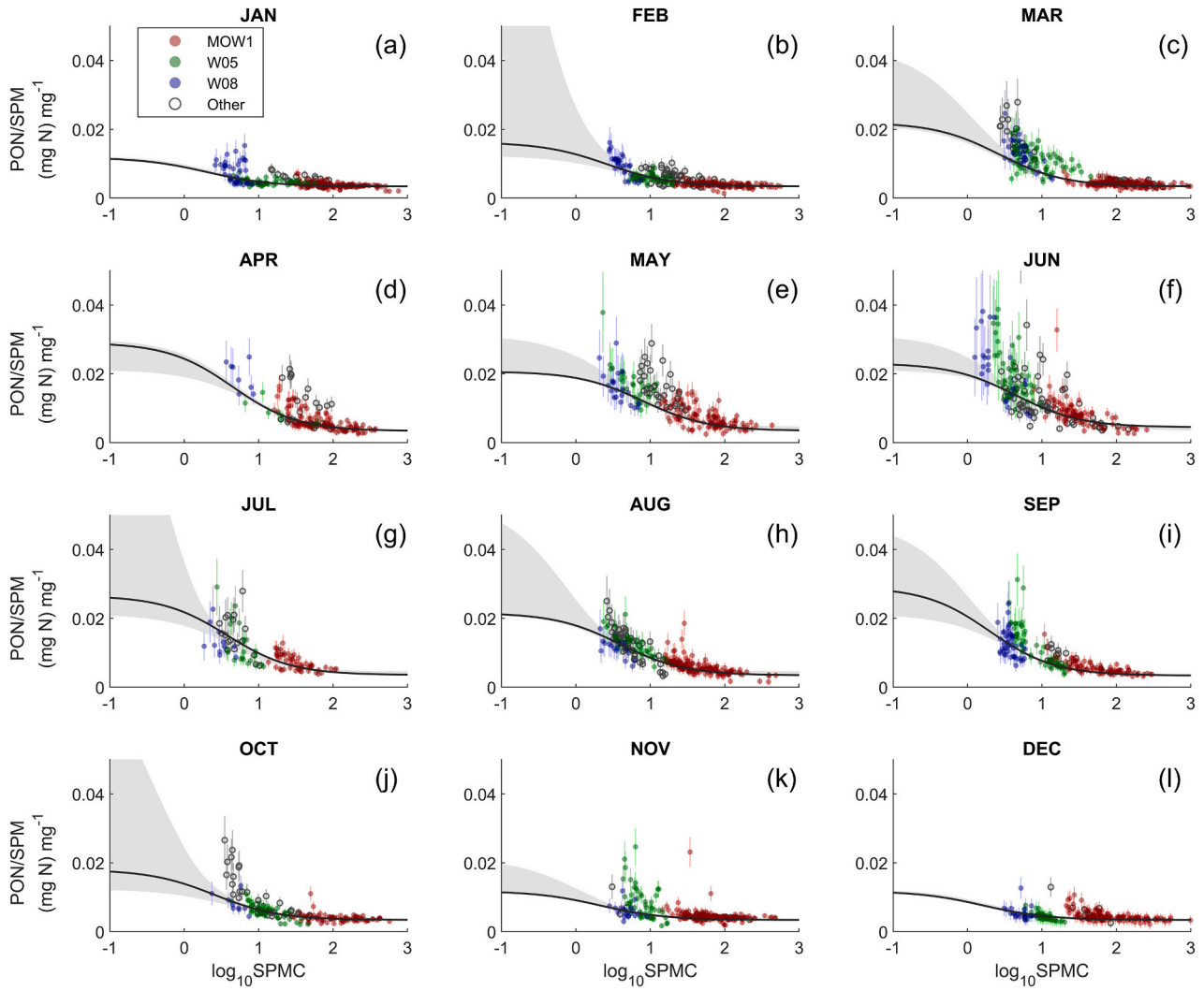

Fig. 3. PON content of SPM [(mg N) mg^{-1}] as a function of SPMC, in situ monthly data sampled at twelve stations along the coastal-offshore gradient on the Belgian shelf. Three stations have been relatively more sampled: MOW1, W05 and W08 (see legend for colours). The black line represents the model fit, and the grey area represents the uncertainty envelope (at the 95 % confidence interval).

Table 1
Monthly model parameters and associated statistics obtained from model fitting for the PON content of SPM along the coastal-offshore gradient on the Belgian shelf.

Month	PON: fitting parameters			Statistics	
	K_{POM}	$f_{1,PON}$	$f_{2,PON}$	RMSE	Cost function
	mg l^{-1}	(mg N) mg^{-1}	(mg N) mg^{-1}	(mg N) mg^{-1}	–
Jan	2.00	0.0095	0.0295	0.0016	1.02
Feb	2.66	0.0145	0.0295	0.0014	1.12
Mar	2.68	0.0210	0.0295	0.0035	1.40
Apr	4.47	0.0290	0.0295	0.0035	1.70
May	8.00	0.0195	0.0300	0.0044	1.73
Jun	4.46	0.0210	0.0390	0.0119	2.10
Jul	3.77	0.0260	0.0310	0.0037	3.19
Aug	3.90	0.0205	0.0300	0.0024	0.88
Sep	1.99	0.0290	0.0295	0.0036	1.23
Oct	2.55	0.0165	0.0295	0.0030	2.29
Nov	2.13	0.0095	0.0295	0.0030	1.78
Dec	1.63	0.0095	0.0295	0.0026	1.80

concentrations than the mineral-associated PON, which leads to negative values of ΔPON. While PON_f concentration in spring is a proxy for phytoplankton biomass, PON_m always reflects the mineral fraction of SPM, which predominantly originates from resuspended sediment particles.

3.3. Monthly variation of PON along cross-shore transects

The monthly variations of PON_f and PON_m have been calculated for the four selected transects. The resulting ΔPON features a high seasonal variability, which is illustrated for the transect 'GE' in Fig. 5c (see Appendix A for the other transects). PON_f is linked to seasonal photosynthesis and organic matter degradation processes. Therefore, PON_f concentration is low in winter and increases during spring and summer in relation to the bloom and post-bloom processes. It decreases in the fall when heterotrophic processes dominate the phototrophic processes. PON_m concentration is proportional to the mineral particle concentration. Therefore, it exhibits a decrease from winter to summer and an increase in the fall, following the seasonal cycle of SPMC (see Section 2.2; Fig. 2). At any time of the year, both PON_m and PON_f show higher concentrations at the coast than offshore. Such a cross-shore difference becomes much less significant for PON_f in winter when plankton growth is minimal. During the growing season, PON_f reaches the highest

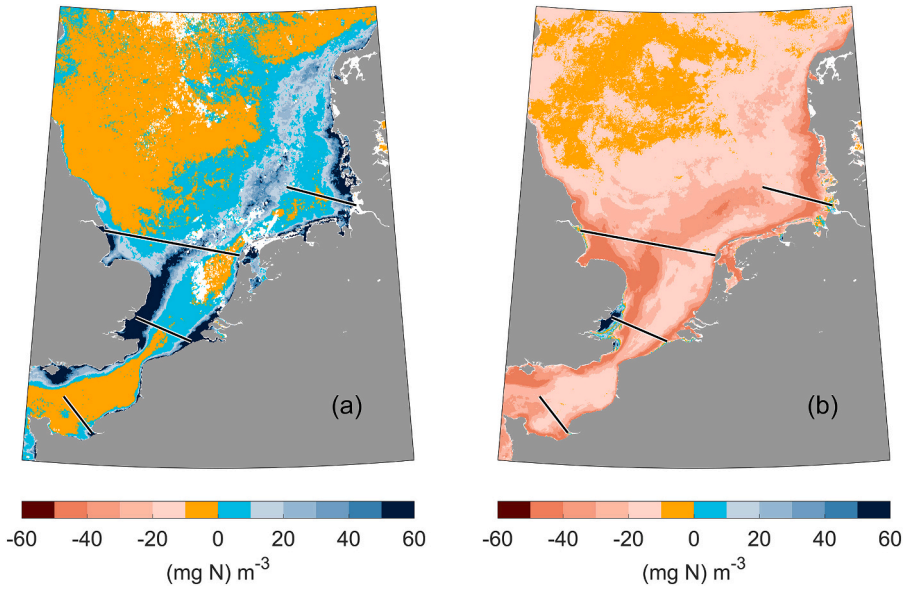

Fig. 4. Surface ΔPON (PON_m-PON_f) concentration [(mg N) m^{-3}] in 2020, January (a) and April (b). Black lines are the transects of interest (see Fig. 1).

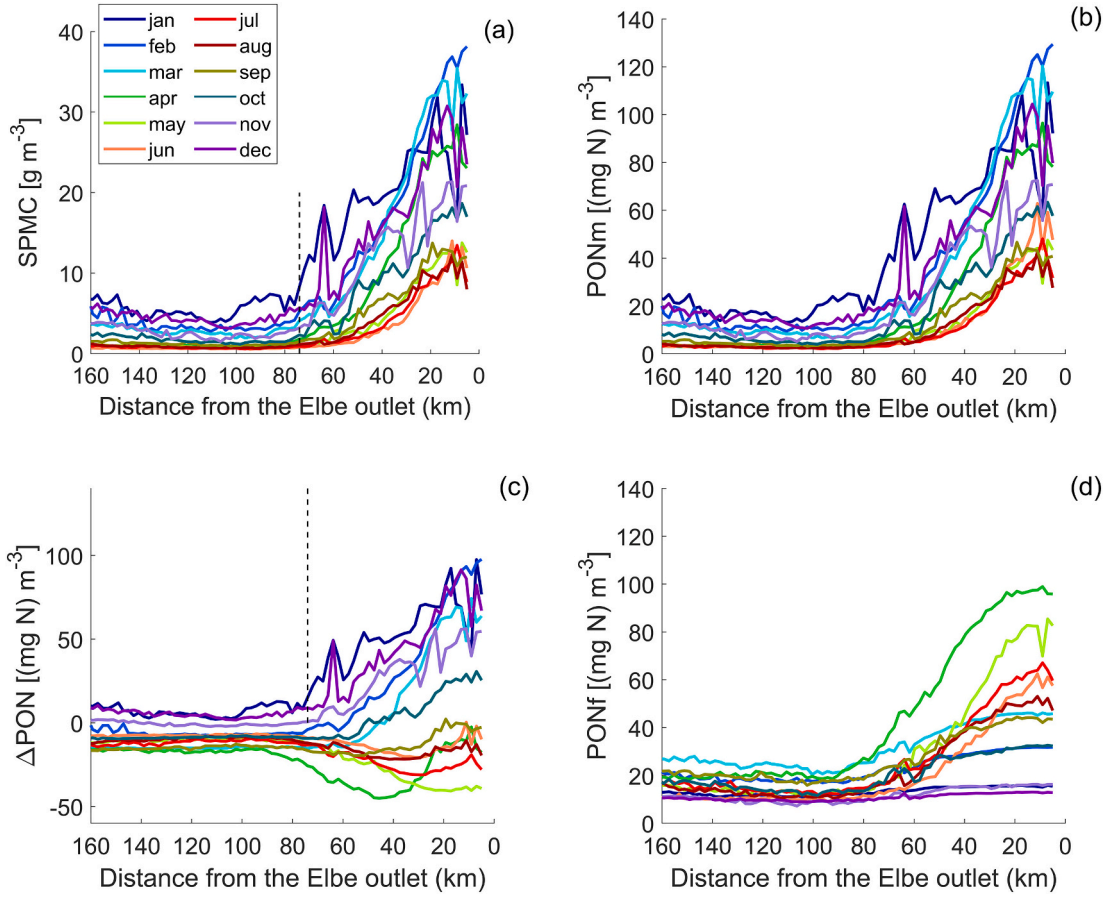

Fig. 5. Monthly surface (a) SPM, (b) PON_m, (c) ΔPON and (d) PON_f concentrations along the transect 'GE' (satellite-derived data). Each line represents the multi-year mean values for one month in the period 2017–2021. The dashed vertical line corresponds to the location where ΔPON reaches its offshore value (see text).

concentrations, especially in April and May at the coast and in March, April and September offshore.

As a result of the seasonal variability of PON_f and PON_m, ΔPON follows a coastal-offshore gradient similar to the one of PON_m during winter months. This cross-shore gradient is characterized by a strong decrease in concentration between the coast up to ~75 km from the Elbe outlet. In the spring and summer, during a period of an increase in PON_f while PON_m decreases, the resulting ΔPON is characterized by lower values (mostly negative values) across the transect. ΔPON shows minimum values from April to September between the coast and ~75 km

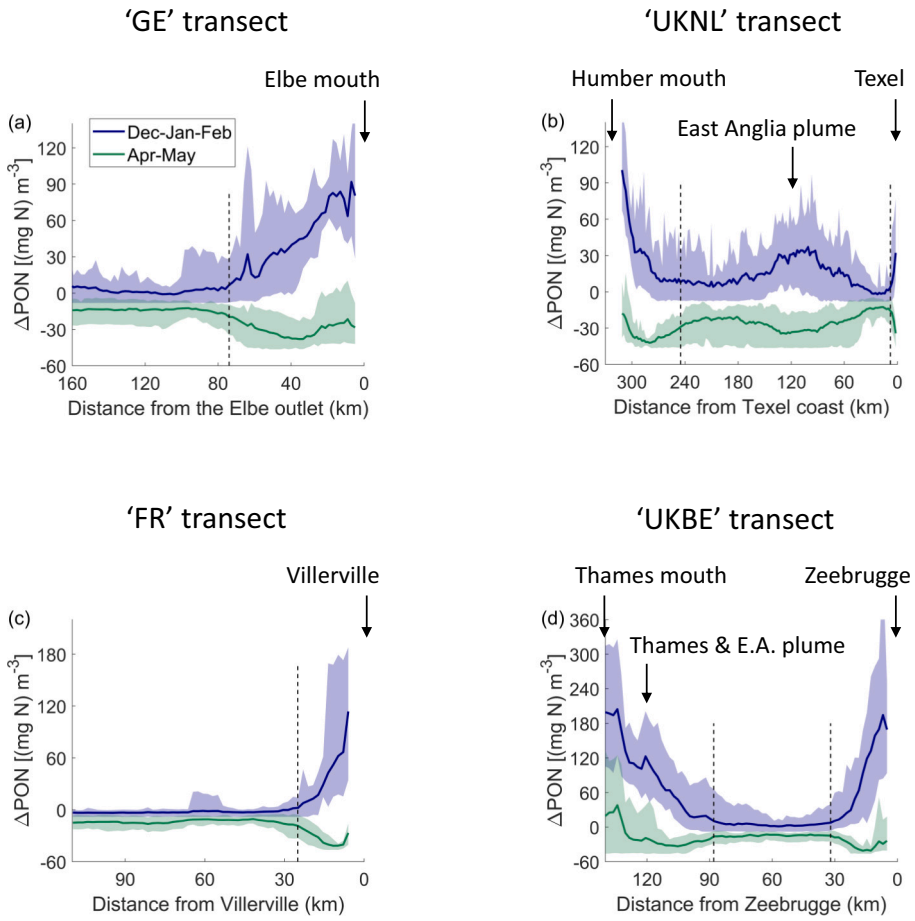

Fig. 6. Surface ΔPON (PON_m-PON_f) concentration [(mg N) m^{-3}] in winter and spring along four transects (a. 'GE' transect; b. 'UKNL' transect; c. 'FR' transect; d. 'UKBE' transect). Lines show the multiyear mean values (2017–2021) and shaded areas illustrate the multiyear minimum and maximum values. The dashed vertical lines correspond to the locations where ΔPON reaches its offshore value (see text).

offshore from the Elbe outlet. In April, when phytoplankton production is at its highest, more negative values of ΔPON occur between km 20 and km 75 from the Elbe outlet. In that zone, although PON_f shows lower concentrations than at the coast, the PON_m concentration has dropped to such an extent that ΔPON reveals its lowest value. This characteristic seems to be a robust feature for many coastal regions, and exceptions or deviations suggest some underlying dynamics, in particular with respect to the cross-shore transport of SPM, that differs from other areas. Over the entire North Sea, such a zone of lowest ΔPON is visible as the dark red narrow area on Fig. 4b, where ΔPON<-40 (mg N) l^{-1}. Typically, it is found as an alongshore feature.

Fig. 6 shows the average winter (blue) and spring (green) ΔPON profiles over the four studied transects. The main characteristics of ΔPON variability across the 'GE' transect are also observable in other coastal zones, whether featuring low turbidity like the Texel coast ('UKNL' transect), moderate turbidity like the Seine Bay ('FR' transect) and the Humber mouth (north of East Anglia; 'UKNL' transect), or high turbidity like the Belgian coast and the Thames mouth (south of East Anglia; 'UKBE' transect). In winter, ΔPON is dominated by PON_m and reflects well the SPMC. In spring, PON_f concentration increases due to biological activity while PON_m decreases concomitantly due to TEP accumulation in the bulk and settling of the flocs, which results in a considerable decrease in ΔPON at the coast (towards negative values). As ΔPON is derived from satellite SPMC, the East Anglia plume and the Thames plume are visible respectively in the 'UKNL' and 'UKBE' transects, especially in winter. The fact that the East Anglia plume is visible in satellite images in winter suggests that the particles have low settling velocities due to their small grain sizes. It is the lateral transport of particles from the Thames that is responsible for the extensive cross-shore spread of SPM, since it is unlikely that particles from the bottom be resuspended towards the surface along the trajectory of the plume, especially when bathymetry increases. Clearly, the other coastal areas, including river mouths and estuaries, do not reveal a similar cross-shore spreading of SPM. In spring, the East Anglia plume is also visible with lower values of ΔPON compared to surrounding waters, which suggests a higher phytoplankton production in the plume. Along the coastal-offshore transects, the annual variability of ΔPON (shaded area in Fig. 6) is lower than the spatial and seasonal variability in the period 2017–2021, suggesting that basin morphology and seasonal processes, such as phytoplankton production, mainly control the particle dynamics. This tends to be less obvious in offshore waters.

3.4. Variations of PON with regard to bathymetry

So far we looked at variations in ΔPON along cross-sections with regard to the distance from the coast. Despite predominant features being similar, the distances at which the spatial gradients in the variation of ΔPON approach their minimum remain elusive. In order to test the dependency of ΔPON on basin morphology, ΔPON can also be represented as a function of the bathymetry along the transects (more specifically along each coastal-offshore sub-transects; Fig. 7). In most of our studied cases, the winter decrease in ΔPON occurs within bathymetry below ~20 m, and likewise in spring we find the trough in ΔPON to occur within the same depth range, with the exceptions of the Elbe and Thames cases where it occurs, respectively, within bathymetry 5–35 m (Fig. 7a) and 15–50 m (Fig. 7d). It should be pointed out that in spite of

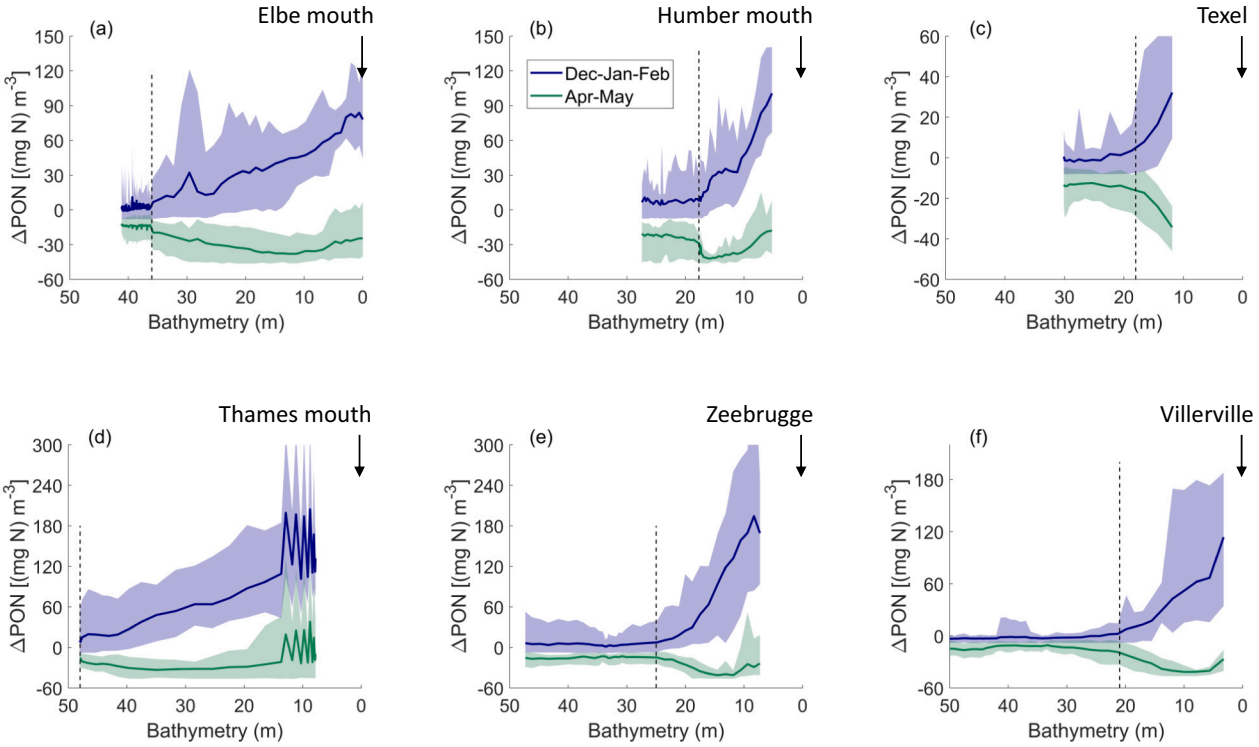

Fig. 7. Surface ΔPON (PON_m-PON_f) concentration [(mg N) m^{-3}] in winter and spring as a function of bathymetry (a. 'GE' transect; b. 'UKNL' transect, Humber plume; c. 'UKNL' transect, Texel coast; d. 'UKBE' transect, Thames plume; e. 'UKBE' transect, Belgian coast; f. 'FR' transect). Lines show the multiyear mean values (2017–2021) and shaded areas illustrate the multiyear minimum and maximum values. The dashed vertical lines correspond to the locations where ΔPON reaches its offshore value (see text).

the complexity of particle dynamics in coastal zones, ΔPON values tend to stabilize in most cases around bathymetry 20 m (or 35 m in the Elbe case; Transect 'GE'), where ΔPON reaches its offshore value while its winter and spring annual variabilities tend to overlap. Also, beyond bathymetry 20 m, the SPM dynamics generally adopt an offshore regime (Fig. 5a and Figs. A.1, A.2, A.3). These results suggest that bathymetry 20–35 m be the location of the virtual 'line of no return', which may also depend locally on river plume dynamics.

4. Discussion

The transition zone between coastal and offshore waters was investigated along four transects as a function of the distance to the coast. We define the transition zone as the part of the coastal area where the ΔPON in April–May (Fig. 6) shows a trough, i.e., where PON_f mostly dominates PON_m. Along the continental coast, it roughly occurs between 20 and 75 km from the Elbe outlet in the GE transect (Fig. 6a), within the first 8 km offshore Texel (Fig. 6b), between 5 and 25 km from Villerville in the Seine Bay (Fig. 6c), and between 10 and 30 km from Zeebrugge in the BE transect (Fig. 6d). It was also represented as a function of bathymetry because of the indirect, though central, influence of the latter on particle dynamics (see below in §4.1). The defined transition zone is located in 4 of the 6 transects shown at Fig. 7 between ~5–20 m water depth. Exceptions are the Thames mouth, where an overlap with the East Anglian plume may distort the pattern, and the Elbe plume, which extends along its Glacial Valley and is not representative, in this respect, of the rest of the German Bight. Beyond the studied transects, the transition zone tends to occur within depths below 20 m in the southern North Sea and the English Channel, as shown in Fig. 8. This zone corresponds to an area where turbulence is decreasing and the settling velocity has a local maximum, as Maerz et al. (2016) derived for the German Bight. In the case of the transition zone overlapping with a region of freshwater influence, the net transport of settled particles during a tidal cycle is directed towards the coast due to ebb-flood asymmetries in the vertical profile (Becherer et al., 2016). These processes cause a net accumulation of particles in the coastal zone (Postma, 1981), shaping the strong horizontal gradients of SPMC. From our point of view, the offshore outer limit of the transition zone (corresponding to a bathymetry of ~20 m) represents the 'line of no return' as put forward by Postma (1984).

4.1. Effect of bathymetry on particle dynamics

Turbulence is a major factor controlling the resuspension and settling of fine-grained particles. Turbulence is due to wind and the tidal dynamics, which cause shear stresses at the surface and bottom boundaries of the water column. While lower levels of turbulence permits flocculation in turbid areas, where the collision probability remains significant, high levels of turbulence will result in floc breakup, leading to a higher number of smaller particles. In addition to the density of particles, the median size of particles is key to predict their settling rates as smaller particles show lower downward flux due to the water viscosity that reduces their terminal velocity. In contrast, larger particles exhibit a higher net downward mass flux. Bathymetry controls the propagation of turbulent kinetic energy between the surface and bottom boundaries of the water column. Bathymetry is therefore a controlling factor determining the median particle size in the water column through floc formation/breakup, and it also determines whether resuspended particles may reach the surface. In shallow waters, there is typically an increased shear stress on the sediment that enhances resuspension of particles. As is known, this effect decreases with increasing water depth, up to the point where the resuspended particles only remain in the lower layers near the bottom. Overall, the net downward flux of particles depends on the vertical profiles of water viscosity and turbulence as well as on the particles' size structure and excess density. These particle properties change with flocculation, which in turn depends not only on the turbulence but also on the abundance and composition of the SPM (Ho et al., 2022; Yu et al., 2023).

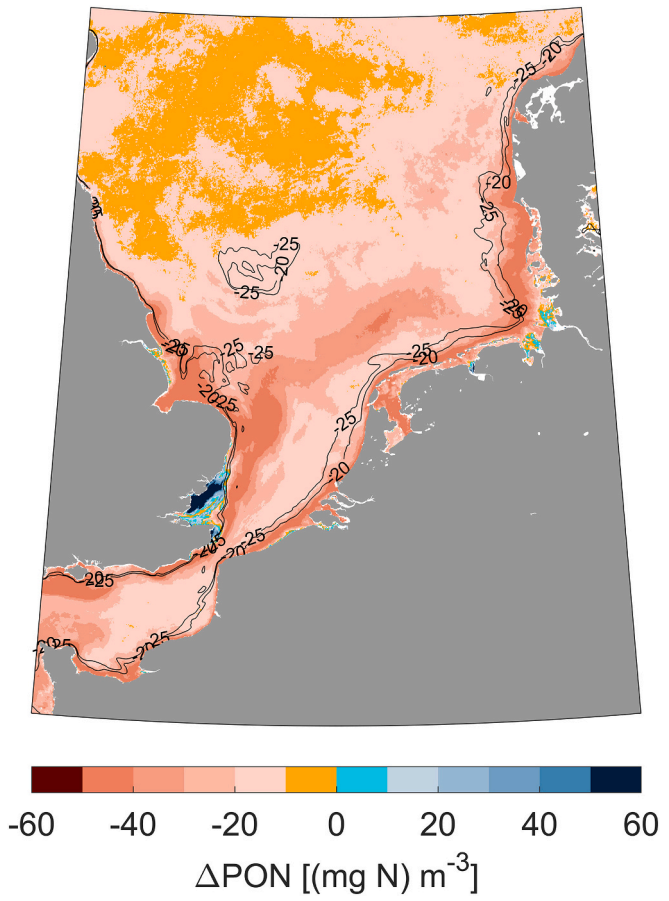

Fig. 8. Surface ΔPON (PON_m-PON_f) concentration in April 2020 with isolines (black) of bathymetry 20 m and 25 m.

4.2. SPM and POM storage and export

Some hypotheses can be made on the influence of the transition zone on SPM and POM storage and export. The well pronounced seasonal variability in PON_f is mainly due to phytoplankton production, whereas the variability seen in PON_m can be attributed to variations in the amount of resuspended matter or the settling behavior of the particles, as, for instance, an increased averaged settling of particles during the growing season due to more effective flocculation. In the case of the German Bight (transect 'GE'), the most upstream values of PON_f concentration increase by ~80 (mg N) m^{-3} (~15–20 (mg N) m^{-3} offshore) between December and April (March, offshore), illustrating the size of the spring bloom (Fig. 5d). Concomitantly, PON_m concentrations decrease by ~100 (mg N) m^{-3} (~13–17 (mg N) m^{-3} offshore) between the end of the winter and the summer, which can be explained by an increase in particle settling in response to the increase in median floc size from the winter to the summer (Fettweis et al., 2022). Even in the absence of any hydrodynamical process responsible for keeping the particles at the coast, several processes can be identified that limit the export of fresh POM to the offshore. In front of the Belgium coast, in winter, when the fresh and sticky components of EPS, including TEP, are found in negligible concentrations in the water column, the SPM remains an assemblage of fine-grained particles, with median floc sizes of ~50–60 μm on average during a tidal cycle (Fettweis and Baeye, 2015). These flocs are deposited and resuspended at tidal scale and, thus, a long-term deposition in the benthic layer is unlikely to occur. During spring and summer, while the fresh and more sticky TEP is accumulating in the bulk, the particles tend to form flocs with median sizes of ~80–150 μm on average during a tidal cycle. A significant part of the SPM settles and remains on the seabed with a lower probability of being resuspended during the tidal cycle than in the winter (Fettweis and Baeye, 2015). As particles settled on the seabed do not move significantly compared to particles in suspension, the increased particle settling in summer also diminish the horizontal transport of SPM and POM. In that sense, the seasonal vertical processes influence the range of the horizontal dispersal of SPM and POM. The line of no return is an emergent property of systems where particles are subject to these coupled vertical and horizontal processes. From a literal point of view, the line of no return inhibits the SPM transport from coastal to offshore waters. We note that this does not exclude a residual, albeit small, net flux of fresh POM produced offshore towards the coast.

Thus, we may hypothesize that a transport of particles is possible between coastal and offshore waters, but it is limited. Such transport is more important during the winter when floc sizes and settling rates are lower, and it is also correlated with the export of mainly mineral-associated POM. In spring and summer, when the SPM is enriched in fresh POM, it is also more subject to local sedimentation and trapping into the benthic fluffy layer. As a consequence, the fate of fresh and mineral-associated POM is different. While fresh POM produced in the coastal zone tends to remain there, the mineral-associated POM may be subject to transport towards the offshore to be eventually stored in the open ocean, predominantly in winter. The remineralization of fresh POM in the coastal zone enriches the system with dissolved nutrients. Those can be locally uptaken or transported away since dissolved substances are not limited by the line of no return (Postma, 1984).

4.3. Criteria for a transition zone in the North Sea

The concept of transition zone as described above, is based on several conditions: elevated SPMC, tidal hydrodynamics that generate strong alongshore and weak cross-shore currents, horizontal salinity gradients (freshwater input), and an area of increased settling velocities controlled by turbulence values that enhance flocculation (bathymetry dependent). Areas that fit these criteria are the east coast of England down to East Anglia, the southeastern coast from the Dover Strait up to the German Bight and Denmark, and the Seine Bay (Fig. 8). In these areas, a strong cross-shore gradient of SPMC is observed. Areas that do not fulfill all these criteria are the southern coast of England from the Isle of Wight up to East Anglia, the Somme Bay and the North Holland coast. In these areas, the cross-shore particle transport mechanism differs from those where the apparent line of no return largely corresponds to the 20 m isobath. The SPM plume offshore the East Anglia coast is not confined to the coast and stretches out across the southern North Sea up to the German Bight. The direction of the strong cross-shore currents corresponds to the flow fields of the cyclonic tidal wave and the inflow of Atlantic waters through the Dover Strait. The area of the Isle of Wight, although rich in SPM, is not subject to significant freshwater input and, thus, hydrodynamical processes keeping the particles at the coast are presumably small. Consequently, the coastal-offshore pattern of SPMC greatly exceeds the 20 m isobath. The Somme Bay exhibits neither high SPMC nor a significant density gradient. The North Holland coast has low SPMC at the surface. However, the influence of the Rhine ROFI may locally perturbate the vertical density gradient, and additionally may cause an underestimation of satellite-derived SPMC (Pietrzak et al., 2011).

5. Conclusion

Coastal areas with elevated SPMC, and with strong alongshore, weak cross-shore currents, and horizontal salinity gradients, feature a land-ocean transition zone that can be identified based on temporal and compositional changes of the particles. Spatial and seasonal variabilities dominate the particle dynamics, suggesting that basin morphology and biological activity mainly control the processes at play. Bathymetry plays an important role in determining the turbulence effects on the flocculation and settling of particles. Our study shows that the coastal

SPMC maximum and thus the maximum settling of particles generally occurs within depths below 20 m. Generally, the seasonal production of phytoplankton should enhance the particle settling and thus the accumulation of freshly produced particles at the bottom during the summer period. Due to vertical and horizontal density gradients and hydrodynamic (tidal) forcings, the particles in the transition zone may become subject to a near-bottom net transport towards the coast, hence maintaining the cross-shore gradient of particles. The offshore limit of the transition zone can thus be regarded as the 'line of no return' put forward by Postma (1984) across which any transport of SPM and its organic matter components becomes small throughout the year, especially in the growing season. The dynamics of particles in the transition zone have an effect on the fate of organic matter. The freshly produced POM and a substantial part of the mineral-associated POM tend to remain in the shallower areas of the coastal waters, while a minor fraction of the mineral-associated POM is exported to the offshore during the winter. The impact of such particle dynamics on the carbon and nitrogen cycles in shelf seas could be further quantified in the future with modeling tools.

Funding section

The research was supported by the Belgian Science Policy (BELSPO) within the BRAIN-be programme (BG-PART, contract nr B2/202/P1/BG-PART, and PiNS, contract nr RV/21/PiNS), the Maritime Access Division of the Flemish Ministry of Mobility and Public Works (MOMO project), and the RBINS BGCMonit program. Scientific input from Markus Schartau and Rolf Riethmüller are integrated in the research topics "Marine and polar life" and "Coastal zones at a time of global change" of the project-oriented funding programme: Changing Earth - Sustaining our Future, funded by the Helmholtz Association of German Research Centers.

CRediT authorship contribution statement

Xavier Desmit: Conceptualization, Data curation, Formal analysis, Funding acquisition, Investigation, Methodology, Project administration, Resources, Software, Supervision, Validation, Visualization, Writing – original draft, Writing – review & editing. **Markus Schartau:** Conceptualization, Formal analysis, Investigation, Methodology, Software, Writing – original draft, Writing – review & editing. **Rolf Riethmüller:** Conceptualization, Investigation, Methodology, Supervision, Writing – review & editing. **Nathan Terseleer:** Conceptualization, Formal analysis, Methodology, Software, Supervision, Visualization, Writing – review & editing. **Dimitry Van der Zande:** Data curation, Formal analysis, Funding acquisition, Methodology, Software, Visualization, Writing – review & editing. **Michael Fettweis:** Conceptualization, Data curation, Formal analysis, Funding acquisition, Investigation, Methodology, Project administration, Resources, Supervision, Validation, Writing – original draft, Writing – review & editing.

Declaration of competing interest

To their best knowledge, the Authors do not have any actual or potential conflict of interest including any financial, personal or other relationships with other people or organizations within three years of beginning the submitted work that could inappropriately influence, or be perceived to influence, their work.

Data availability

Data used in this study (in situ concentrations, bathymetry) are available online. See Acknowledgements section for references.

Acknowledgements

Ship time with the RV Belgica was provided by BELSPO and RBINS-OD Nature. The SPM and POC analysis have been done in RBINS's ECOCHEM Laboratory. Data of in situ SPM and PON concentrations are freely available on request at https://www.bmdc.be/NODC/search_data.xhtml. Bathymetry information and images were derived from GEBCO Compilation Group (2022), GEBCO 2022 Grid (doi:https://doi.org/10.5285/e0f0bb80-ab44-2739-e053-6c86abc0289c). Maps were performed in Matlab with M_Map (Pawlowicz, 2020).

Appendix A

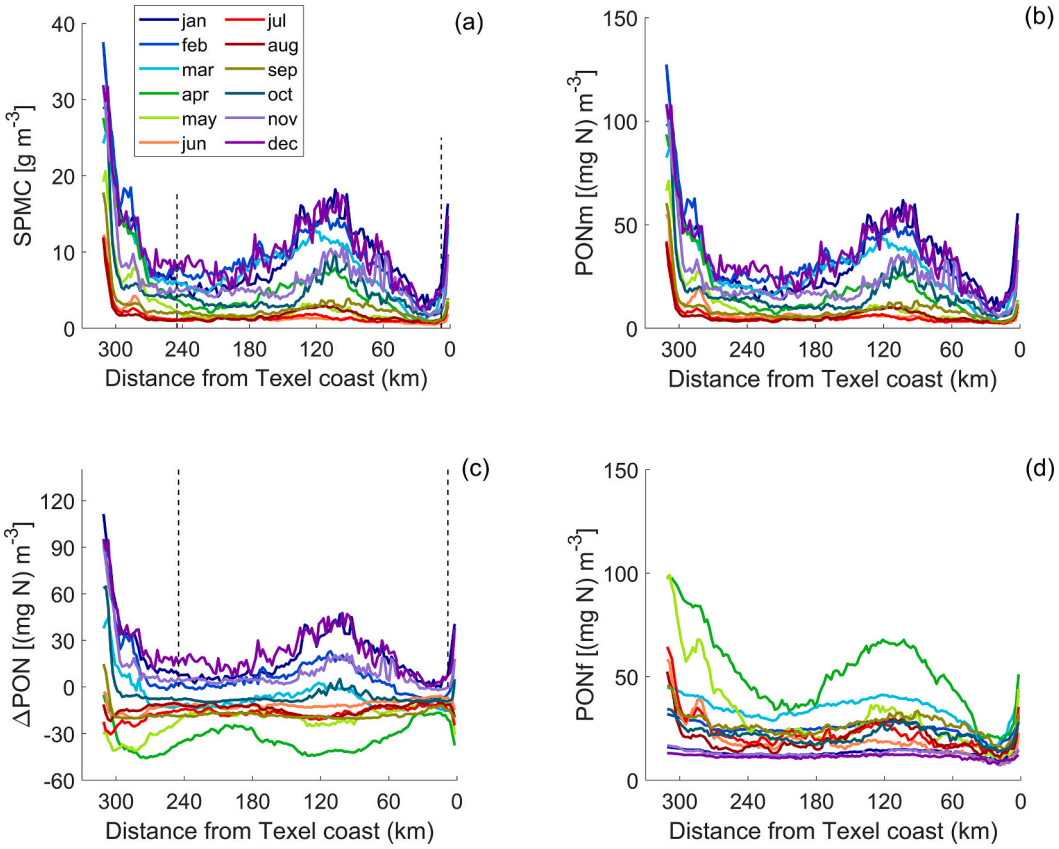

Fig. A.1. Monthly surface (a) SPM, (b) PON_m, (c) ΔPON and (d) PON_f concentrations along the transect 'UKNL' (satellite-derived data). Each line represents the multi-year mean values for one month in the period 2017–2021. The dashed vertical lines correspond to the locations where ΔPON reaches its offshore value (see text).

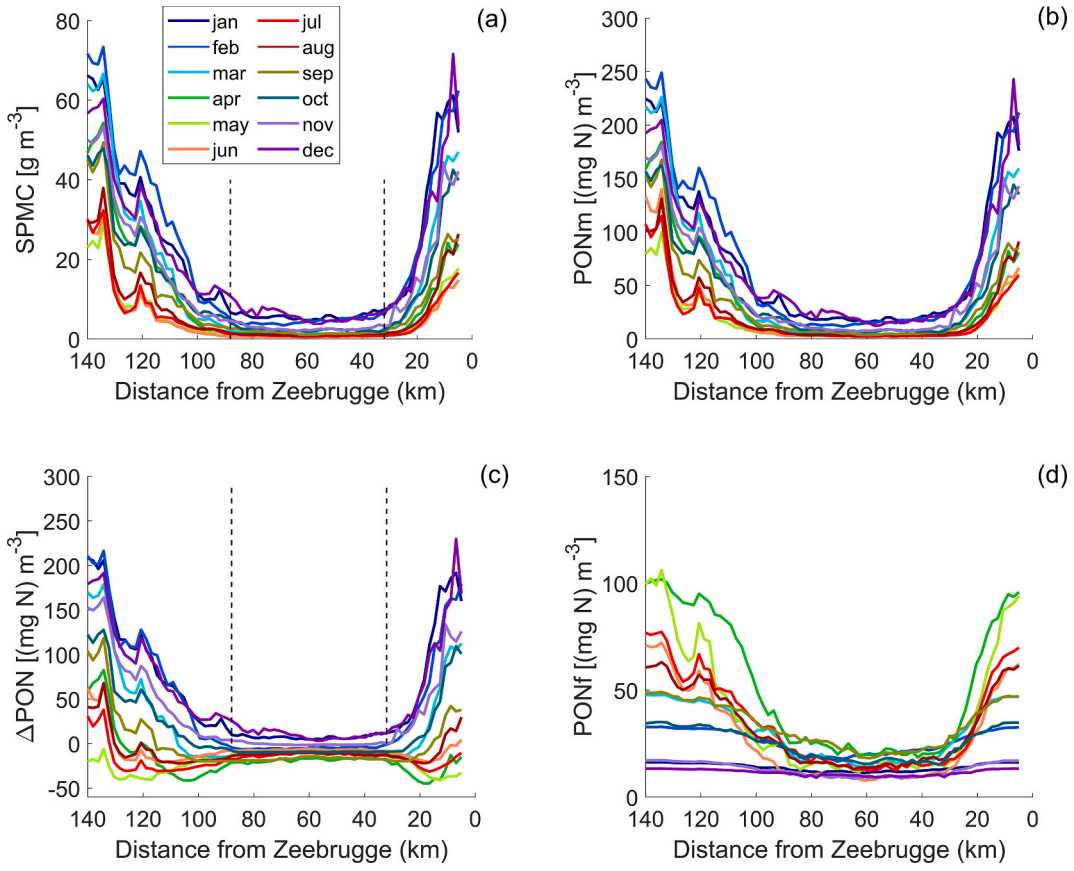

Fig. A.2. Monthly surface (a) SPM, (b) PON_m, (c) ΔPON and (d) PON_f concentrations along the transect 'UKBE' (satellite-derived data). Each line represents the multi-year mean values for one month in the period 2017–2021. The dashed vertical lines correspond to the locations where ΔPON reaches its offshore value (see text).

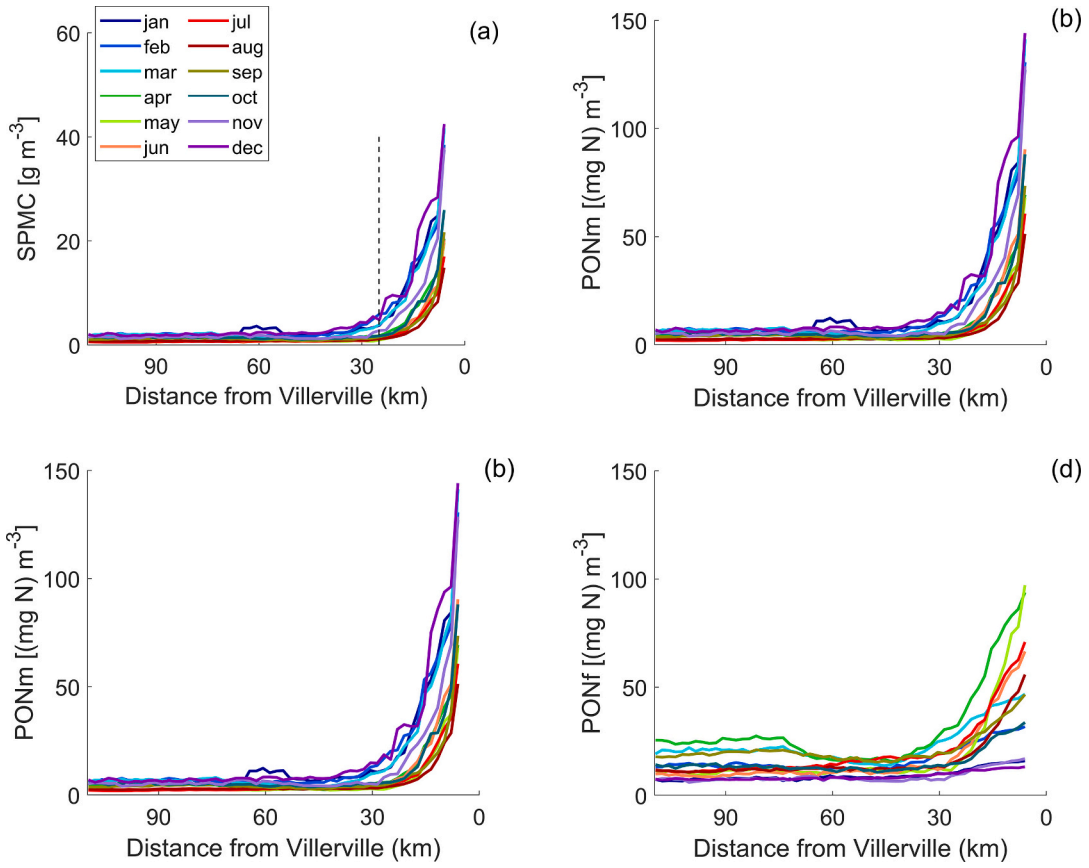

Fig. A.3. Monthly surface (a) SPM, (b) PON_m, (c) ΔPON and (d) PON_f concentrations along the transect 'FR' (satellite-derived data). Each line represents the multi-year mean values for one month in the period 2017–2021. The dashed vertical line corresponds to the location where ΔPON reaches its offshore value (see text).

References

Adriaens, R., Zeelmaekers, E., Fettweis, M., et al., 2018. Quantitative clay mineralogy as provenance indicator for recent muds in the southern North Sea. Mar. Geol. 398, 48–58. https://doi.org/10.1016/J.MARGEO.2017.12.011.

Asmala, E., Carstensen, J., Conley, D.J., Slomp, C.P., Stadmark, J., Voss, M., 2017. Efficiency of the coastal filter: nitrogen and phosphorus removal in the Baltic Sea. Limnol. Oceanogr. 62, S222–S238. https://doi.org/10.1002/lno.10644.

Becherer, J., Flöser, G., Umlauf, L., Burchard, H., 2016. Estuarine circulation versus tidal pumping: sediment transport in a well-mixed tidal inlet. J. Geophys. Res. Ocean. 121, 6251–6270. https://doi.org/10.1002/2016JC011640.

Becker, G.A., Dick, S., Dippner, J.W., 1992. Hydrography of the German bight. Mar. Ecol. Prog. Ser. 91, 9–18.

Blattmann, T.M., Liu, Z., Zhang, Y., Zhao, Y., Haghipour, N., Montluçon, D.B., Plötze, M., Eglinton, T.I., 2019. Mineralogical control on the fate of continentally derived organic matter in the ocean. Science 366, 742–745. https://doi.org/10.1126/science.aax5345.

Brenon, I., Le Hir, P., 1999. Modelling the turbidity maximum in the Seine estuary (France): identification of formation processes. Estuar. Coast. Shelf Sci. 49, 525–544. https://doi.org/10.1006/ECSS.1999.0514.

Du, Z., Yu, Q., Peng, Y., Wang, L., Lin, H., Wang, Y., Gao, S., 2022. The formation of coastal turbidity maximum by tidal pumping in well-mixed inner shelves. J. Geophys. Res. Ocean. 127 https://doi.org/10.1029/2022JC018478.

Dyer, K.R., 1989. Sediment processes in estuaries: future research requirements. J. Geophys. Res. Ocean. 94, 14327–14339. https://doi.org/10.1029/JC094IC10P14327.

Dyer, K.R., Moffat, T.J., 1998. Fluxes of suspended matter in the East Anglian plume, Southern North Sea. Cont. Shelf Res. 18, 1311–1331. https://doi.org/10.1016/S0278-4343(98)00045-4.

Ehrhardt, M., Koeve, W., 1999. Determination of particulate organic carbon and nitrogen. In: Grasshoff, K., Kremling, K., Ehrhardt, M. (Eds.), Methods of Seawater Analysis, 3rd ed. Wiley, pp. 437–444. https://doi.org/10.1002/9783527613984.ch17.

Eisma, D., 1981. Supply and deposition of suspended matter in the North Sea. In: Nio, S.-D., Shüttenhelm, R.T.E., Van Weering, T.C.E. (Eds.), Holocene Marine Sedimentation in the North Sea Basin. Blackwell Publishing Ltd., Oxford, UK, pp. 415–428.

Eisma, D., 1986. Flocculation and de-flocculation of suspended matter in estuaries. Neth. J. Sea Res. 20, 183–199. https://doi.org/10.1016/0077-7579(86)90041-4.

Eisma, D., Kalf, J., 1987. Distribution, organic content and particle size of suspended matter in the North Sea. Neth. J. Sea Res. 21, 265–285. https://doi.org/10.1016/0077-7579(87)90002-0.

Engel, A., Endres, S., Galgani, L., Schartau, M., 2020. Marvelous marine microgels: on the distribution and impact of gel-like particles in the oceanic water-column. Front. Mar. Sci. 7 https://doi.org/10.3389/FMARS.2020.00405/FULL.

Fettweis, M., Baeye, M., 2015. Seasonal variation in concentration, size and settling velocity of muddy marine flocs in the benthic boundary layer. J. Geophys. Res. Oceans 120, 5648–5667. https://doi.org/10.1002/2014JC010644.

Fettweis, M., Houziaux, J.-S., Du Four, I., et al., 2009. Long-term influence of maritime access works on the distribution of cohesive sediments: analysis of historical and recent data from the Belgian nearshore area (southern North Sea). Geo-Marine Lett. 29, 321–330. https://doi.org/10.1007/S00367-009-0161-7/METRICS.

Fettweis, M., Schartau, M., Desmit, X., Lee, B.J., Terseleer, N., Van der Zande, D., Parmentier, K., Riethmüller, R., 2022. Organic matter composition of biomineral flocs and its influence on suspended particulate matter dynamics along a nearshore to offshore transect. J. Geophys. Res. Biogeosciences 127, e2021JG006332. https://doi.org/10.1029/2021JG006332.

Flemming, B.W., Delafontaine, M.T., 2000. Mass physical properties of muddy intertidal sediments: some applications, misapplications and non-applications. Cont. Shelf Res. 20, 1179–1197. https://doi.org/10.1016/S0278-4343(00)00018-2.

Gerritsen, H., Boon, J.G., Van der Kaaij, T., Vos, R.J., 2001. Integrated modelling of suspended matter in the North Sea. Estuar. Coast. Shelf Sci. 53, 581–594. https://doi.org/10.1006/ECSS.2000.0633.

Ho, Q.N., Fettweis, M., Spencer, K.L., Lee, B.J., 2022. Flocculation with heterogeneous composition in water environments: a review. Water Res. 213, 118147 https://doi.org/10.1016/j.watres.2022.118147.

Huthnance, J.M., 1991. Physical oceanography of the North Sea. Ocean Shorel. Manag. 16, 199–231. https://doi.org/10.1016/0951-8312(91)90005-M.

Ittekkot, V., Laane, R.W.P.M., 1991. Fate of riverine particulate organic matter. In: Degens, E.T., Kempe, S., Richey, J.E. (Eds.), Biogeochemistry of Major World Rivers, SCOPE Report 42. Wiley, Chichester, pp. 229–239.

Jago, C.F., Bale, A.J., Green, M.O., et al., 1994. Resuspension processes and seston dynamics, southern North Sea, p. 97–113. In: Charnock, H., Dyer, K.R., Huthnance, J.M., Liss, P.S., Simpson, J.H., Tett, P.B. (Eds.), Understanding the North Sea System. Chapman & Hall, for the Royal Society, Springer, Dordrecht.

Jung, A.S., Bijkerk, R., Van Der Veer, H.W., Philippart, C.J.M., 2017. Spatial and temporal trends in order richness of marine phytoplankton as a tracer for the

exchange zone between coastal and open waters. J. Mar. Biol. Assoc. United Kingdom 97, 477–489. https://doi.org/10.1017/S0025315416001326.
Keil, R.G., Montluçon, D.B., Prahl, F.G., Hedges, J.I., 1994. Sorptive preservation of labile organic matter in marine sediments. Nature 370, 549–552. https://doi.org/10.1038/370549a0.
Kopte, R., Becker, M., Holtermann, P., Winter, C., 2022. Tides, stratification, and counter rotation: the German bight ROFI in comparison to other regions of freshwater influence. J. Geophys. Res. Ocean. 127, e2021JC018236 https://doi.org/10.1029/2021JC018236.
Maerz, J., Hofmeister, R., Van Der Lee, E.M., Gräwe, U., Riethmüller, R., Wirtz, K.W., 2016. Maximum sinking velocities of suspended particulate matter in a coastal transition zone. Biogeosciences 13, 4863–4876. https://doi.org/10.5194/BG-13-4863-2016.
Maggi, F., Tang, F.H.M., 2015. Analysis of the effect of organic matter content on the architecture and sinking of sediment aggregates. Mar. Geol. 363, 102–111. https://doi.org/10.1016/j.margeo.2015.01.017.
Manheim, T.F., Hathaway, J.C., Uchupi, E., 1972. Suspended matter in surface waters of the Northern Gulf of Mexico. Limnol. Oceanogr. 17, 17–27. https://doi.org/10.4319/lo.1972.17.1.0017.
Moulton, M., Suanda, S.H., Garwood, J.C., Kumar, N., Fewings, M.R., Pringle, J.M., 2023. Exchange of plankton, pollutants and particles across the nearshore region. Ann. Rev. Mar. Sci. 15 (1), 167–202. https://doi.org/10.1146/annurev-marine-032122-115057.
Nechad, B., Ruddick, K., Neukermans, G., 2009. Calibration and validation of a generic multisensor algorithm for mapping of turbidity in coastal waters. In: SPIE "Remote Sensing of the Ocean, Sea Ice, and Large Water Regions" Conference held in Berlin (Germany), 31 August 2009. Proc. SPIE Vol. 7473, 74730H.
Nechad, B., Ruddick, K.G., Park, Y., 2010. Calibration and validation of a generic multisensor algorithm for mapping of total suspended matter in turbid waters. Remote Sens. Environ. 114, 854–866.
Neukermans, G., Ruddick, K., Loisel, H., 2012. Optimization and quality control of suspended particulate matter concentration measurement using turbidity measurements. Limnol. Oceanogr. Methods 10, 1011–1023. https://doi.org/10.4319/LOM.2012.10.1011.
Novoa, S., Doxaran, D., Ody, A., et al., 2017. Atmospheric corrections and multi-conditional algorithm for multi-sensor remote sensing of suspended particulate matter in low-to-high turbidity levels coastal waters. Remote Sens. (Basel) 9, 61. https://doi.org/10.3390/RS9010061.
Otto, L., Zimmerman, J.T.F., Furnes, G.K., Mork, M., Saetre, R., Becker, G., 1990. Review of the physical oceanography of the North Sea. Netherlands J. Sea Res. 26, 161–238. https://doi.org/10.1016/0077-7579(90)90091-T.
Pawlowicz, R., 2020. M_Map: A mapping package for MATLAB, version 1.4 m [Computer software], available online at www.eoas.ubc.ca/~rich/map.html.
Pietrzak, J.D., de Boer, G.J., Eleveld, M.A., 2011. Mechanisms controlling the intra-annual mesoscale variability of SST and SPM in the southern North Sea. Cont. Shelf Res. 31, 594–610. https://doi.org/10.1016/j.csr.2010.12.014.
Postma, H., 1981. Exchange of materials between the North Sea and the Wadden Sea. Mar. Geol. 40, 199–213. https://doi.org/10.1016/0025-3227(81)90050-5.
Postma, H., 1984. Introduction to the symposium on organic matter in the Wadden Sea. Netherlands Inst. Sea Res. - Publ. Ser. 10, 15–22.
Prandle, D., Ballard, G., Flatt, D., et al., 1996. Combining modelling and monitoring to determine fluxes of water, dissolved and particulate metals through the Dover Strait. Cont. Shelf Res. 16, 237–257. https://doi.org/10.1016/0278-4343(95)00009-P.
Prandle, D., Hydes, D.J., Jarvis, J., McManus, J., 1997. The seasonal cycles of temperature, salinity, nutrients and suspended sediment in the southern North Sea in 1988 and 1989. Estuar. Coast. Shelf Sci. 45, 669–680. https://doi.org/10.1006/ecss.1996.0227.
Rijnsburger, S., van der Hout, C., van Tongeren, O., de Boer, G., van Prooijen, B.C., Borst, W.G., Pietrzak, J.D., 2016. Simultaneous measurements of tidal straining and advection at two parallel transects far downstream in the Rhine ROFI. Ocean Dyn. 66, 719–736. https://doi.org/10.1007/s10236-016-0947-x.
Röttgers, R., Heymann, K., Krasemann, H., 2014. Suspended matter concentrations in coastal waters: methodological improvements to quantify individual measurement uncertainty. Estuar. Coast. Shelf Sci. 151, 148–155. https://doi.org/10.1016/j.ecss.2014.10.010.
Schartau, M., Riethmüller, R., Flöser, G., van Beusekom, J.E.E., Krasemann, H., Hofmeister, R., Wirtz, K., 2019. On the separation between inorganic and organic fractions of suspended matter in a marine coastal environment. Prog. Oceanogr. 171, 231–250. https://doi.org/10.1016/j.pocean.2018.12.011.
Simpson, J.H., Brown, J., Matthews, J., Allen, G., 1990. Tidal straining, density currents, and stirring in the control of estuarine stratification. Estuaries 13, 125–132. https://doi.org/10.2307/1351581/METRICS.
Stavn, R.H., Rick, H.J., Falster, A.V., 2009. Correcting the errors from variable sea salt retention and water of hydration in loss on ignition analysis: implications for studies of estuarine and coastal waters. Estuar. Coast. Shelf Sci. 81, 575–582. https://doi.org/10.1016/j.ecss.2008.12.017.
Van Leeuwen, S., Tett, P., Mills, D., van der Molen, J., 2015. Stratified and nonstratified areas in the North Sea: long-term variability and biological and policy implications. J. Geoph. Res. Ocean. 120, 4670–4686. https://doi.org/10.1002/2014JC010485.
Yu, M., Yu, X., Mehta, A.J., Manning, A.J., 2023. Persistent reshaping of cohesive sediment towards stable flocs by turbulence. Sci. Rep. 13, 1760. https://doi.org/10.1038/s41598-023-28960-y.

APPENDIX 3

Tidal cycle at MOW1 January 2019 (2019/01)

23/01 18h00 – 24/01 06h00

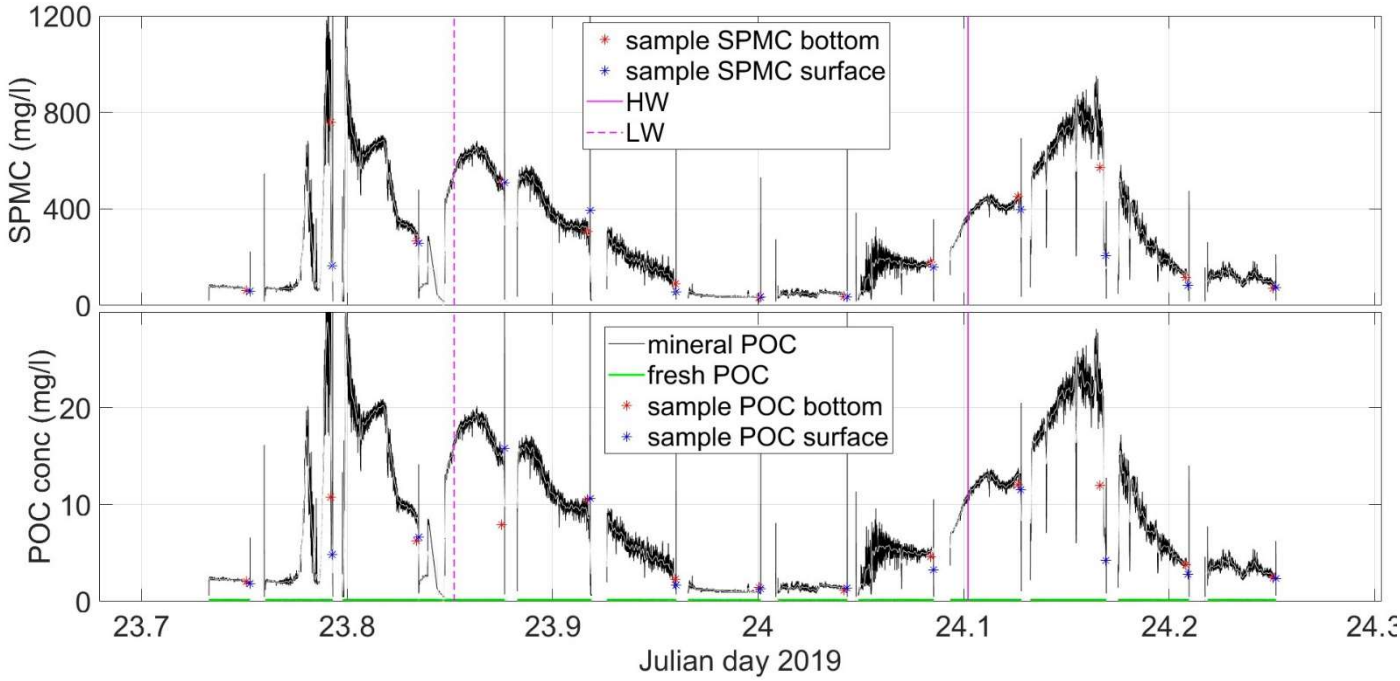

Figure A3.1: Time series of OBS-derived SPM concentration and SPM-derived mineral and fresh POC during a tidal cycle. The sample SPM and POC concentrations are shown. Period: 23/01/2019 18h00 – 24/01/2019 06h00; LW: 23/01 20h27, HW: 24/01 02h27.

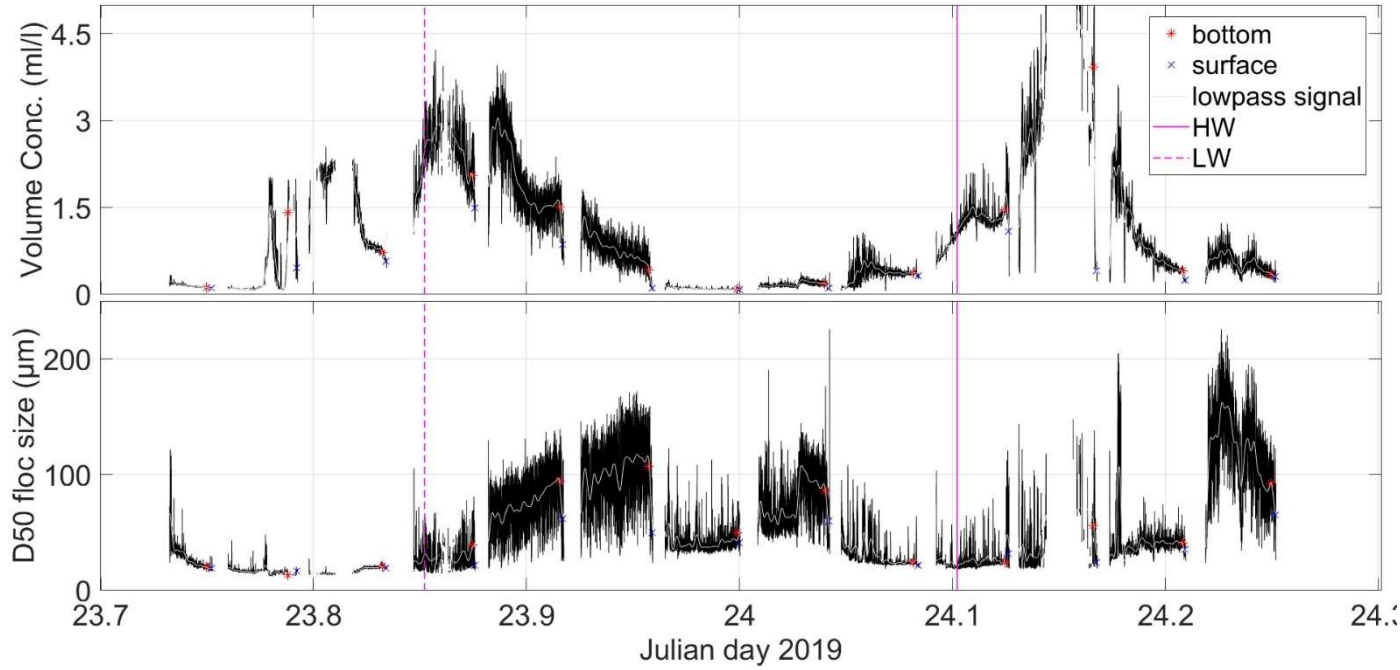

Figure A3.2: Time series of LISST-derived SPM volume concentration and median floc size during a tidal cycle. The values at surface and bottom are are shown. . Period: 23/01/2019 18h00 – 24/01/2019 06h00; LW: 23/01 20h27, HW: 24/01 02h27.

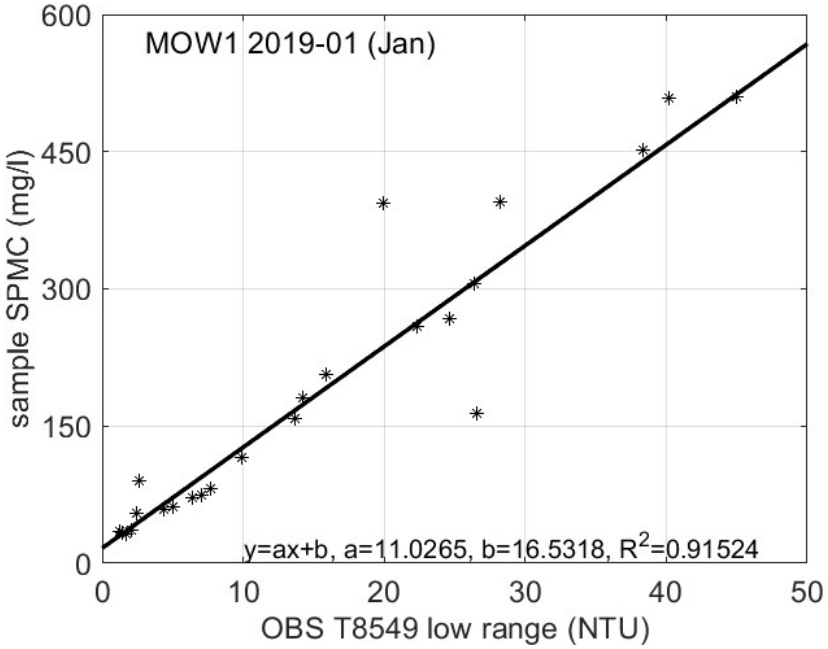

Figure A3.3: Calibration of OBS with water samples

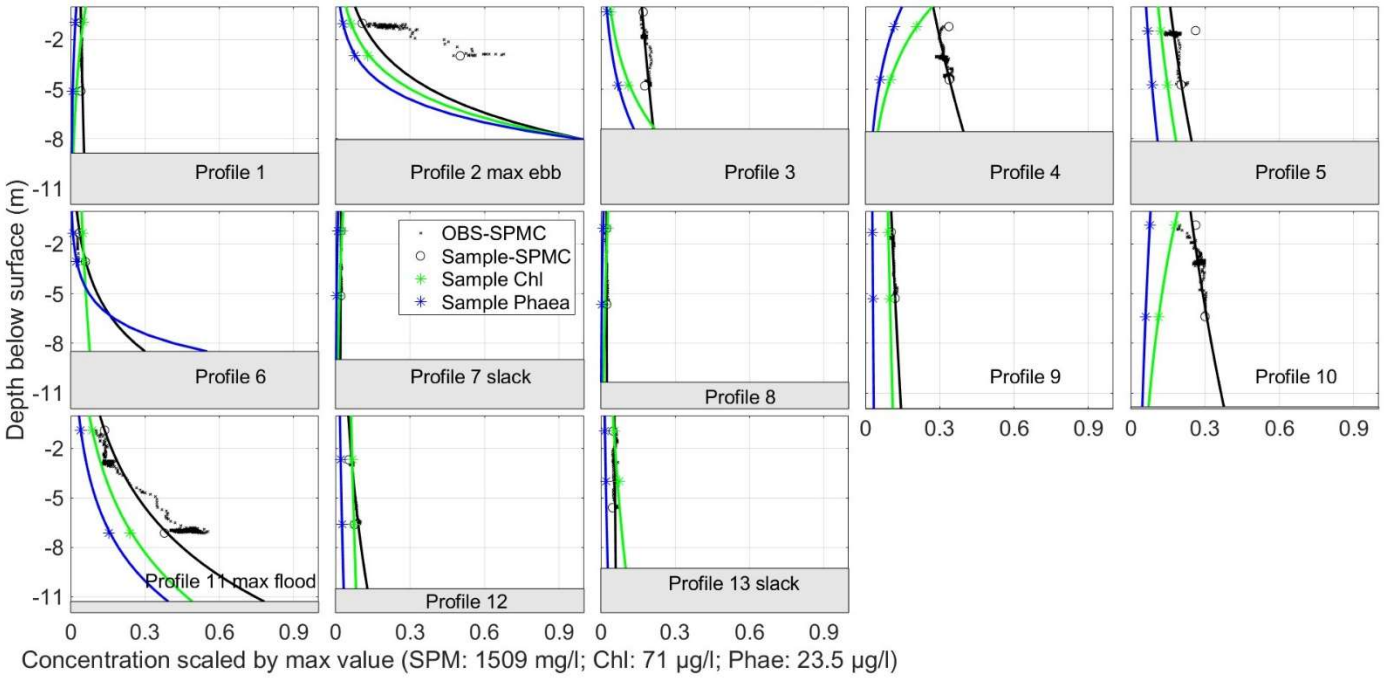

Figure A3.4: OBS and sample-derived SPM concentration profile (black), sample-derived Chl profiles (green) and sample-derived Phaeophytin-a (blue). Values are scaled by maximum value. Period: 23/01/2019 18h00 – 24/01/2019 06h00.

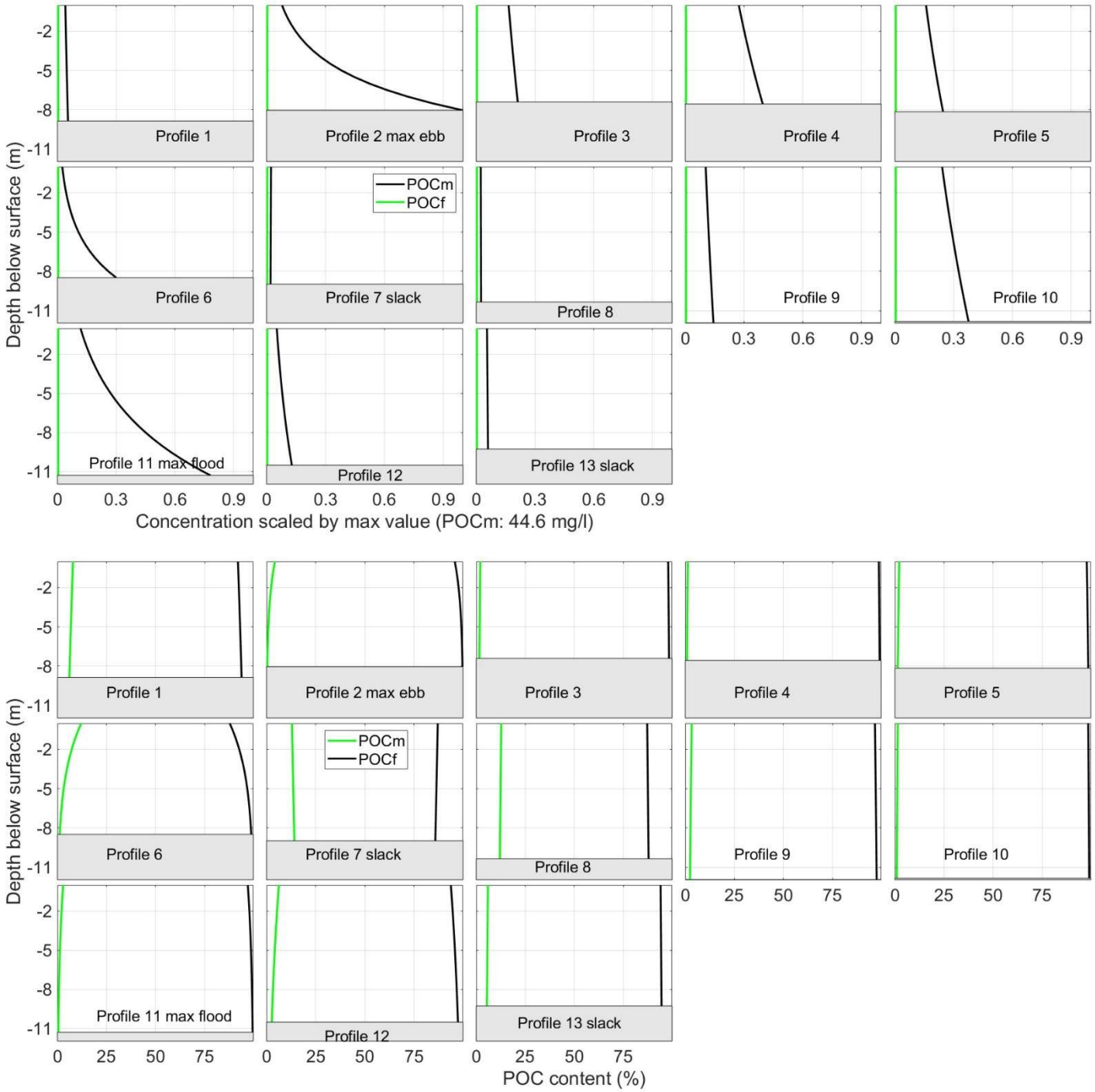

Figure A3.5: (above) Model-derived fresh and mineral-attached POC concentration profiles (values are scaled by maximum POCm); (below) relative content of fresh and mineral attached POC profiles. Period: 23/01/2019 18h00 – 24/01/2019 06h00.

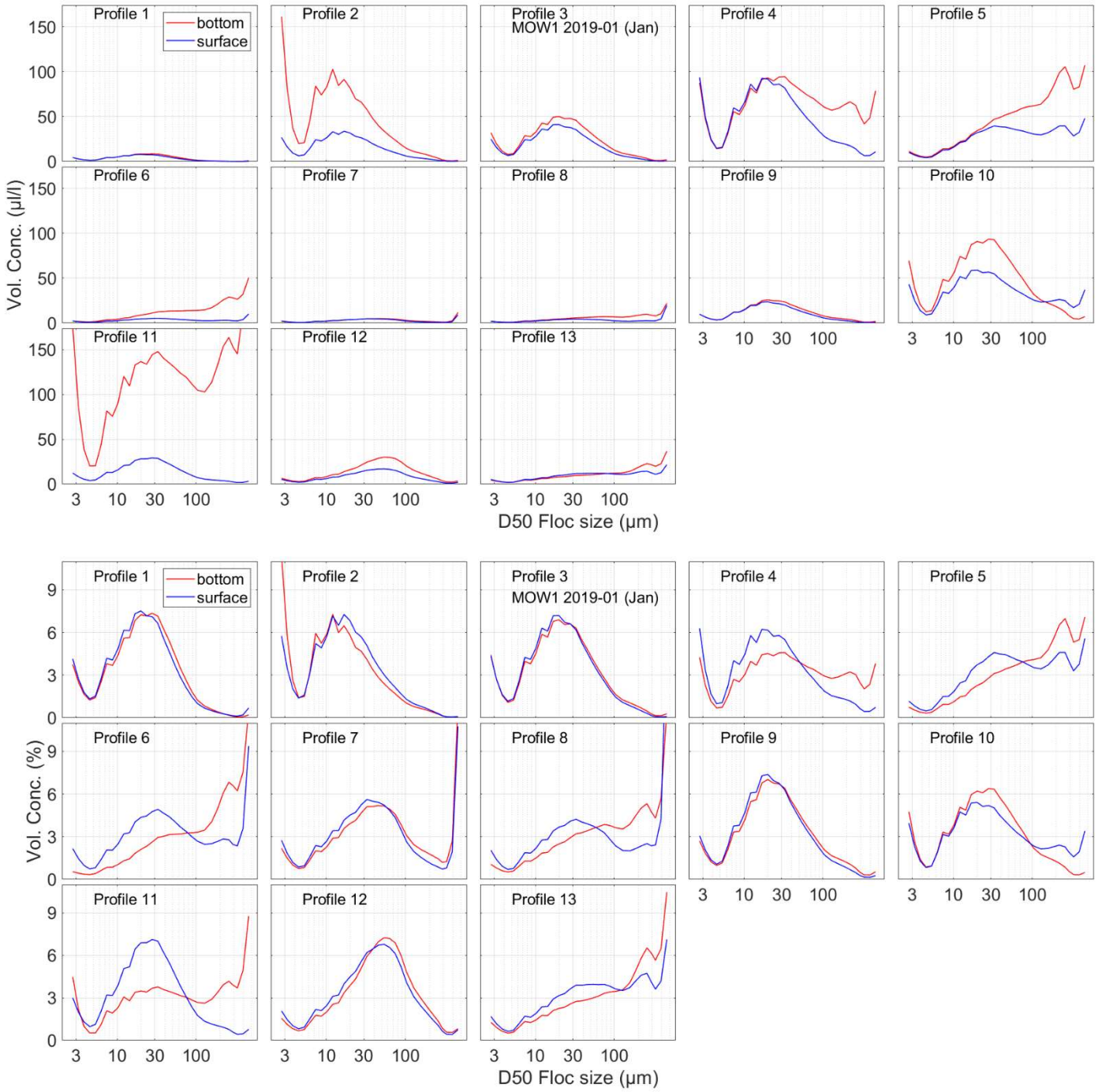

Figure A3.6: Floc size distribution (above in µl/l, below in %) at bottom and surface. Period: 23/01/2019 18h00 – 24/01/2019 06h00.

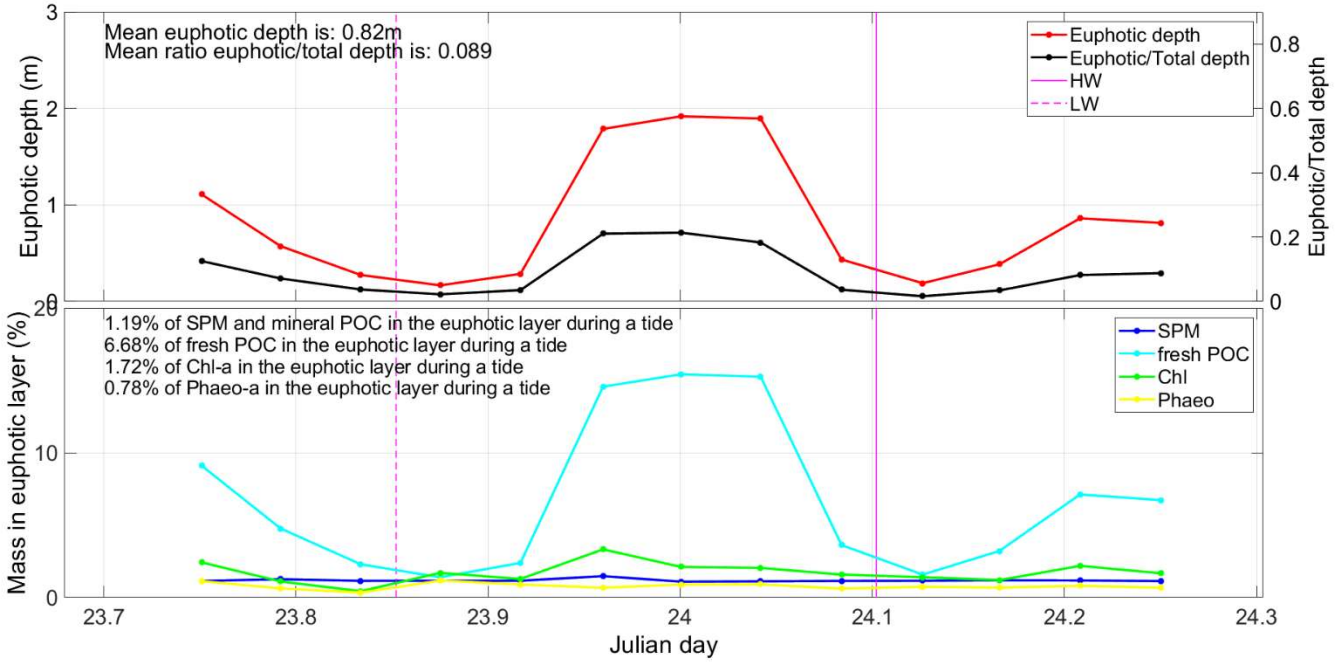

Figure A3.7: (Above) Euphotic layer depth and the ratio euphotic:total depth; (below) Probability of SPM and POC (fresh and mineral) of being in the euphotic layer. Period: 23/01/2019 18h00 – 24/01/2019 06h00; LW: 23/01 20h27, HW: 24/01 02h27.

APPENDIX 4

Tidal cycle at MOW1 February 2019 (2019/03)

12/02 18h00 – 13/02 06h00

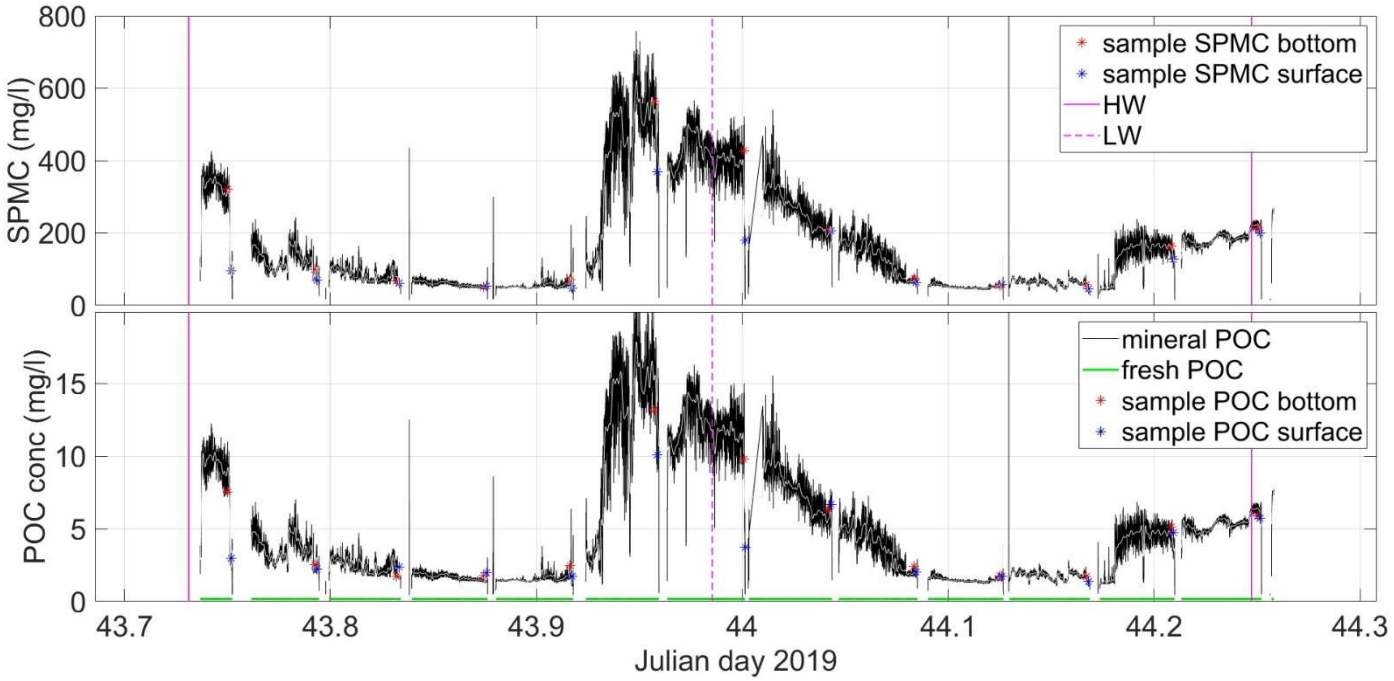

Figure A4.1: Time series of OBS-derived SPM concentration and SPM-derived mineral and fresh POC during a tidal cycle. The sample SPM and POC concentrations are also shown. Period: 12/02/2019 18h00 – 13/02/2019 06h00; HW 12/03 18h33; LW: 12/03 23h39; HW: 13/0305h56.

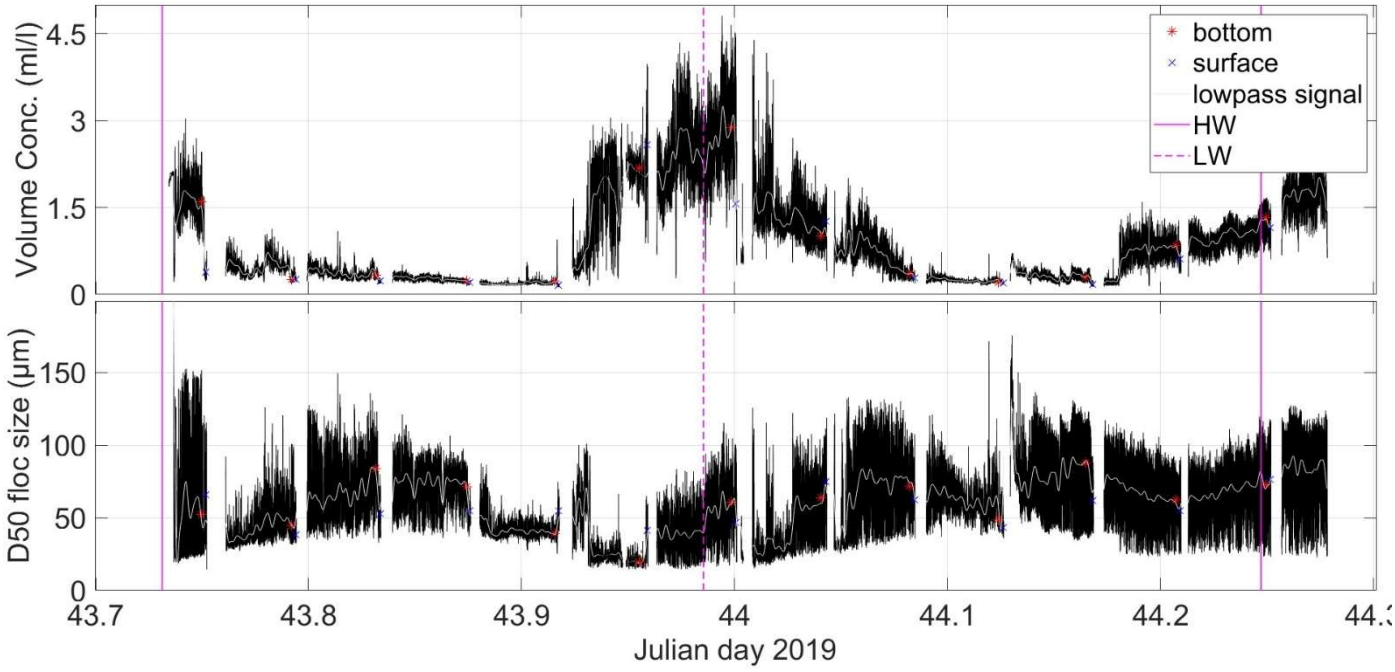

Figure A4.2: Time series of LISST-derived SPM volume concentration and median floc size during a tidal cycle. The values at surface and bottom are are also shown. Period: 12/02/2019 18h00 – 13/02/2019 06h00; HW 12/03 18h33; LW: 12/03 23h39; HW: 13/0305h56.

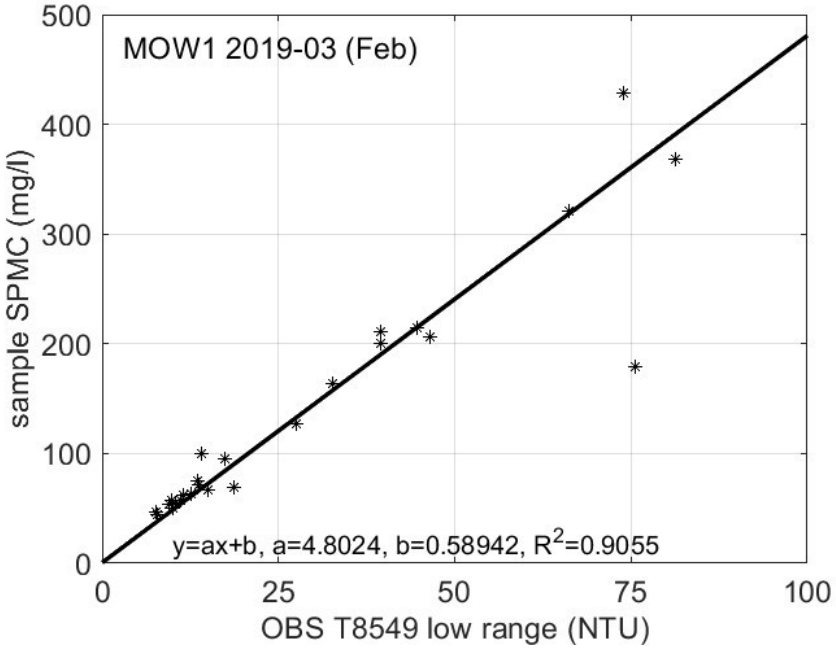

Figure A4.3: Calibration of OBS with water samples

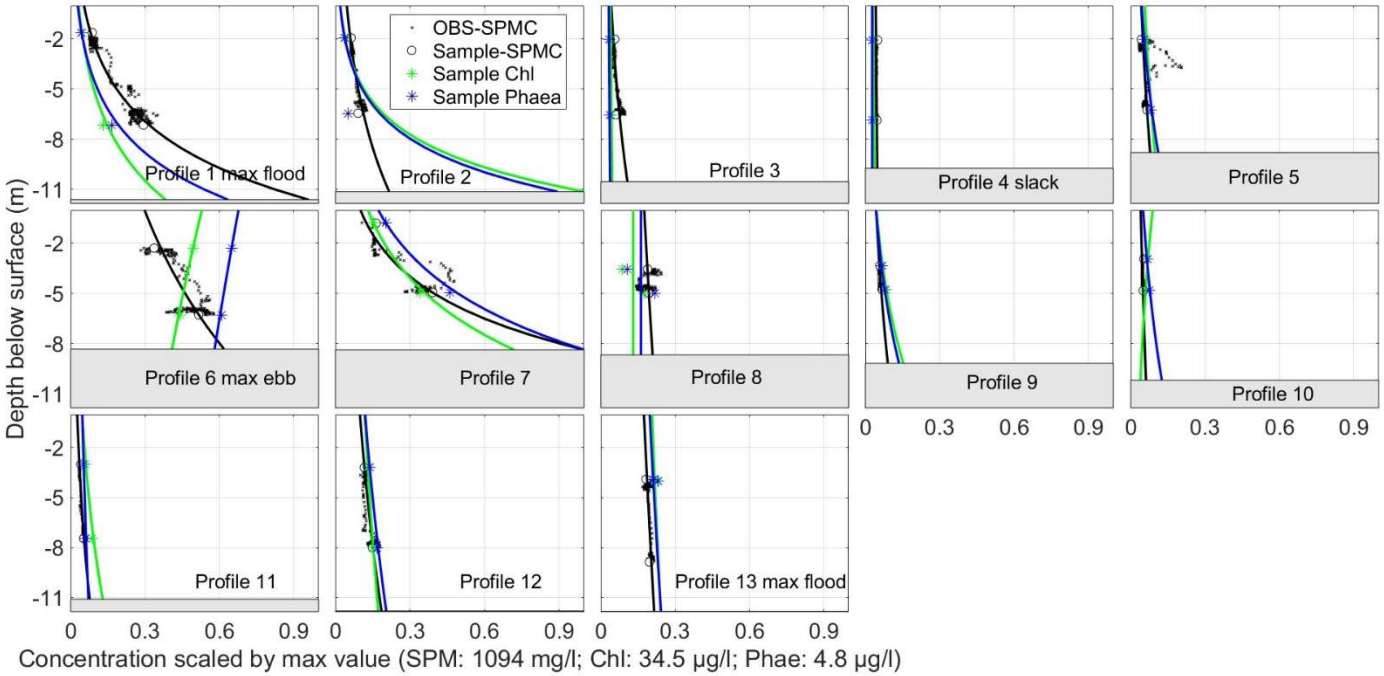

Figure A4.4: OBS and sample-derived SPM concentration profile (black), sample-derived Chl profiles (green) and sample-derived Phaeophytin-a (blue). Values are scaled by maximum value. Period: 12/02/2019 18h00 – 13/02/2019 06h00.

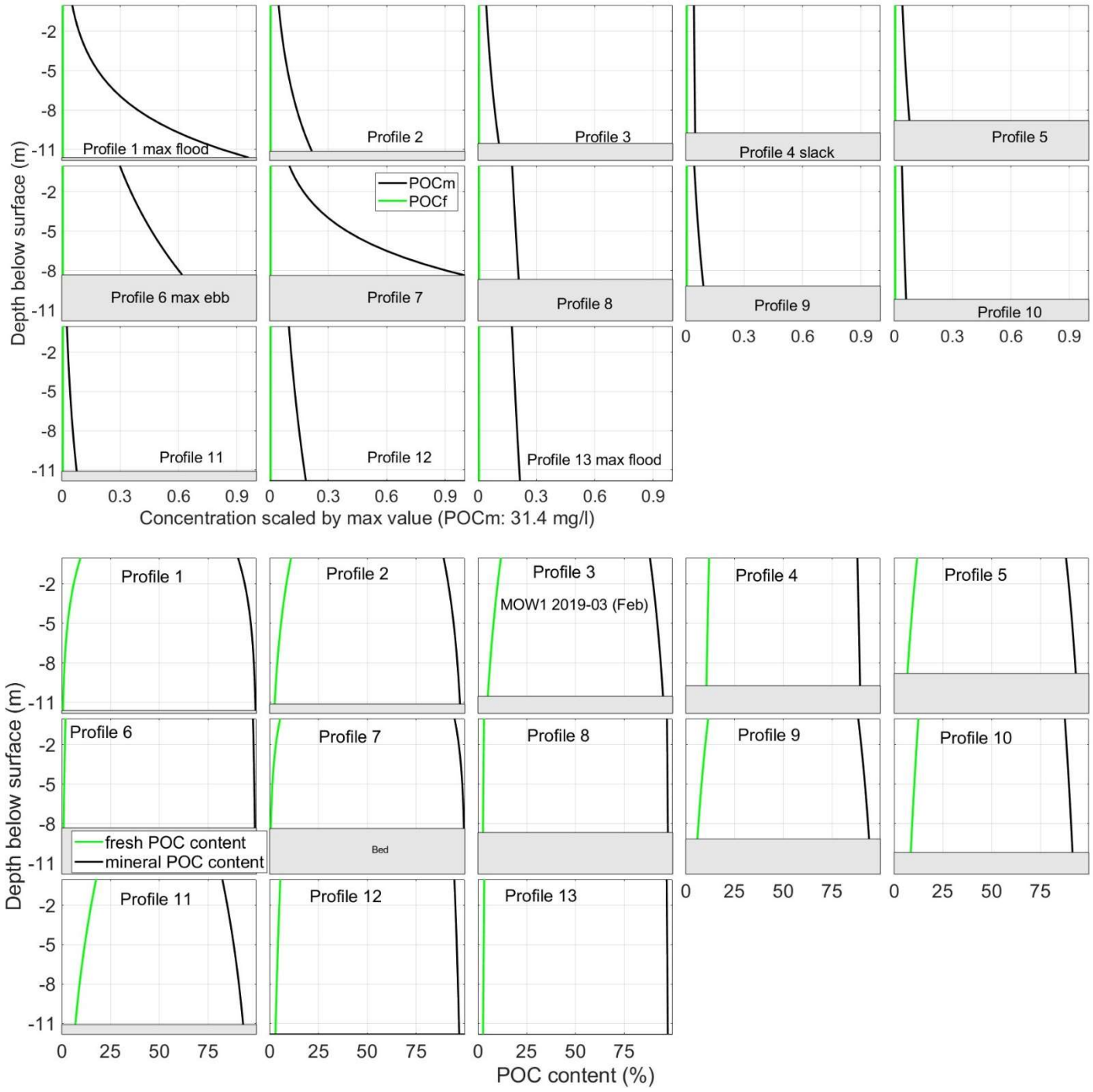

Figure A4.5: (above) Model-derived fresh and mineral-attached POC concentration profiles (values are scaled by maximum POCm); (below) relative content of fresh and mineral attached POC profiles. Period: 12/02/2019 18h00 – 13/02/2019 06h00

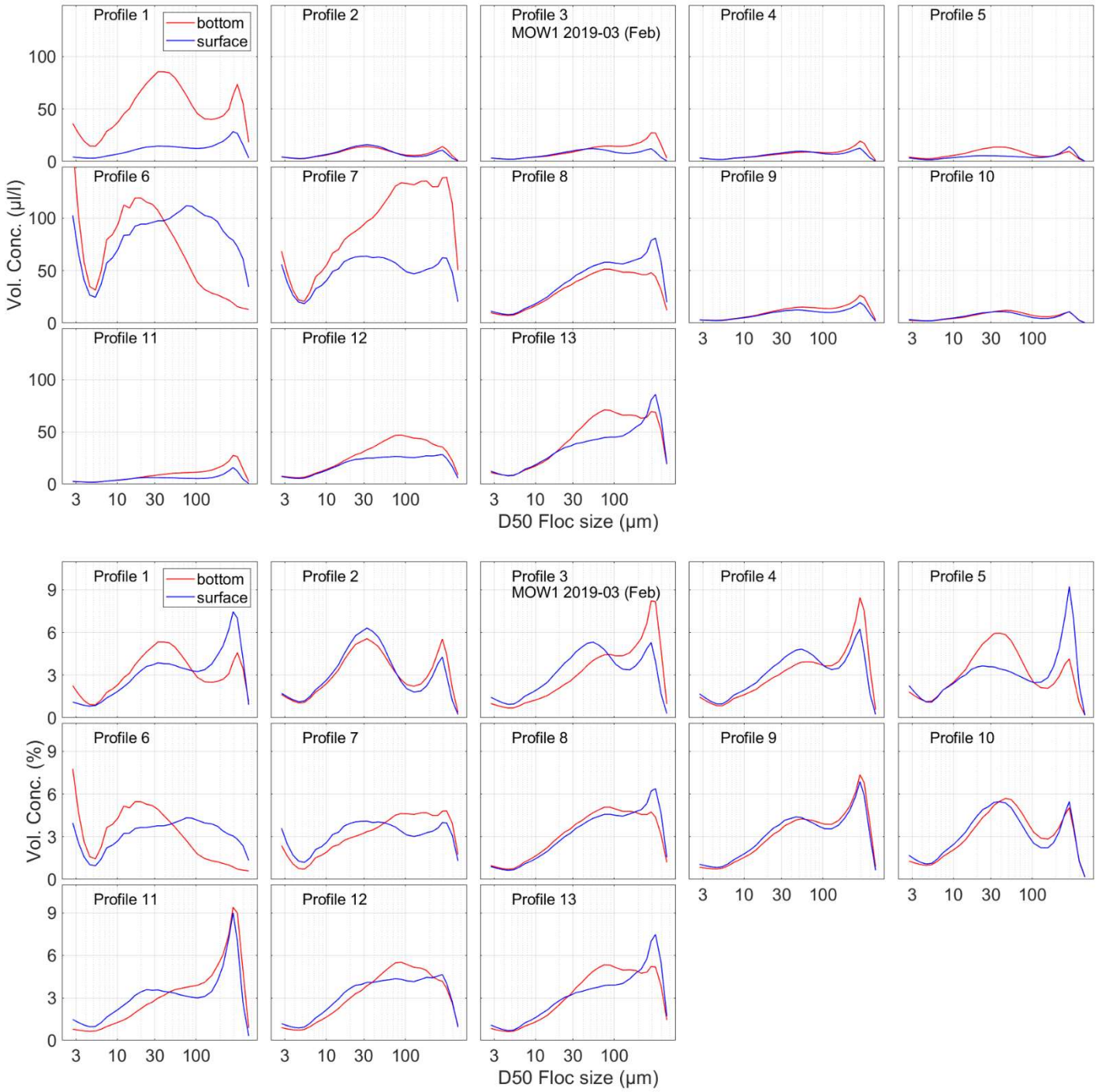

Figure A4.6: Floc size distribution (above in µl/l, below in %) at bottom and surface. Period: 12/02/2019 18h00 – 13/02/2019 06h

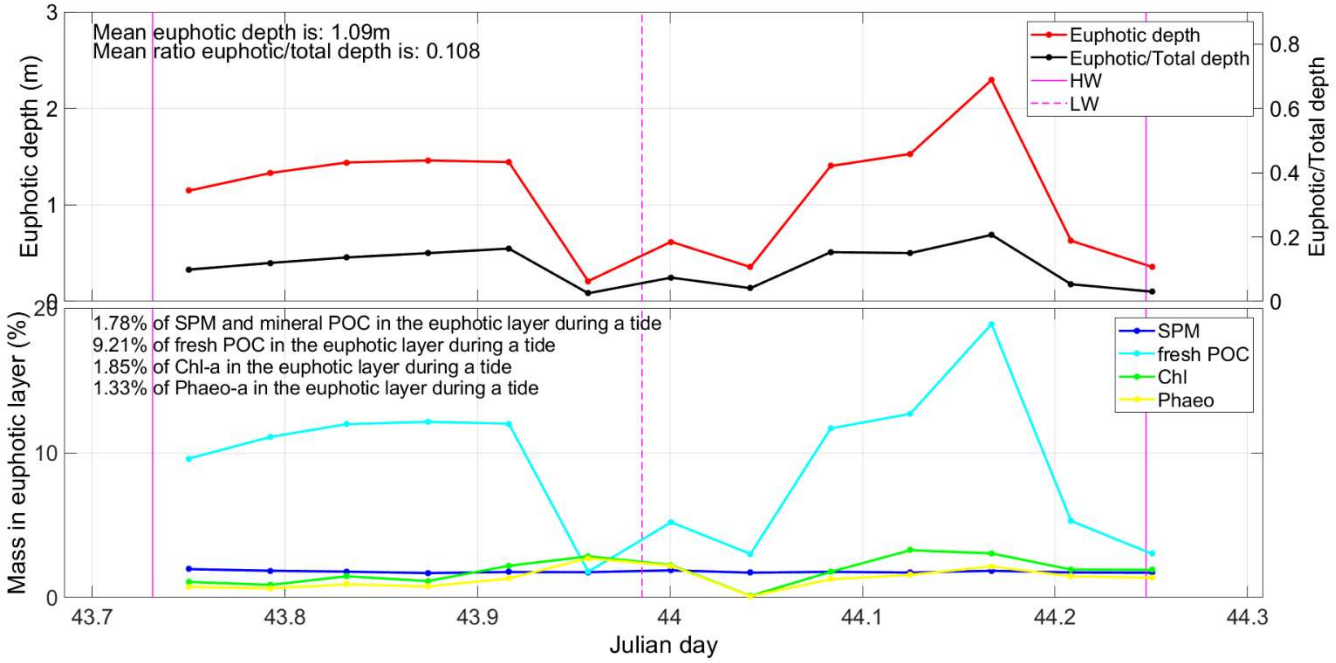

Figure A4.7: (Above) Euphotic layer depth and the ratio euphotic:total depth; (below) Probability of SPM, Chl, Phaeophytine and POC (fresh and mineral) of being in the euphotic layer. Period: 12/02/2019 18h00 – 13/02/2019 06h00; HW 12/03 18h33; LW: 12/03 23h39; HW: 13/0305h56.

APPENDIX 5

Tidal cycle at MOW1 March 2019 (2019/07)

11/03 20h00 – 12/03 08h00

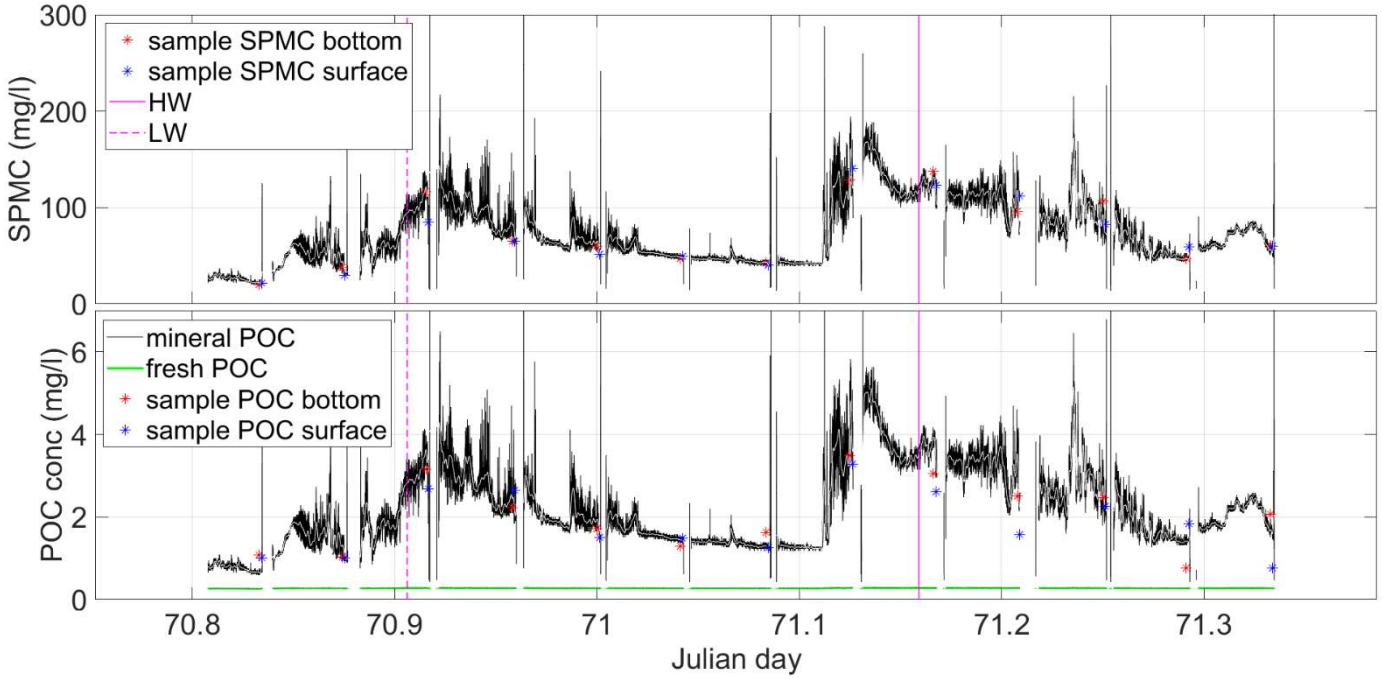

Figure A5.1: Time series of OBS-derived SPM concentration and SPM-derived mineral and fresh POC during a tidal cycle. The sample SPM and POC concentrations are also shown. Period 11/03/2019 20h00 – 12/03/2019 08h00; LW: 12/03 22h23; HW: 13/03 04h32.

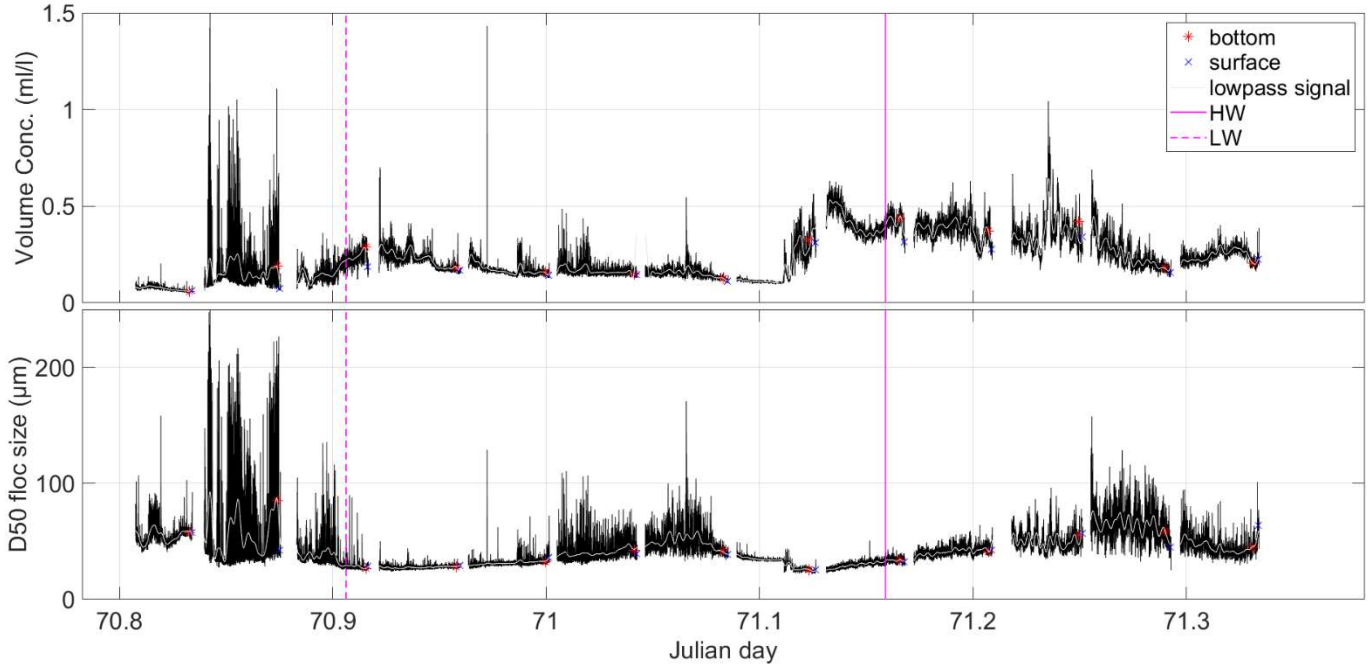

Figure A5.2: Time series of LISST-derived SPM volume concentration and median floc size during a tidal cycle. The values at surface and bottom are are also shown. Period 11/03/2019 20h00 – 12/03/2019 08h00; LW: 12/03 22h23; HW: 13/03 04h32.

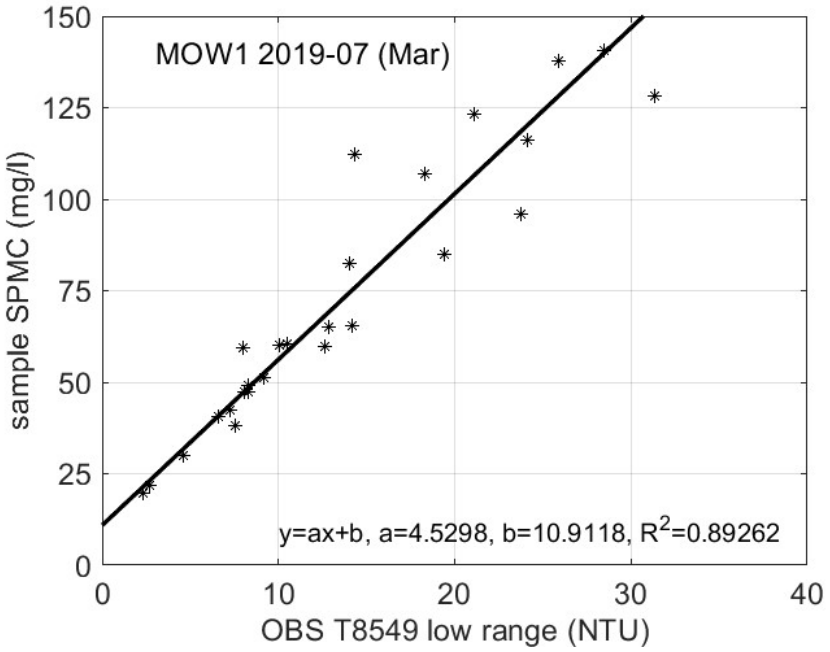

Figure A5.3: Calibration of OBS with water samples

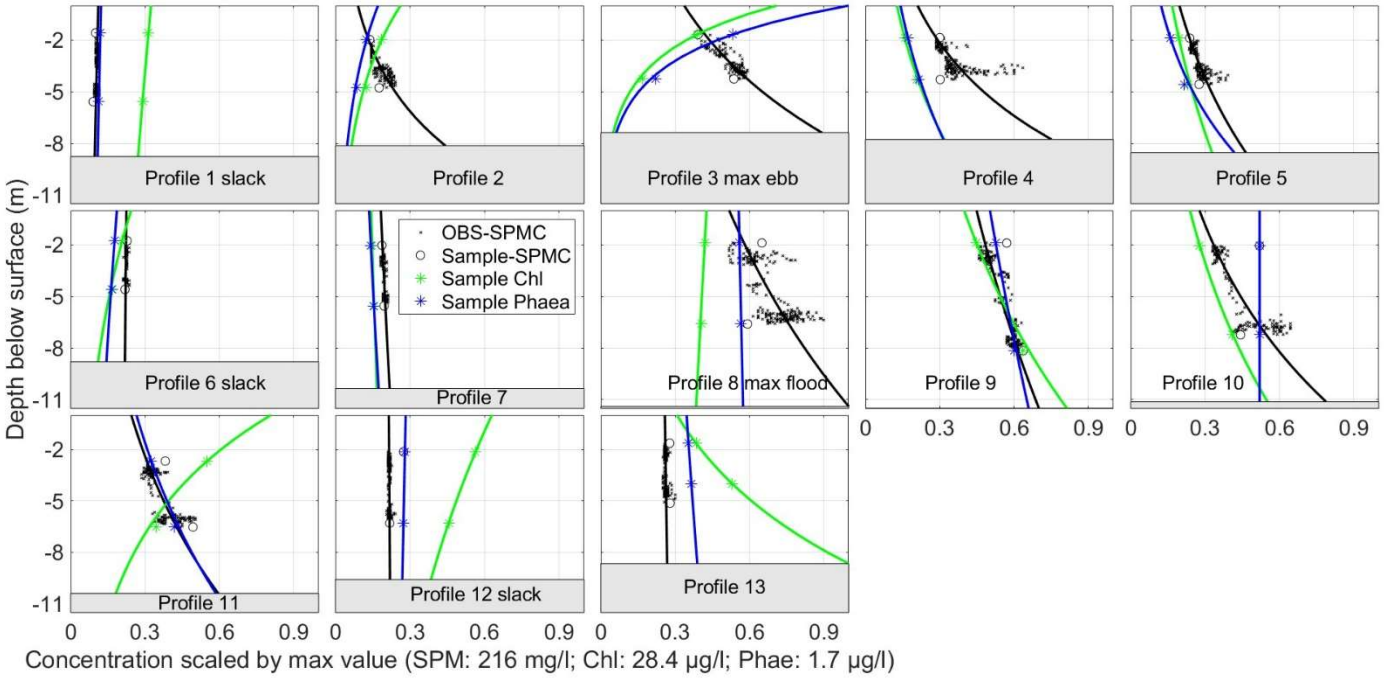

Figure A5.4 : OBS and sample-derived SPM concentration profile (black), sample-derived Chl profiles (green) and sample-derived Phaeophytin-a (blue). Values are scaled by maximum value. Period 11/03/2019 20h00 – 12/03/2019 08h00.

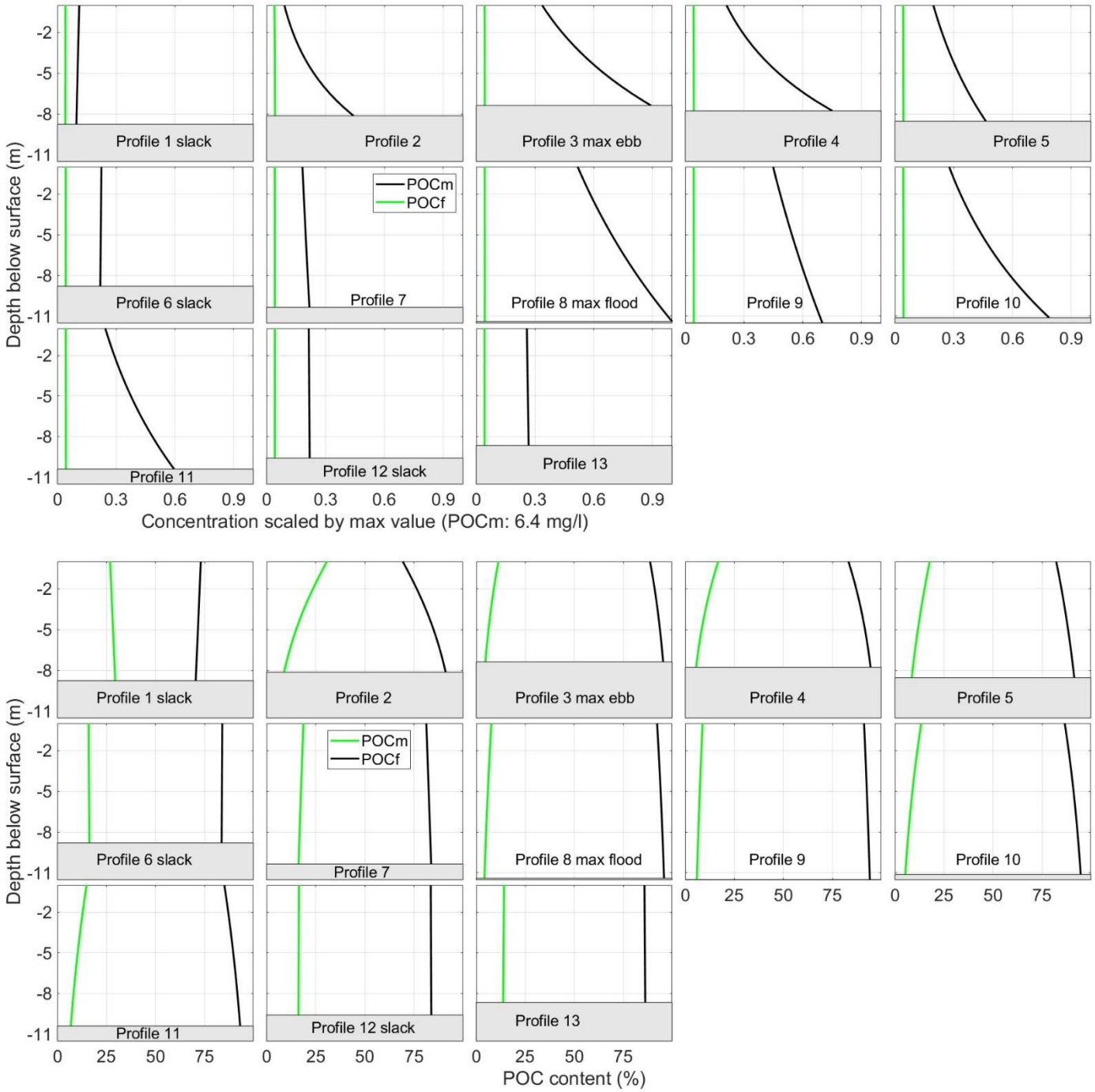

Figure A5.5: : (above) Model-derived fresh and mineral-attached POC concentration profiles (values are scaled by maximum POCm); (below) relative content of fresh and mineral attached POC profiles. Period 11/03/2019 20h00 – 12/03/2019 08h00.

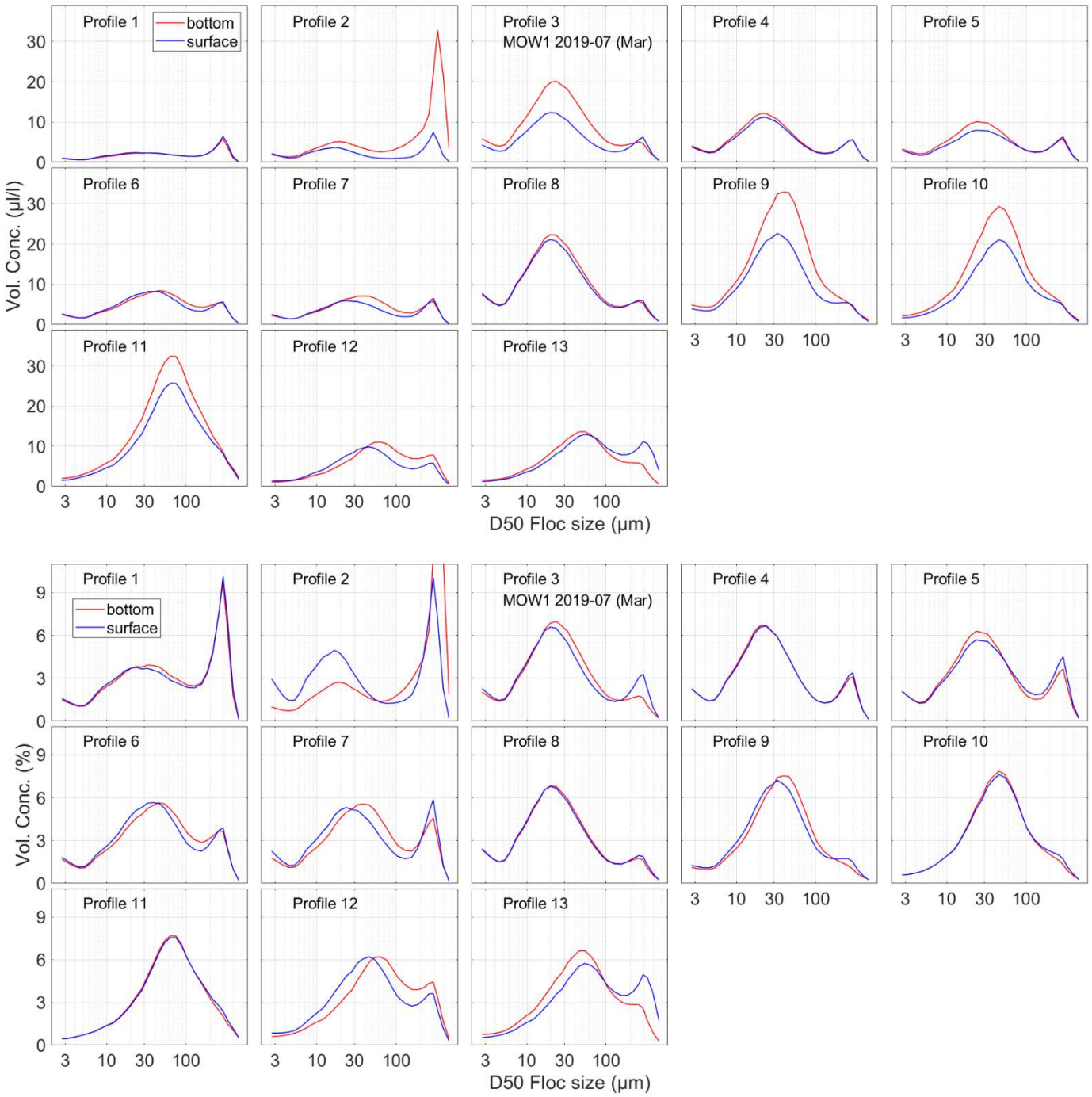

Figure A5.6: Floc size distribution (above in µl/l, below in %) at bottom and surface. Period 11/03/2019 20h00 – 12/03/2019 08h00.

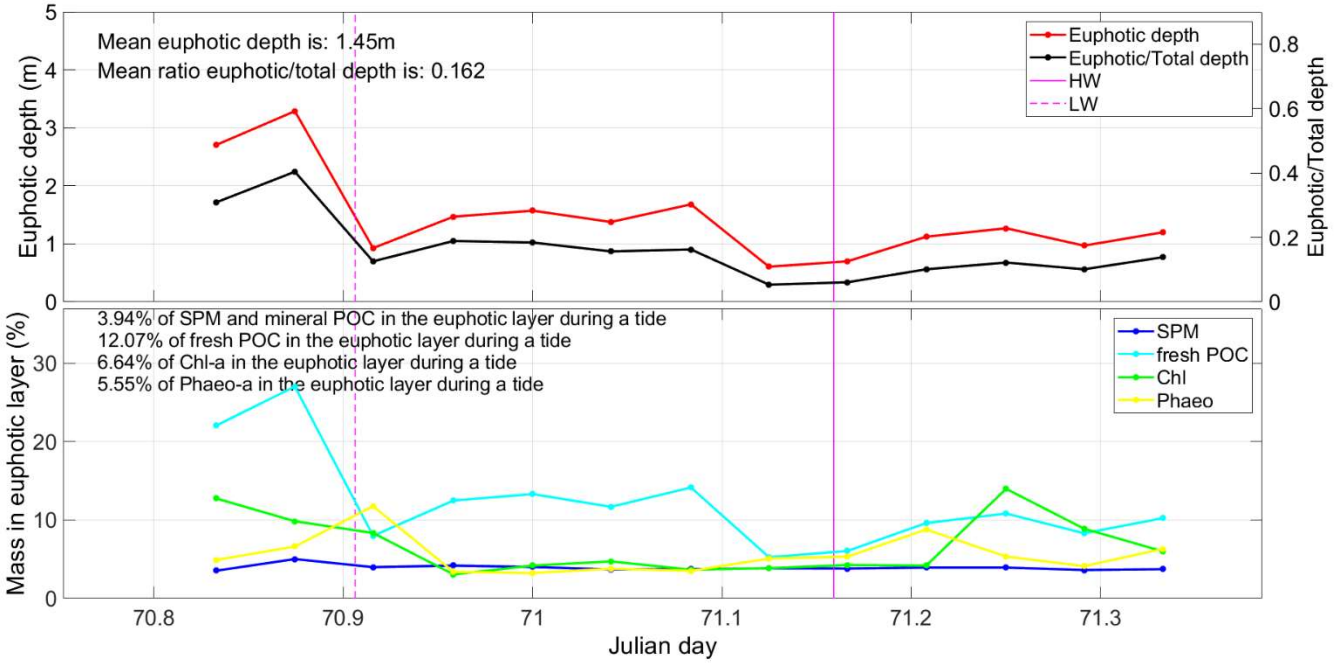

Figure A5.7: (Above) Euphotic layer depth and the ratio euphotic:total depth; (below) Probability of SPM, Chl, Phaeophytine and POC (fresh and mineral) of being in the euphotic layer. Period 11/03/2019 20h00 – 12/03/2019 08h00; LW: 12/03 22h23; HW: 13/03 04h32.

APPENDIX 6

Tidal cycle at MOW1 April 2019 (2019/11)

09/04 11h00 – 09/04 23h00

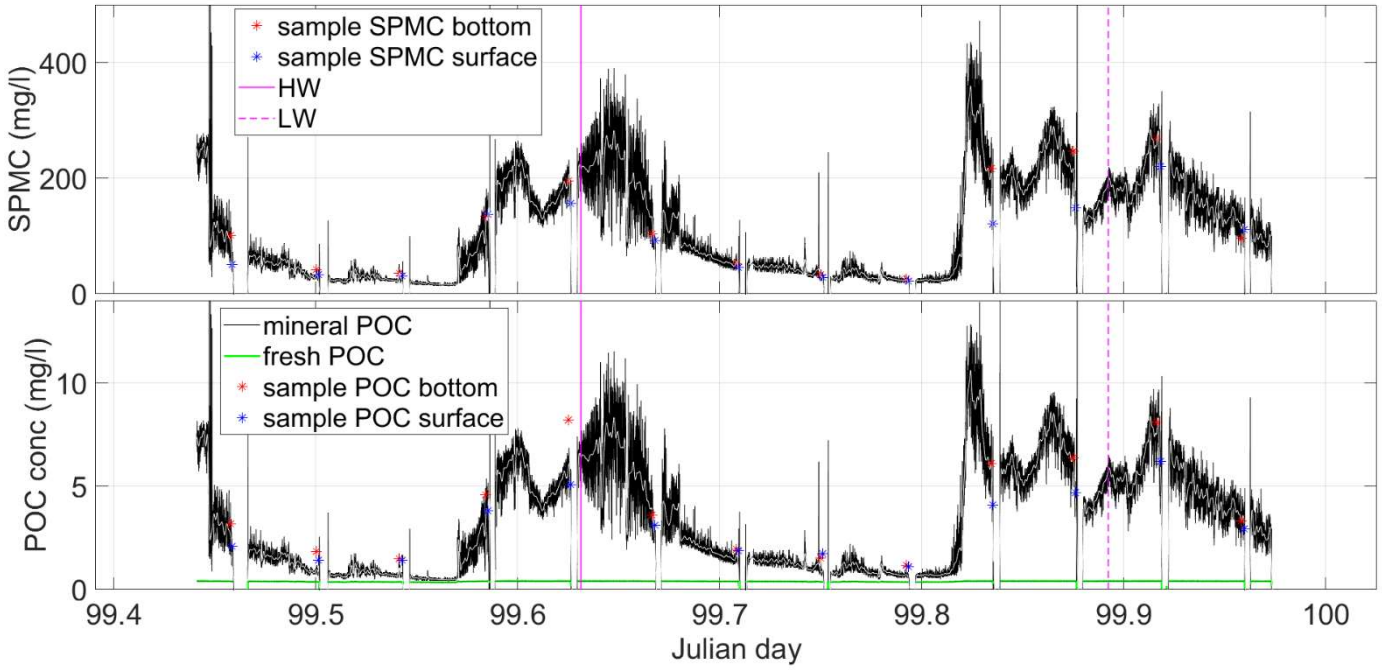

Figure A6.1: Time series of OBS-derived SPM concentration and SPM-derived mineral and fresh POC during a tidal cycle. The sample SPM and POC concentrations are also shown. Period: 9/04/2019 11h00-23h00. HW: 15h09; LW: 21h25

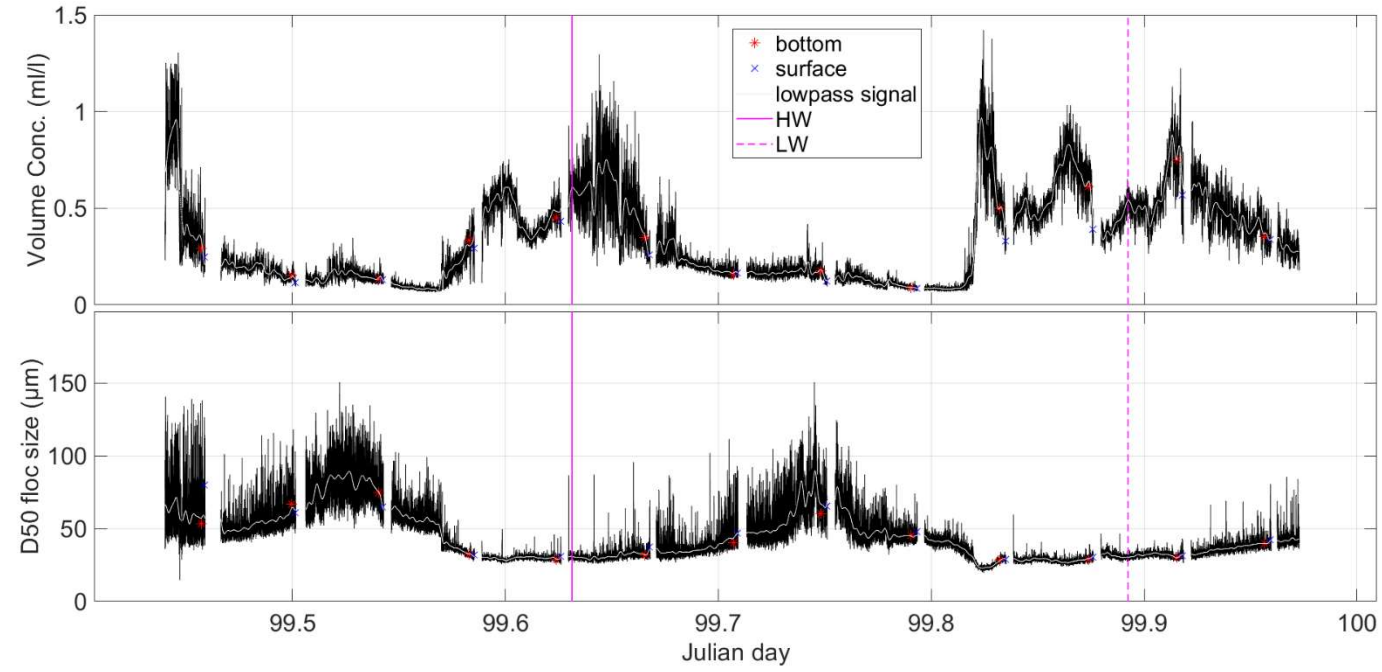

Figure A6.2: Time series of LISST-derived SPM volume concentration and median floc size during a tidal cycle. The values at surface and bottom are are also shown. Period: 9/04/2019 11h00-23h00. HW: 15h09; LW: 21h25

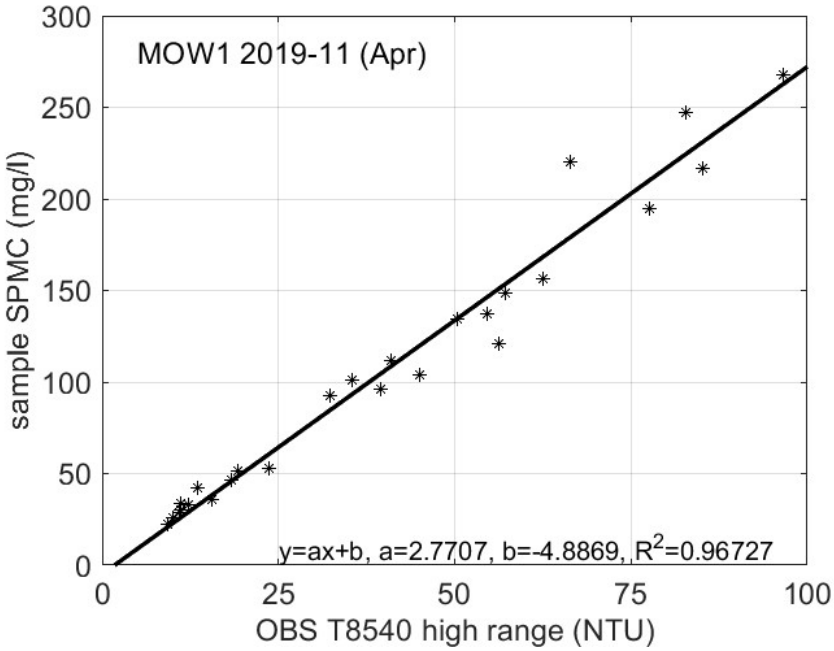

Figure A6.3: Calibration of OBS with water samples

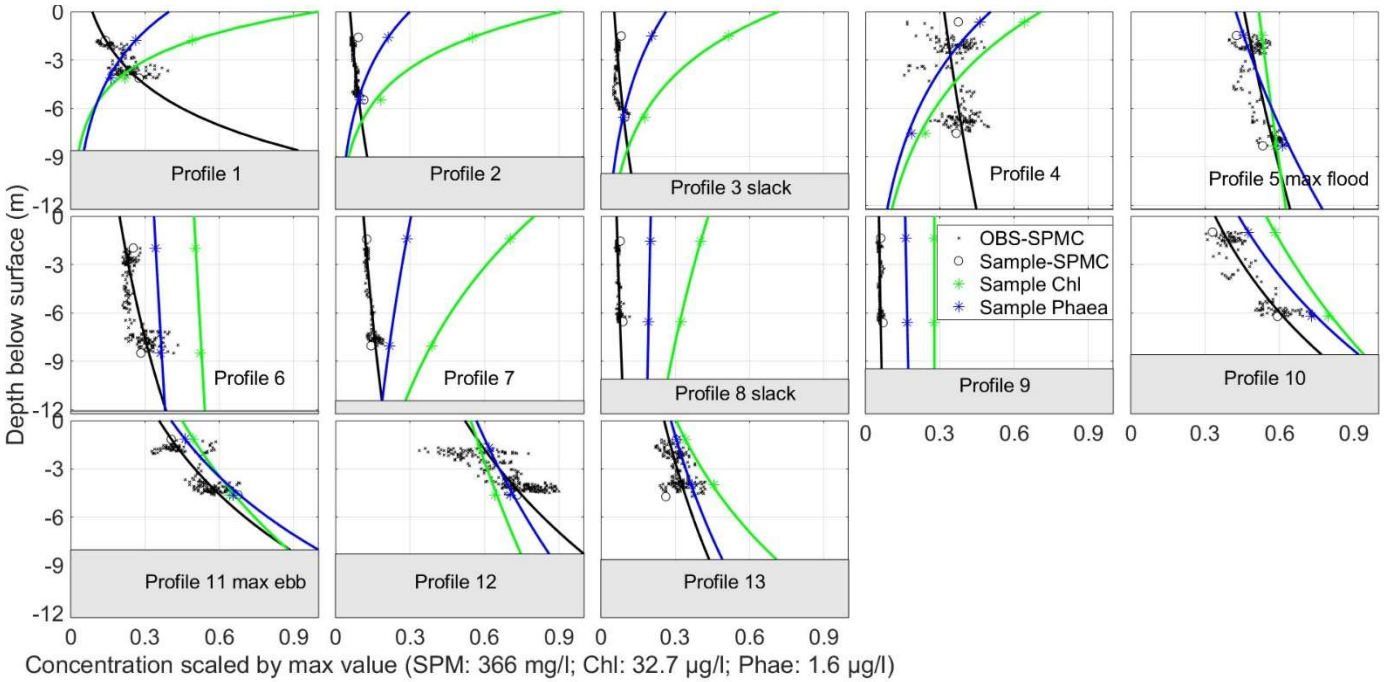

Figure A6.4 Sample-derived SPM concentration profile (black), sample-derived Chl profiles (green) and sample-derived Phaeophytin-a (blue). Values are scaled by maximum value. Period: 9/04/2019 11h00-23h00.

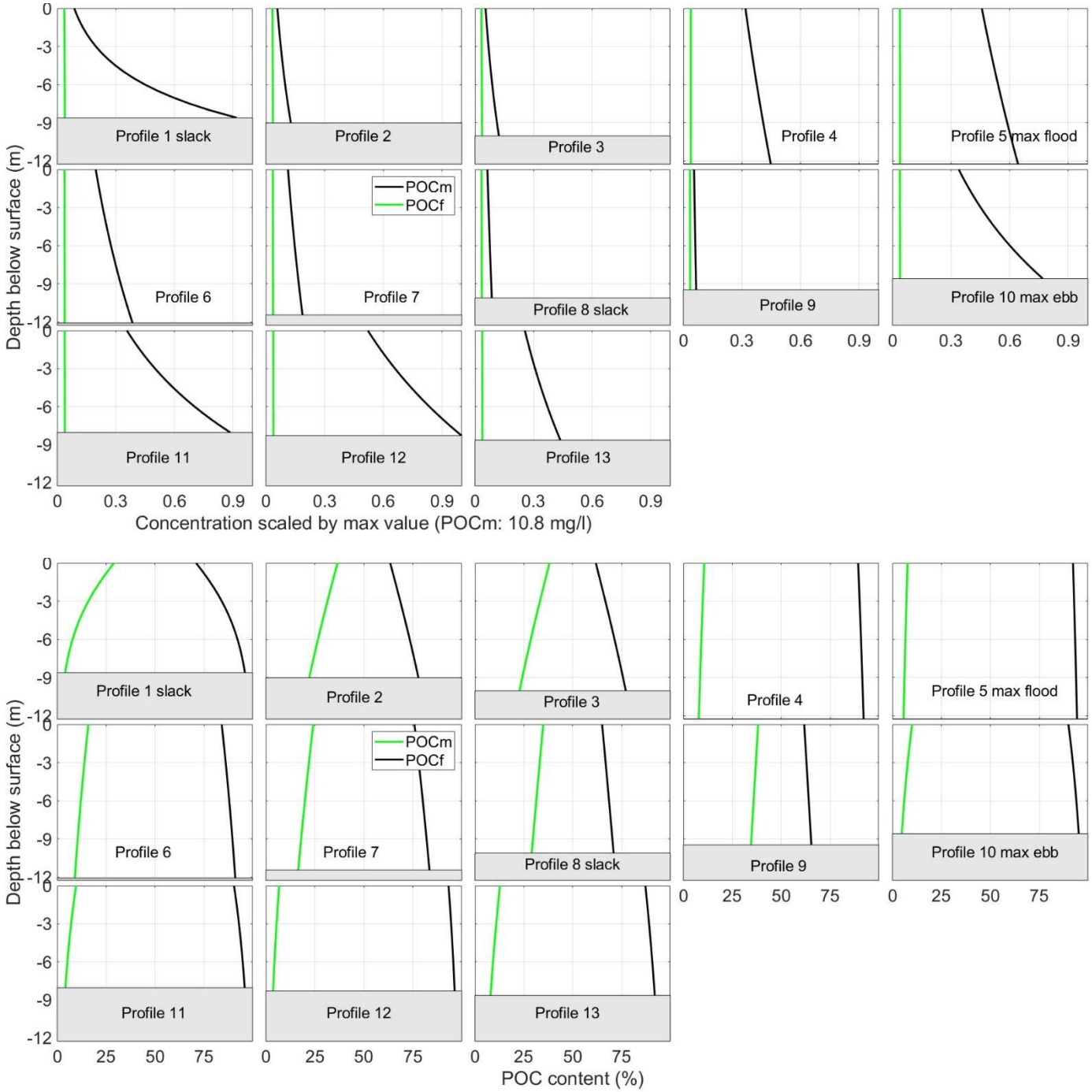

Figure A6.5: : (above) Model-derived fresh and mineral-attached POC concentration profiles (values are scaled by maximum POCm); (below) relative content of fresh and mineral attached POC profiles. Period: 9/04/2019 11h00-23h00.

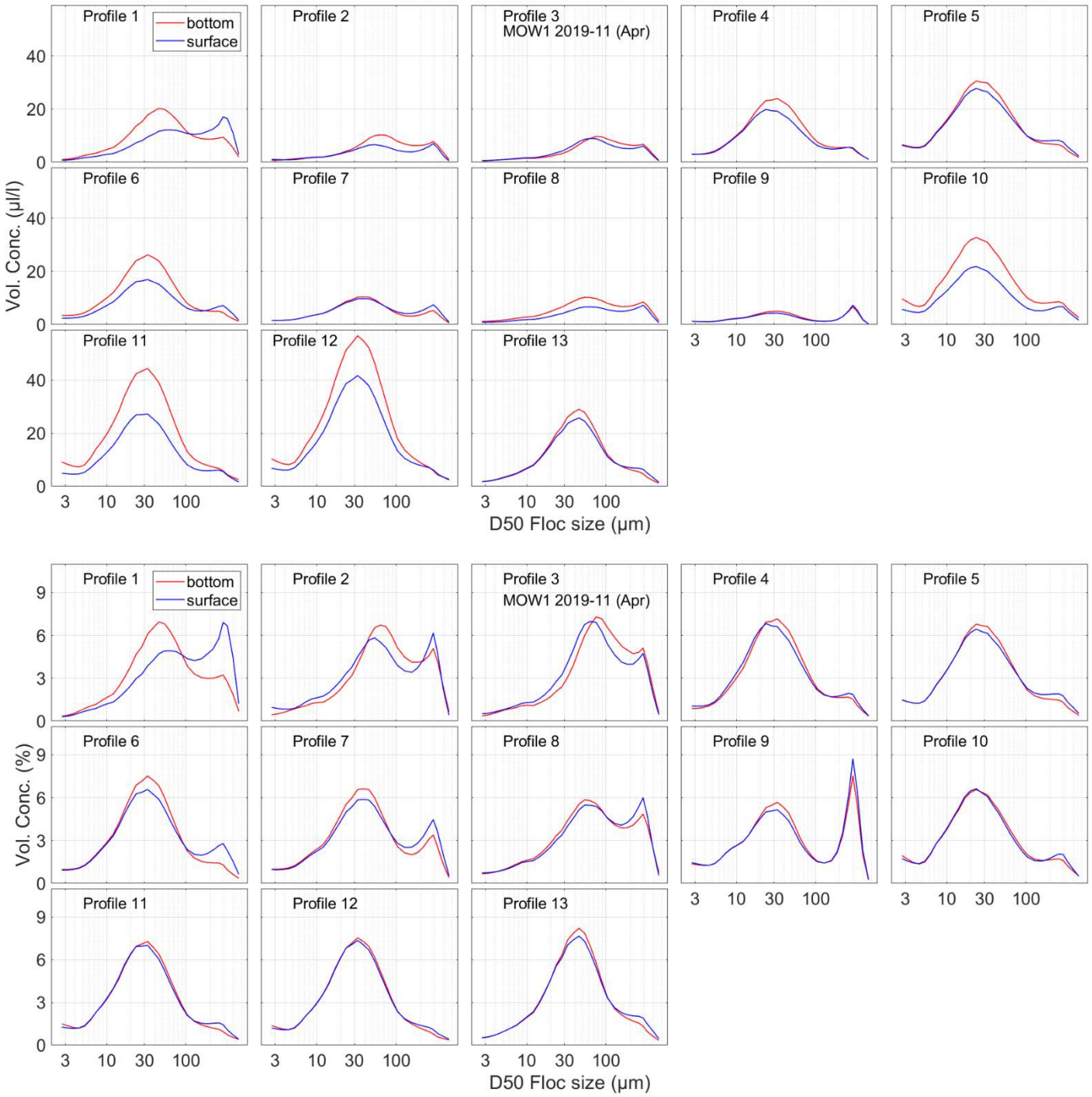

Figure A6.6: Floc size distribution (above in µl/l, below in %) at bottom and surface. *Period: 9/04/2019 11h00-23h00.*

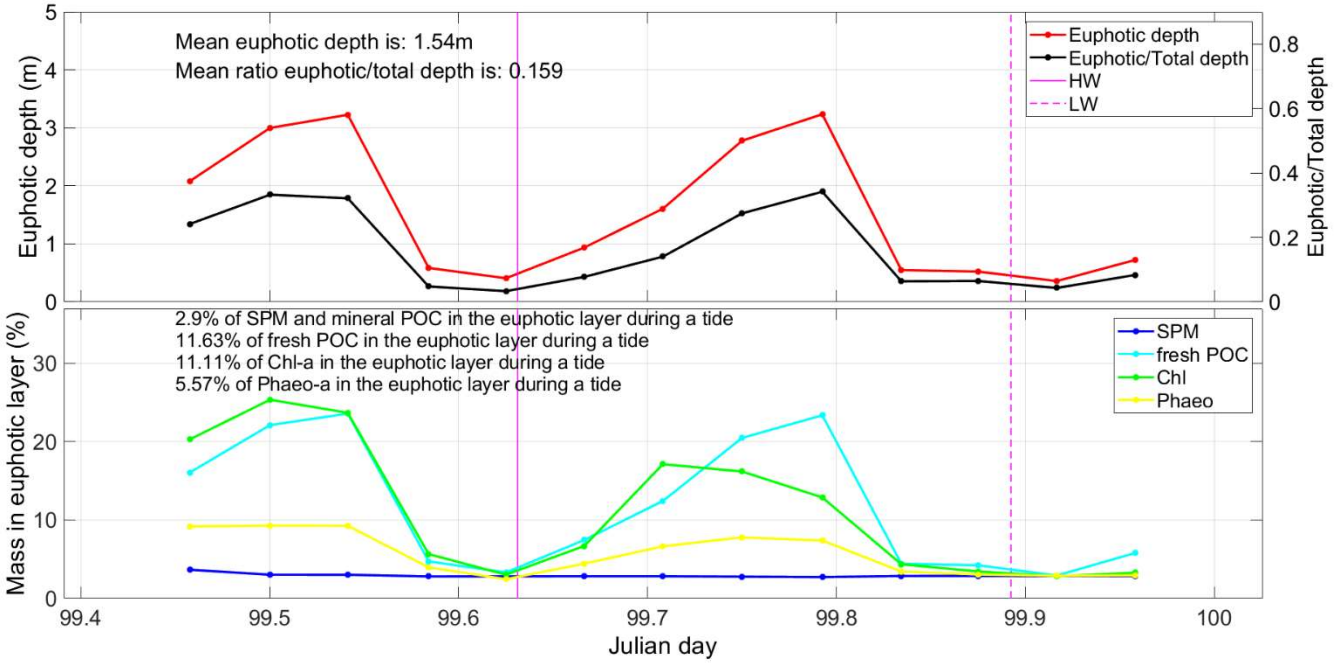

Figure A6.7: (Above) Euphotic layer depth and the ratio euphotic:total depth; (below) Probability of SPM, Chl, Phaeophytine and POC (fresh and mineral) of being in the euphotic layer. Period: 9/04/2019 11h00-23h00. HW: 15h09; LW: 21h25

APPENDIX 7

Tidal cycle at MOW1 May 2019 (2019/14)

20/05 14h00 – 21/05 02h00

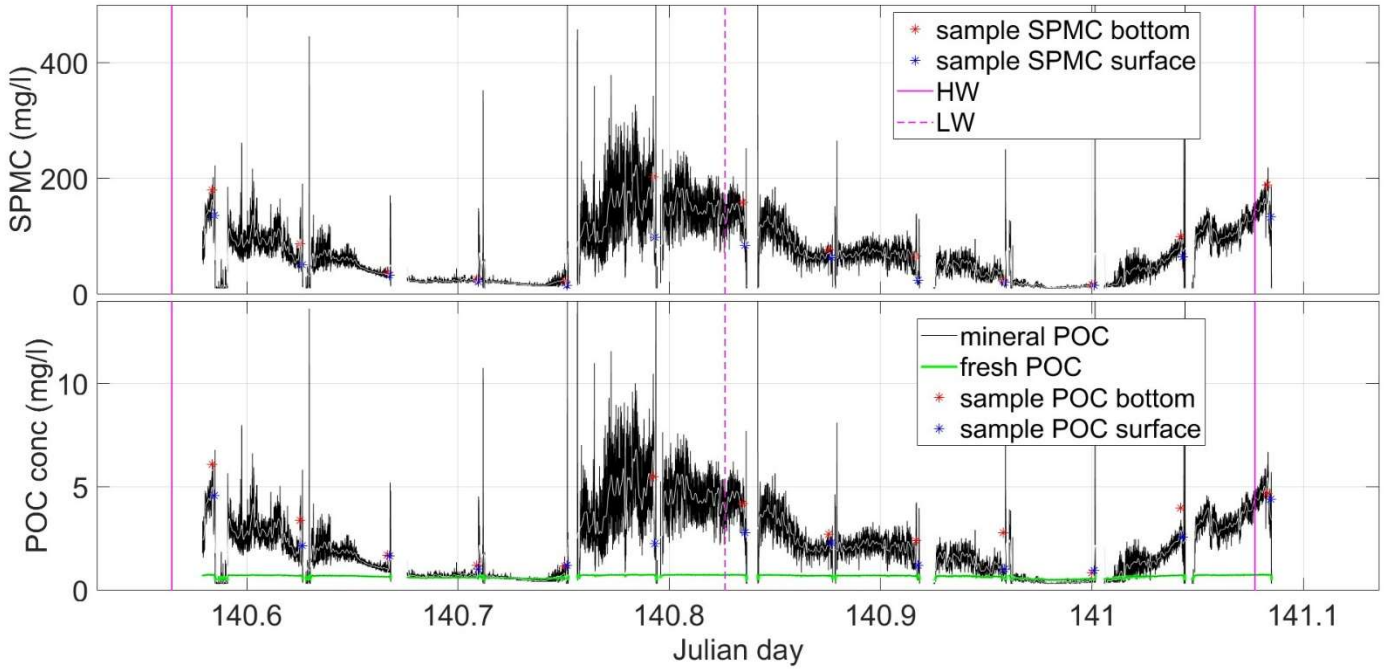

Figure A7.1: Time series of OBS-derived SPM concentration and SPM-derived mineral and fresh POC during a tidal cycle. The sample SPM and POC concentrations are also shown. Period 20/05/2019 14h00 – 21/05/2019 02h00; HW: 13h33; LW 19h50: HW1h51.

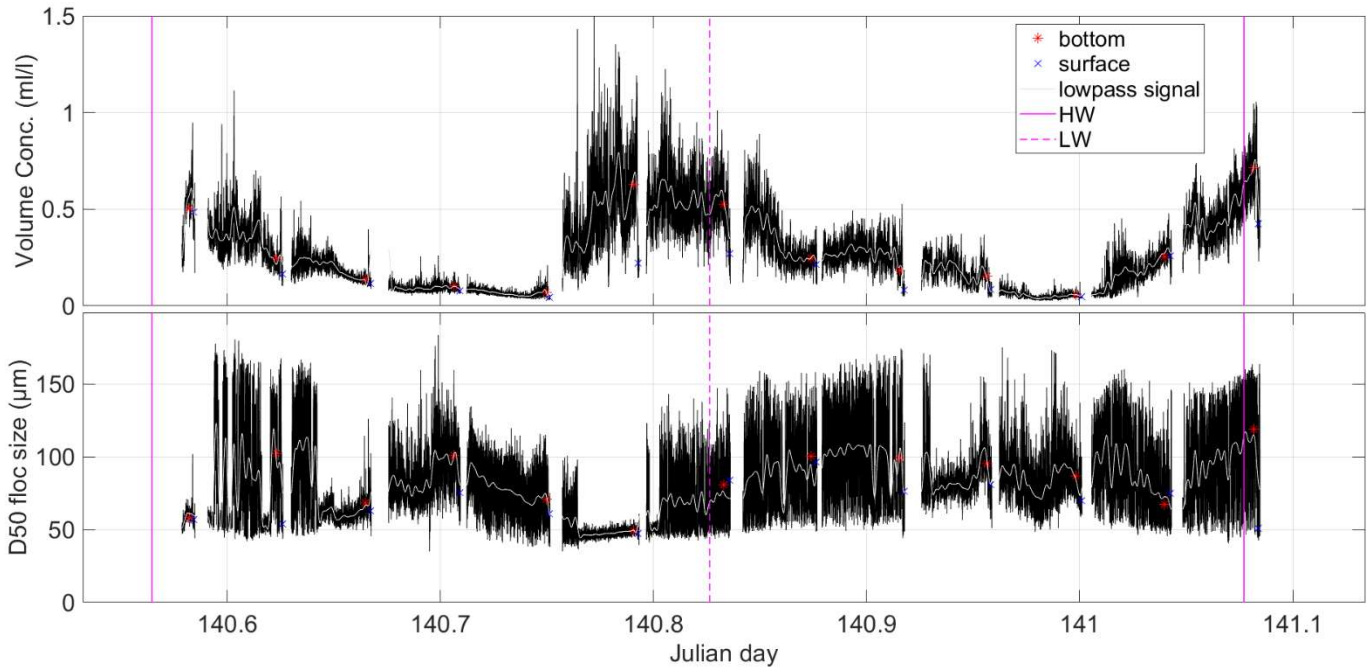

Figure A7.2: Time series of LISST-derived SPM volume concentration and median floc size during a tidal cycle. The values at surface and bottom are are also shown. Period 20/05/2019 14h00 – 21/05/2019 02h00; HW: 13h33; LW 19h50: HW1h51.

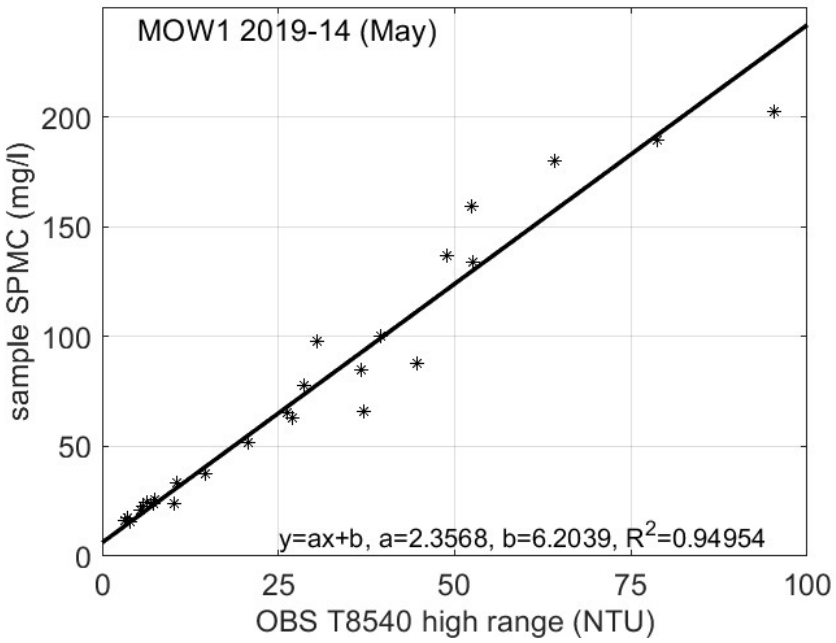

Figure A7.3: Calibration of OBS with water samples

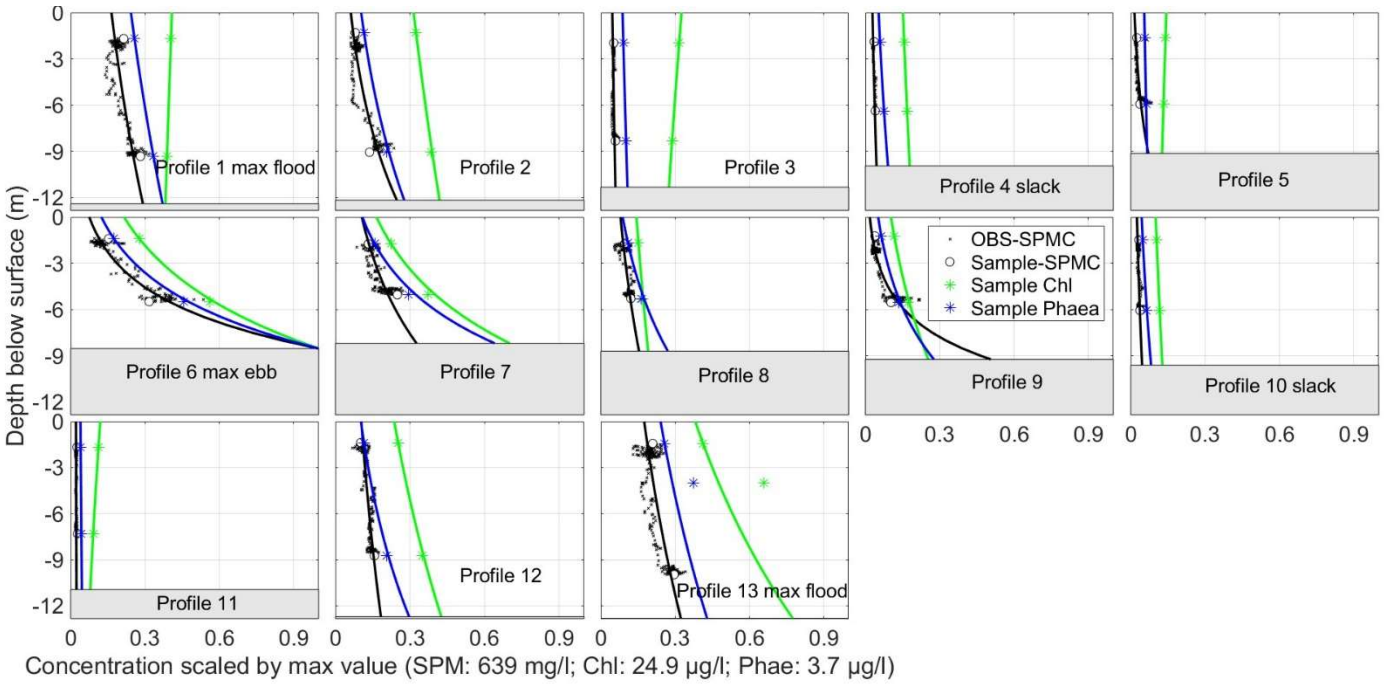

Figure A7.4 Sample-derived SPM concentration profile (black), sample-derived Chl profiles (green) and sample-derived Phaeophytin-a (blue). Values are scaled by maximum value. Period 20/05/2019 14h00 – 21/05/2019 02h00.

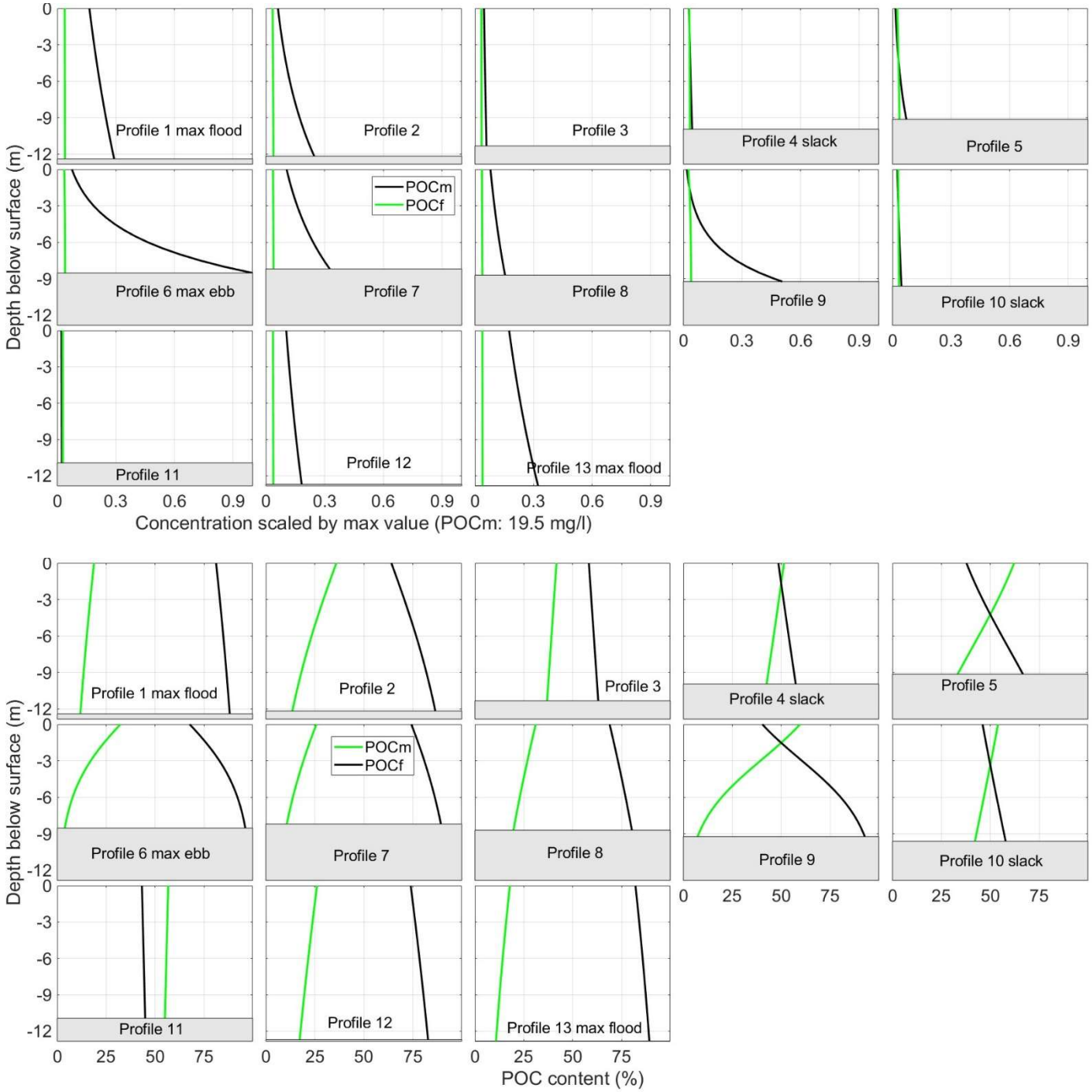

Figure A7.5: : (above) Model-derived fresh and mineral-attached POC concentration profiles (values are scaled by maximum POCm); (below) relative content of fresh and mineral attached POC profiles. Period 20/05/2019 14h00 – 21/05/2019 02h00.

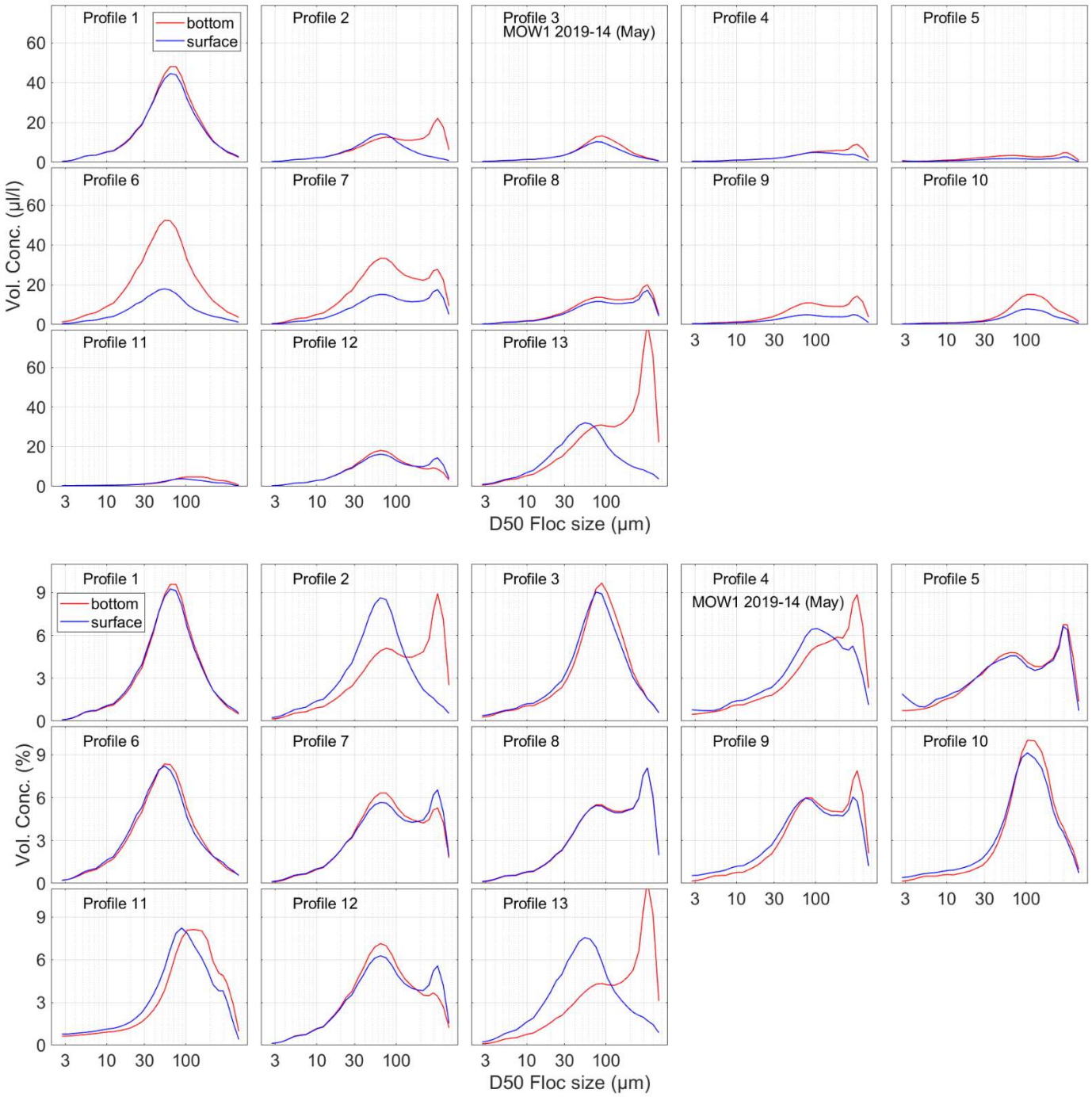

Figure A7.6: Floc size distribution (above in µl/l, below in %) at bottom and surface. Period 20/05/2019 14h00 – 21/05/2019 02h00

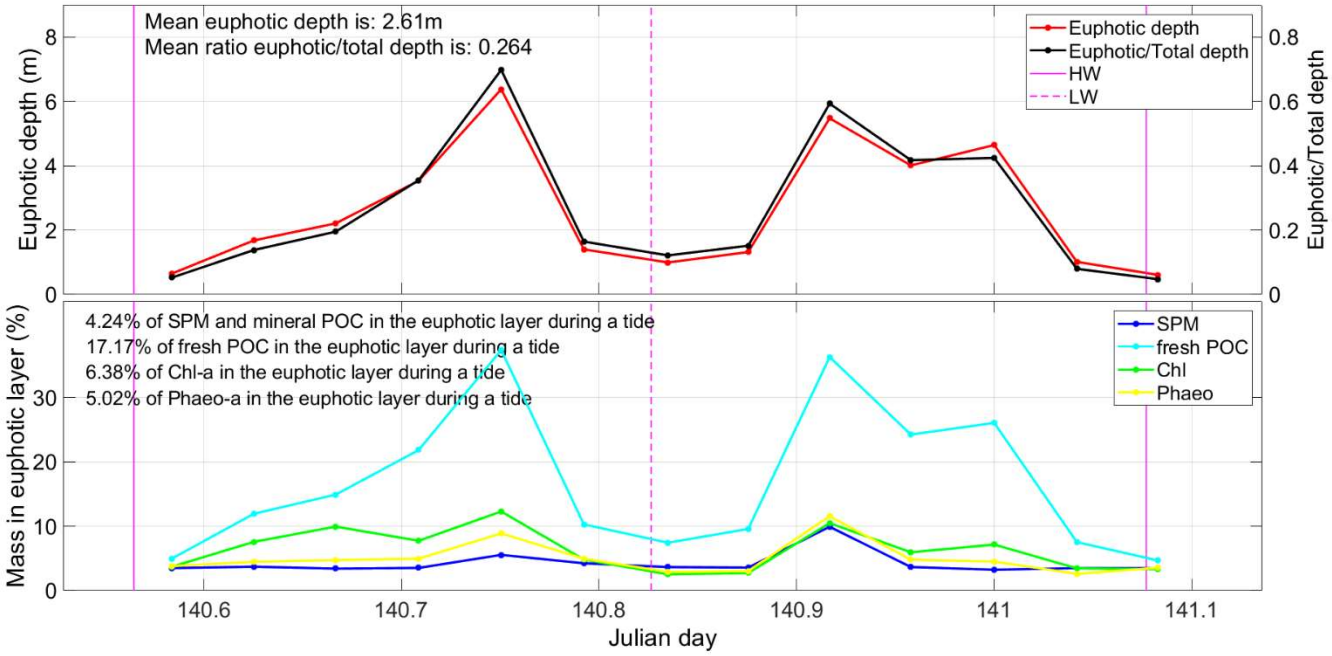
Mean euphotic depth is: 2.61m
Mean ratio euphotic/total depth is: 0.264
Euphotic depth
Euphotic/Total depth
HW
LW
Euphotic depth (m)
Euphotic/Total depth
4.24% of SPM and mineral POC in the euphotic layer during a tide
17.17% of fresh POC in the euphotic layer during a tide
6.38% of Chl-a in the euphotic layer during a tide
5.02% of Phaeo-a in the euphotic layer during a tide
SPM
fresh POC
Chl
Phaeo
Mass in euphotic layer (%)
Julian day

APPENDIX 8

Tidal cycle at MOW1 June 2019 (2019/17)

26/06 09h30 – 26/06 21h30

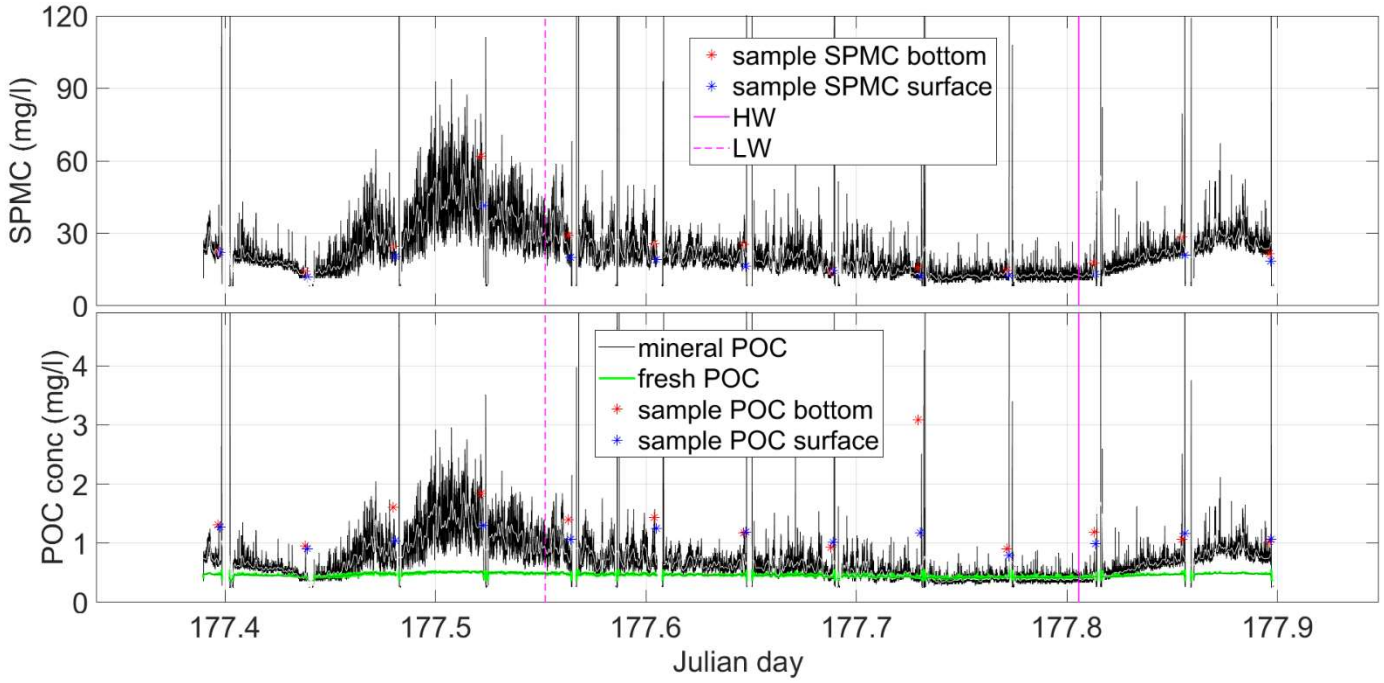

Figure A8.1: Time series of OBS-derived SPM concentration and SPM-derived mineral and fresh POC during a tidal cycle. The sample SPM and POC concentrations are also shown. Period: 26/06/2019 09h30-21h30; LW: 13h15; HW: 19h20.

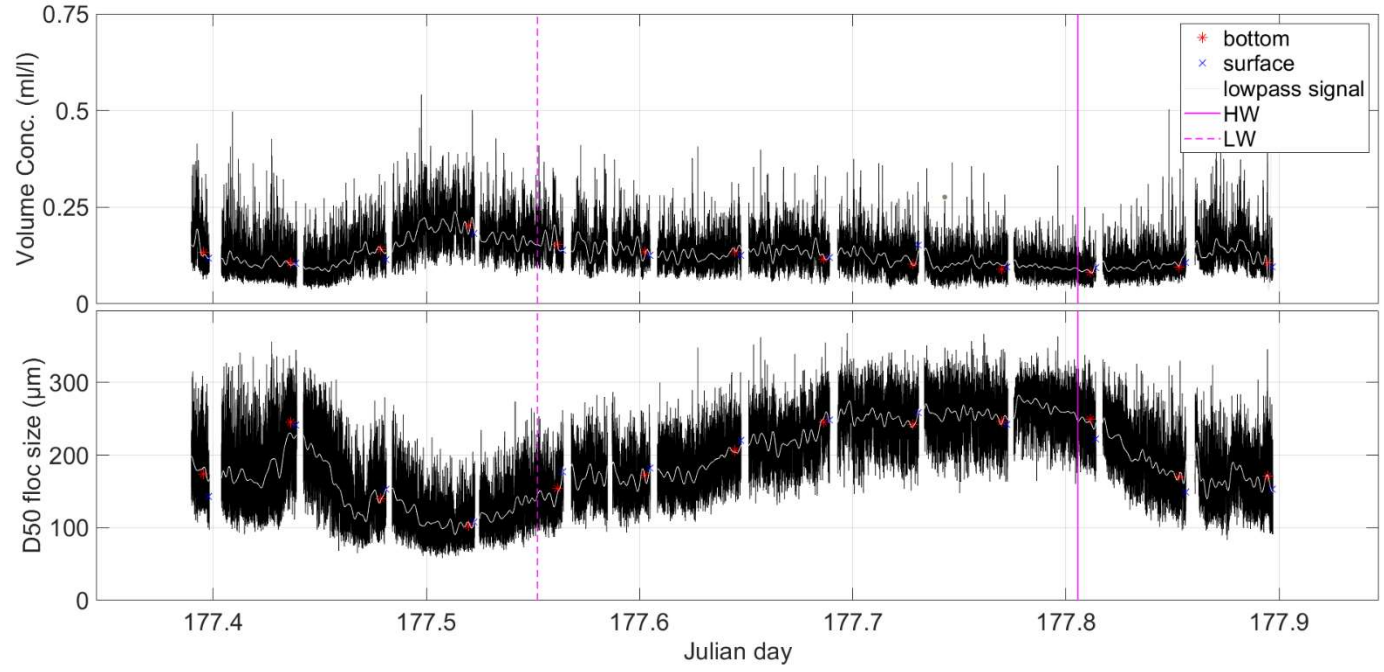

Figure A8.2: Time series of LISST-derived SPM volume concentration and median floc size during a tidal cycle. The values at surface and bottom are also shown. Period: 26/06/2019 09h30-21h30; LW: 13h15; HW: 19h20.

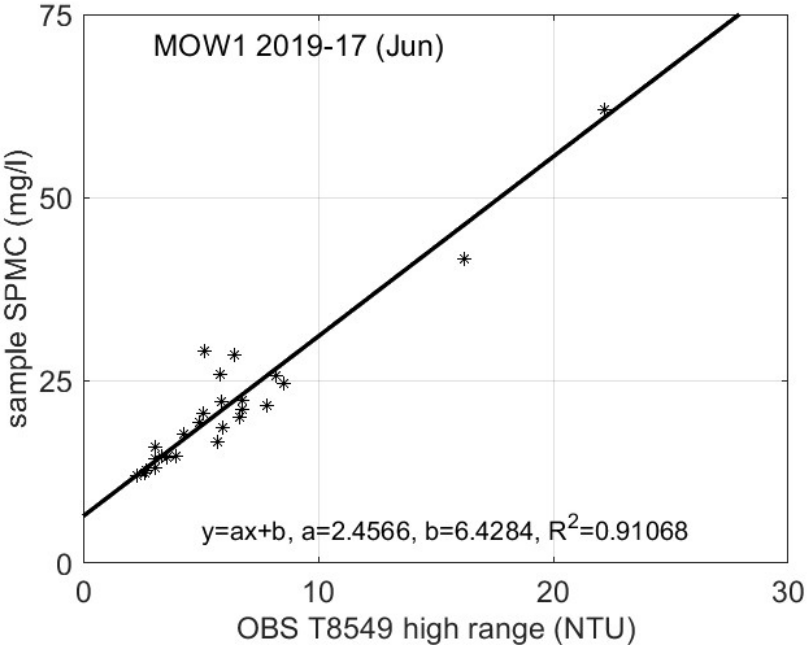

Figure A8.3: Calibration of OBS with water samples

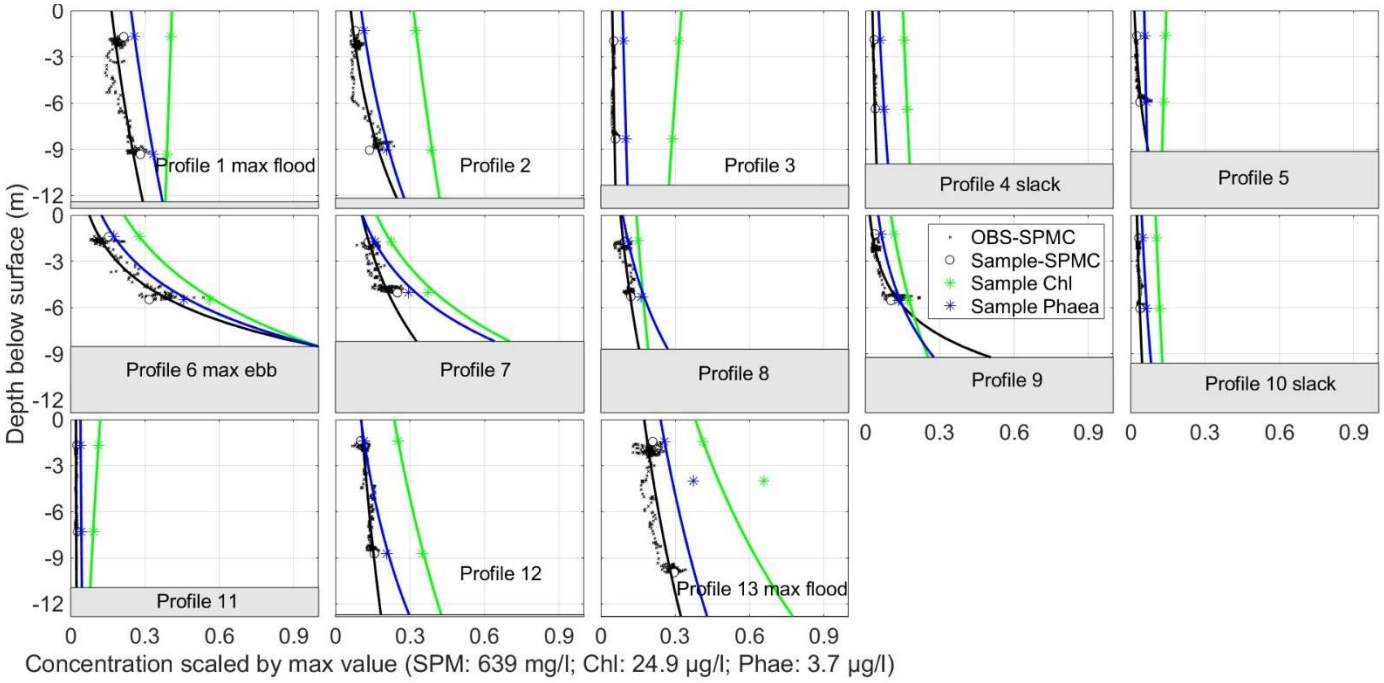

Figure A8.4 Sample-derived SPM concentration profile (black), sample-derived Chl profiles (green) and sample-derived Phaeophytin-a (blue). Values are scaled by maximum value. Period: 26/06/2019 09h30-21h30.

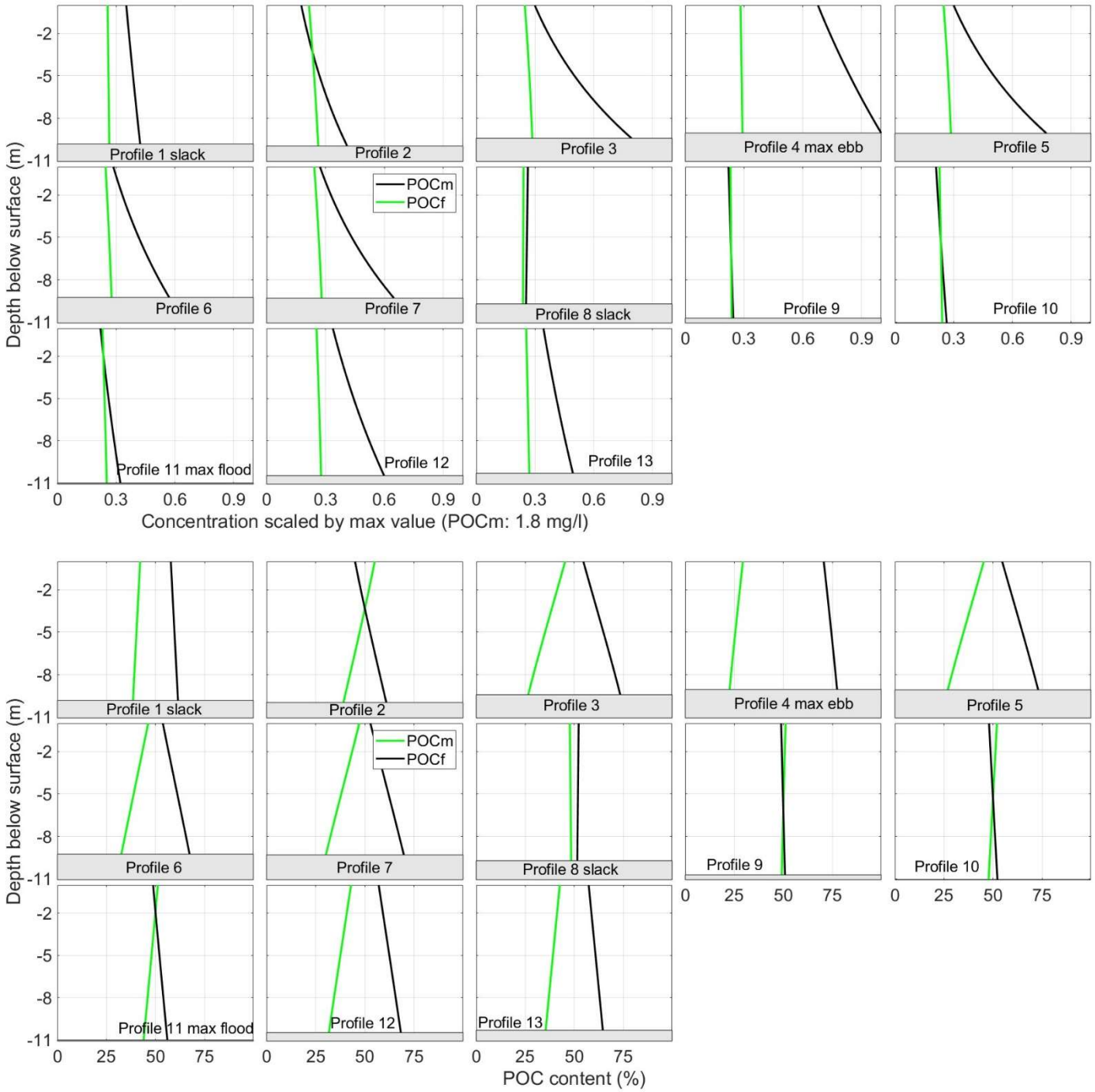

Figure A8.5: (above) Model-derived fresh and mineral-attached POC concentration profiles (values are scaled by maximum POCm); (below) relative content of fresh and mineral attached POC profiles. Period: 26/06/2019 09h30-21h30.

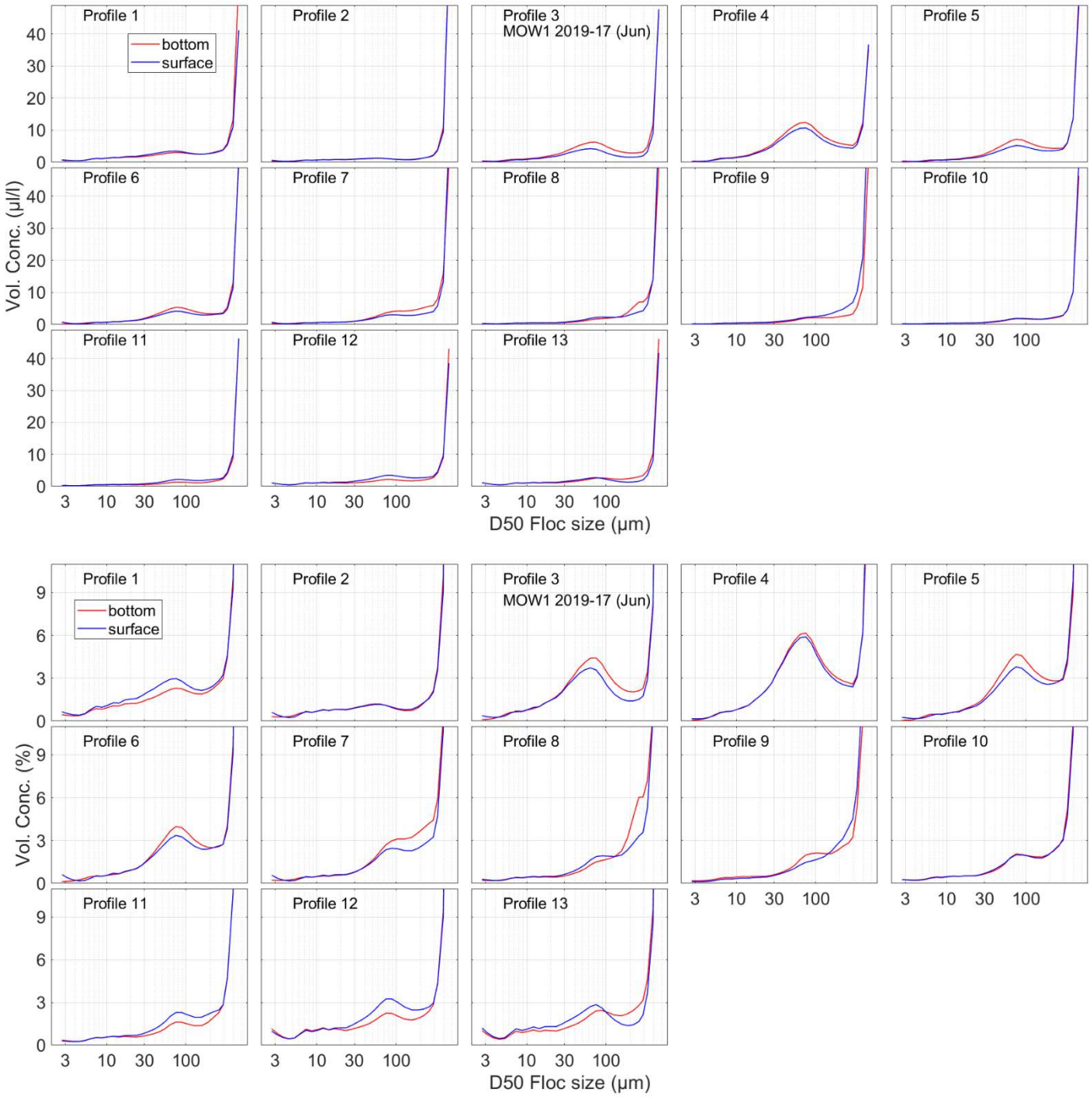

Figure A8.6: Floc size distribution (above in µl/l, below in %) at bottom and surface. Period: 26/06/2019 09h30-21h30

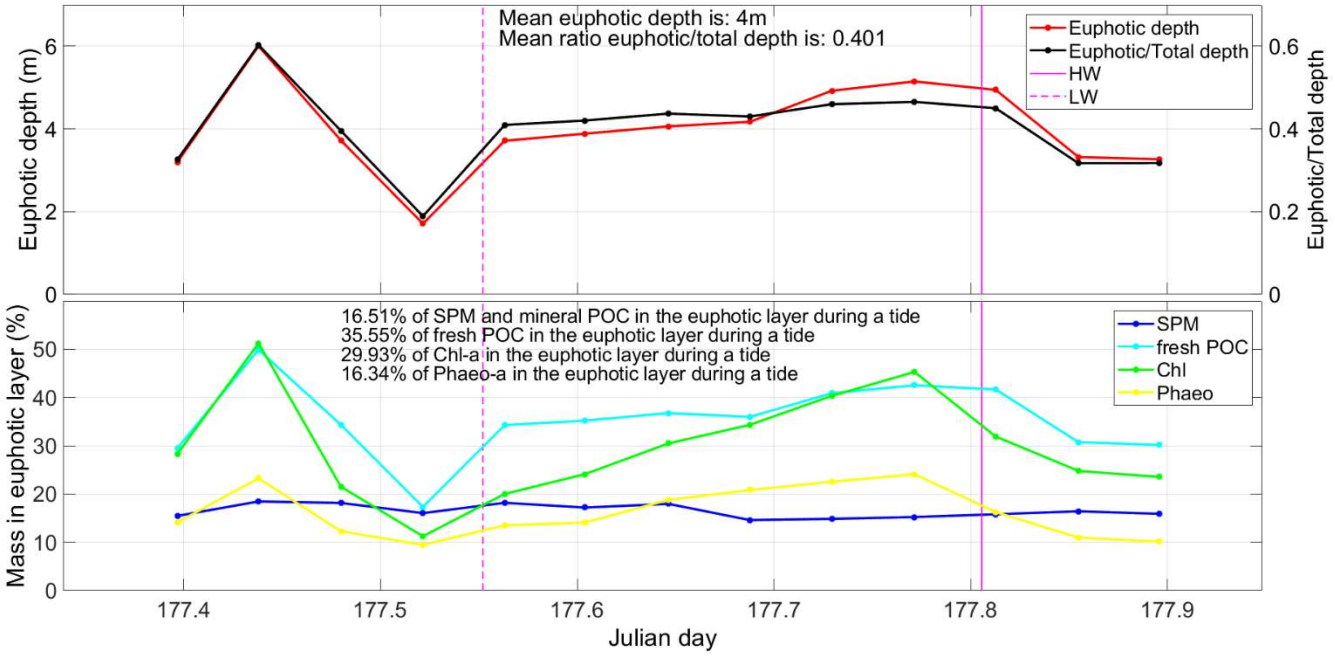

Figure A8.7: (Above) Euphotic layer depth and the ratio euphotic:total depth; (below) Probability of SPM, Chl, Phaeophytine and POC (fresh and mineral) of being in the euphotic layer. Period: 26/06/2019 09h30-21h30; LW: 13h15; HW: 19h20.

APPENDIX 9

Tidal cycle at MOW1 August 2019 (2019/20)

22/08 13h00 – 23/08 01h00

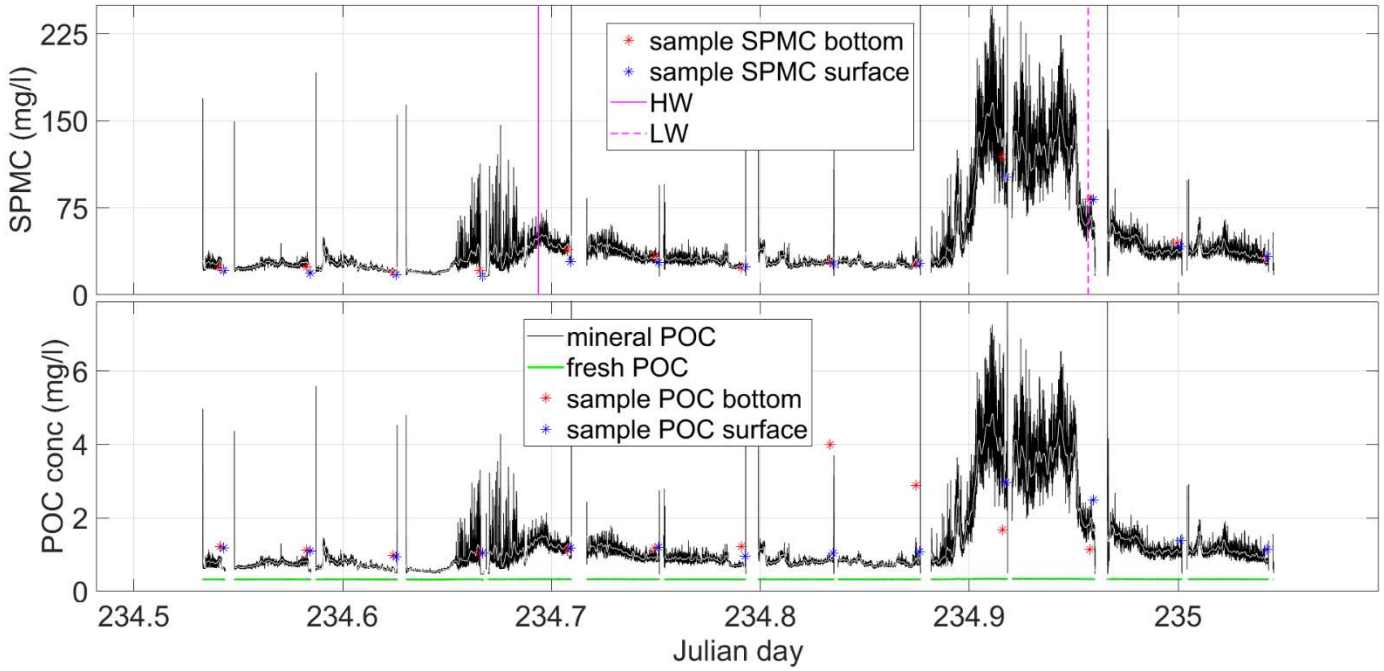

Figure A9.1: Time series of OBS-derived SPM concentration and SPM-derived mineral and fresh POC during a tidal cycle. The sample SPM and POC concentrations are also shown. Period: 22/08/2019 13h00 – 23/08/2019 01h00; HW: 16h39; LW: 22h58.

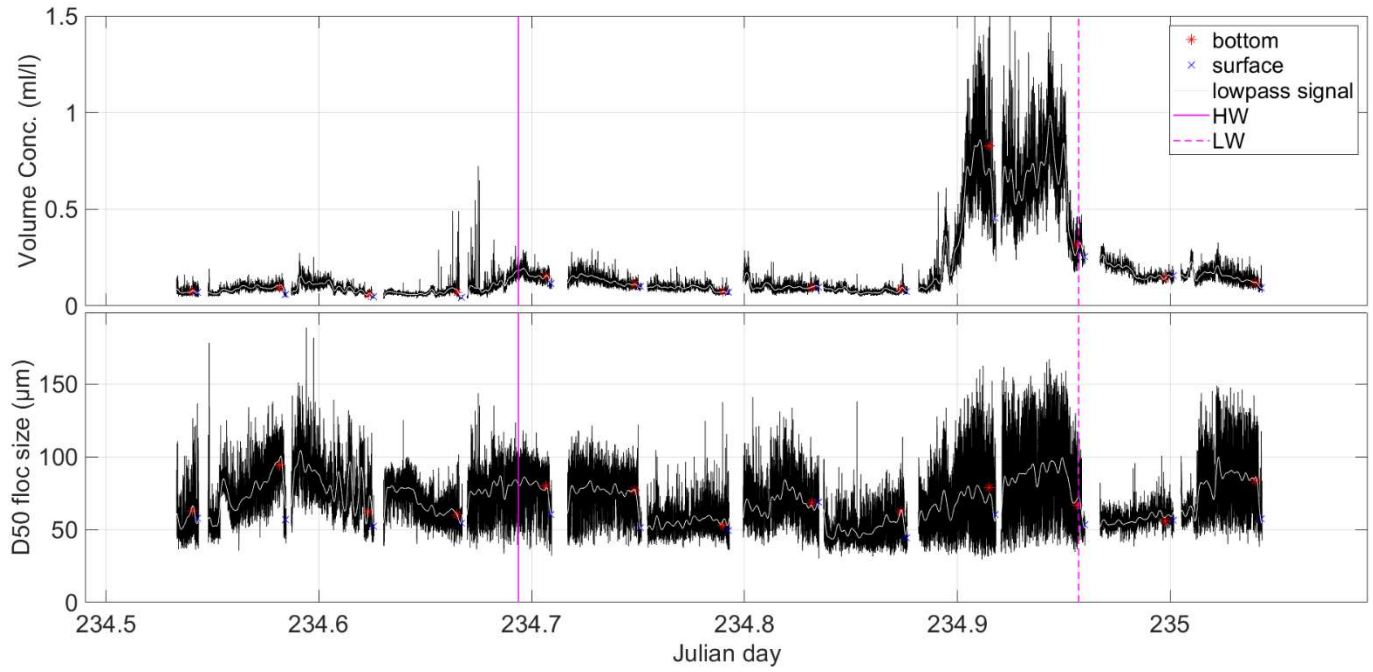

Figure A9.2: Time series of LISST-derived SPM volume concentration and median floc size during a tidal cycle. The values at surface and bottom are are also shown. Period: 22/08/2019 13h00 – 23/08/2019 01h00; HW: 16h39; LW: 22h58.

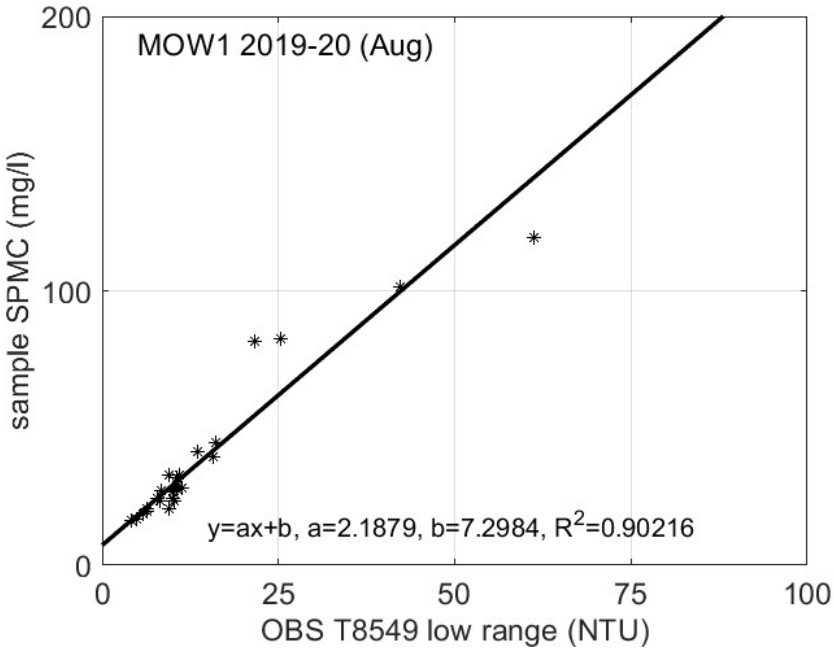

Figure A9.3: Calibration of OBS with water samples

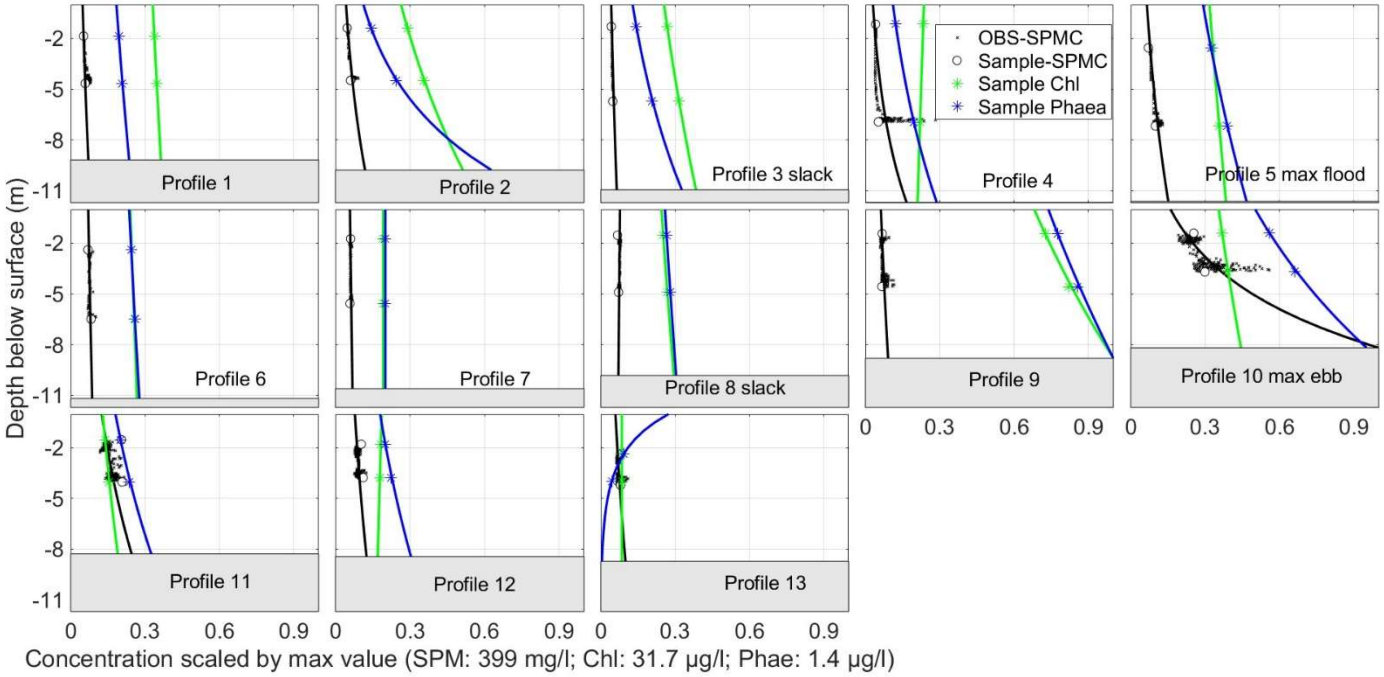

Figure A9.4: Sample-derived SPM concentration profile (black), sample-derived Chl profiles (green) and sample-derived Phaeophytin-a (blue). Values are scaled by maximum value. Period: 22/08/2019 13h00 – 23/08/2019 01h00.

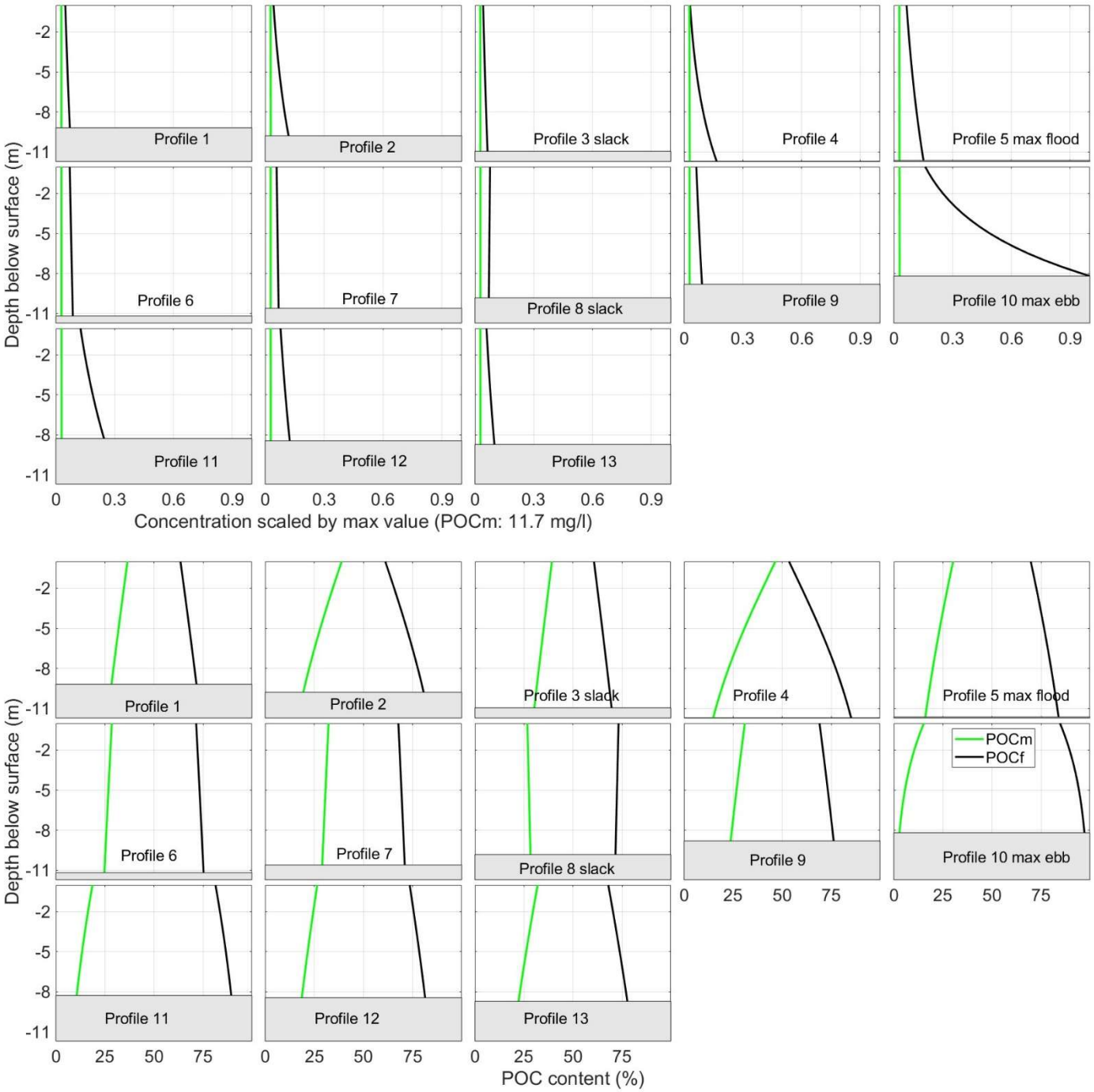

Figure A9.5: (above) Model-derived fresh and mineral-attached POC concentration profiles (values are scaled by maximum POCm); (below) relative content of fresh and mineral attached POC profiles. Period: 22/08/2019 13h00 – 23/08/2019 01h00

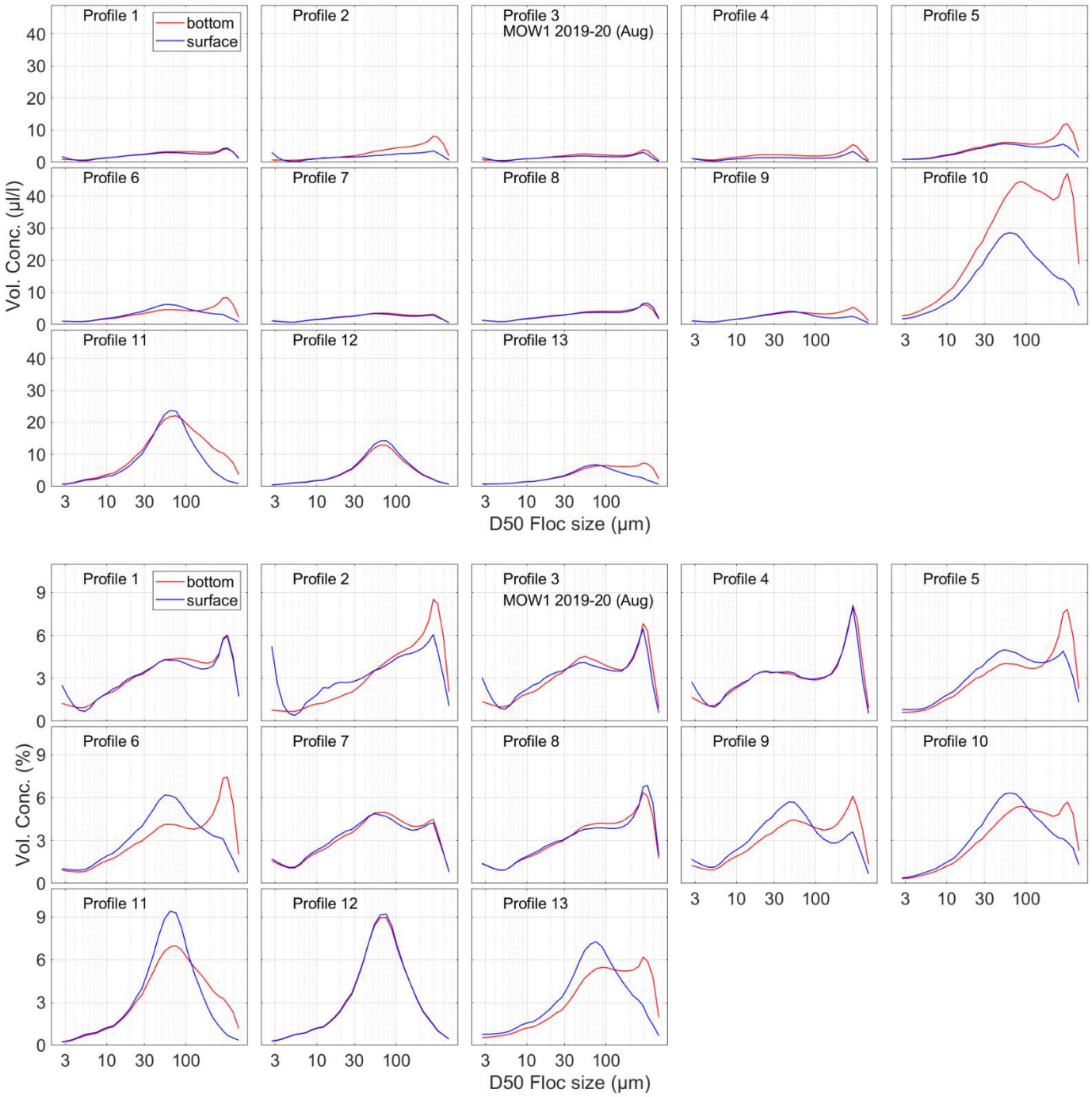

Figure A8.4: Floc size distribution (above in µl/l, below in %) at bottom and surface. *Period: 22/08/2019 13h00 – 23/08/2019 01h00*

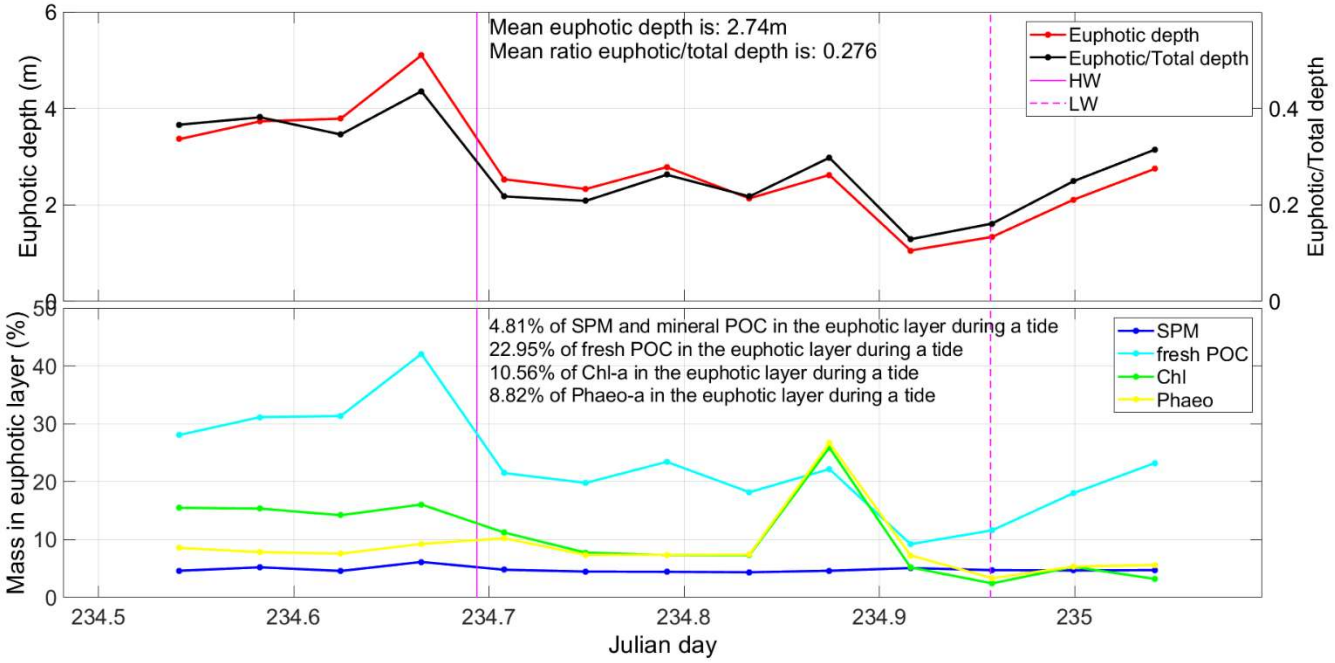

Figure A9.7: (Above) Euphotic layer depth and the ratio euphotic:total depth; (below) Probability of SPM, Chl, Phaeophytine and POC (fresh and mineral) of being in the euphotic layer. Period: 22/08/2019 13h00 – 23/08/2019 01h00; HW: 16h39; LW: 22h58.

APPENDIX 10

Tidal cycle at MOW1 September 2019 (2019/22)

11/09 06h00 – 11/09 18h00

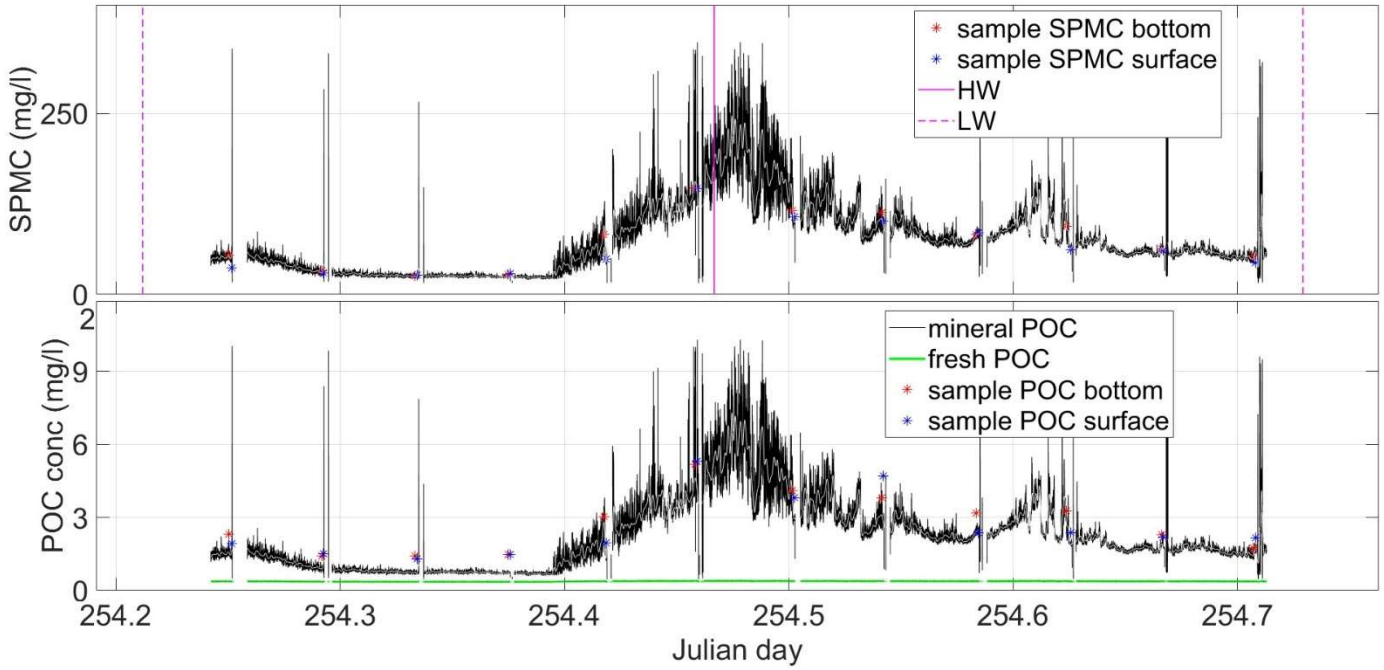

Figure A10.1: Time series of OBS-derived SPM concentration and SPM-derived mineral and fresh POC during a tidal cycle. The sample SPM and POC concentrations are also shown. Period: 11/09/2019 06h00-18h00; LW: 05h05; HW: 11h12; LW: 17h30.

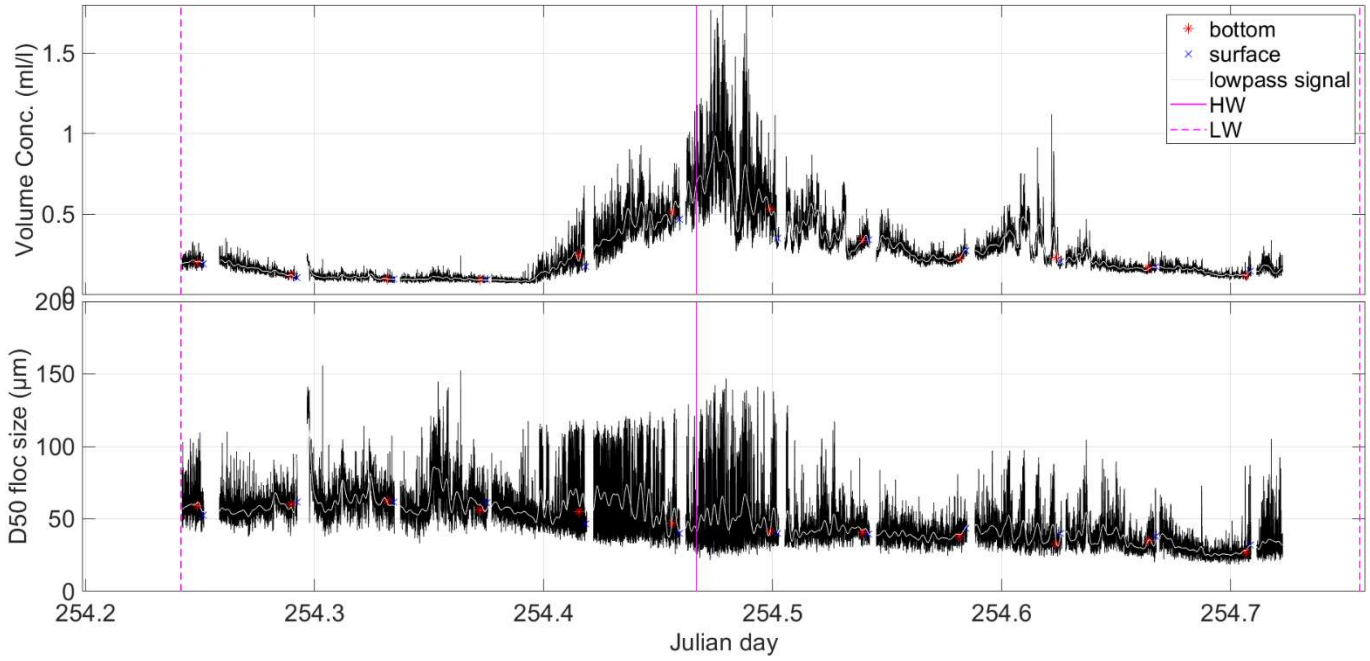

Figure A10.2: Time series of LISST-derived SPM volume concentration and median floc size during a tidal cycle. The values at surface and bottom are are also shown. Period: 11/09/2019 06h00-18h00; LW: 05h05; HW: 11h12; LW: 17h30.

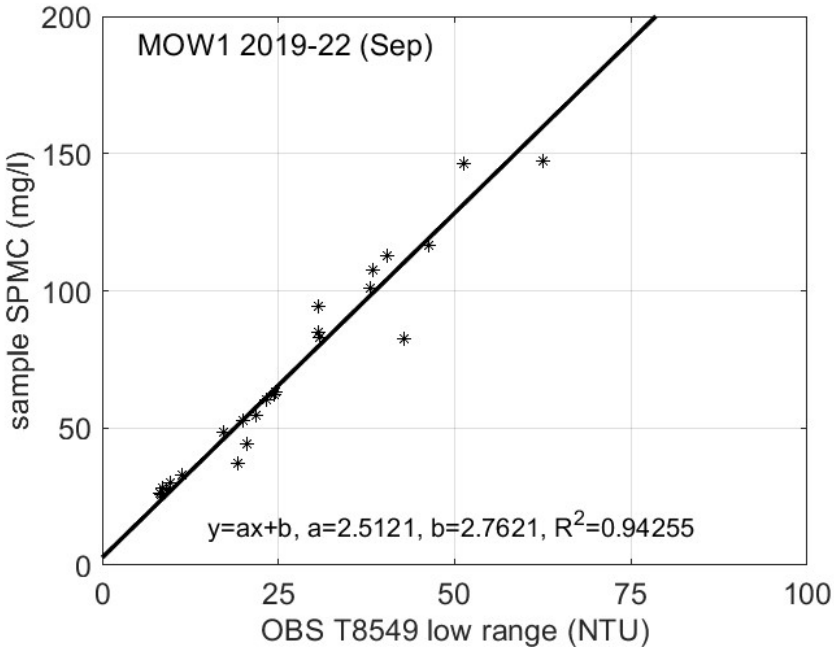

Figure A10.3: Calibration of OBS with water samples

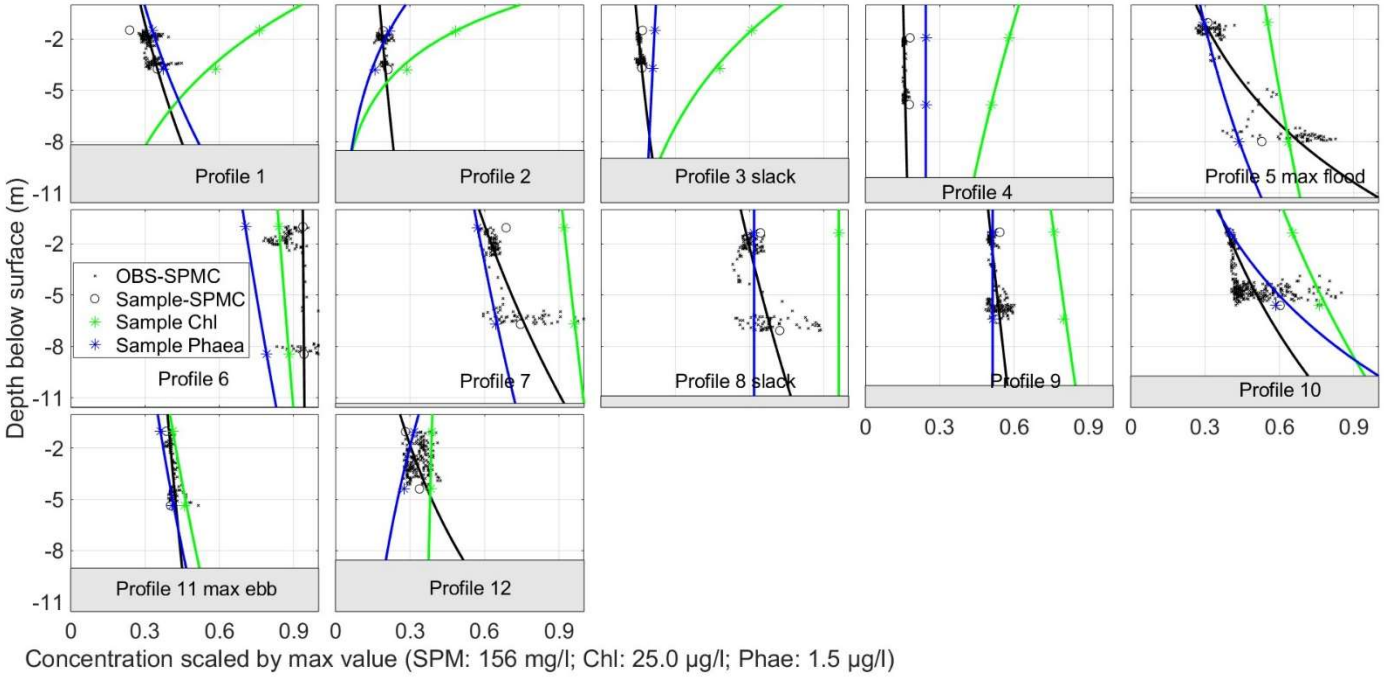

Figure A10.4: Sample-derived SPM concentration profile (black), sample-derived Chl profiles (green) and sample-derived Phaeophytin-a (blue). Values are scaled by maximum value. Period: 11/09/2019 06h00-18h00.

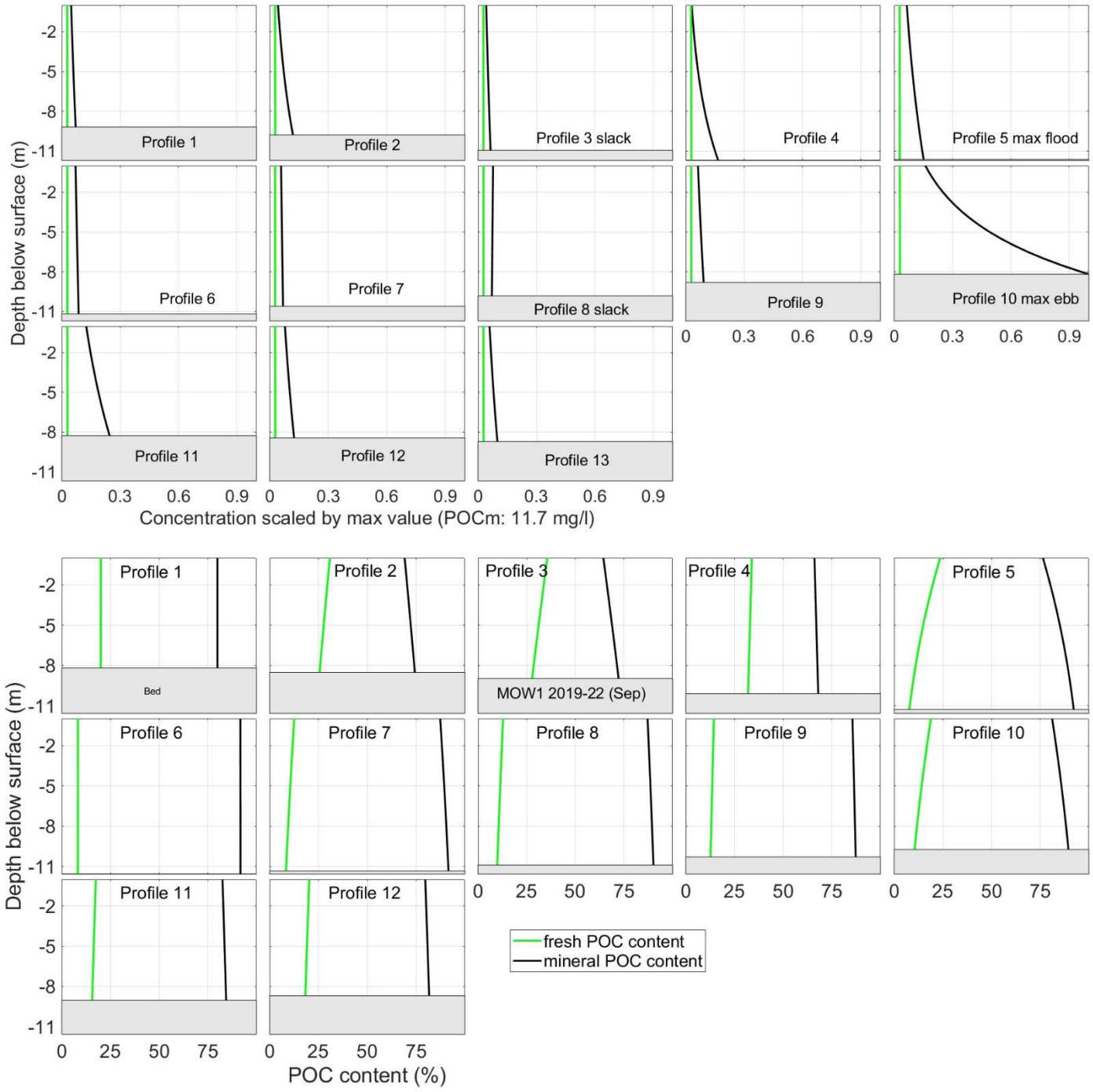

Figure A10.5: (above) Model-derived fresh and mineral-attached POC concentration profiles (values are scaled by maximum POCm); (below) relative content of fresh and mineral attached POC profiles. Period: 11/09/2019 06h00-18h00.

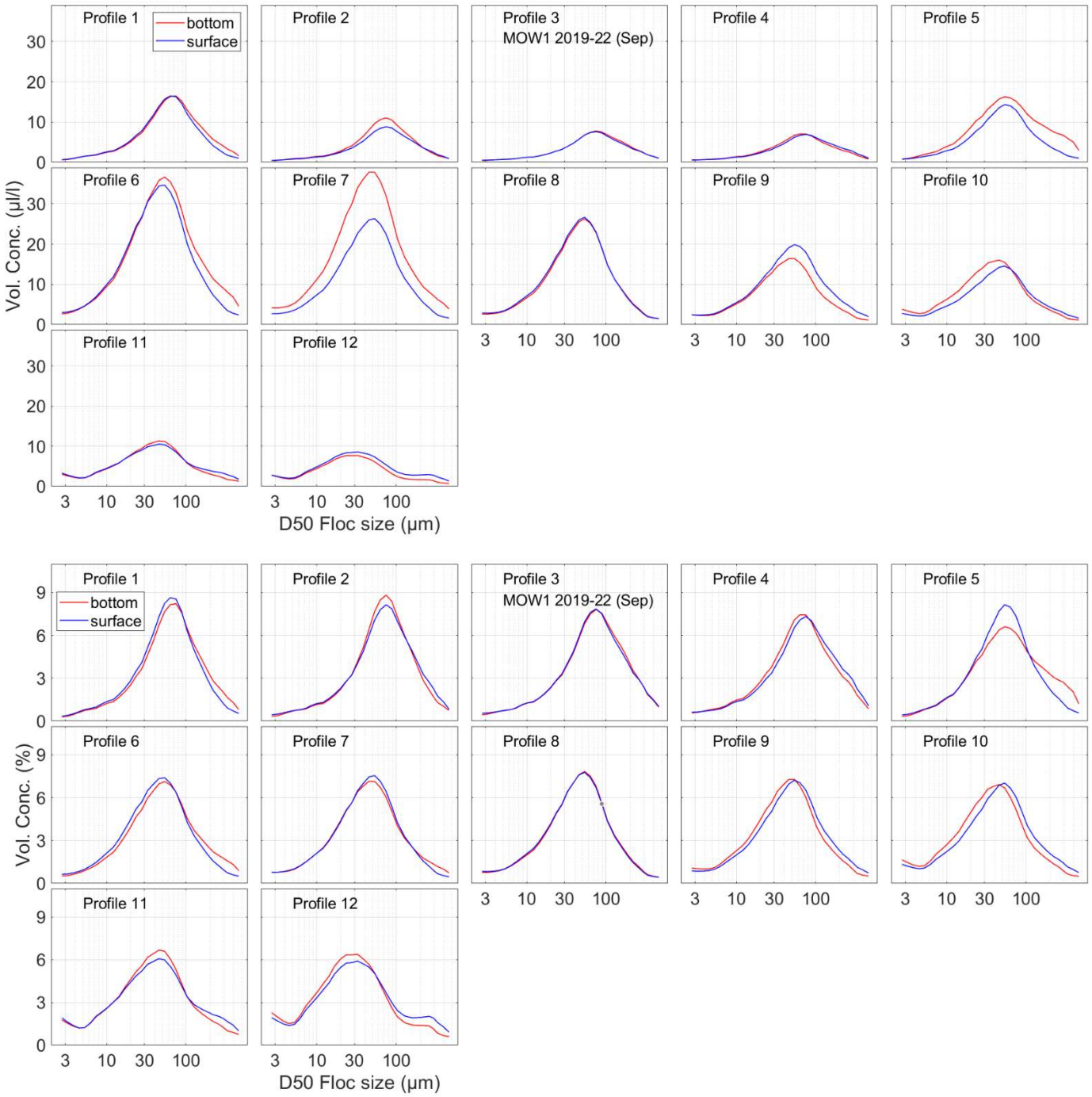

Figure A10.6: Floc size distribution (above in µl/l, below in %) at bottom and surface. Period: 11/09/2019 06h00-18h00

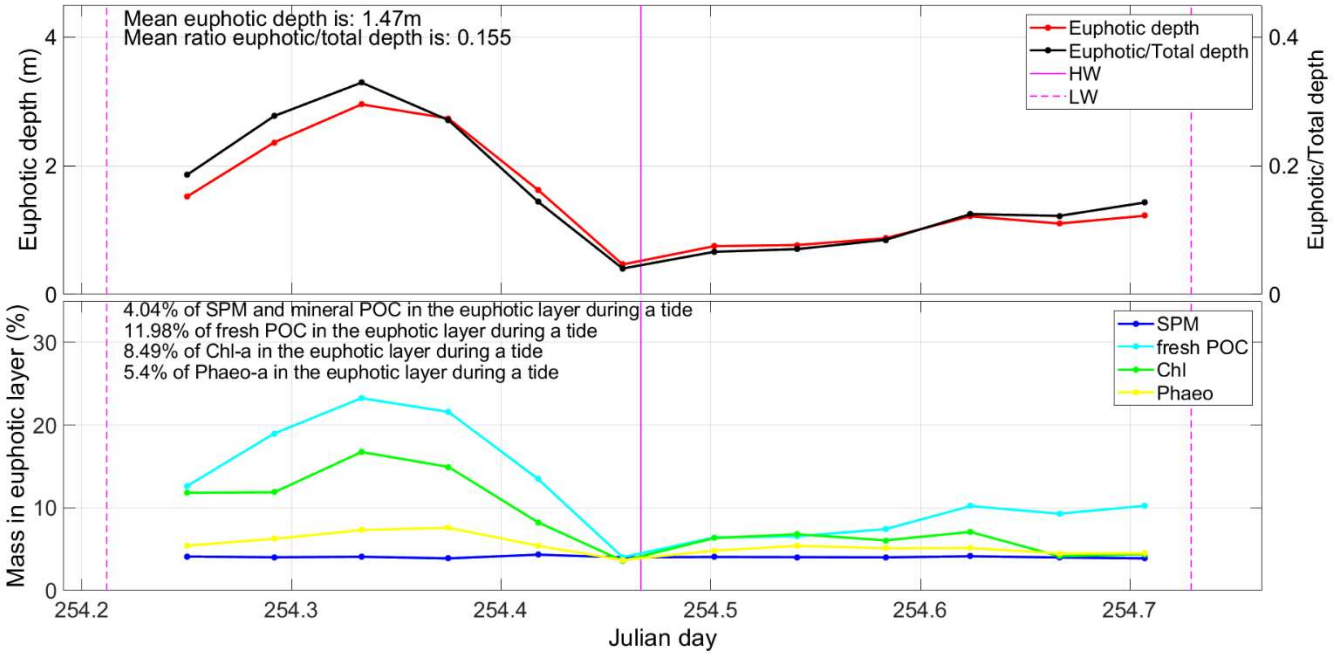

Figure A10.7: (Above) Euphotic layer depth and the ratio euphotic:total depth; (below) Probability of SPM, Chl, Phaeophytine and POC (fresh and mineral) of being in the euphotic layer. Period: 11/09/2019 06h00-18h00; LW: 05h05; HW: 11h12; LW: 17h30.

APPENDIX 11

Tidal cycle at MOW1 October 2019 (2019/25)

16/10 11h00 – 16/10 23h00

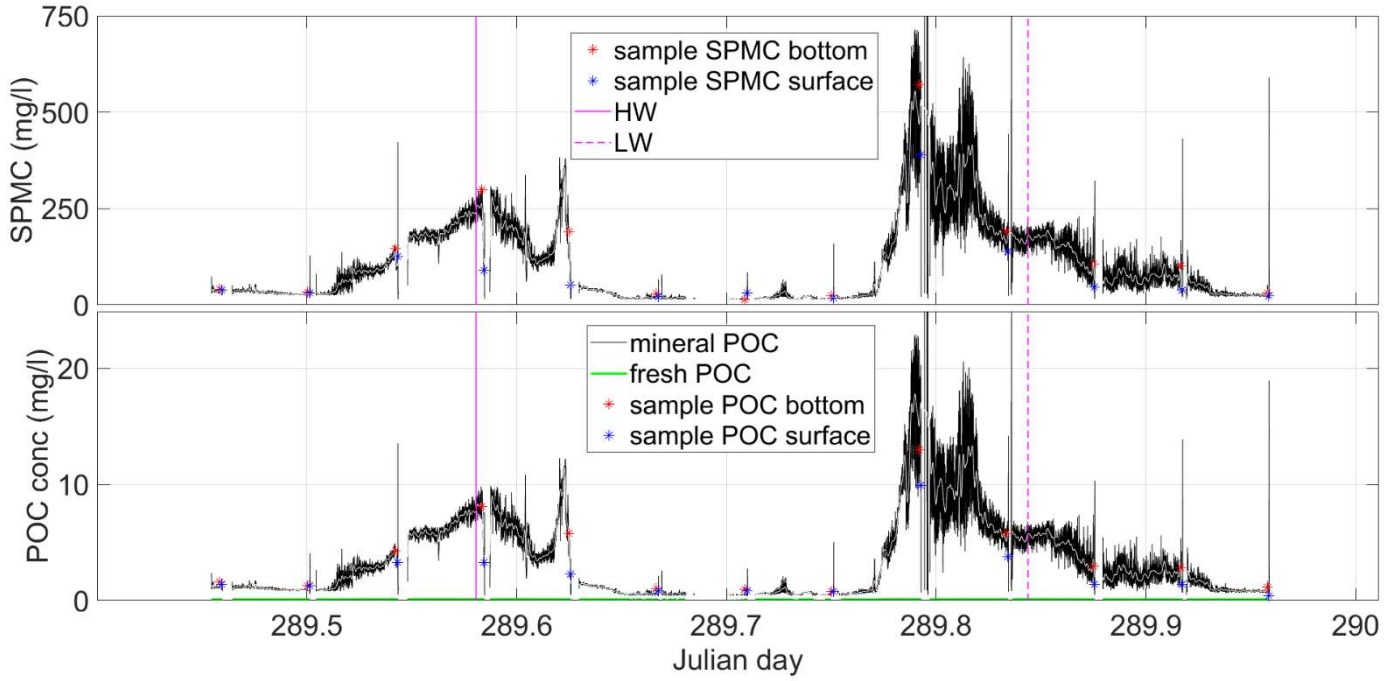

Figure A11.1: Time series of OBS-derived SPM concentration and SPM-derived mineral and fresh POC during a tidal cycle. The sample SPM and POC concentrations are also shown. Period: 16/10/2019 11h00-23h00, HW: 13h56; LW: 20h15.

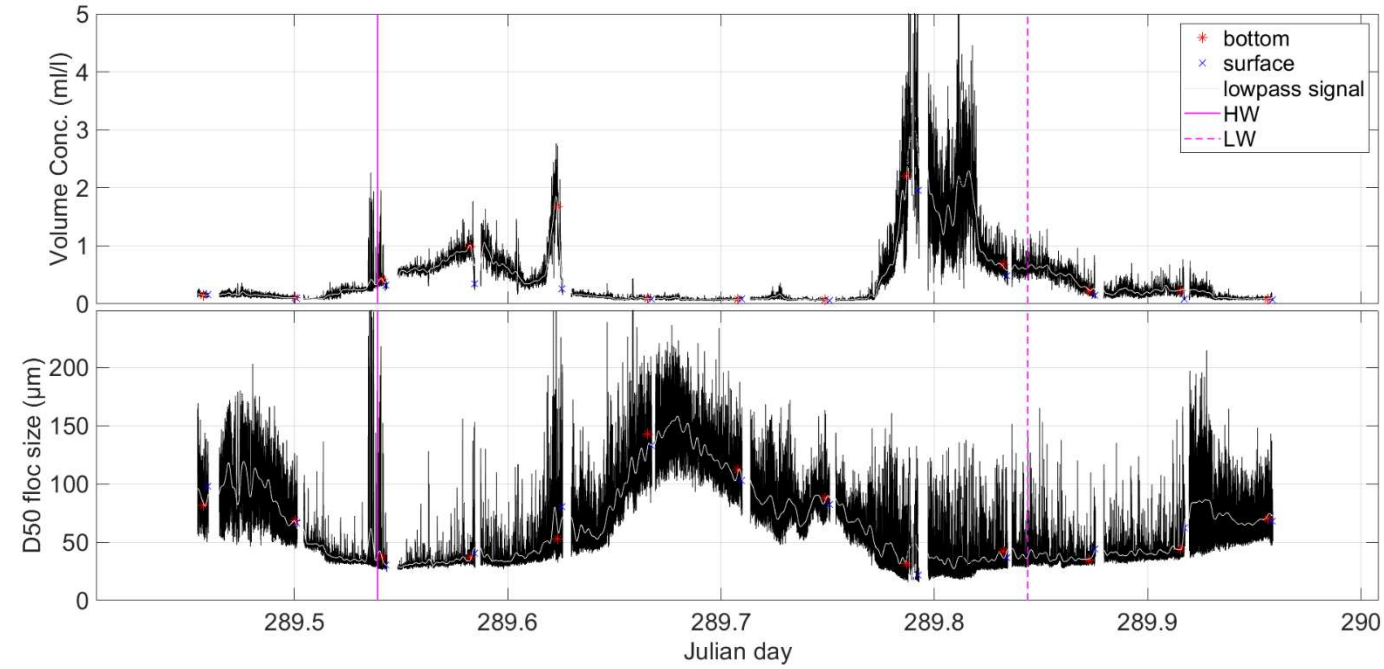

Figure A11.2: Time series of LISST-derived SPM volume concentration and median floc size during a tidal cycle. The values at surface and bottom are are also shown. Period: 16/10/2019 11h00-23h00, HW: 13h56; LW: 20h15.

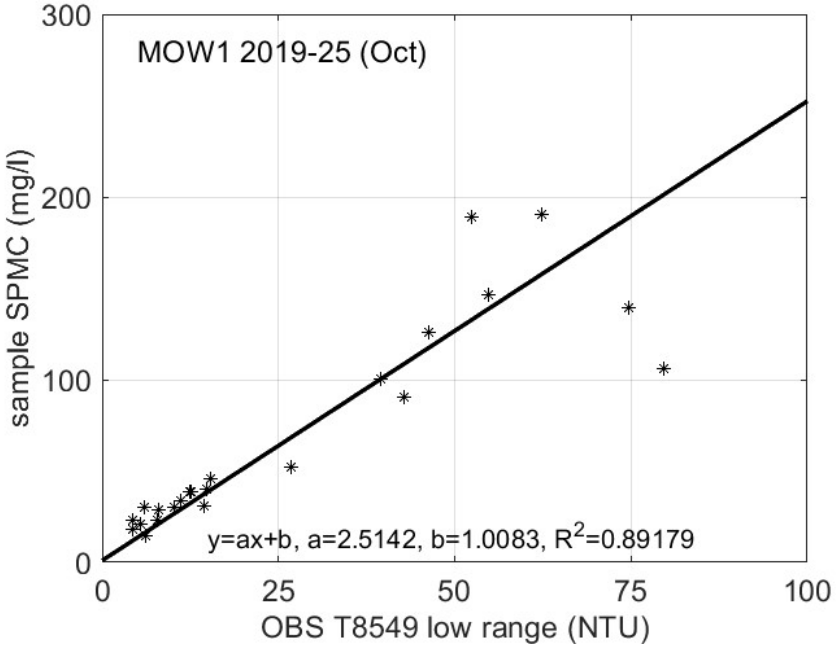

Figure A11.3: Calibration of OBS with water samples

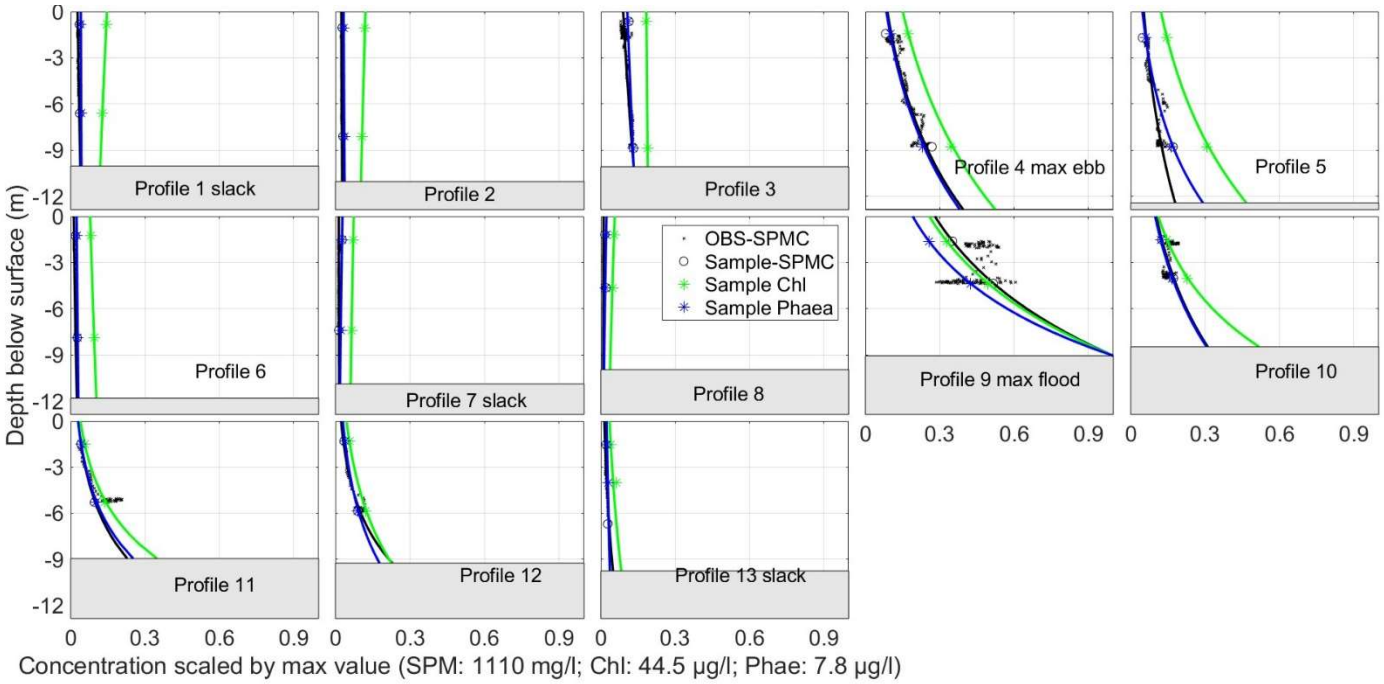

Figure A11.4: Sample-derived SPM concentration profile (black), sample-derived Chl profiles (green) and sample-derived Phaeophytin-a (blue). Values are scaled by maximum value. Period: 16/10/2019 11h00-23h00.

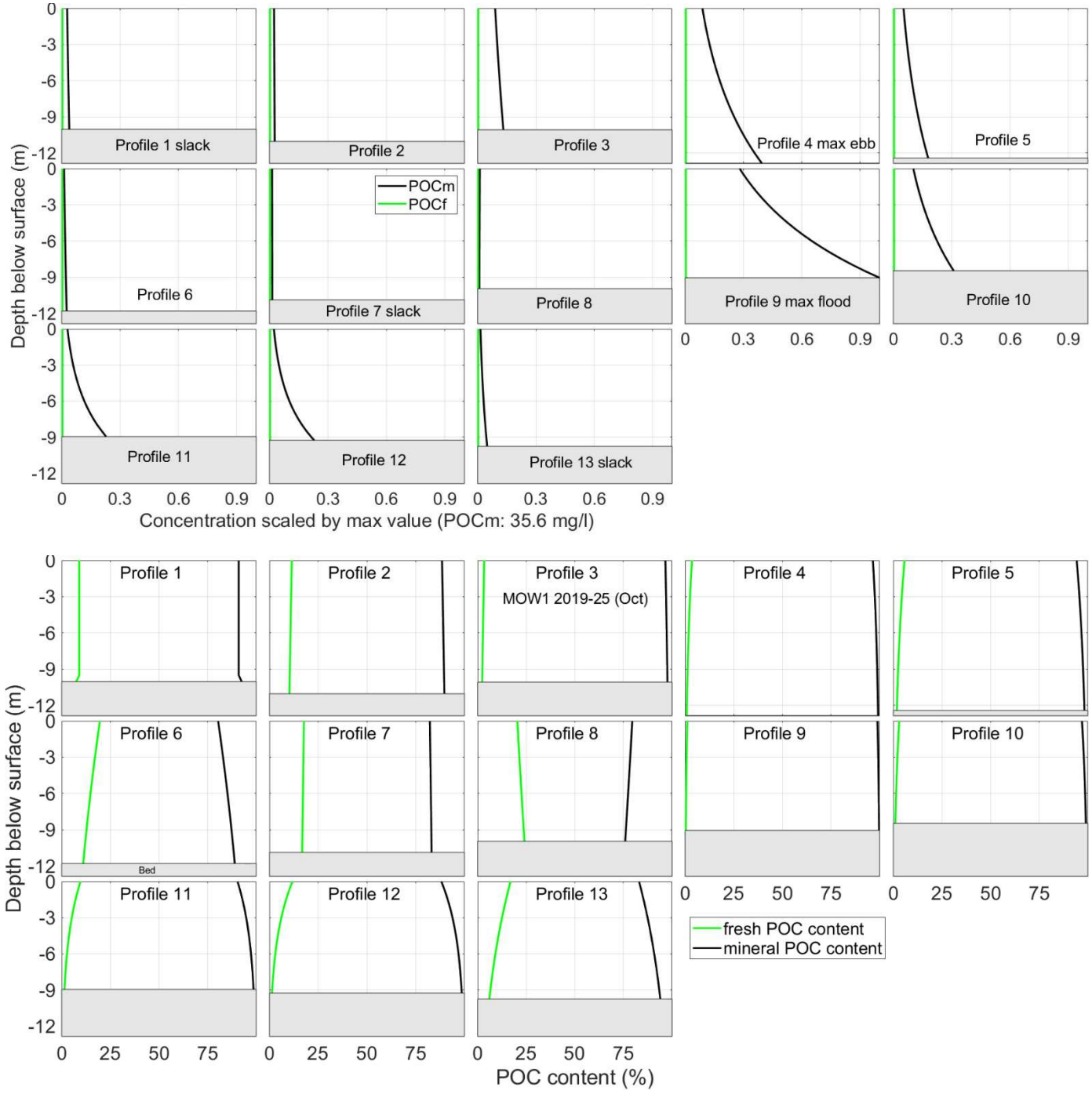

Figure A11.5: (above) Model-derived fresh and mineral-attached POC concentration profiles (values are scaled by maximum POCm); (below) relative content of fresh and mineral attached POC profiles. Period: 16/10/2019 11h00-23h00.

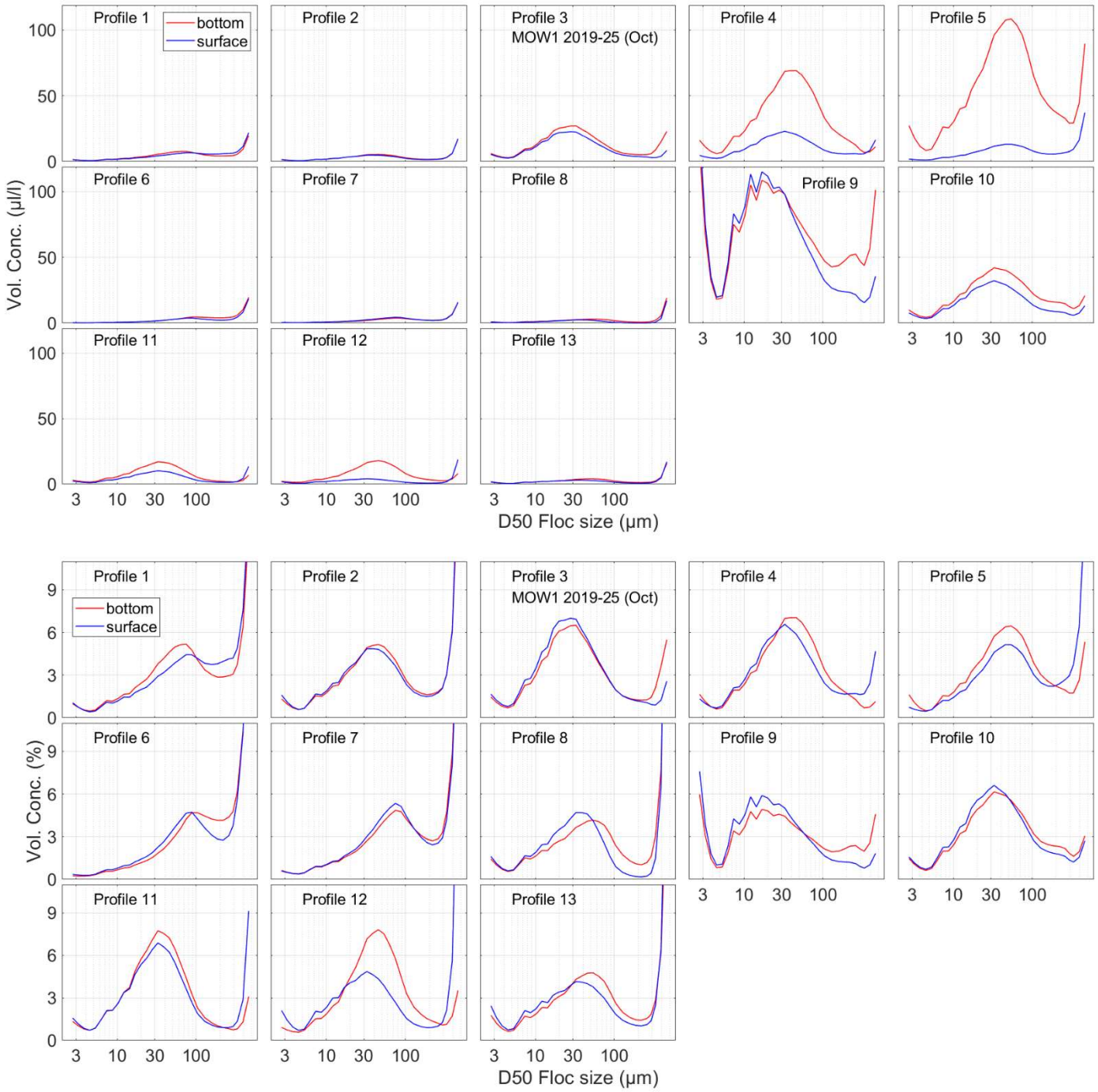

Figure A11.6: Floc size distribution (above in µl/l, below in %) at bottom and surface. Period: 16/10/2019 11h00-23h00.

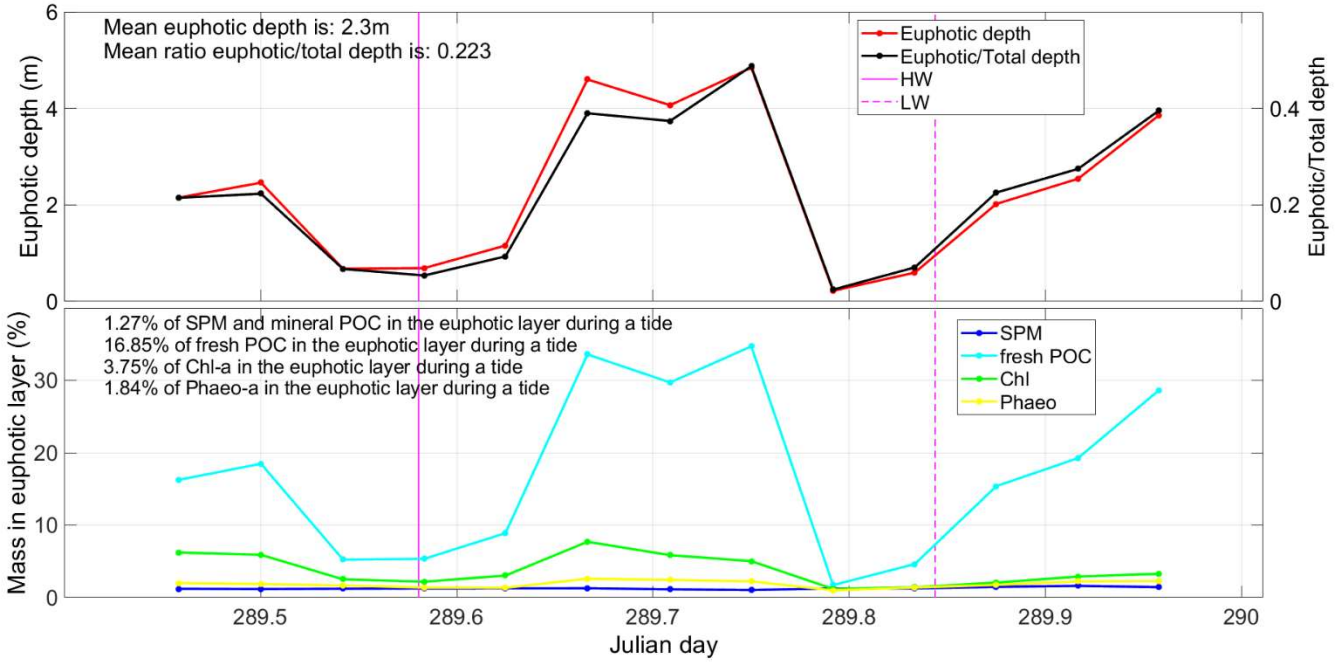

Figure A11.7: (Above) Euphotic layer depth and the ratio euphotic:total depth; (below) Probability of SPM, Chl, Phaeophytine and POC (fresh and mineral) of being in the euphotic layer. Period: 16/10/2019 11h00-23h00, HW: 13h56; LW: 20h15.

APPENDIX 12

Tidal cycle at MOW1 November 2019 (2019/29)

20/11 08h00 – 20/11 20h00

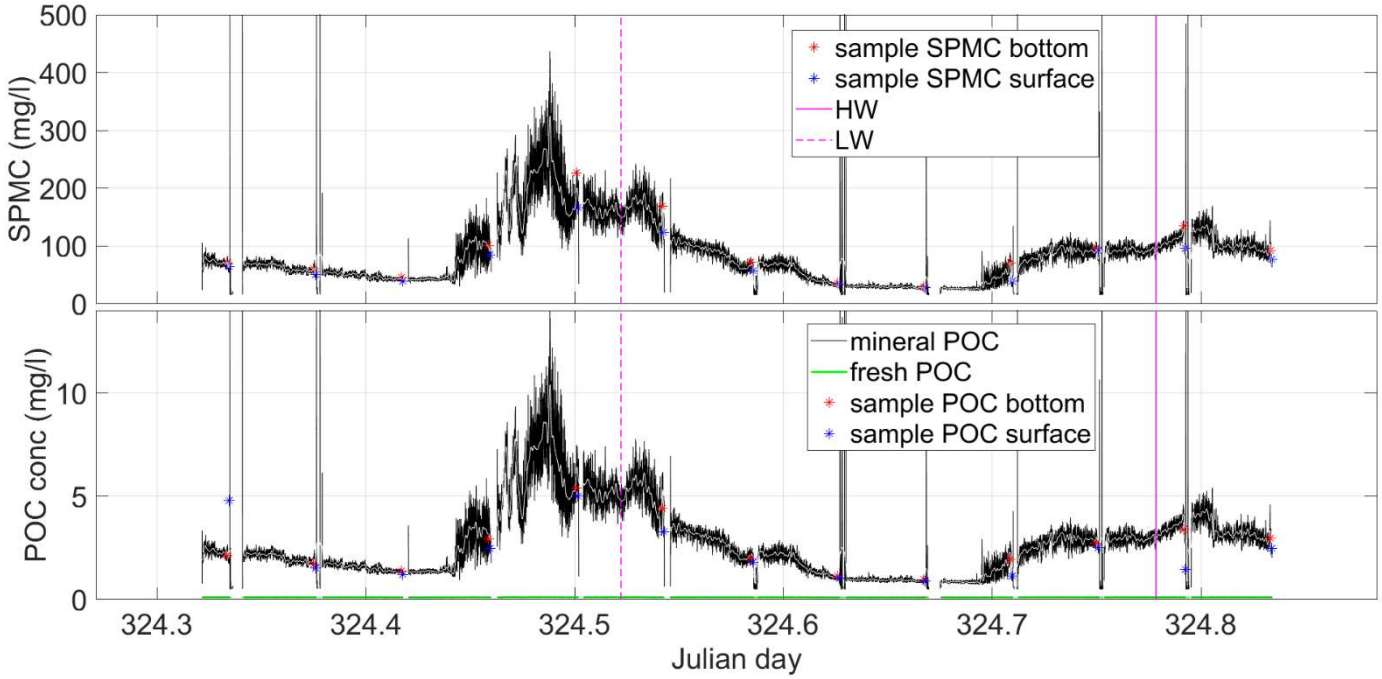

Figure A12.1: Time series of OBS-derived SPM concentration and SPM-derived mineral and fresh POC during a tidal cycle. The sample SPM and POC concentrations are also shown. Period: 20/11/2019 08h00-20h00; HW: 5h52; LW: 12h32; HW: 18h41.

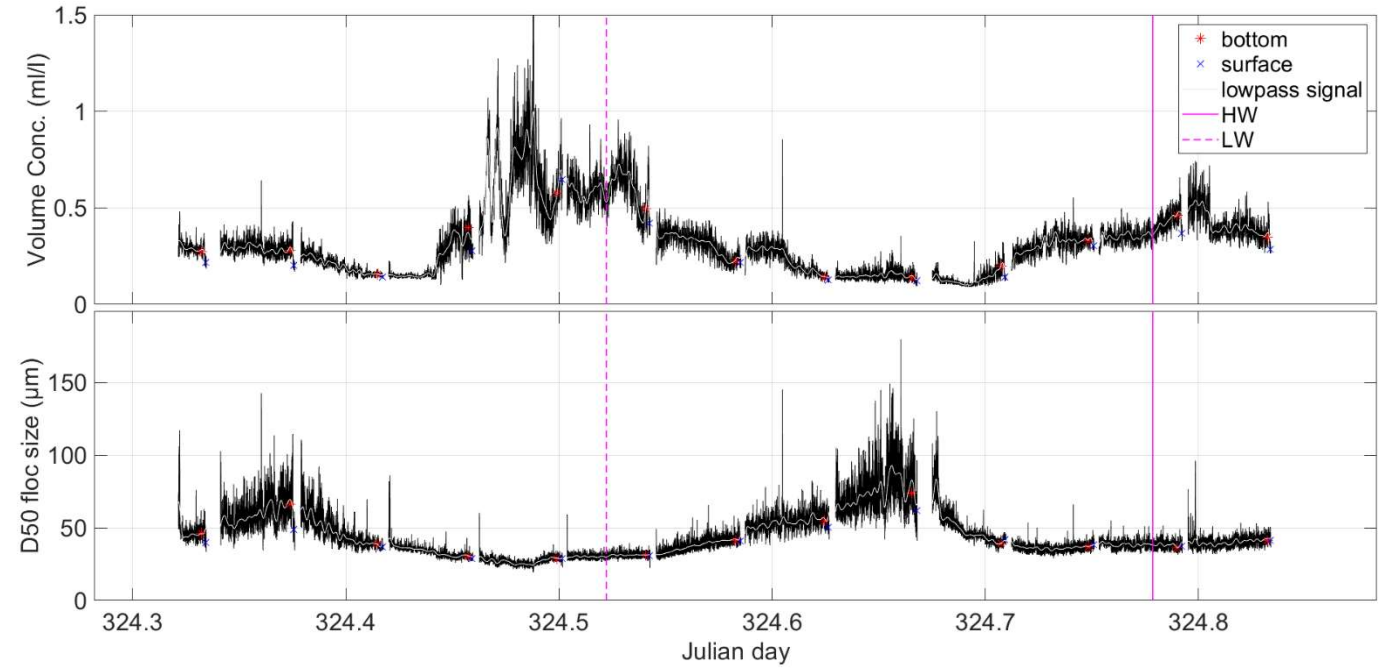

Figure A12.2: Time series of LISST-derived SPM volume concentration and median floc size during a tidal cycle. The values at surface and bottom are are also shown. Period: 20/11/2019 08h00-20h00; HW: 5h52; LW: 12h32; HW: 18h41.

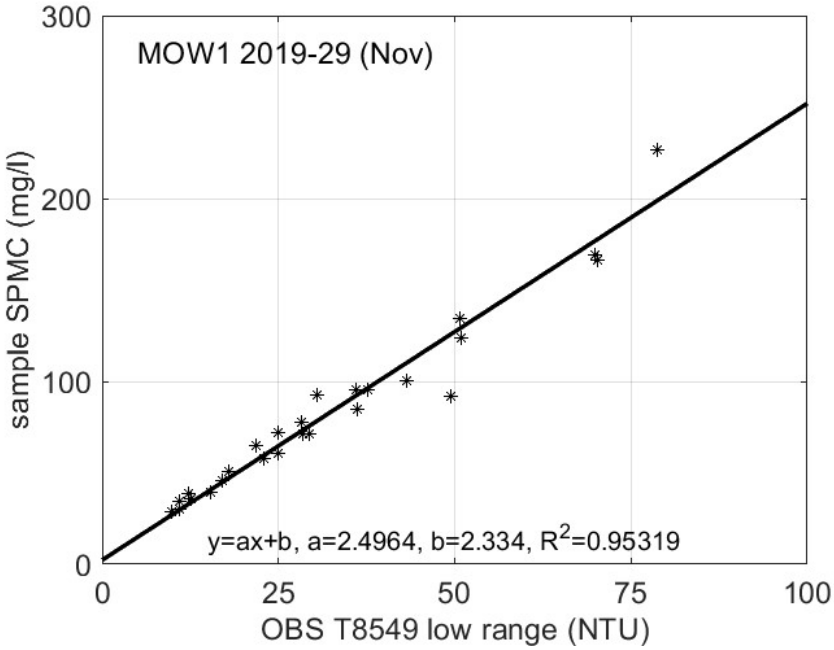

Figure A12.3: Calibration of OBS with water samples

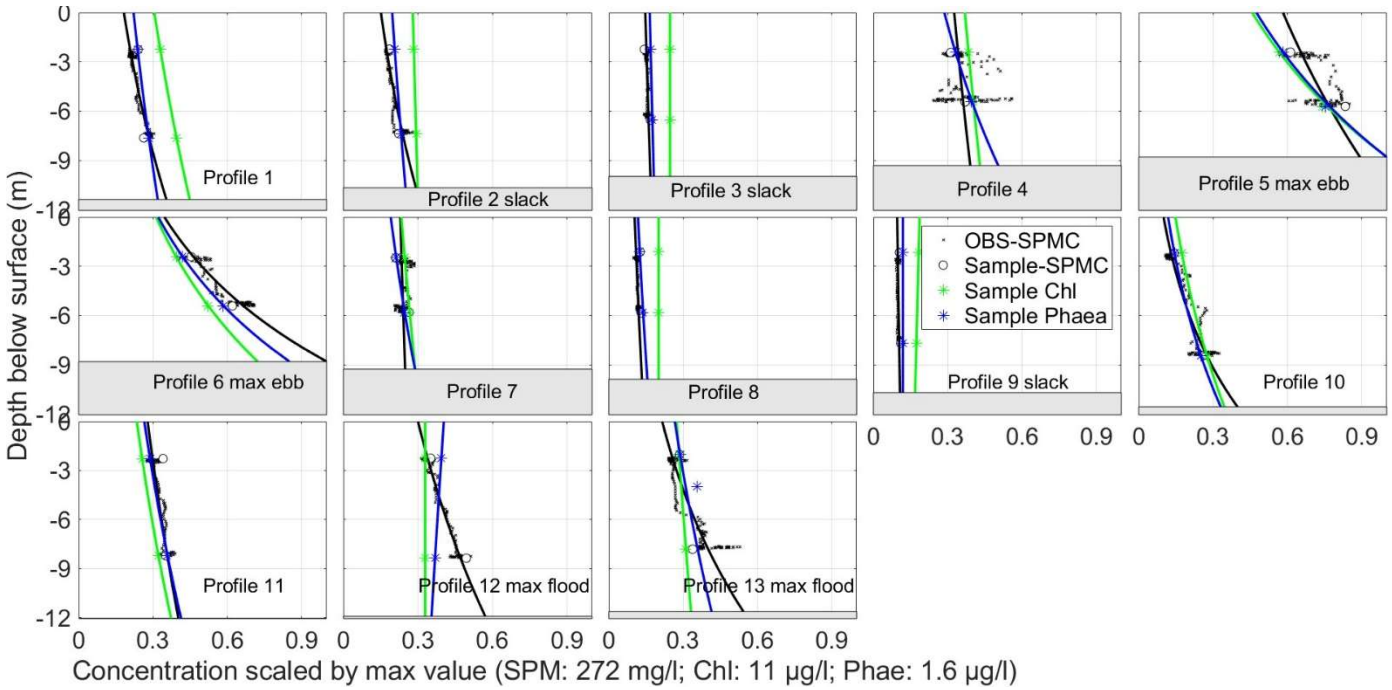

Figure A12.4: Sample-derived SPM concentration profile (black), sample-derived Chl profiles (green) and sample-derived Phaeophytin-a (blue). Values are scaled by maximum value. Period: 20/11/2019 08h00-20h00.

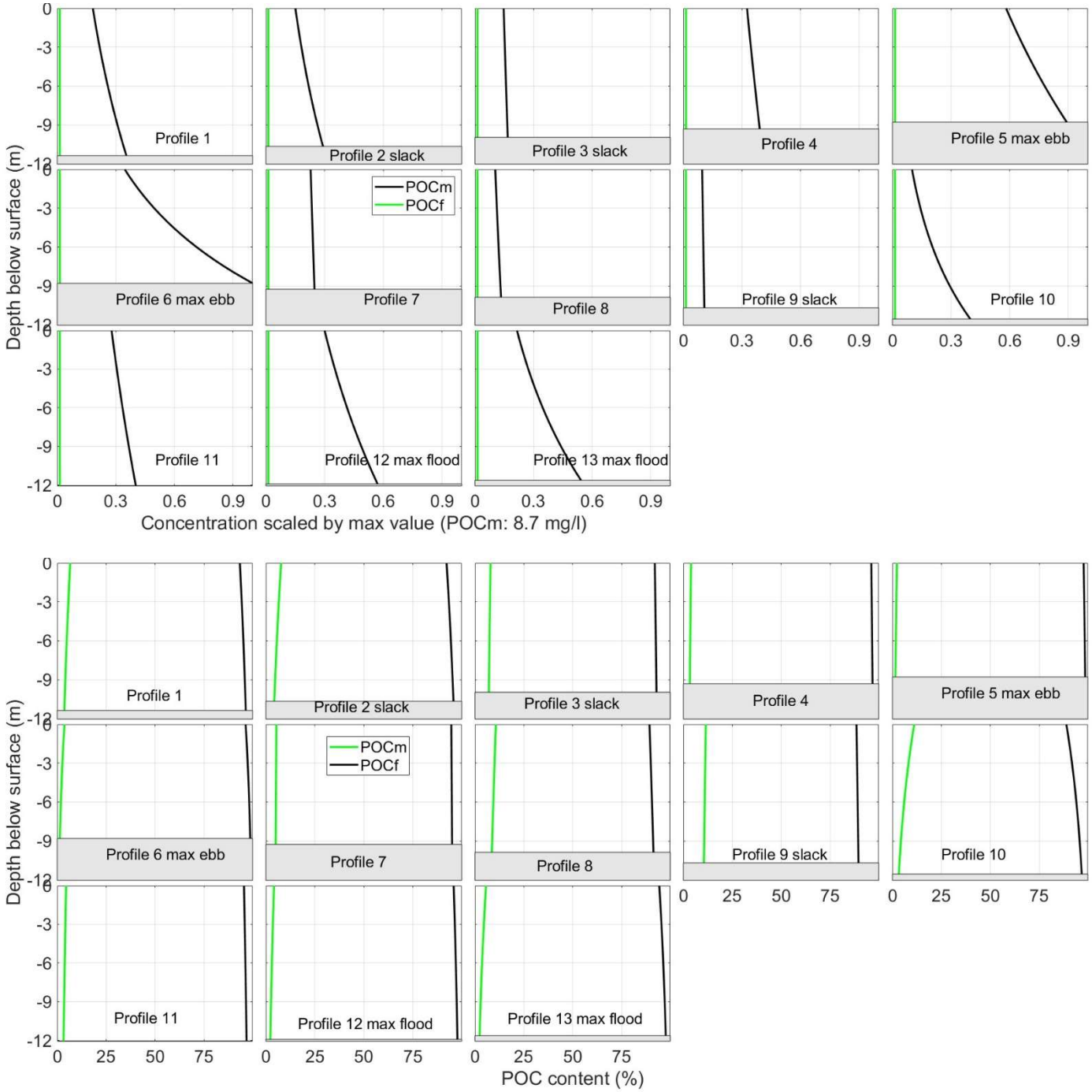

Figure A12.5: (above) Model-derived fresh and mineral-attached POC concentration profiles (values are scaled by maximum POCm); (below) relative content of fresh and mineral attached POC profiles. Period: 20/11/2019 08h00-20h00.

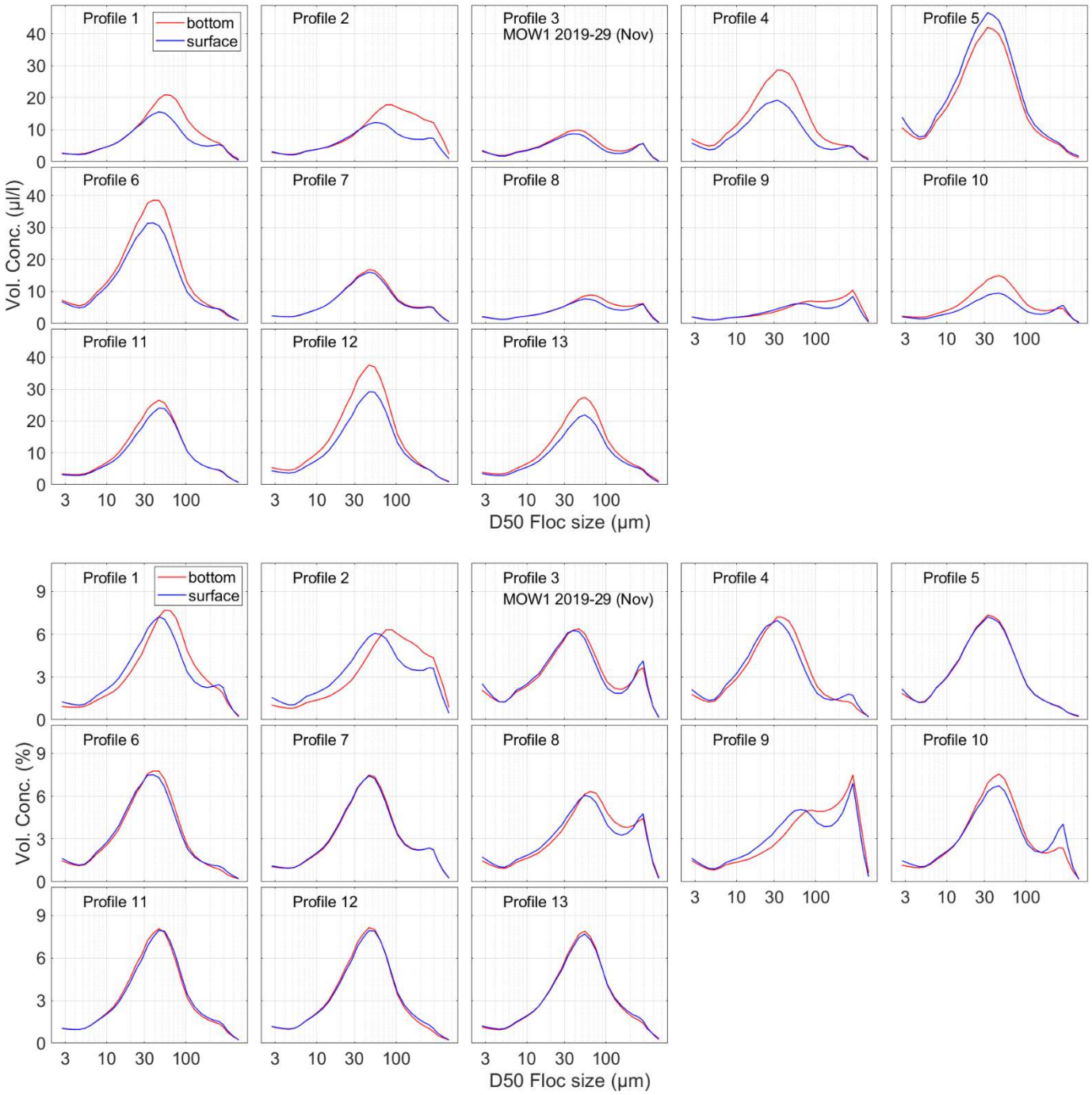

Figure A12.6: Floc size distribution (above in µl/l, below in %) at bottom and surface. Period: 20/11/2019 08h00-20h00.

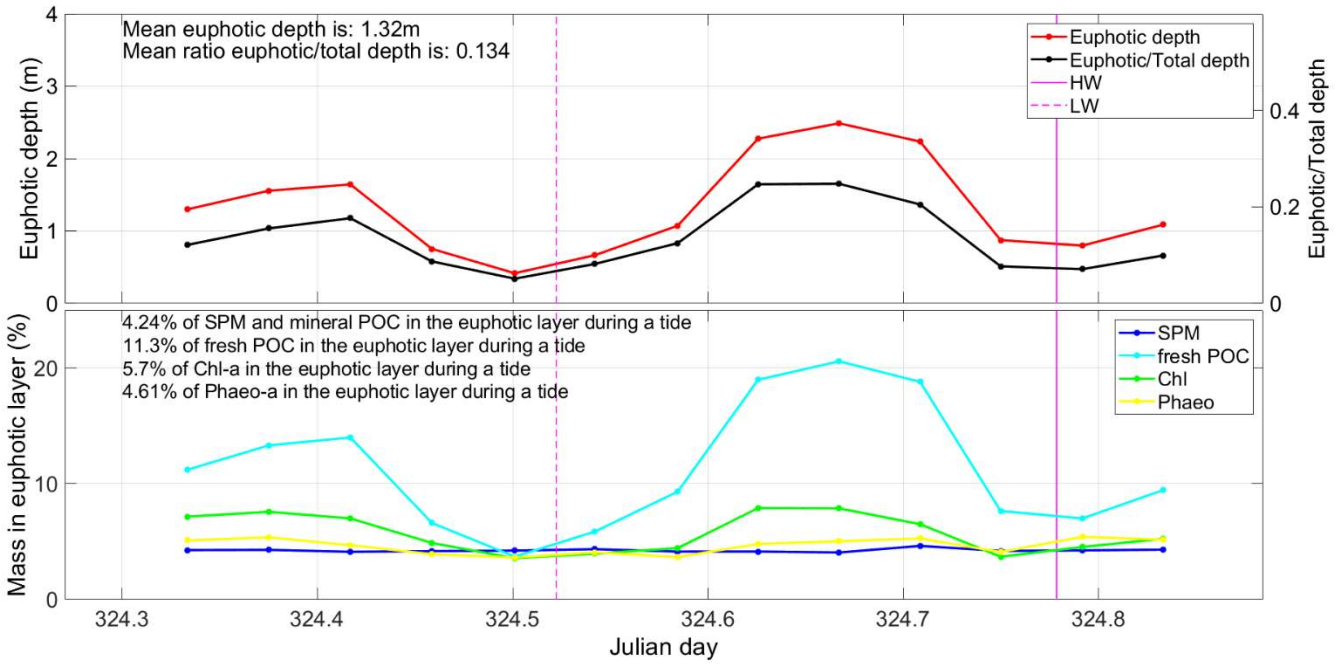

Figure A12.7: (Above) Euphotic layer depth and the ratio euphotic:total depth; (below) Probability of SPM, Chl, Phaeophytine and POC (fresh and mineral) of being in the euphotic layer. Period: 20/11/2019 08h00-20h00; HW: 5h52; LW: 12h32; HW: 18h41.

APPENDIX 13

Tidal cycle at MOW1 December 2019 (2019/32)

17/12 09h00 – 17/12 21h00

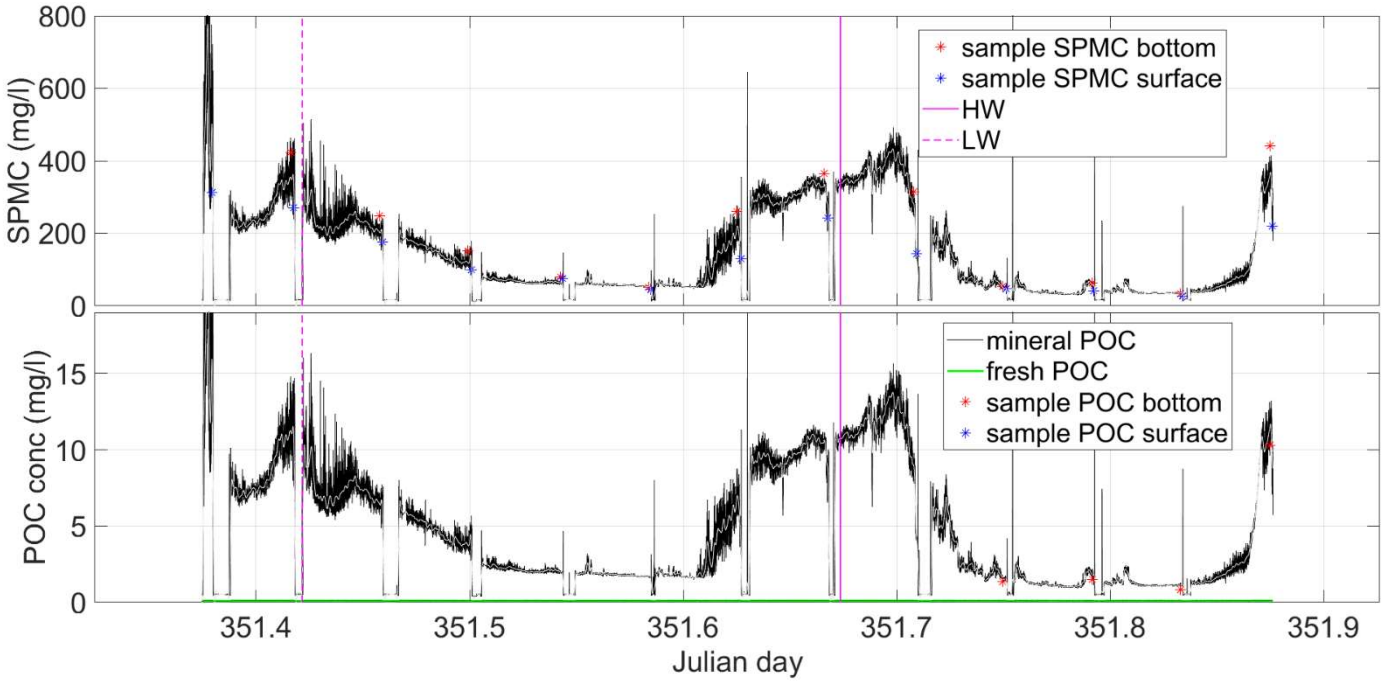

Figure A13.1: Time series of OBS-derived SPM mass concentration and SPM-derived mineral and fresh POC mass concentration during a tidal cycle. The sample SPM and POC concentrations are also shown. Period 17/12/2019 09h00-21h00; LW: 10h07; HW: 16h10.

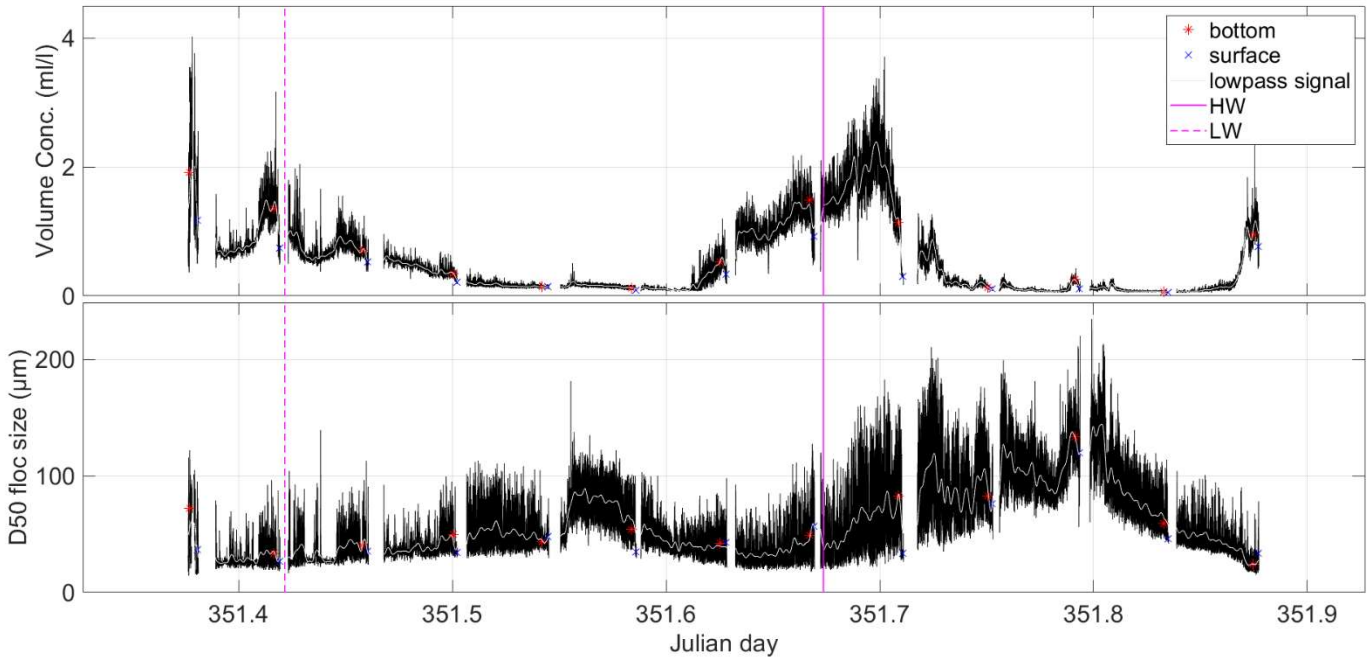

Figure A13.2: Time series of LISST-derived SPM volume concentration and median floc size during a tidal cycle. The values at surface and bottom are are also shown. Period 17/12/2019 09h00-21h00; LW: 10h07; HW: 16h10.

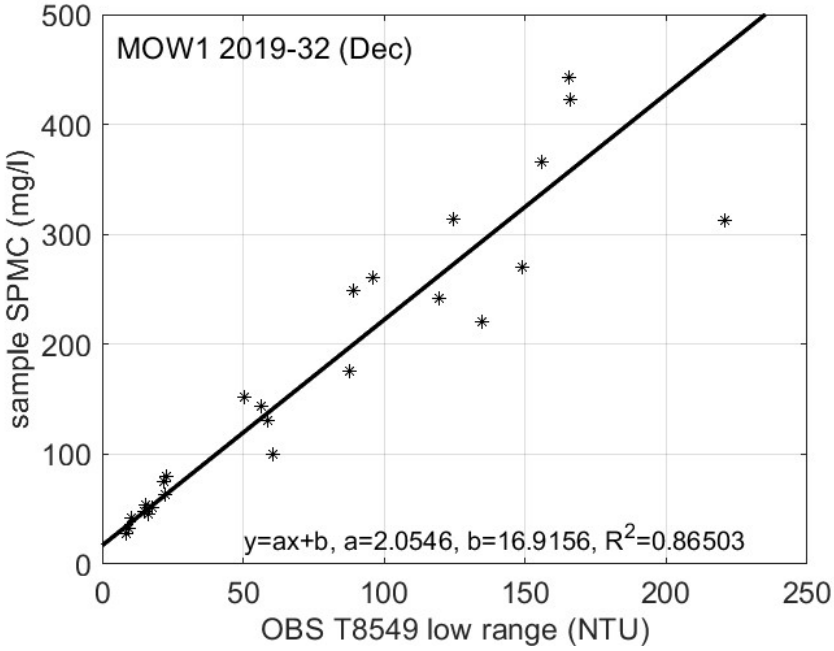

Figure A13.3: Calibration of OBS with water samples

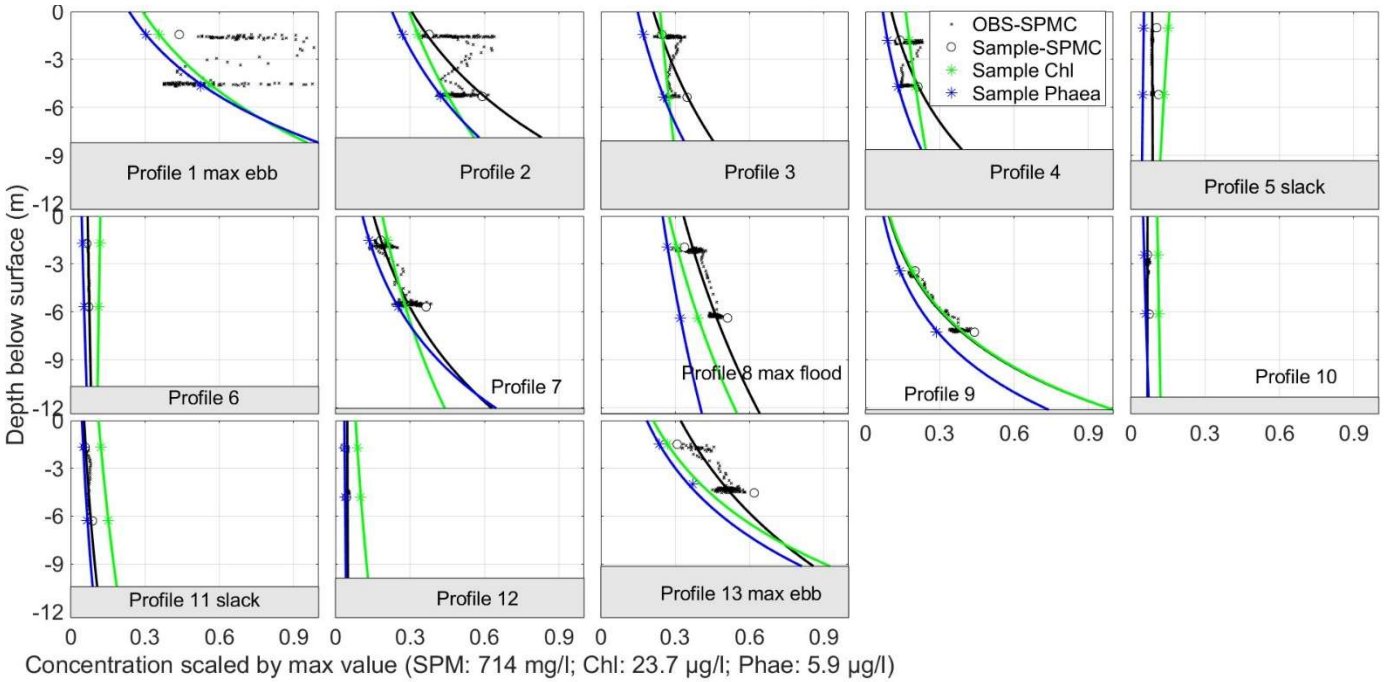

Figure A13.4: Sample-derived SPM concentration profile, profile 1 is not drawn (black), sample-derived Chl profiles (green) and sample-derived Phaeophytin-a (blue). Values are scaled by maximum value. The missing near bed Chl values in profiles 9 and 13 have been scaled by Pheophytin-a such that the ratio is equal. Period 17/12/2019 09h00-21h00.

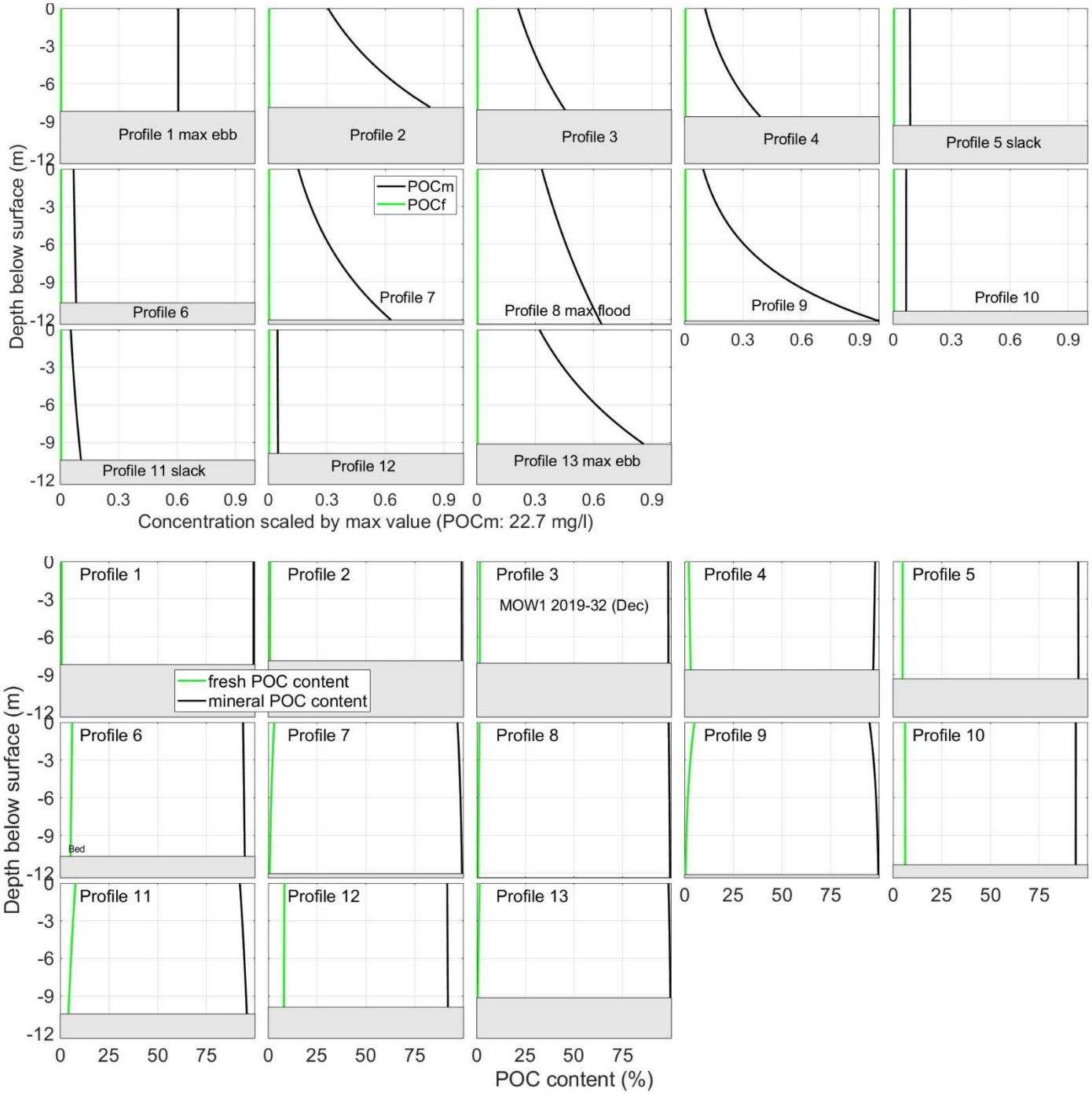

Figure A13.5: (above) Model-derived fresh and mineral-attached POC concentration profiles (values are scaled by maximum POCm); (below) relative content of fresh and mineral attached POC profiles. Period 17/12/2019 09h00-21h00.

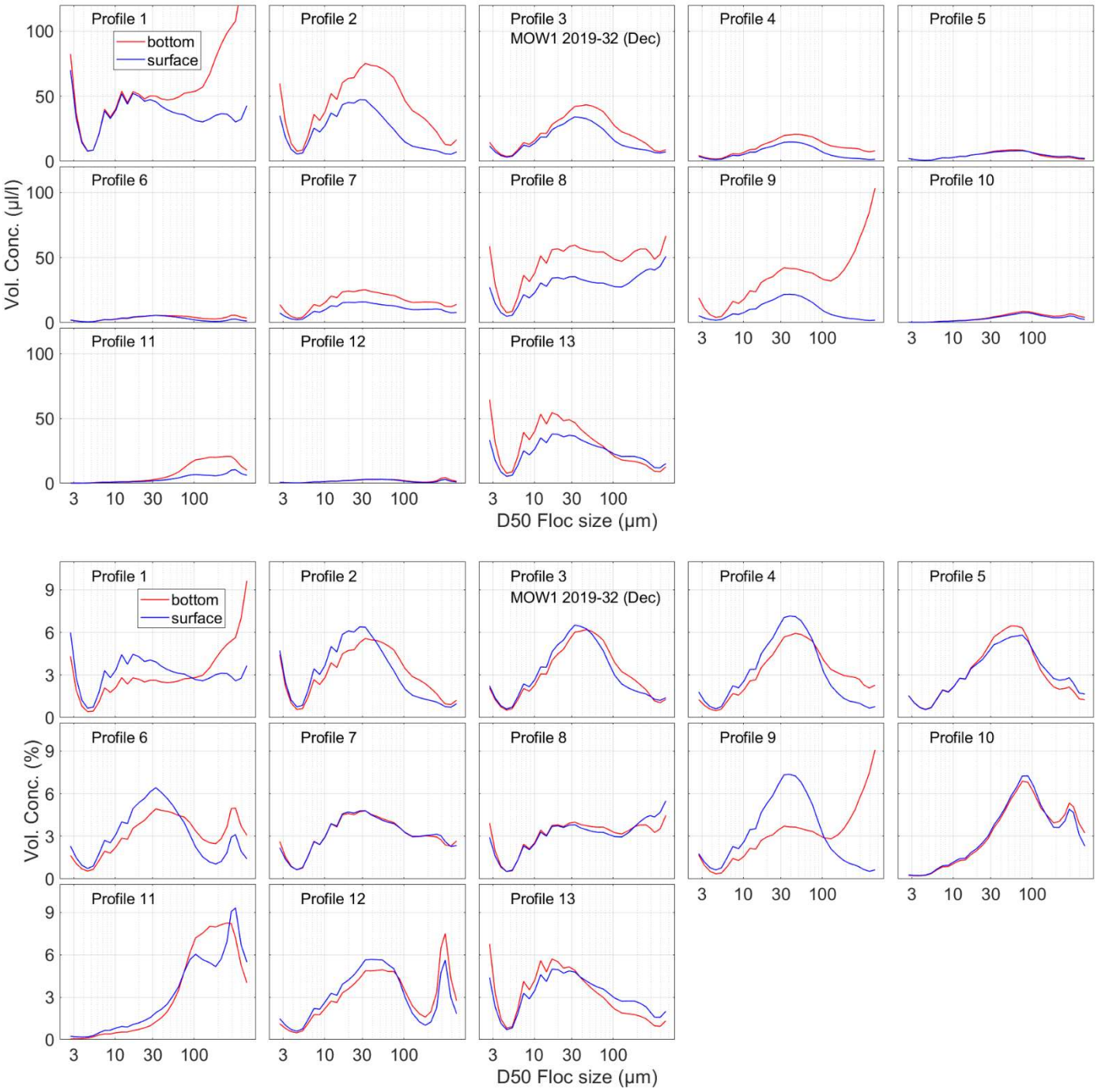

Figure A13.6: Floc size distribution (above in µl/l, below in %) at bottom and surface. *Period 17/12/2019 09h00-21h00.*

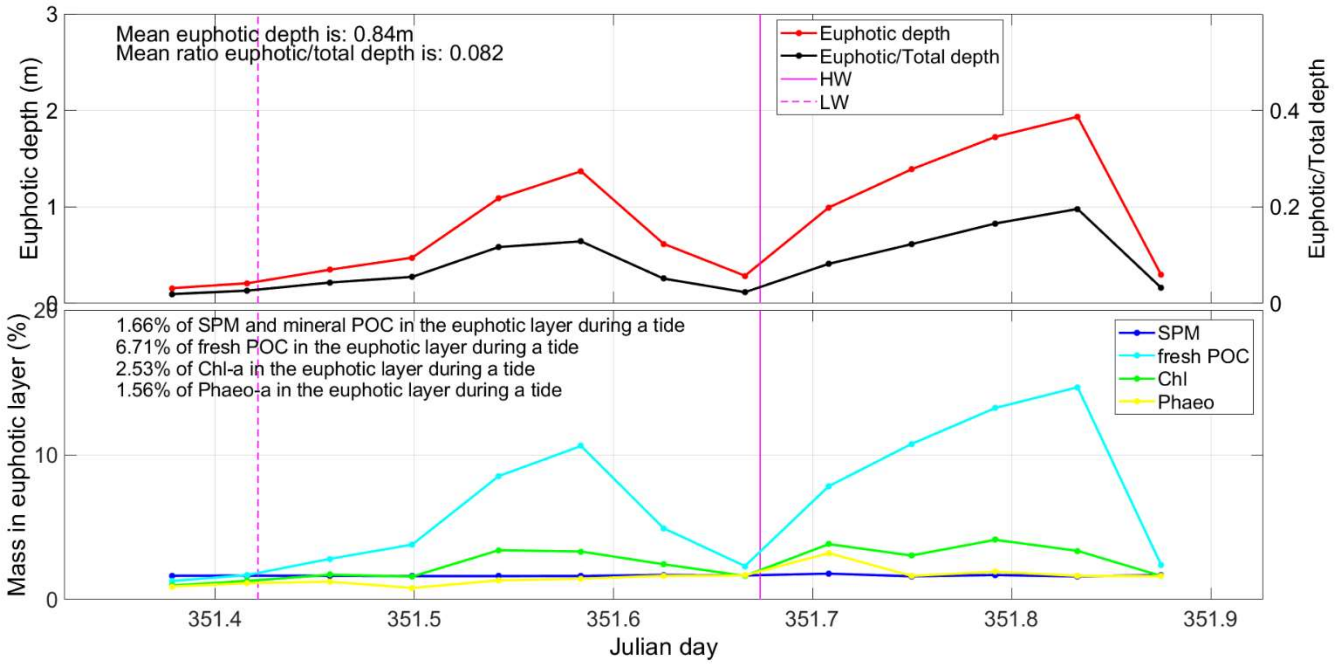

Figure A13.7: (Above) Euphotic layer depth and the ratio euphotic:total depth; (below) Probability of SPM, Chl, Phaeophytine and POC (fresh and mineral) of being in the euphotic layer. Period 17/12/2019 09h00-21h00; LW: 10h07; HW: 16h10.